Intrusions of Sub-antarctic Surface Water across the Subtropical Convergence southwest of Africa.

Submitted in fulfilment of the requirements for the degree of
Master of Science

C. S. Fillis

University of Cape Town
2001

University of Cape Town

The copyright of this thesis vests in the author. No quotation from it or information derived from it is to be published without full acknowledgement of the source. The thesis is to be used for private study or non-commercial research purposes only.

Published by the University of Cape Town (UCT) in terms of the non-exclusive license granted to UCT by the author.

University of Cape Town

This work is dedicated to my parents.

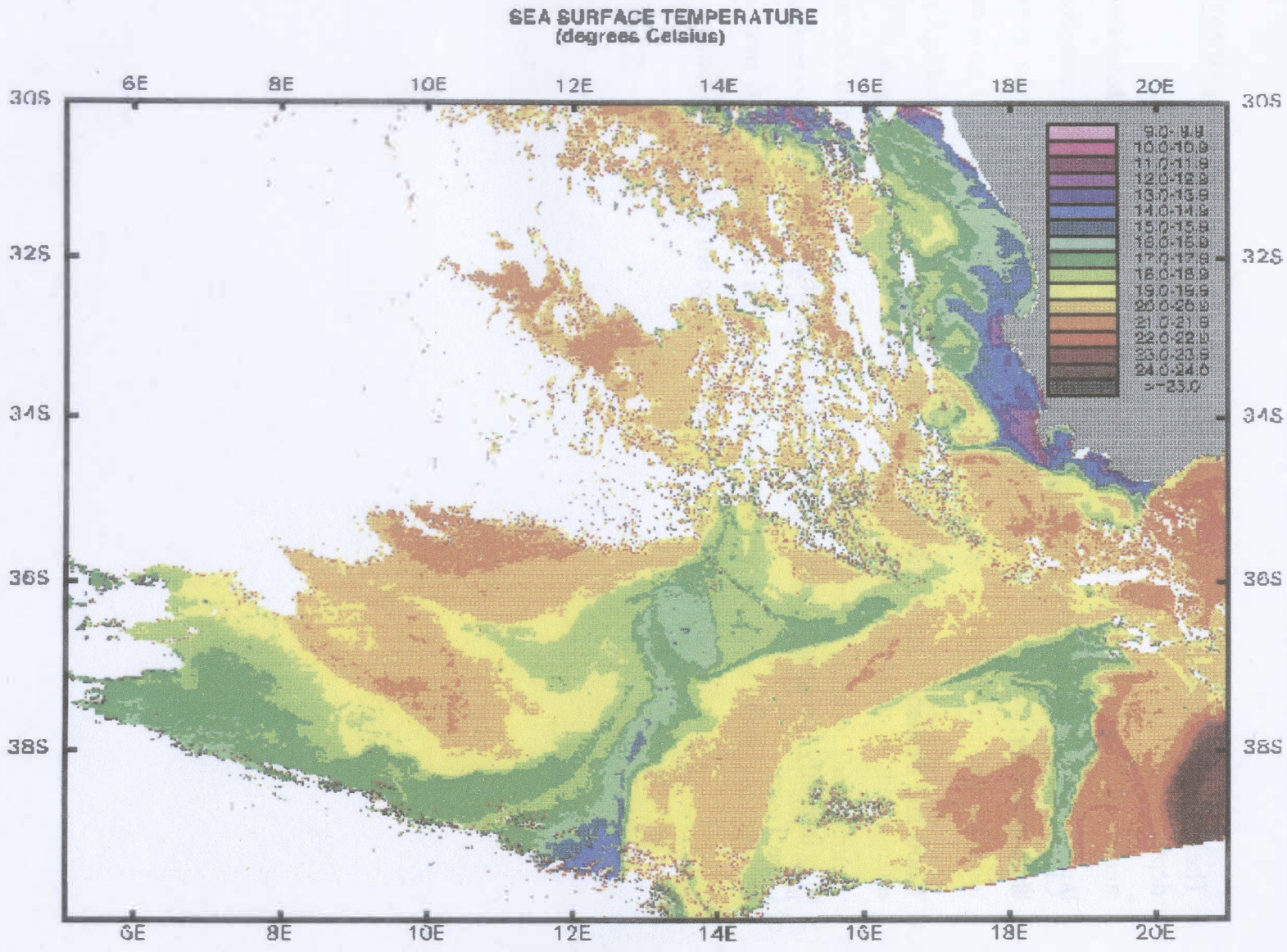
SEA SURFACE TEMPERATURE
(degrees Celsius)
6E
8E
10E
12E
14E
16E
18E
20E
30S
32S
34S
36S
38S
9.0-9.9
10.0-10.9
11.0-11.9
12.0-12.9
13.0-13.9
14.0-14.9
15.0-15.9
16.0-16.9
17.0-17.9
18.0-18.9
19.0-19.9
20.0-20.9
21.0-21.9
22.0-22.9
23.0-23.9
24.0-24.0
>=25.0

Frontis piece

Declouded and geometrically corrected thermal infrared NOAA image of the oceanic environment around South Africa on 28 February 1988. This image shows the lateral extent of cold Sub-antarctic Surface Water (SAASW) intrusions at longitudinal positions 12 °E and 19 °E (green on the diagram). The surface thermal expression of an Agulhas ring embedded between these intrusions (its core at approximately 18° E, 39°S) suggests an association with the process of ring shedding at the Agulhas Retroflection, identified as a patch of warm water directly south of the continent. Furthermore, the extensive geographical coverage of this SAASW intrusion event suggests that it may have important implications for the dynamics of the Agulhas Retroflection as well as the oceanic region to the west of the Retroflection.

Declaration

No portion of this thesis has been previously submitted in support
of an application for any other degree or qualification
in this or any other University.

C. S. Fillis
2001

Acknowledgements.

My sincere thanks to the Department of Environmental Affairs and Tourism for funding this project through its Antarctic Program;

Everyone in the Ocean Climatology Research Group of the Department of Oceanography, University of Cape Town, for creating such a friendly and cooperative environment in which I was privileged to finish this thesis;

Prof. Geoff Brudritt (HOD: Oceanography) for affording me the opportunity to register for the degree within the Department of Oceanography;

Mrs. L. Staegemann for her expert administrative and logistical support, which was vital for the completion of this work;

My family and friends for their unwavering believe in my abilities;

Miss Louise Watt at the CSIR, Stellenbosch, for going out of her way in supplying me with SADCO data housed in that data centre in such a workable format;

My supervisor, Prof. J. R. E. Lutjeharms for his tireless supervision for the duration of the thesis. My most sincere thanks to him for a chance to learn from someone whom I greatly admire;

Last, but not least, I would like to thank God for seeing me through the toughest times of my life during the completion of this thesis.

Acronyms used in the Text

AABW : Antarctic Bottom Water
AAIW : Antarctic Intermediate Water
AC : Agulhas Current
APF : Antarctic Polar Front
AVHRR : Advanced Very High Resolution Radiometer
CSIR : Council for Scientific and Industrial Research
CTD : Conductivity-Temperature-Depth meter
CWB : Continental Water Boundary
EMC : East Madagascar Current
ENSO : El Niño Southern Oscillation
LC : Leeuwin Current
METEOSAT : Meteorological Satellite
MOC : Mozambique Current
NADW : North Atlantic Deep Water
NOAA : National Oceanic and Atmospheric Administration
R. V. : Research Vessel
SAASW : Sub-antarctic Surface Water
SADCO : Southern African Data Centre for Oceanography
SAF : Sub-antarctic Front
SANAE : South African National Antarctic Expedition
SASW : South Atlantic Surface Water
SCARC : Subtropical Convergence and Agulhas Retroflection Cruise
SEC : South Equatorial Current
SIOC : South Indian Ocean Current
SICW : South Indian Central Water
SST : Sea Surface Temperature
STC : Subtropical Convergence
SWIO : Southwest Indian Ocean
VOS : Voluntary Observing Ships
VHRR : Very High Resolution Radiometer
WAC : West Australian Current
XBT : Expendable Bathythermograph

Symbols used in the text.

kg : kilogram
J : Joules
m : meter
Sv : Sverdrup (10^6 $m^3.s^{-1}$)
db : decibar (100 bar) 1db is approximately the equivalent of 1 m dept in the water column
+ or - δ : Positive or negative anomaly.
~ : Approximately

Index

Frontis piece v

Declaration vi

Acknowledgements vii

Acronyms used in the Text viii

Symbols used in the Text viii

Index ix

Abstract xi

Chapter 1 : Introduction 1

Chapter 2 : The oceanic environment around Southern Africa 6

2.1. Bathymetry 6
2.2. Water masses 9
2.3. Geostrophic transport of surface and thermocline water 13
2.3.1. Meso-scale features associated with the Agulhas Current 19
2.4. Geostrophic flow at depth 23
2.5. The Southern Ocean 26

Chapter 3 : Review of what is known about SAASW intrusions 30

3.1. The Process of ring shedding 30
3.2. Structure of an extreme event 34
3.3. Environmental changes 38

Chapter 4 : Remaining Questions and Research Objectives 41

Chapter 5 : Data and Methodology 43

5.1. Mean sea surface thermal and salinity expression 43
5.2. Thermal infrared analysis 47
5.2.1. Analysis of satellite thermal infrared images 48
5.2.2. Determination of SAASW intrusion frequency 48
5.3. Altimetric observations 50
5.4. Hydrographic data 51

Chapter 6 : Mean oceanic environment and satellite infrared analysis 54

6.1. Mean flow field southwest of Africa 54
6.2. Types of intrusions 60
6.3. Satellite Composite analysis 65
6.4. Composite diagrams of individual SAASW intrusion events 68
6.5. Frequency of SAASW intrusions 70

Chapter 7 : Altimetry 82

Chapter 8 : Hydrographic structure of SAASW intrusions 121

8.1. The Agulhas Retroflection Cruise (ARC) 121
8.2. The Subtropical Convergence and Agulhas Retroflection Cruise 135

Chapter 9 : Summary and Conclusion 144

9.1. The lateral dimensions of SAASW intrusions 144
9.2. Location of SAASW intrusions 144
9.3. Frequency and persistence 145
9.4. Hydrographic structure 145

References 147

Addenda 156

A.1. Composite diagrams of Meteosat images (1983 to 1990). 156
A.2. Yearly composite diagrams 165
A.3. Summary of the statistical 168
A. 4. Weathership data 174

Abstract

The terminal region of the Agulhas Current south of Africa is characterized by the complete retroflection of the Current. The region has been shown to be populated by a range of eddies and rings. It has been observed that the spawning of an Agulhas Current ring at the retroflection is preceded by the northward wedging of the Subtropical Convergence (STC) through the retroflection loop to effectively "pinch" off these rings. The resultant entrainment of cold Sub-antarctic Water Surface (SAASW) behind the displaced STC is of climatic and oceanographic interest in light of the concurrent interruption and eastward retreat of the warm Agulhas Current. The leakage of Agulhas Current water into the Southeastern Atlantic Ocean in the form of filaments may also be temporarily terminated during these SAASW intrusion episodes. In order to investigate intrusions of SAASW into the Agulhas Retroflection region, all available data of any kind have been accessed and analyzed.

A serial satellite study, using both METEOSAT and NOAA images, suggests that approximately four intrusions of SAASW are observed per year. These intrusions generally occur between 11° E and 19° E; the westerly intrusions being more prevalent during extreme episodes of SAASW intrusions. The mean temperature and salinity distribution at the retroflection shows that the longitudinal location of SAASW intrusions seems to be geographically invariant suggesting a possible topographic influence by prominent geographical features such as the Agulhas Ridge (~ 18 °E) and the Panzarini seamount (~ 11 °E) in the region southwest of South Africa.

Hydrographic analysis of sub-antarctic water intrusions leads one to believe that they are not just shallow, short term phenomena but may reach to depths of approximately 800 m to 1000 m, persisting for about 28 days on average. These intrusions introduce low temperature (~ 14 °C), low salinity (< 35) water into the retroflection region with an average areal geographical coverage of 158 000 ± 118 256 km^2. This suggests that

these sub-antarctic water intrusions may have important oceanographic and biologic implications to the dynamics of the Agulhas Retroflection and the oceanic region to the west of it in light of the sheer magnitude of the amount of water involved.

Chapter 1

Introduction

This chapter provides an orientation to the diverse oceanographic flow field around southern Africa; in particular how SAASW intrusions fit into this circulation. It also introduces some meso-scale oceanographic circulation features that will be discussed more comprehensively in the next two chapters. The general layout of the thesis is presented at the end of the chapter.

South Africa is in a unique geographical location for oceanographic research [Siegfried and Lutjeharms, 1990] owing to the fact that it is surrounded by three of the world's oceans (Figure 1.1).

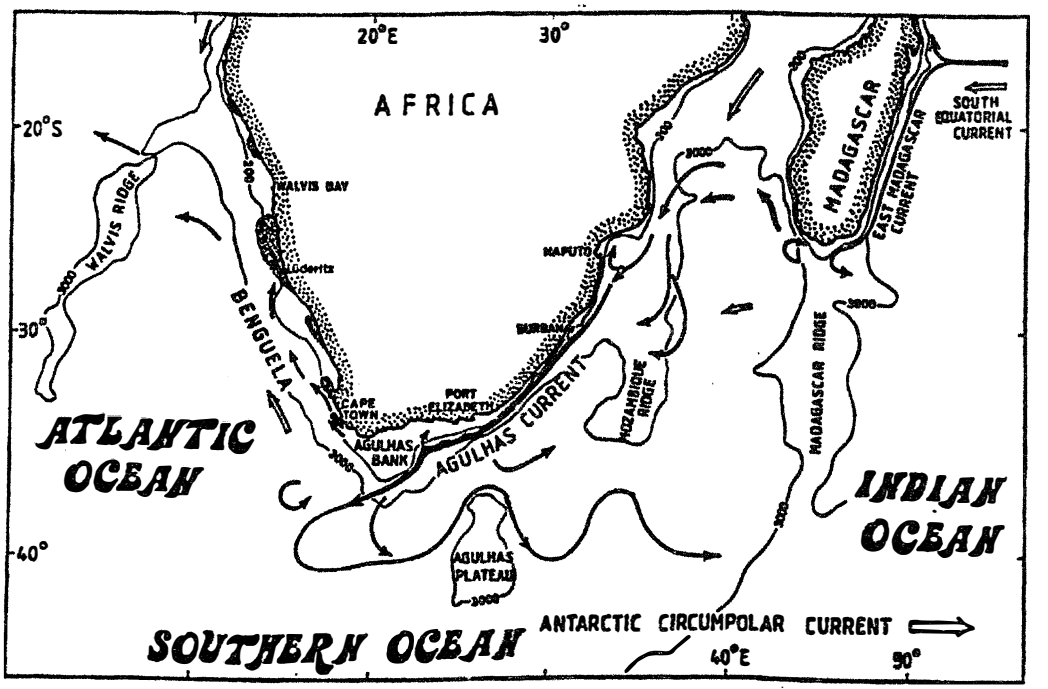

Figure 1.1. The Southern African oceanic environment showing the location of the Agulhas Current and the Benguela upwelling cells as well as part of the Southern Ocean. The arrows indicate the basic circulation features within these three oceanic systems. Bathymetric contours are in meters. [Schumann, 1990]

Marine research in South Africa in the past decades seems to have been polarized largely into the study of the Benguela upwelling system to the west and the Agulhas Current system to the east and south and specialization into one or the other system has become the norm [Lutjeharms, 1991]. Little interaction between the two systems has been observed except on the continental shelf [*e.g.* Duncumbe Rae *et al.*, 1992; Lutjeharms and Cooper, 1996].

The western coastline of South Africa forms the southeastern boundary of the South Atlantic anticyclonic gyre. Being one of four major eastern boundary regions of the world ocean, it is archetypically dominated by coastal upwelling on the continental shelf [Shannon, 1985; Lutjeharms and Valentine, 1987; Shannon, 1990; Shannon and Nelson, 1996]. Centres of upwelling (identified on Figure 1.1 as tongue-like patches of water along the Southern African west coast) are of economic value to the South African and Namibian fishing industries. Therefore, much oceanographic research in the area has been in support of biological studies linked to Southern African fisheries on the west coast [as summarized by Shannon and Nelson, 1996]. The Benguela Current itself may be described as the broad, slow-moving eastern boundary current of the South Atlantic Ocean [*e.g.* Shannon, 1990].

The Agulhas Current system forms the southern component of the western boundary currents associated with the South Indian anticyclonic ocean gyre [Wyrtki, 1971] and stands in stark contrast to the Benguela regime. It is a warm, fast-moving current that follows the continental slope (200 m depth) very closely. The current axis migrates offshore upon encountering the Agulhas Bank (Figure 1.1), overshoots the southern terminus of the continent and turns back on itself (retroflects) to form the Agulhas Return Current. The Agulhas Return Current then executes a northward meridional loop over the Agulhas Plateau generating planetary waves downstream of the Plateau. The greater Agulhas Current system has enjoyed a wealth of oceanographic attention over the past few decades [summarized by Lutjeharms, 1991; Lutjeharms, 1996].

The Agulhas Current plays an important role in the global ocean circulation through the exchange of thermocline water between the Indian Ocean and the Atlantic Ocean [Gordon, 1986; Gordon, 1996; Lutjeharms, 1996; Feron *et al.*, 1992; Schmitz, 1996] and exerts a marked influence over the weather of the South African east and south coasts. [Preston-Whyte and Tyson, 1988].

To the south, the Antarctic Circumpolar Current (ACC) in the Southern Ocean has a major influence on the South African as well as the whole globe's weather. It is the only ocean in direct contact with all the rest of the world's oceans; Atlantic, Indian and Pacific. Research on the Southern Ocean south of Africa has only recently received serious (local) oceanographic interest [Lutjeharms, 1991; Gründlingh and Lutjeharms, 1990]. The region directly to the south of the African continent, where the three surrounding oceans meet and interact, is of particular importance to global ocean circulation [Lutjeharms and van Ballegooyen, 1988; van Ballegooyen *et al.*, 1994; Lutjeharms, 1996, Gordon, 1986, Gordon, 1996]. Vast amounts of heat, salt and water are exchanged here between the oceans in a dynamic and complex way [Gordon, 1986; Gordon *et al.*, 1987; Lutjeharms and Cooper, 1996]. Inter-ocean exchange of heat and salt from the Indian Ocean to the Atlantic Ocean occurs at the Agulhas Retroflection region in the form of rings and plumes emanating from the Agulhas retroflection [Lutjeharms and van Ballegooyen, 1988; Lutjeharms and Cooper, 1996; Lutjeharms, 1996]; details of which are not shown on Figure 1.1.

At times the Agulhas retroflection loop may occlude and form annulus-shaped vortices termed Agulhas rings. This spawning of Agulhas Current rings has been observed to result in an entrainment of cold water from the south, called Sub-antarctic Surface Water (SAASW), across the Subtropical Convergence (STC) southwest of the African continent [Lutjeharms and Gordon, 1987; Lutjeharms and van Ballegooyen, 1988; Shannon *et al.*, 1989; Meeuwis and van Rensburg, 1995] (see Frontis piece). The oceanographic nature and extent (both temporally and spatially) of these SAASW intrusions have not been adequately established and are the focus of this investigation. The importance of this

water mass as well as the present knowledge concerning SAASW intrusion events are discussed at length in Chapter 3.

However, understanding the nature of these SAASW intrusions south of Africa and their role within the Agulhas Retroflection dynamics warrants a more detailed description of the oceanic environment around southern Africa. Such a description will be given in the next chapter. Chapter 3 therefore augments Chapter 2, by providing a more in-depth discussion of the current knowledge concerning these SAASW intrusions in particular. Chapter 4 details the gaps in our present knowledge on SAASW intrusions and gives the scope of this investigation in attempting to fill these gaps. In Chapter 5 the Data and Methodology used to study the intrusions are described. This chapter also outlines the shortcomings and sources of error within the data and methods used.

The results of an analysis using thermal infrared images from geostationary and polar orbiting satellites are reported and discussed in Chapter 6. The surface thermal expressions of these SAASW intrusions were used to determine the geographic extent, duration as well as the frequency of these intrusions. These thermal infrared analyses are augmented by an altimetry study in Chapter 7, in which sea surface height anomalies were measured in the vicinity of SAASW intrusions, thus avoiding the problem with cloud cover usually encountered when using thermal infrared images.

Results of a hydrographic analysis are reported and discussed in Chapter 8. These give an indication of the vertical extent of these intrusions and how these vertical characteristics change with time. The data were also used to verify whether the intrusions indeed consist of SAASW.

Chapter 9 presents a synoptic review and summary of what has been learned here about SAASW intrusions and explains the importance of SAASW intrusions south-west of Africa to the global thermohaline circulation.

The Addendum consists of a set of satellite composite sketches of the thermal sea surface expressions of cold SAASW intrusions as well as summarising statistics on the lateral dimensions and position of SAASW intrusions. Thermograph data obtained from a weather ship, *F. H. Hughes,* over the Retroflection region is also analysed. The uncertainty regarding the quality of the data does not warrant it to be put in the body of the thesis, however useful information was indeed extracted from this data source to justify putting it at least in the addendum.

Chapter 2

The oceanic environment around Southern Africa

This chapter does not present an encyclopaedic account of the complex marine circulation around southern Africa; it describes most of the meso-scale oceanic features in sufficient detail for the purposes of this thesis. It commences with a description of the general bathymetry of the region. Thereafter, the oceanic characteristics of the different marine environments are discussed. Information presented includes the general geostrophic flow field within the different marine regions and the characteristics of the different water masses within these regions.

2.1. Bathymetry

A chart depicting the sea bottom topography around Southern Africa between 14 °S to 45 °S and 0 °E to 26 °E is given on Figure 2.1. The abyssal plain of the southeastern Atlantic Ocean east of the Mid-Atlantic Ridge comprises the Cape and Angola Basins, which are clearly separated by the Walvis Ridge. The Walvis Ridge has been shown to impede the northward and southward flow of Antarctic Bottom Water (AABW) between the two basins [Shannon, 1985; Shannon and Nelson, 1996] although some leakage through this ridge has been observed [*e.g.* Shannon and Chapman, 1991].

The Agulhas Ridge forms a prominent geological feature towards the southwest of the African continental terminus. It is believed that this ridge could be responsible for mesoscale meridional instabilities within the STC (a strong thermal oceanic front located at ~ 40 °S) at longitude 15 °E [Shannon *et al.*, 1989; Harris and Stavropoulos, 1978] giving rise to episodic northward displacement of this front.

The continental shelf off the Southern African west coast varies from the wide Agulhas Bank (up to 230 km wide) to the south of the continent to approximately 40 km off the Cape Peninsula, widening towards the north to ~ 180 km in the vicinity of

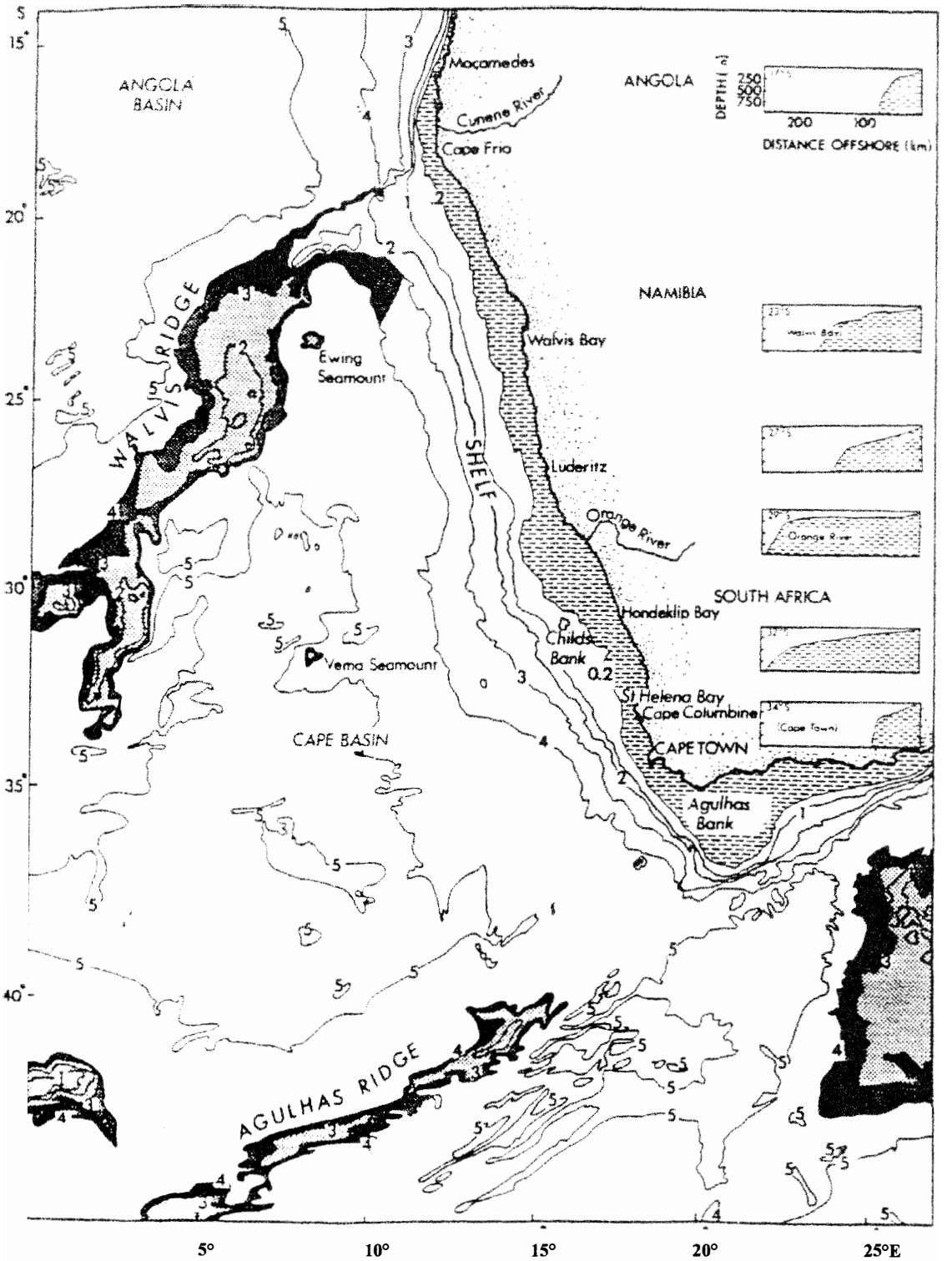

Figure 2.1 Bathymetric chart of the South-east Atlantic Ocean showing the major bathymetric features off the South-western African and Southern African coastline. Depth contours are in hundreds of metres and the continental shelf is hatched. [Shannon and Nelson, 1996].

the Orange River. The width of the continental shelf north of Lüderitz varies between 40 and 75 km becoming very narrow off Angola (~ 20 km wide).

The continental shelf on the east coast of southern Africa is considerably narrower than that along the west coast (*cf.* Figure 2.9), but shows some widening north of Durban (called the Natal Bight) and off Maputo (called the Delagoa Bight). The Natal Bight is believed to be the spawning site of an extreme solitary meander of the Agulhas Current [Lutjeharms and Roberts, 1988]. This wave migrates southward along the coast and is conjectured to bring about early retroflection of the Agulhas Current [Lutjeharms and Roberts, 1988; van Leeuwen *et al.*, 2000].

The Agulhas Plateau southeast of the continent (~40 °S, 26 °E on Figure 2.1) constitutes a conspicuous hindrance to the water flow of the Agulhas Return Current [*cf.* Figure 1.1]. It forces the Current to loop northward at the Plateau initiating planetary Rossby waves downstream of the Current path.

From the above description it is clear that the bottom topography of the region around southern Africa contributes to the pattern of the water circulation not only at depth, but also at the surface. However, before the geostrophic transport field can be discussed in more detail, an understanding of the different water masses within this circulation field is needed.

2.2. Water masses.

The principal water masses present in the Southeastern Atlantic Ocean are depicted in a Potential Temperature–Salinity (Θ-S) diagram (Figure 2.2).

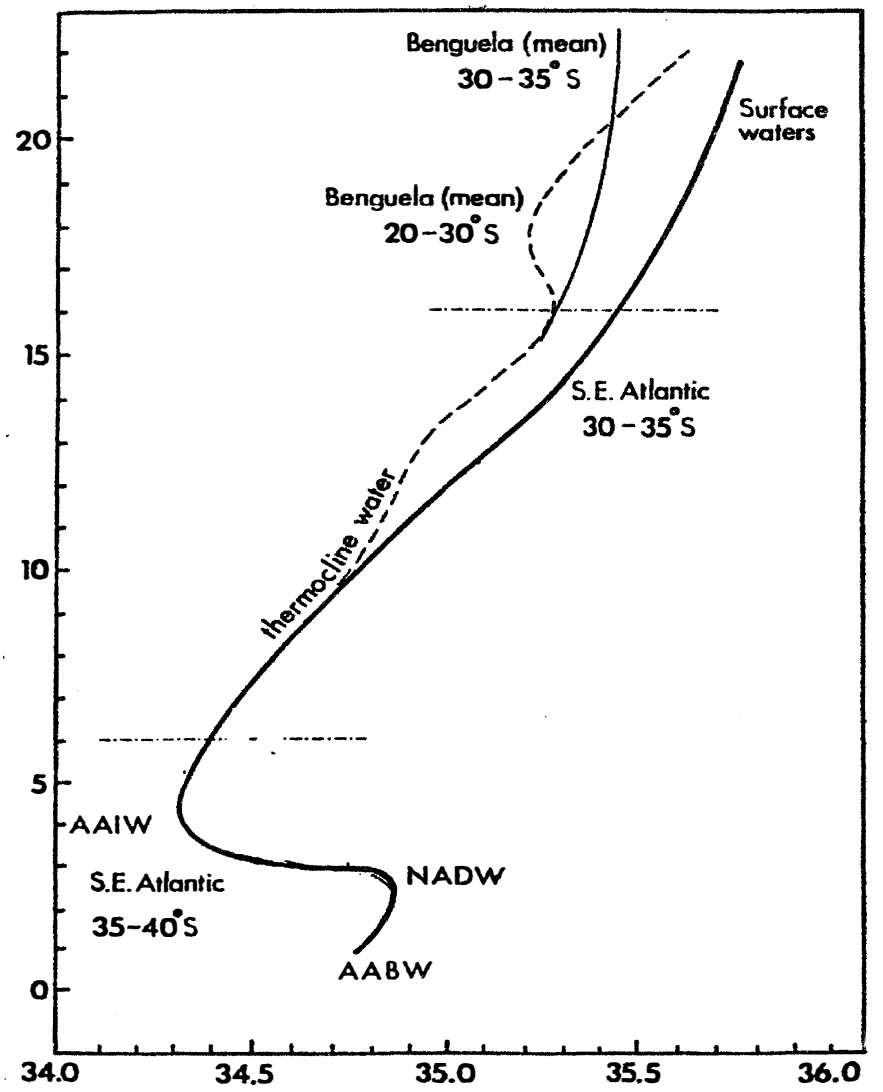

Figure 2.2. Potential Temperature–Salinity diagram showing the principal water masses present within the Southeast Atlantic Ocean and the Benguela upwelling system (horizontal axis denotes salinity and vertical axis denote potential temperature in °C). Horizontal broken lines indicate the limits of the thermocline water. AAIW= Antarctic Intermediate Water, NADW= North Atlantic Deep Water, AABW= Antarctic Bottom Water. [Modified from Shannon and Nelson, 1996].

There are a number of distinct water masses present off the south and southwestern coast of southern Africa [Gordon *et al.*, 1987; Lutjeharms and Valentine, 1987; Shannon and Nelson, 1996]. These water masses include Tropical and Subtropical Surface Water (> 16 °C and 35,5), Thermocline Water which comprises South Atlantic Central Water and South Indian Central Water (SICW) and spans the linear portion of the potential temperature-salinity curve from approximately 6 °C, 34,5 to 16 °C, 35,5. Antarctic Intermediate Water (AAIW) marks a deep, local salinity minimum of ~ 34.4 while the NADW marks a local deep salinity maximum of ~ 34.9 above the AABW stratum. From Figure 2.2 the upwelling of Thermocline Water along the coastal regions (marked Benguela on the diagrams) can be seen in the freshening of the water warmer than 10 °C by more that 0,2 for the same temperature over much of the Thermocline Water range (broken line) [see Lutjeharms and Valentine, 1987].

Gordon *et al.* (1987) have carried out a detailed analysis of the water masses entering and moving through the Agulhas Retroflection region. The different water masses entering the Agulhas Retroflection region are depicted on a Θ-S diagram (Figure 2.3). This diagram shows the presence of five distinct water masses:

Tropical Thermocline Water is formed by the excess of precipitation over evaporation in the tropics and has a relatively low surface salinity. Subtropical Surface Water has a high surface salinity due to the excess of evaporation over precipitation experienced in the subtropical regions of the Indian Ocean. SICW spans the linear part of the Θ-S curve from the surface salinity maximum of the Subtropical Surface Water to the deep salinity minimum of AAIW. AAIW is located at the base of the SICW. The large range of values at the intermediate depth indicates some influence (although weak) of the salty Red Sea Water. The Red Sea Water influence at the 27,35 sigma-θ level (approximately AAIW depth) has been observed within the Mozambique Basin and traced through the Mozambique Channel (e.g. Gründlingh, 1985). The data set used to

produce the Θ-S diagrams were taken only to 2000 m depth and hence did not reach the deep-water masses.

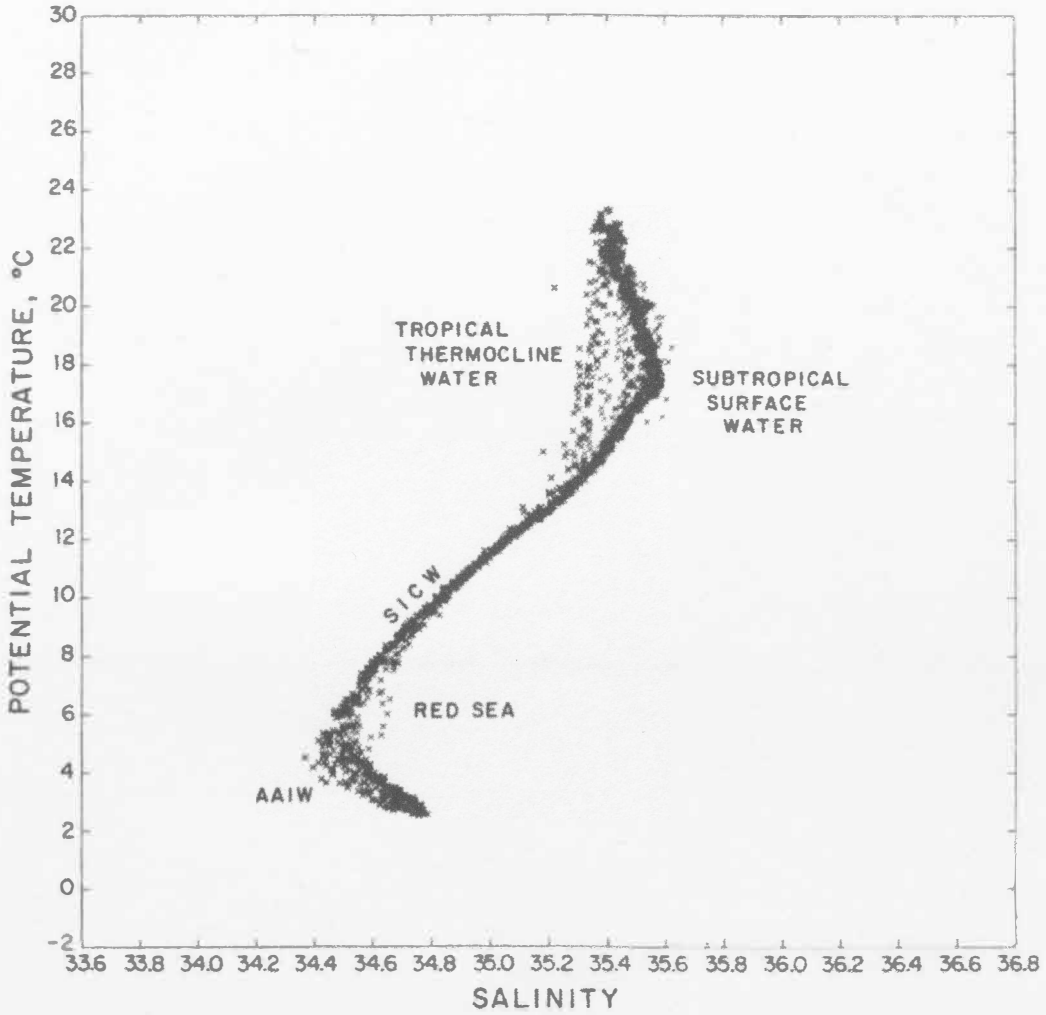

Figure 2.3. Potential Temperature–Salinity diagram of Agulhas Current water entering the Agulhas Retroflection region showing the presence of five distinct water masses: Tropical Thermocline Water, Subtropical Surface Water, South Indian Central Water (SICW), Antarctic Intermediate Water (AAIW) and Red Sea Water [Gordon *et al.*, 1987].

An illustrative Θ-S diagram of the water masses at the Agulhas Retroflection region is given on Figure 2.4. This figure displays a broad range of salinities at nearly every isotherm. Gordon *et al.* (1987) have shown that the characteristics of the water masses entering the Agulhas Retroflection corresponds to the high salinity edge of this Θ-S curve. The freshening of the water upon entering the retroflection region, therefore, reflects the influence of the fresher South Atlantic Ocean water (*cf.* Figure 2.2) and, conceivably, water from south of the STC.

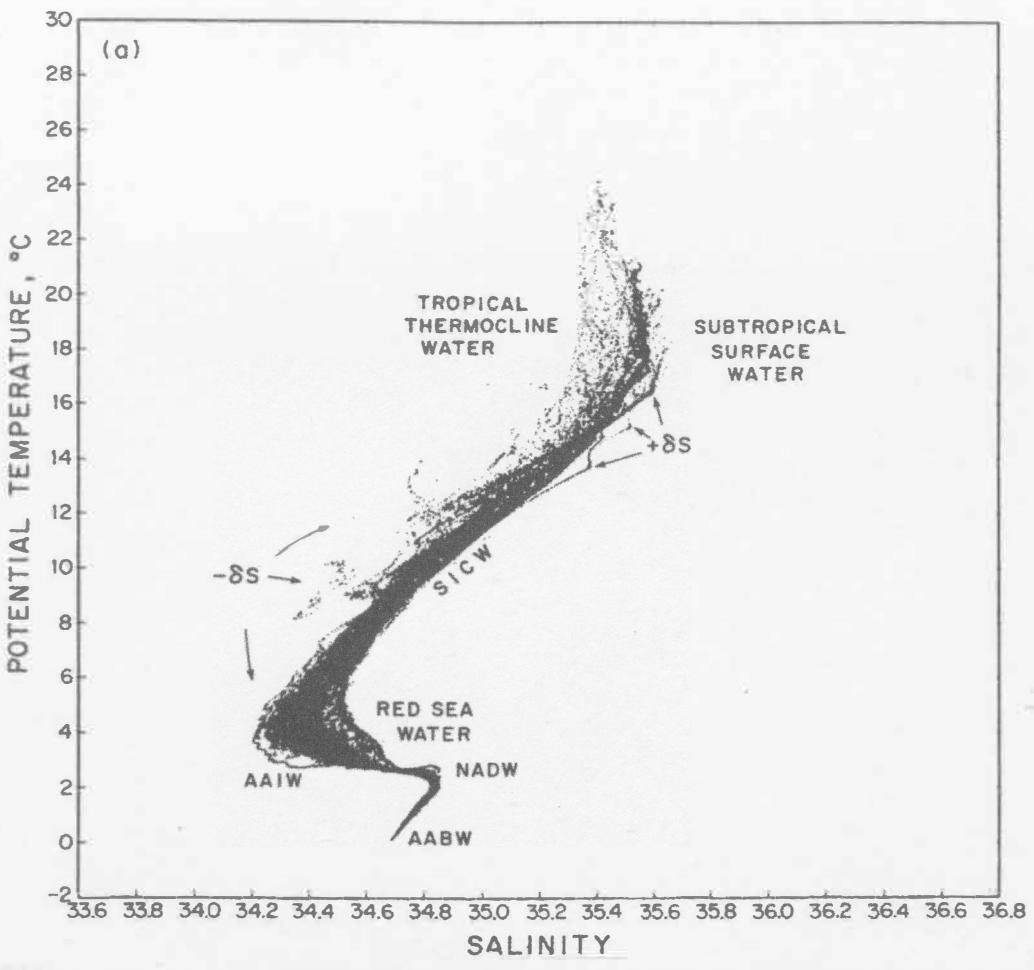

Figure 2.4. Potential Temperature – Salinity diagram of the water at the Agulhas Retroflection region. Positive (+δ) and negative (-δ) salinity anomalies are marked. SICW= South Indian Central Water, AAIW= Antarctic Intermediate Water, NADW= North Atlantic Deep Water, AABW= Antarctic Bottom Water [Gordon *et al.*, 1987].

Essentially the same water masses are found in the retroflection region as those that enter it, which are: Tropical Thermocline Water, Subtropical surface water, SICW mixed with North Atlantic Central Water, AAIW and Red Sea Water. Below the AAIW and Red Sea Water is the North Atlantic Deep Water (NADW) marking a deep local salinity maximum. The bottom water is marked by cold, high oxygen (not shown on the θ-S diagram) Antarctic Bottom Water (AABW).

Positive salinity anomalies (marked +δ on Figure 2.4) at the surface are believed to be induced by interaction with the local atmosphere while Gordon *et al.* (1987) have attributed the negative salinity anomalies (marked -δ on the Figure 2.4) at the central and intermediate water depths to interaction with intrusions of Atlantic Water. It will be shown later in this thesis that this is not Atlantic surface water as was believed at the time but indeed Subantarctic Surface Water.

2.3. Geostrophic Transport of Surface and Thermocline Water.

A considerable amount of research has been done to increase the understanding of the upwelling process that characterizes the southeast Atlantic Ocean and of the winds that cause this upwelling [Shannon, 1985; Shannon and Nelson, 1996].

The Benguela Current is one of the four major eastern boundary currents of the world oceans and may be defined as the broad northward flow of the eastern South Atlantic Ocean [Shannon, 1990]. The surface movement of Benguela water is largely wind-driven. Like similar regions off California, Peru and North West Africa, it is dominated by coastal upwelling [Shannon, 1985; Chapman and Shannon, 1985; Shannon and Nelson, 1996].

Since upwelling along the South African west coast is wind-induced and the winds do not blow with uniform intensity throughout the year along the west coast [e.g. Tyson,

1986], there are seasonal and regional variation in the intensity of upwelling along the coast. The regional variation of upwelling gives rise to specific centres of upwelling as illustrated by the dark, tongue-like patches seen on Figure 1.1.

Figure 2.5 illustrates the flow of surface and thermocline water in the southeastern region of the Atlantic Ocean. The strongest surface currents within the Benguela system is often associated with the shelf edge (200 m depth) and may take the form of a jet (7 to 10 Sv.) around Cape Town (Figure 2.5). This jet extends from the Agulhas Bank around Cape Agulhas and plays an important role in the transport of fish eggs and larvae from spawning areas on the Agulhas Bank to the nursery areas of St Helena Bay and farther north [Shannon, 1985; Shannon, 1990]. Close to the coast the subsurface flow is often southward (0 to 25 cm. s^{-1}) and is believed to be important for occasionally flushing small fish out of areas such as St Helena Bay [Shannon, 1990]. A poleward undercurrent (10 to 30 cm. s^{-1}) is believed to be a compensation for the equatorward displacement of water from the inner shelf [Shannon and Nelson, 1996]. This forms part of a more extensive poleward movement stretching from the shelf and into the Cape Basin [Stramma and Peterson, 1989; Shannon and Nelson, 1996].

About 7 Sv of water is received from the Agulhas Current in the form of rings and filaments [see also Gordon *et al.*, 1987]. This influx of Agulhas Current water forms part of the total northward transport of 15 Sv of water above 1 500 m within the Southeastern limb of the South Atlantic gyre.

By contrast to the South Atlantic gyre, the Subtropical Gyre of the South Indian Ocean is composed of two anticyclonic circulation cells (Figure 2.6) - one centred near 20° to 25° S, 60° E and the other near 35° S, 30° E [Wyrtki, 1971]. The Agulhas Current forms the western boundary current associated with the southwestern circulation cell.

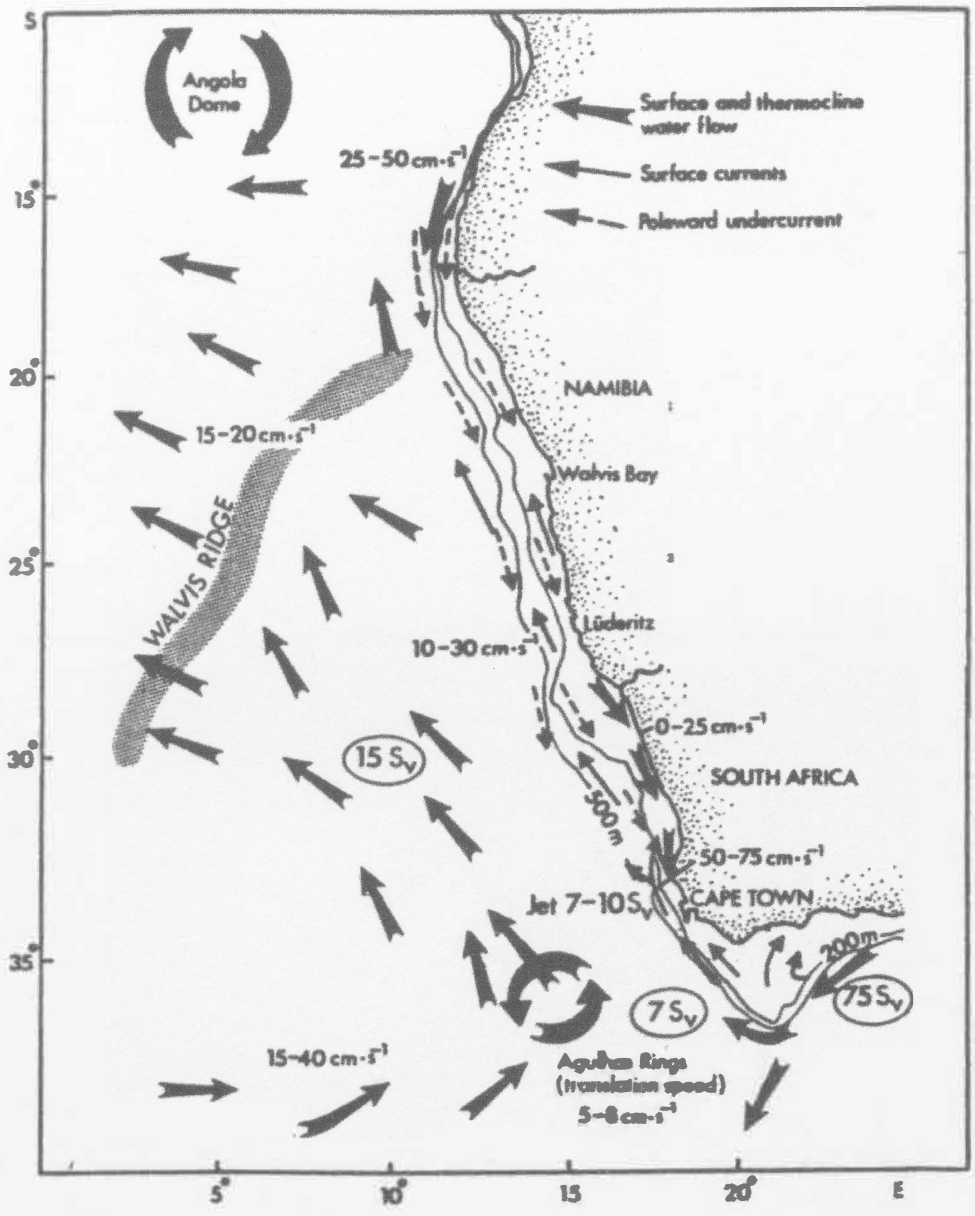

Figure 2.5. Schematic illustration of the flow field within the southeastern Atlantic Ocean of the surface and thermocline water. Current speeds refer to surface values. Circled transports refer to total transport above 1 500 db [Shannon and Nelson, 1996].

A schematic illustration of the flow field within the South Indian Ocean is given on Figure 2.7. This figure shows the transport magnitudes in Sv of the different water sources for the Agulhas Current. Agulhas Current water seems to stem primarily from recirculation within the Southwest Indian Ocean (SWIO). However, secondary inputs through the Mozambique Channel (approximately 5 Sv) and from the East Madagascar Current (approximately 25 Sv) have also been suggested [Stramma and Lutjeharms, 1997; Gordon *et al.*, 1987].

One particular oceanographic survey of the Agulhas Retroflection region (Figure 2.8) shows that approximately 70 Sv of Agulhas Current water enters the retroflection region of which approximately 5 Sv continues westward into the South Atlantic Ocean while ~ 60 Sv of water enters the Agulhas Retroflection [Gordon *et al.*, 1987]. Approximately 35 Sv feeds the Agulhas Return Current, while the rest of the water entering the Agulhas Retroflection is lost to the South-East Atlantic Ocean in the form of filaments (~ 10 Sv) [e.g. Lutjeharms and Cooper, 1996] and rings (~ 30 to 35 Sv) [e.g. Feron *et al.*, 1992; van Ballegooyen *et al.*, 1994].

Figure 2.8 also shows an the unusual flow of water of approximately 15 Sv between the Agulhas Retroflection and the Retroflection Eddy, which Gordon *et al.* (1987) have attributed to South Atlantic Surface Water (SASW). Eddies towards the south of the Agulhas Return Current carried approximately 30 Sv and 10 Sv respectively into the Southern Ocean.

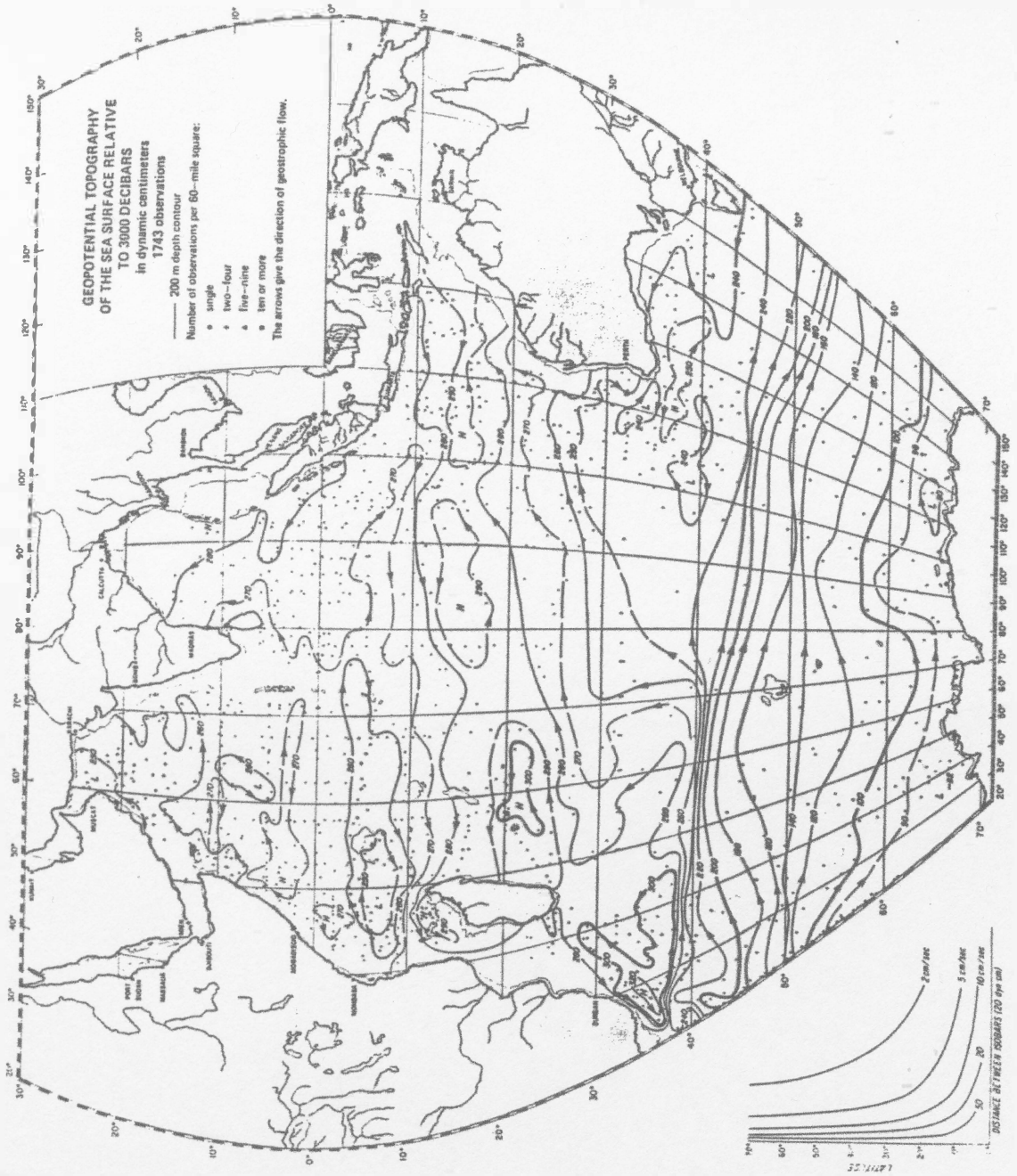

Figure 2.6. Geopotential topography of the sea surface relative to the 3 000 db (in dynamic meters) showing two circulation cells within the SIO. The northern cell in located at approximately 15 °S and extends from east Madagascar right across the SIO. The Southern cell is located at approximately 35 °S and extends to about 70 °E [Wyrtki, 1971]

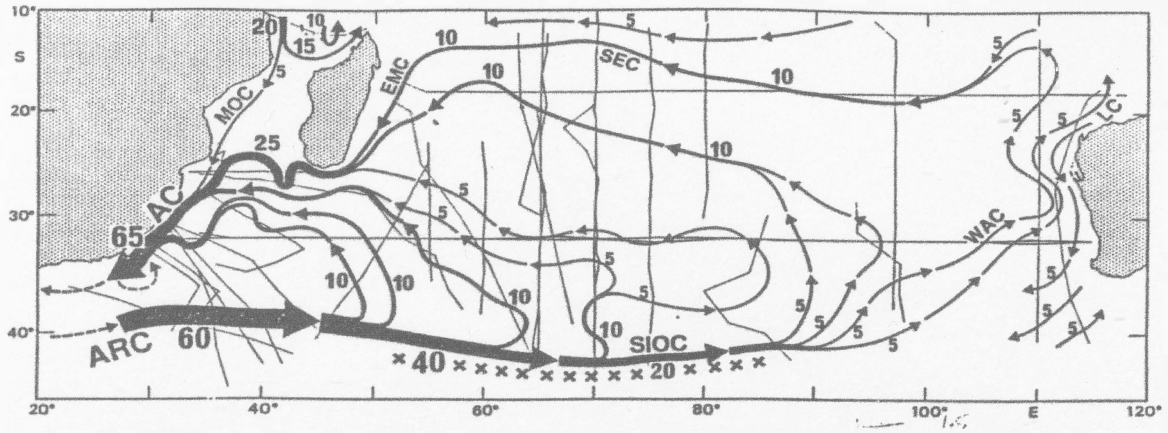

Figure 2.7. Schematic illustration of the flow field in the South Indian Ocean. The transport for the upper 1000 m is given in 5 Sv steps. Current bands for the Agulhas Current (AC), Agulhas Return Current (ARC), East Madagascar Current (EMC) and the Mozambique Current (MOC) are marked. Other currents marked on the diagram include the South Indian Ocean Current (SIOC), the West Australian Current (WAC) , the Leeuwin Current (LC) and the Southern Equatorial Current (SEC). Thin lines show the distribution of the hydrographic data used to calculate the transport magnitudes of the different currents. [Stramma and Lutjeharms, 1997].

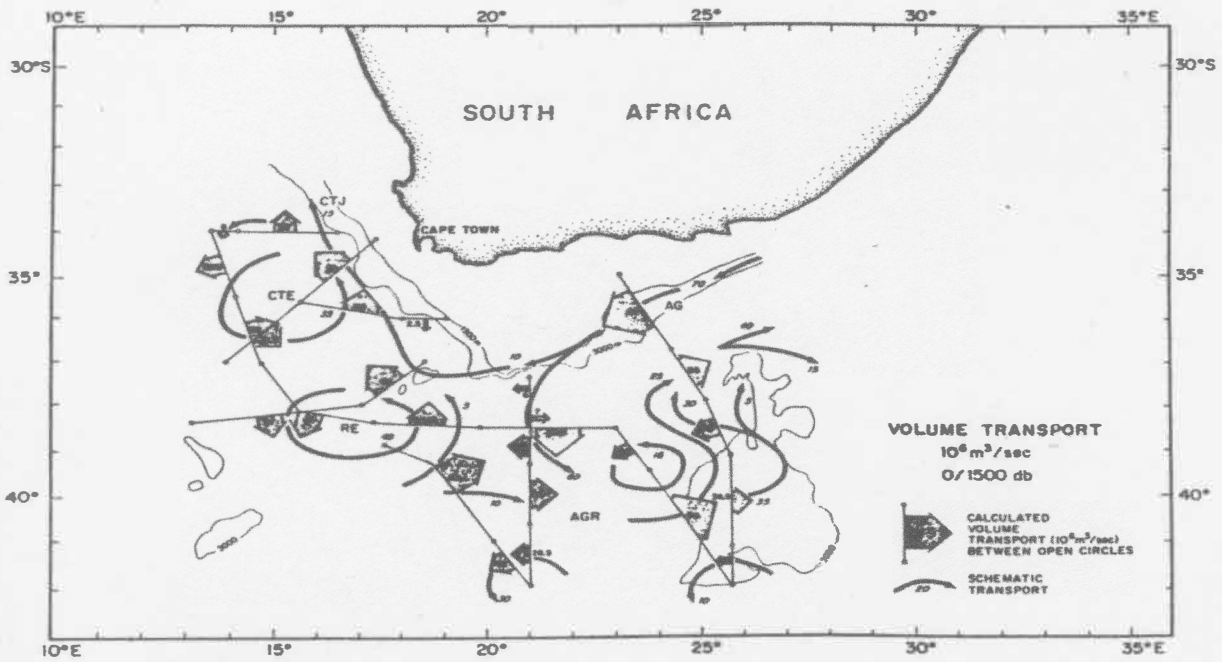

Figure 2.8. Schematic illustration of the volumetric transport within the Agulhas Current system for the upper 1 500 m relative to the 1 500 db surface. AGR : Agulhas Retroflection, RE : Retroflection Eddy, CTE : Cape Town Eddy [Gordon *et al.*, 1987].

2.3.1. Meso-scale features associated with the Agulhas Current.

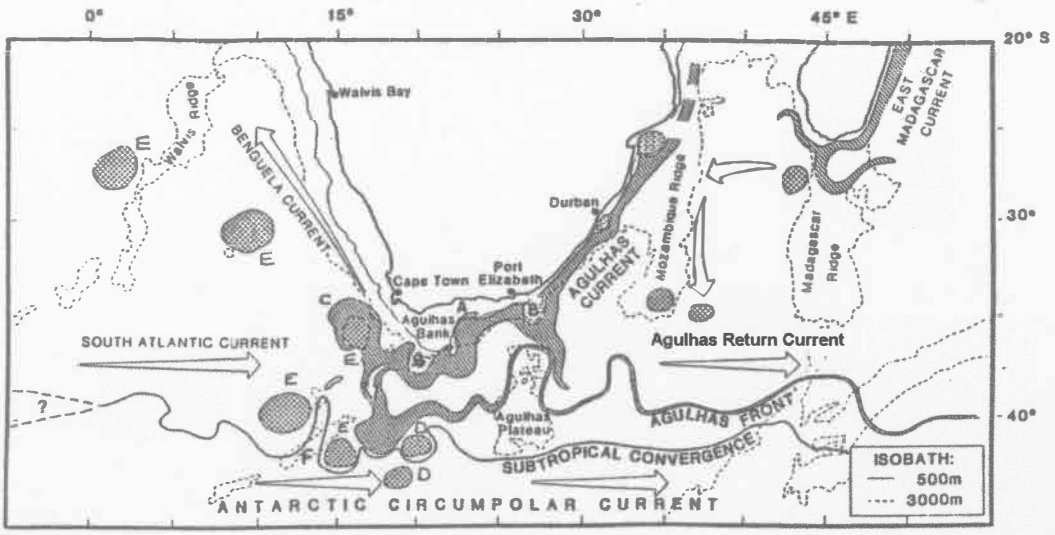

Figure 2.9. Schematic illustration of the flow field within the greater Agulhas Current depicting various features associated with it. A: Meandering of the Current. B:Solitary meanders at the inshore edge of the Agulhas Current termed Natal Pulses. C: Warm Agulhas Current filaments may penetrate deep into the South Indian Ocean. D: Warm eddies from the Agulhas Return Current. E: Agulhas Current Rings. F: Kink within the STC marking the intrusion of colder water from south of the STC into the Retroflection region [modified from van Ballegooyen *et al.*, 1991].

Figure 2.9 presents an overview of the flow field within the Agulhas Current system at the surface and the meso-scale features associated with the Current. A study of the eddies and plumes associated with the landward boundary of the Agulhas Current [Lutjeharms *et al.*, 1989] has revealed that the offshore migration of the Current downstream of Port Elizabeth is usually marked by the meandering of the Current (A: Figure 2.9). Solitary meanders at the inshore edge of the Agulhas Current are associated with Natal Pulses (B) [Lutjeharms and Roberts, 1988].

Agulhas filaments (C) which emanate from the Agulhas Retroflection consist mostly of Subtropical Surface Water and are known to transport heat, salt and water from the Indian Ocean to the Atlantic Ocean in a south-easterly north-westerly direction (Figure 2.10) [Lutjeharms and Cooper, 1996; Shannon *et al.*, 1990; Lutjeharms and Stockton, 1987]. Lutjeharms and Cooper (1996), in a study using satellite remote sensing images from the METEOSAT and NOAA series have shown that these filaments are on average 50 km wide and 50 m deep. Furthermore, each filament may carry excess heat of approximately 3,5 x 10^{19} J as well as excess salt of about 1 to 5 x 10^{11} kg from the Indian Ocean to the South Atlantic Ocean. Most of the excess heat is rapidly lost to the overlying atmosphere but the excess salt carried by these plumes constitute an annual salt flux of approximately 3 to 9 x 10^{19} kg, approximately 15 % of the total salt flux generated by the Agulhas Current. Based on the study by Lutjeharms and Cooper (1995) these plumes are evident in satellite remote sensing approximately 56 % of the time.

Warm eddies (D in Figure 2.9) south of the STC are pinched off the Agulhas Current as a result of instabilities at the retroflection region or at the Agulhas Plateau [Lutjeharms and Valentine, 1988]. These eddies are generally 200 to 300 km in diameter and lose their heat to the overlying atmosphere very quickly. Therefore, their heat contribution to the Southern Ocean is small [Webb, 1996]. However, on occasion [Lutjeharms and Valentine, 1988] they are found as far north as 43 °S in various stages of decay.

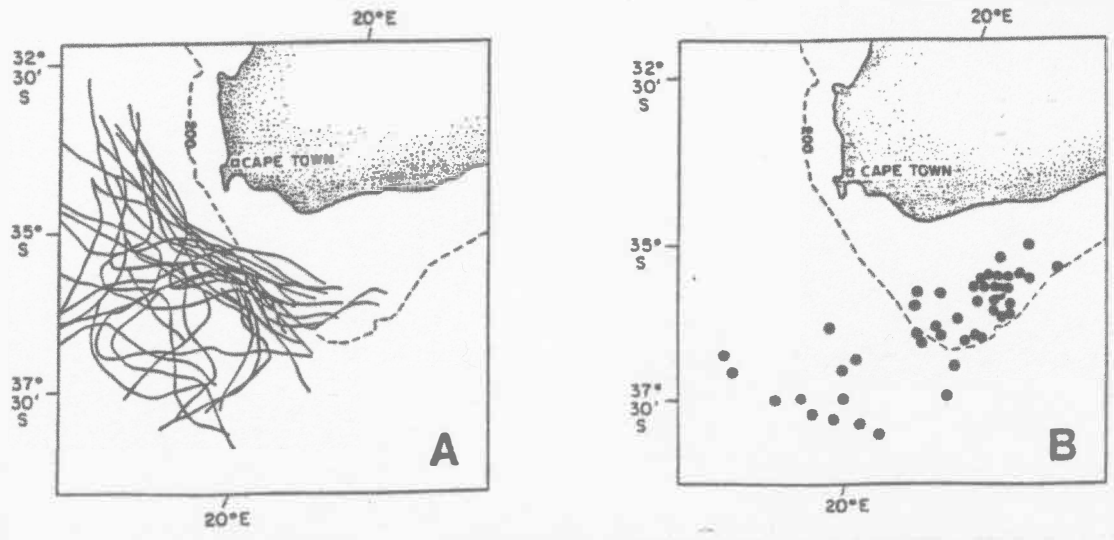

Figure 2.10. Illustrative examples of Agulhas filaments identified in satellite imagery for the years 1983 to 1985 showing (A) the trajectories and (B) the geographic location of the source points of these filaments on the Agulhas Current border. The dashed 200 m isobath represents the edge of the Agulhas Bank [after Lutjeharms and Stockton,1987].

Lutjeharms (1981), in a study using satellite remote sensing, has shown for the first time that the Agulhas retroflection loop is unstable and can coalesce and thus form Agulhas rings (E) with an average diameter of 320 km. These rings may move north-westward into the South Atlantic Ocean or south or south-eastward into the Southern Ocean [Lutjeharms *et al.*, 1989]. It has been estimated that the heat anomaly contained within a representative ring may be 2,4 x 10^{20} J and the salt anomaly 13 x 10^{12} kg [van Ballegooyen *et al.*, 1994]. Approximately 6 to 9 rings are shed per year [Lutjeharms and van Ballegooyen, 1988; Feron *et al.*, 1992, has suggested 4 to 8 rings]. They drift into the South Atlantic Ocean in a northwesterly direction [Gordon and Haxby, 1990; Duncombe Rae, 1991] (see Figure 2.11.) where they lose their heat and excess salt to the ambient waters at an as yet undetermined rate. The importance of these rings in the processes of water, heat and water mass transfer between the Indian and Atlantic oceans has been summarised by Lutjeharms (1996).

An anomalous "kink" within the STC (F in Figure 2.9) is associated with the mechanism of Agulhas ring shedding [Lutjeharms and van Ballegooyen, 1988; Lutjeharms, 1996]. This entrainment of cold water from south of the Subtropical Convergence into the retroflection region can have far reaching consequences for the retroflection dynamics [Shannon *et al.*, 1989]. The current knowledge of these intrusions will be discussed in more detail in the next chapter.

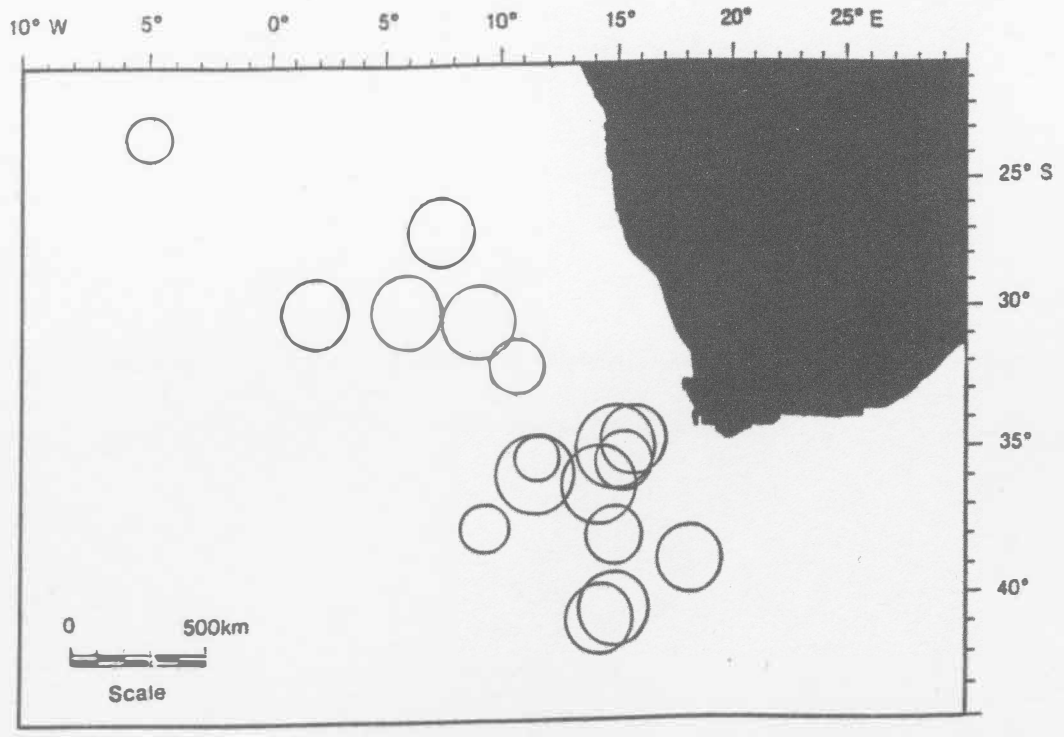

Figure 2.11. The dimensions and geographic locations of seventeen Agulhas rings that have been detected in hydrographic data in the South-Eastern Atlantic Ocean from 1969 to 1990 [Duncombe Rae, 1991 (modified by Lutjeharms, 1996)]

2.4. Geostrophic flow at depth.

Figure 2.12 shows a conceptual image of the flow of water in the SWIO and the Southeast Atlantic Ocean associated with the deep salinity minimum of AAIW. The flow pattern mimics that of the upper layer flow within the Agulhas Current and even reproduces the water flux from the Indian Ocean to the Atlantic Ocean at the Agulhas Retroflection. Within the Benguela system the flow field follows that of the poleward undercurrent, while the broader flow associated with the South Atlantic Ocean gyre is also reflected.

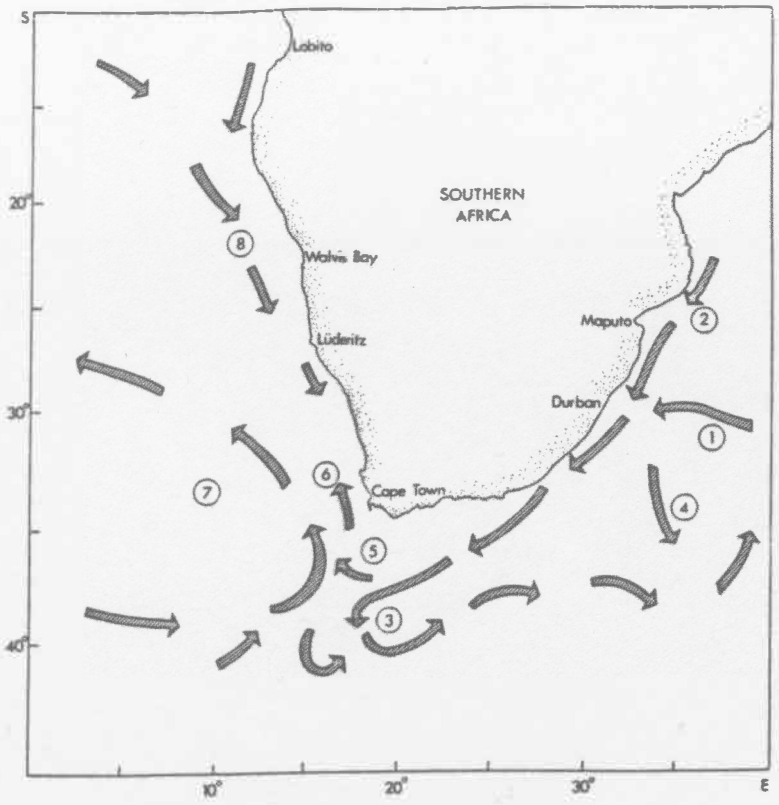

Figure 2.12. Conceptual representation of AAIW flow around Southern Africa. 1. Primary Agulhas Current source. 2. Secondary Agulhas Current source. 3. Retroflection. 4. Short circuit flow. 5. Flux from Agulhas Current into the South Eastern Atlantic Ocean. 6. Relatively fresh AAIW from the Southwest. 7. Anticyclonic AAIW gyre. 8. Poleward flow from the tropical eastern Atlantic [Shannon and Nelson, 1996].

A curious "short circuit" flow off Durban (4 on Figure 2.12) is believed to be associated with the Agulhas Plateau and the topographically induced meanders in the Agulhas Return Current [Shannon and Hunter, 1988].

The flow of NADW is of particular importance to the global ocean circulation [Gordon, 1986; Gordon, 1996; Lutjeharms, 1996; Schmitz, 1996]. This high salinity, high (deep) temperature water mass is formed in the northern Atlantic Ocean at a rate of ~ 20 Sv and exported to the rest of the world ocean (e.g. Figure 2.13). It is incorporated within the Circumpolar Deep Water (CDW) at the STC [Toole and Warren, 1993; Whitworth and Nowlin, 1987] south of Africa and transported to the Indian and Pacific Oceans. As compensation for the export of NADW Gordon (1986) proposed that the warm, saline upper layer flow from the Agulhas Current into the Atlantic Ocean (~13,5 Sv.) is significant [also Gordon, 1996].

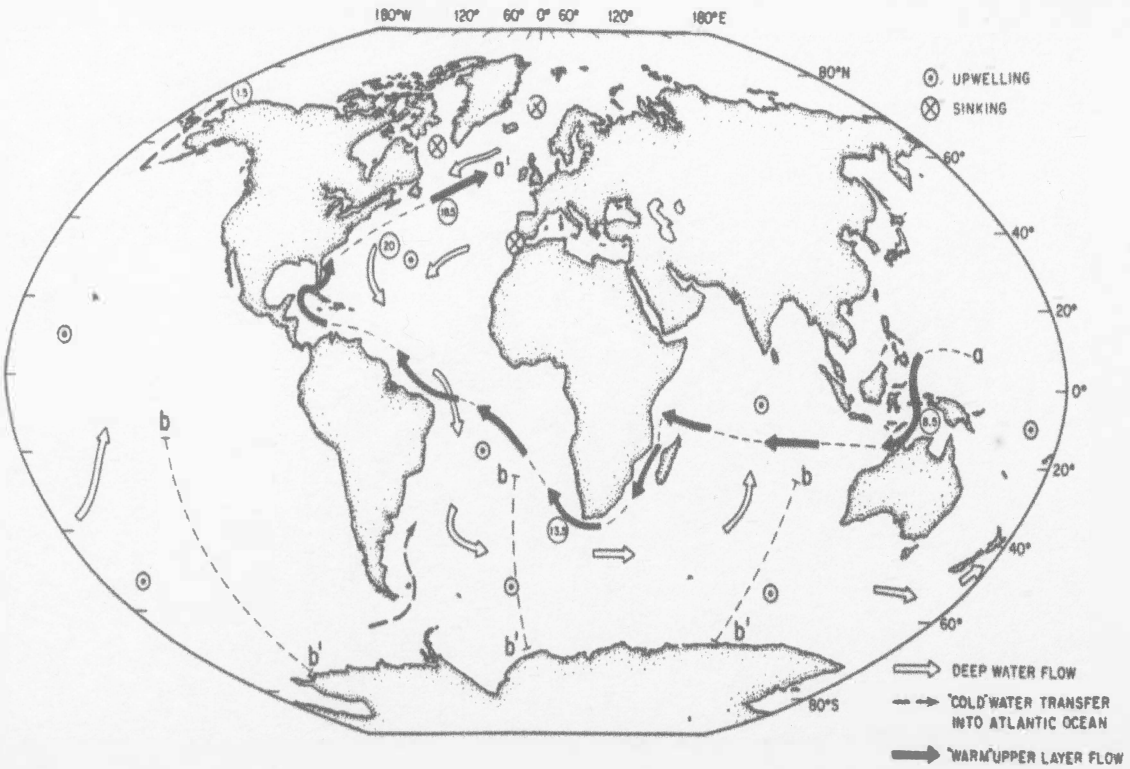

Figure 2.13. Conceptual representation of the global structure of the thermohaline circulation cell associated with NADW production. The circled values are volume flux in Sv. The production rate in the North Atlantic Ocean of 18,5 Sv and the compensation flow of 13,5 Sv around Southern Africa are derived from the assumption that the flow of cold water via the Drake Passage (broken arrow around South America) is of minor importance [Gordon, 1986].

The flow field associated with bottom water is ill understood and falls outside the scope necessary for the discussion of the features presented within this thesis.

2.5. The Southern Ocean.

The Southern Ocean is the enormous area of water encircling the Antarctic continent (see Figure 1.1). It has become usual to define the northern boundary of the Southern Ocean as the STC near 40 °S [e.g. Lutjeharms, 1985; Shannon and Agenbag, 1990; Matthysen, 1997]. The front is found south of the Agulhas Return Current, where the denser SAASW (~12 °C and < 34) subducts and spreads northward beneath the Subtropical Surface Water to form South Atlantic and South Indian Central Water [Matthysen, 1997].

The STC has a variable nature within the South Atlantic Ocean and across the South Indian Ocean [Belkin, 1989 and 1993]. It exhibits the strongest horizontal thermal and salinity gradients of all the major fronts of the Southern Ocean both at the sea surface and at depth (Lutjeharms, 1985) south of Africa e.g. Figure 2.14. Considerable latitudinal variability in the position of the front occurs directly south of Africa with the formation of planetary waves and the shedding of eddies [Lutjeharms, 1985; Harris and Stavropoulos, 1978; Matthysen, 1997]. [1]Matthysen [1997] has found that, in general, the STC has very high chlorophyll levels (Figure 2.15).

The importance of the Southern Ocean to the southern African oceanic environment and weather is well known. The ACC, the largest ocean current in the world, encircles the Antarctic continent and is connected to the other oceans such as the Indian, Atlantic and the Pacific oceans. Many of the weather systems that affect the southern African continent are generated over the Southern Ocean [Preston-Whyte and Tyson, 1988].

[1]Matthysen also states that this peak in chlorophyll concentration does not necessarily coincide with the thermal front but does coincide with the salinity front of the STC.

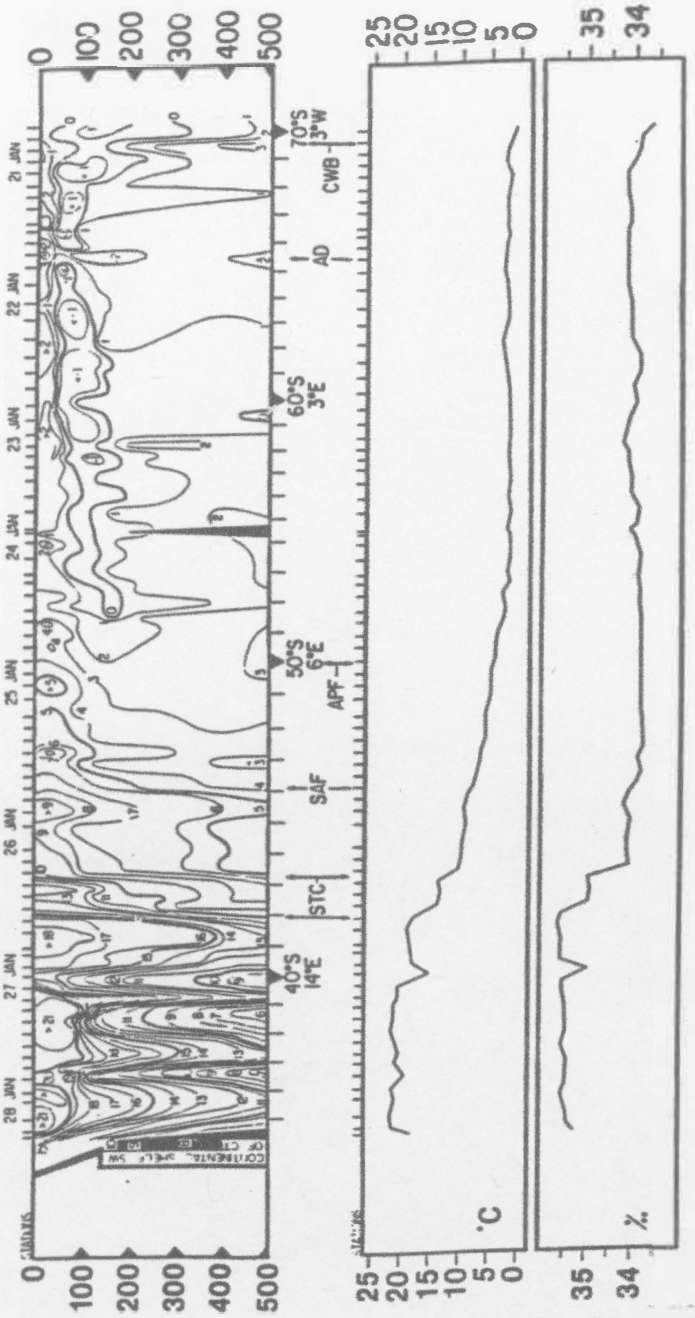

Figure 2.14(a) Characteristic temperature section of the upper 500 m of the water column between Africa and Antarctica in January 1981. (b) Surface temperature and (c) Salinity are portrayed as well. The geographical location of the STC, the Sub-Antarctic Front (SAF), the Antarctic Polar Front (APF) and the Continental Water Boundary (CWB) are indicated as well as the position of the thermal feature assumed to be the Antarctic Divergence [Lutjeharms, 1985].

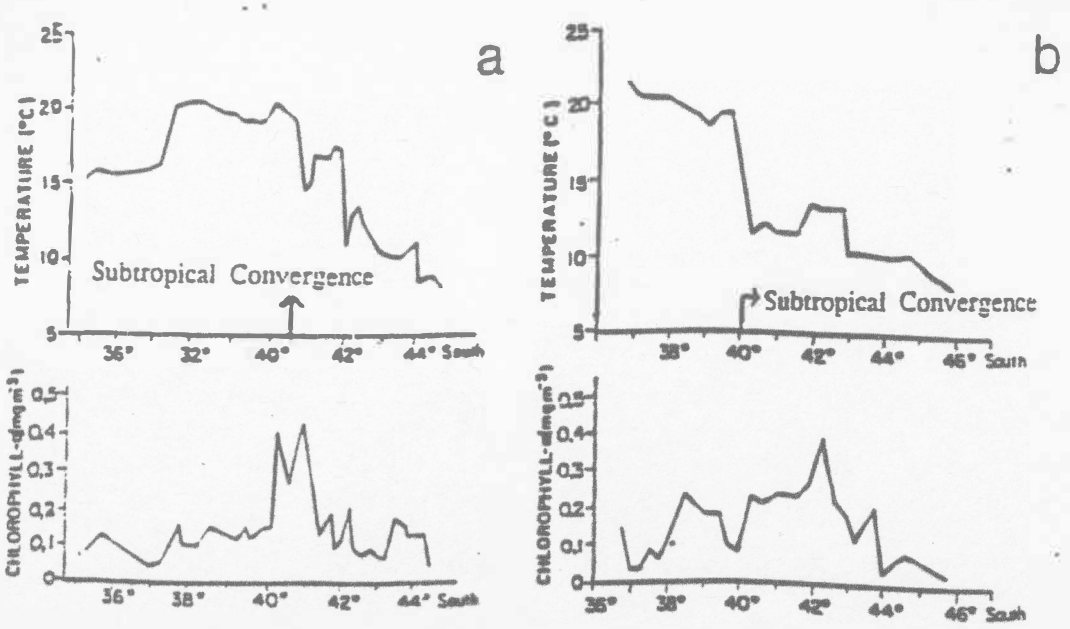

Figure 2.15. The relationship between surface chlorophyll and sea surface temperature from north to south across the STC showing the peak in chlorophyll concentration on two separate occasions at the STC. a: 8 to 12 November 1983, and b. 18 to 21 November 1983 [Matthysen, 1997].

Figure 2.16 gives a representative illustration of the water masses present within the Southern Ocean clearly indicating the characteristics of SAASW (termed Subantarctic Upper Water on the diagram). The temperature range of SAASW spans 4 to 10 °C in Winter and 4 to 14 °C in Summer, with a salinity varying between 33,9 and 34,9; reaching as low as 33,0 in Summer as the ice melts [Tomczak and Godfrey, 1994]. Therefore the difference between the full line and the dashed line on Figure 2.16 of the "Upper Waters" represents a difference in season.

For the purposes of this thesis the region of interest is confined to the northern sector of the Southern Ocean between 40 °S to the Antarctic convergence *i.e.* the region indicating the characteristics of SAASW. A discussion of the water masses at depth will therefore not be presented. However, their location on the θ-S diagram and mixing processes are indicated in Figure 2.16.

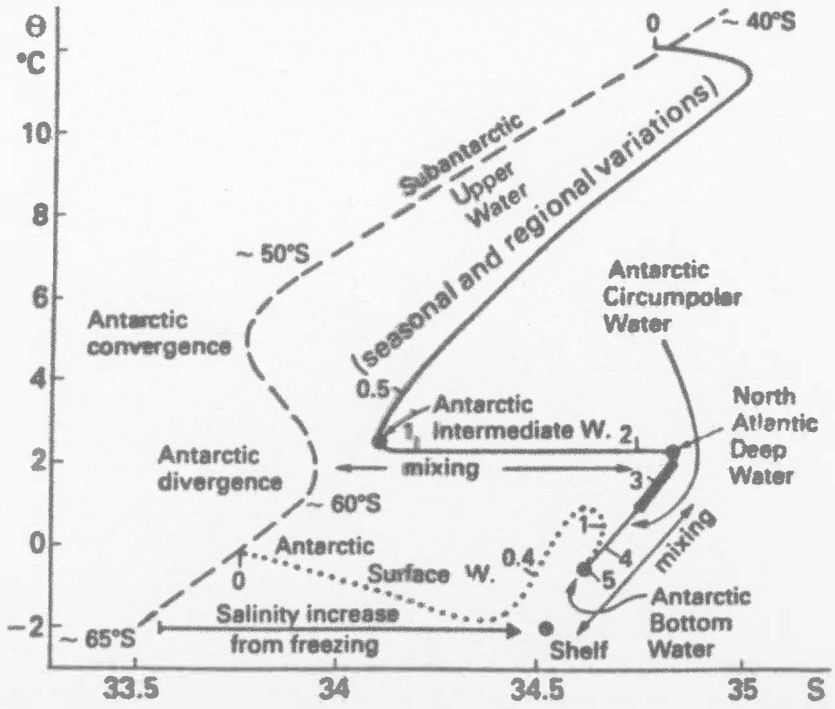

Figure 2.16. Θ-S diagram for a representative station in the Sub-antarctic (full line). The dashed line were plotted from surface observations along crossings of the Antarctic Polar front and Divergence. The dotted line indicates the mixing between the low salinity surface water of the Antarctic zone, where the ice melts, and the deeper water. Depth in the vertical Θ-S profiles is indicated in km [Tomczak and Godfrey, 1994].

From the above discussion it is clear that the marine environment around Southern Africa is complex and comprises a variety of oceanic regimes. The region directly south of the continent is observed to be particularly important to interoceanic exchanges between the South Atlantic and the South Indian Ocean through the exchange of heat, salt and water by rings, plumes and eddies. Agulhas rings, in particular, play an integral part in this process. The process of ring shedding has been linked to the northward entrainment of SAASW across the STC. This process will be discussed in the next chapter.

Chapter 3

Review of what is known about SAASW Intrusions south of Africa.

This chapter outlines the process of ring shedding at the STC and presents our present knowledge concerning SAASW entrainment in the wake of these rings. It also describes the environmental changes that occurred at the Agulhas Retroflection between 1983and 1988.

3.1. The Process of Ring shedding.

Lutjeharms and Van Ballegooyen (1988) have given a fairly descriptive account of the process of ring shedding by the Agulhas Current. A conceptual diagram of this process is given on Figure 3.1 and a sketch of an example of such an occurrence is given in Figure 3.2.

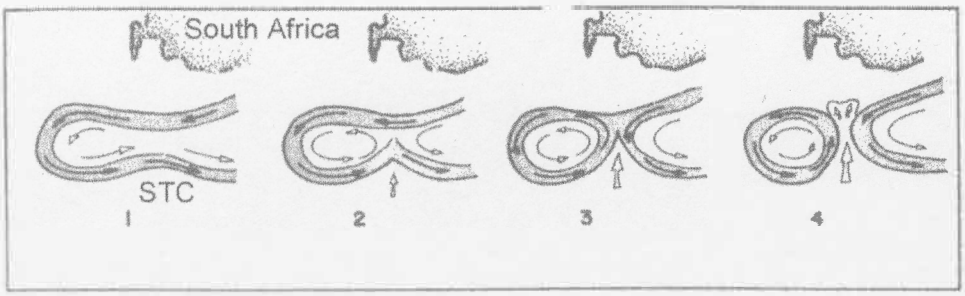

Figure 3.1. Conceptual diagram showing the (1) initiation, (2) development and (3) growth of the wedge of cold SAASW. (4) The lateral spread of the SAASW into the retroflection region is also shown [Lutjeharms and van Ballegooyen, 1988].

Using satellite data from 1978 to 1983 Lutjeharms and van Ballegooyen (1988) were able to show that the formation of these rings is usually preceded by the westward progression of the retroflection loop of the Agulhas Current at a rate of 12 cm. s^{-1} over a period of 39 days. This westward movement of the retroflection is then followed by the genesis and growth of a wedge of cold SAASW at the STC that penetrates through the retroflection loop over a period of five days. This cold water wedge then proceeds to effectively separate the newly formed ring from the retroflection loop and spreads laterally

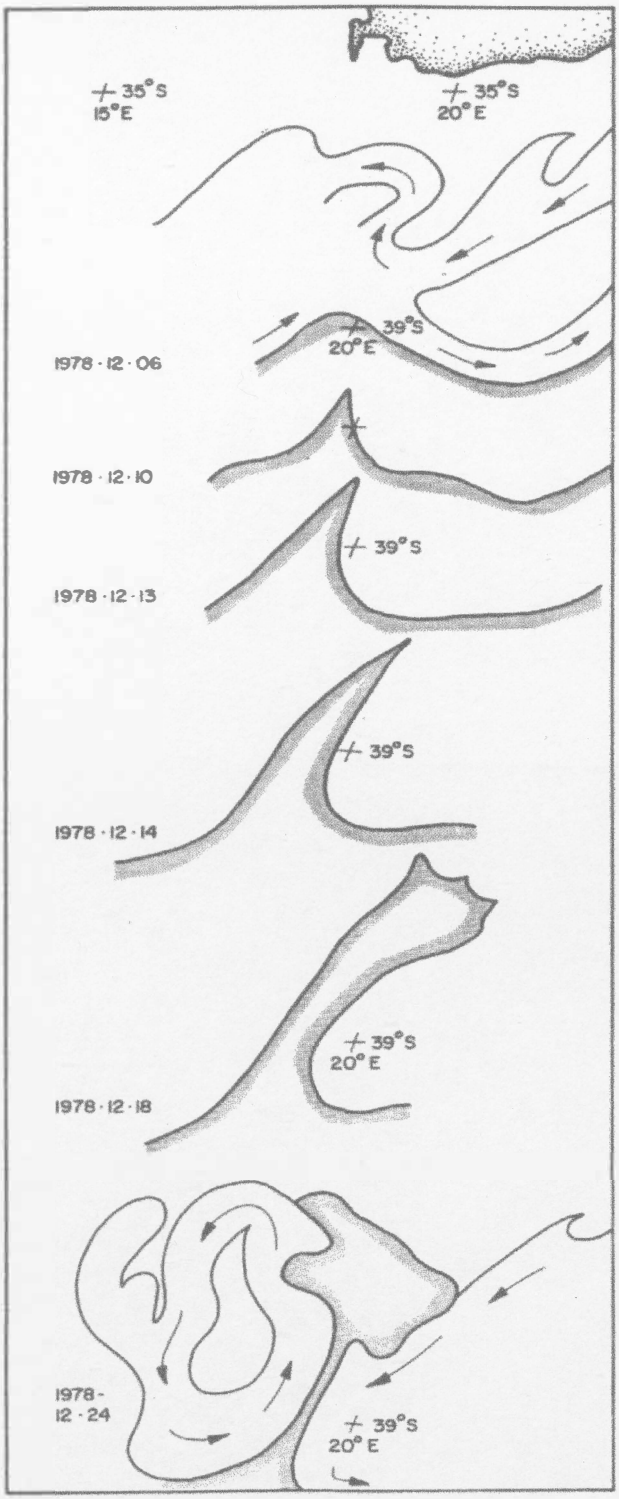

Figure 3.2. The characteristically rapid initiation and growth of a wedge of SAASW and its role in the separation of an Agulhas ring from the retroflection region over a period of less than three weeks in December 1978. The thermal data were from METEOSAT I [Lutjeharms and van Ballegooyen, 1988].

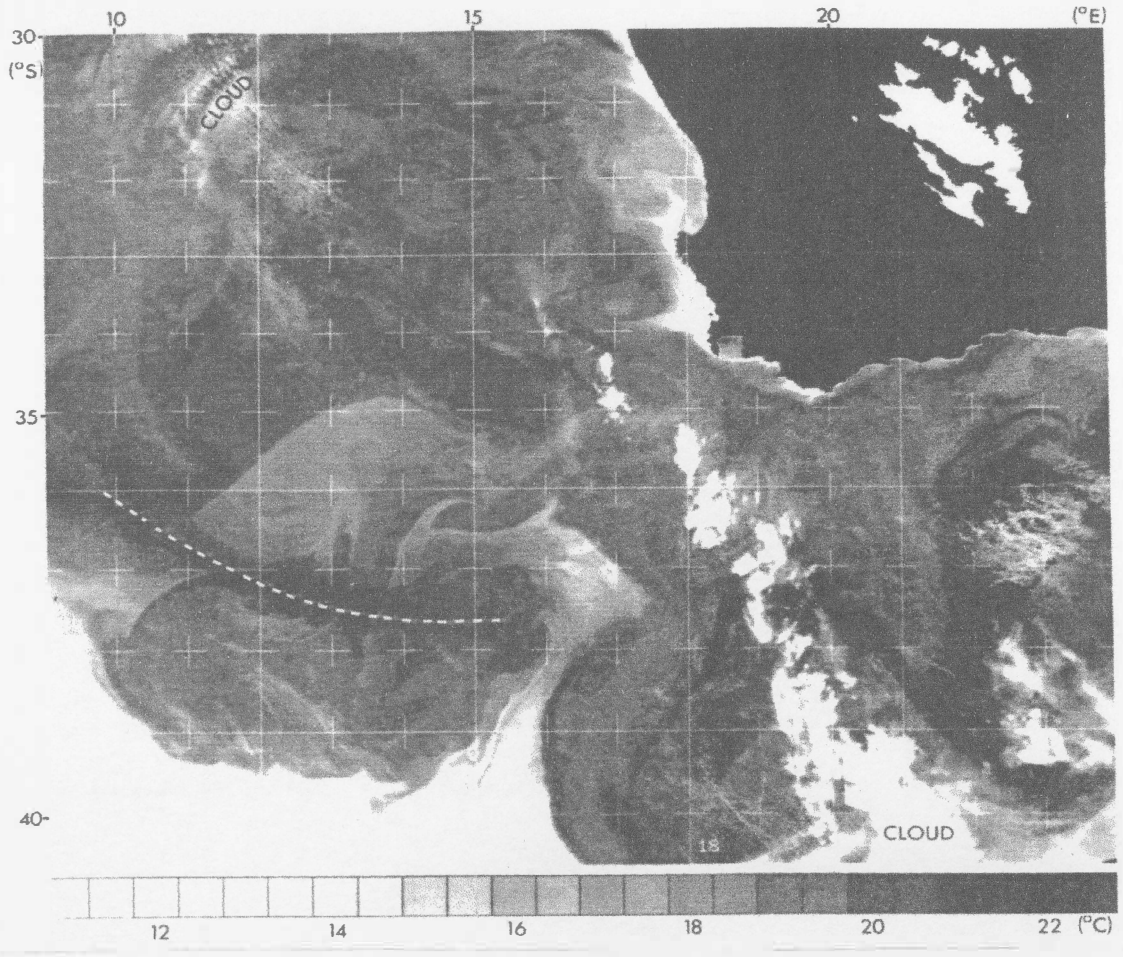

Figure 3.3. Geographically corrected and calibrated thermal infrared image of the sea surface temperature distribution as depicted by NOAA 9 AVHRR on 10 December 1986. Bright white areas over the ocean and land on the satellite image may be attributed to cloud cover; some clouds over the ocean are labelled. The white filament-like protrusions emanating from the South African west coast reflect the cooling effect of coastal upwelling as described in the previous chapter. The warm water between the cold water intrusions are attributed to an embedded Agulhas current ring and the Agulhas Retroflection may be observed in the warm water to the east of the easternmost intrusion. The dashed line marking a "false" warm water feature is attributed to sensor interference and should be ignored [Shannon *et al.*, 1989].

northward to cover a relatively wide zone which may extend over 300 to 500 km [Meeuwis and van Rensburg, 1995].

Shannon *et al.* (1989) have described an extreme case of SAASW penetration across the STC. This event involved the presence of two intrusions, one situated at approximately 9 °E and the other at approximately 15 °E (Figure 3.3). The estimates on the location of these features agree fairly well with those found by Meeuwis and van Rensburg (1995) of 12 °E (standard deviation 2,0 °) and 15 °E (standard deviation of 1,7 °). This particular SAASW intrusion event resulted in an extensive zone of the retroflection region being covered with water ranging between 11°C and 14 °C in temperature.

The intrusions described by Lutjeharms and van Ballegooyen (1988) may generally reach northward to between 39 °S and 34 °S [Meeuwis and van Rensburg, 1995]. In the extreme case of SAASW intrusion as described by Shannon *et al.* (1989) however, a substantially larger area was covered by the SAASW (50 000 to 70 000 km^2). This water was observed to penetrate as far north as 33 °S. Shannon *et al.* (1989) have also suggested that these intrusions may hinder the penetration of Agulhas Current filaments into the South Atlantic Ocean; both due to their conflicting path orientation (see Figure 2.10 for Agulhas filament orientation) and the fact that plumes are shallow features reaching ~ 50 m in depth [Lutjeharms and Cooper, 1996].

3.2. Structure of extreme event

Shannon *et al.* (1989) have presented the only hydrographic description of these SAASW intrusions to date using *in sito* measurements of temperature and salinity from the Subtropical Convergence and Agulhas Retroflection Cruise (SCARC) undertaken during the austral summer of 1986/1987. The cruise track is given on Figure 3.4 and temperature sections along three legs and salinity sections along two legs of the cruise are given in Figure 3.5.

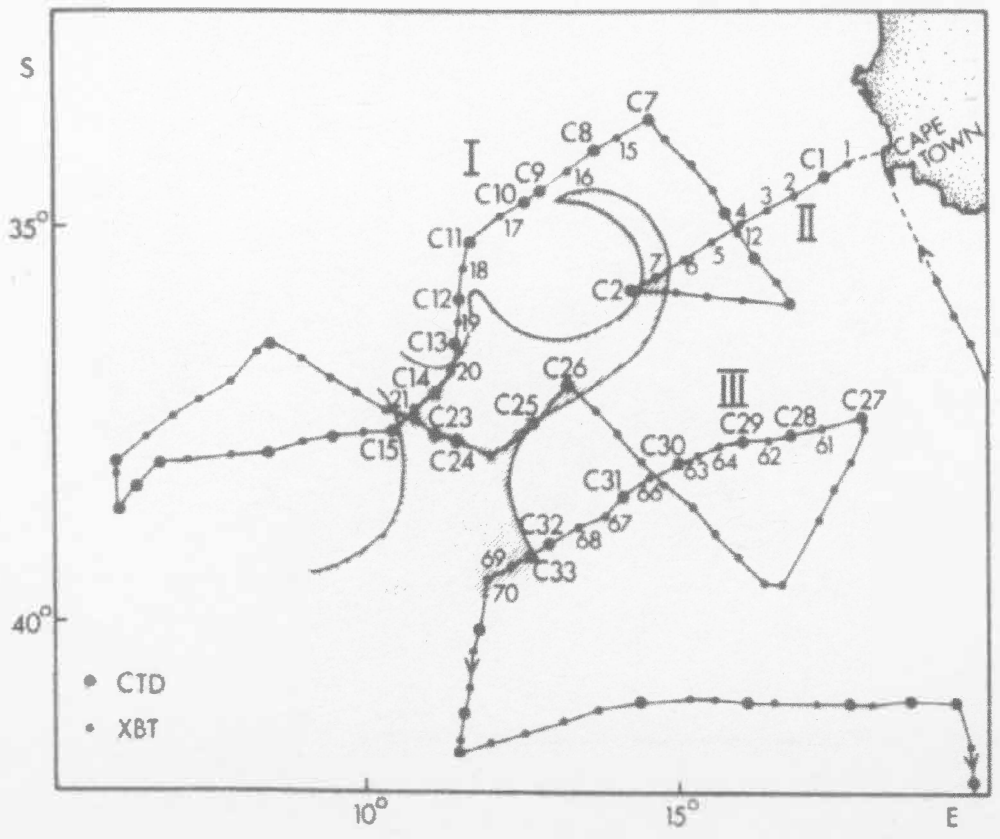

Figure 3.4. Cruise track of the Subtropical Convergence and Agulhas retroflection (SCARC) cruise between 12 February and 4 March 1987. C denotes Conductivity-Temperature-Depth (CTD) probe stations while numbers alone denote Expendable Bathythermograph (XBT) stations [Shannon *et al.*, 1989].

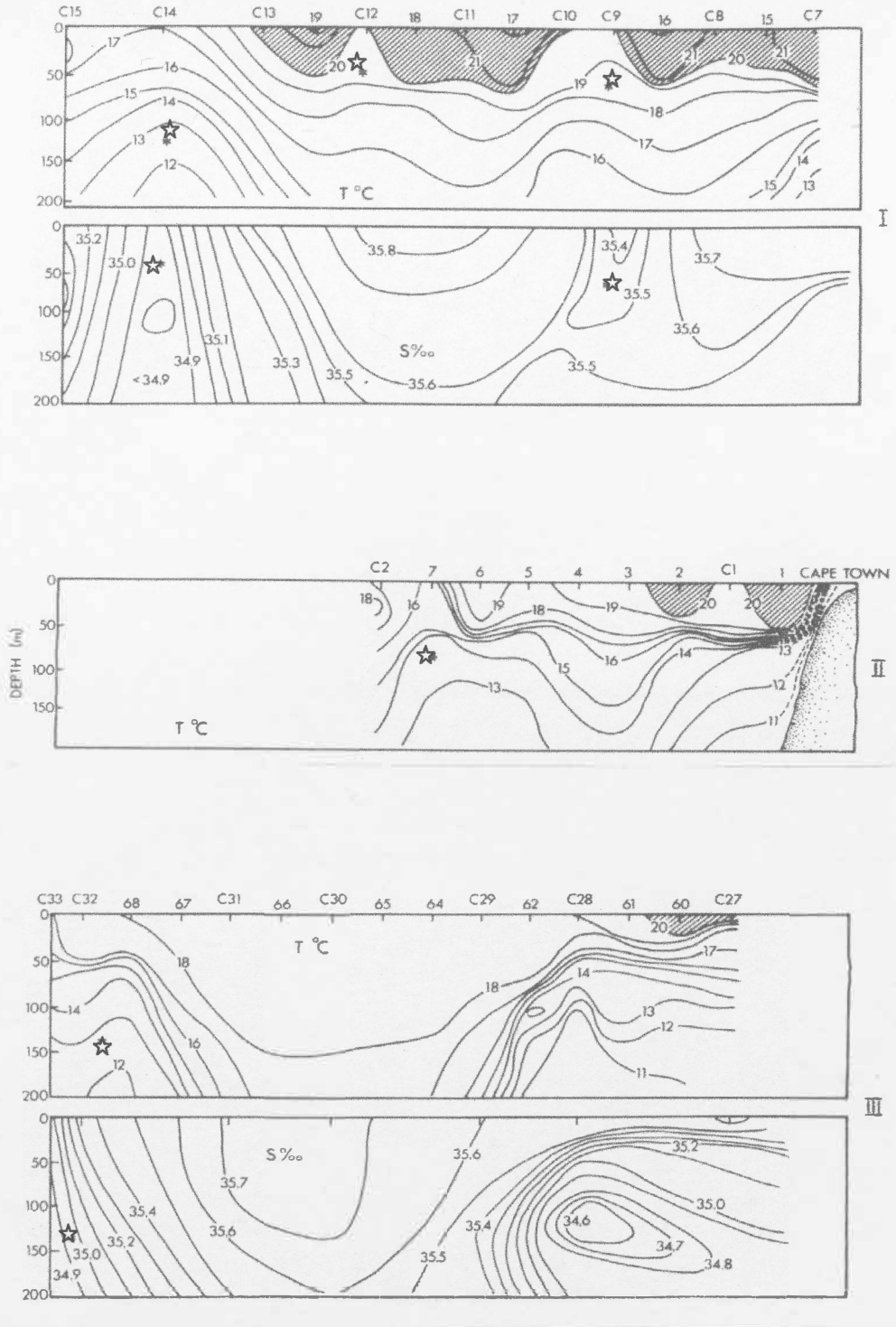

Figure 3.5. Temperature and salinity sections of three legs of the SCARC cruise denoted I, II, III respectively on Figure 3.4. (no salinity section could be drawn for leg II since only 2 CTDs were deployed for the entire leg - one at the beginning and one at the end of the leg). SAASW intrusions are marked ☆ on the sections. [Shannon *et al.*, 1989].

In the northern section (I), three cold water intrusions can be seen. The main intrusion path seems to be situated at station C14 and appears to extend below 200 m while the more easterly ones (at C12 and C9) seem to be shallower and extend only to about 75 m. The intrusion along the more coastally located leg (II) seems to extend to about 100 m depth while the most southerly intrusion (along leg III) seems to extend below 200 m. This suggests that these cold fluxes of SAASW shoal as they penetrate northward into the southeastern Atlantic Ocean. All the sections depict the wedge-like nature of the cold fluxes (marked ☆ on the diagrams).

No focused research on these intrusion events has been carried out to date. Lutjeharms and van Ballegooyen (1988) have given a descriptive account of Agulhas retroflection features (the retroflection itself, eddies and rings) and these cold water intrusions are described only in terms of their association with ring shedding. Although Shannon *et al.* (1989) have presented a description of the structure of an extreme event their results were based on one occurrence only.

The statistical analysis of the surface characteristics of these intrusions by Meeuwis and van Rensburg (1995) gives a fairly sound estimate of the longitudinal position and temperature of these intrusions. Apart from it being only surface information, their results were based on only three years of satellite data with a very poor spatial resolution. This means that their results represent at least a coarse first estimate of the longitudinal location of SAASW intrusions.

Intrusions of SAASW introduce a substantial amount of cold, low salinity water into the Agulhas Retroflection region. This may result in a negative heat flux and a freshening of the region and may also introduce sub-antarctic fish species into the region. Such a wide expanse of cold water may, conceivably, influence the path of low pressure frontal systems *en route* to South Africa. However, a considerable amount of research still needs to be done to augment the current knowledge of the structure and dynamics of these

intrusions as well as their climatic and oceanographic importance to the Agulhas Retroflection region.

In order to do this, it would be instructional to consider the environmental changes that occurred in the Agulhas Retroflection region between 1983 and 1988.

3.3. Environmental changes.

A large-scale study on the interannual variability of the environment in the southeast Atlantic Ocean between the years 1983 and 1988 was carried out by Shannon and Agenbag (1990).

Cooling of the oceans was evident between August and October 1983 followed by the warming of the waters during the summer of 1983. This event seemed to be at the tail end of a regional response to the 1983 Pacific El Niño - Southern Oscillation (ENSO) [Preston-Whyte and Tyson, 1988].

Gillooly and Walker (1984) have pointed to an unusual situation as regards the location of the STC in the 1982/1983 summer. The cooling south of Africa in the period August - October 1983 could, therefore, also be the aftermath of the 1982/83 ENSO reflected by the northward displacement of the STC.

During 1984, the surface Equatorial Counter Current in the SAO was unusually well developed, and in the Gulf of Guinea there was very little westward flow. This unusual situation in the Gulf of Guinea was associated with the rapid relaxation of the zonal winds over the subtropical western Atlantic between November 1983 and January 1984, following on an extended period of stronger trades [Shannon and Agenbag, 1990].

The year 1984 was characterised by the presence of an anomalous flow of warm water with a temperature > 17 °C along the west coast of Angola and Namibia. This event is similar to a southward flow of warm water along the Peruvian coast; the original definition of the Pacific El Niño Southern Oscillation [Shannon *et al.*, 1986]. Shannon *et al.* (1986) have therefore named the anomalous flow "Benguela Niño". High rainfall and even flooding over the Namib Desert were recorded during the year 1984. For a more extensive account on the 1984 Benguela Niño and similar recorded events in 1950 and 1963, see Shannon *et al.* (1986).

The warming in 1984 was followed by substantial cooling over much of the South Atlantic during the first half of 1985 with cold water being present over the Benguela almost continuously between 1984 and 1985 [Shannon and Agenbag, 1990].

In 1986 anomalies in the distribution of wind stress over a large part of the Indian Ocean and over the retroflection region south of Africa seem to have given rise to an extensive Agulhas Current water intrusion into the Benguela region [Shannon *et al.*, 1990]. This pronounced intrusion of Agulhas Current water into the south-east Atlantic appeared to have started in September 1985 and ended abruptly at the end of 1986 followed by extensive cooling during the first half of 1987.

The Shannon *et al.* (1989) SAASW intrusion was discussed earlier. This episodic incursion was caused by major instabilities in the STC at 15 and 11 °E where a large wedge-like filament of SAASW developed and moved northward at a speed of about 14 $cm.s^{-1}$. This intrusion retained it's surface signature for approximately 2 months and effectively blocked the leakage of Agulhas Current water into the Atlantic during December 1986 and January 1987.

During the summer of 1987/88 abnormally high SSTs in the northern Benguela were followed by a substantial cooling over a large part of the South Atlantic [Shannon and

Agenbag, 1990]. This was probably in response to the 1987/88 El Niño - La Nina event during that time [Preston-Whyte and Tyson, 1988].

From the above discussion it is clear that the complex oceanic environment around South Africa has been subjected to a range of episodic environmental changes in the 1980s. With this in mind and considering the lack of knowledge concerning SAASW intrusions across the STC, clear research objectives can be formulated in the next chapter.

Chapter 4

Remaining Questions and Research Objectives

This chapter outlines the shortcomings to the present knowledge of SAASW intrusions discussed in the previous chapter and gives the scope of this thesis in attempting to fill some of the gaps in our understanding of SAASW intrusion episodes.

At least one extreme case of SAASW intrusion has been observed in satellite remote sensing in the thermal infrared that lasted for more than a month at the sea surface. Furthermore, it was detectable by oceanographic instruments for up to 2 months to a depth of more than 200 m [Shannon *et al.*, 1989]. This suggests that these events are not just shallow, short-term phenomena but may have a prominent function in the dynamics of the Agulhas Retroflection region with regards to the heat, water and biomass exchange between the Southern and Atlantic Oceans.

It is also believed that such an extensive aerial coverage of cold water southeast of Cape Town may be climatically important. Brundrit and Shannon (1989) have, for instance, shown that during periods when the Agulhas retroflection region was covered extensively by warm water, such as at the end of July 1989, this water had the effect of greatly enhancing buoyancy-driven turbulence in the lower atmosphere and that the transfer of the considerable amount of sensible and latent heat from the ocean to the atmosphere can thus fuel low pressure systems to storm intensity. Therefore it is suggested that an extensive aerial cover of cold water over the Agulhas retroflection area may, in turn, suppress the development of low-pressure systems and may even delay the progression of a cold front.

This thesis attempts to fill some of the gaps in our present knowledge concerning these SAASW intrusions and to serve as a base from which further research can continue. The aim of this dissertation is therefore to:

i. Determine the lateral dimensions of SAASW intrusions at the Agulhas Retroflection in terms of their width and length.

ii. Establish the location of these features at the STC in an infrared serial satellite study spanning 11 years. Their annual and seasonal frequency will be estimated from the available satellite data. It is believed that approximately 5 intrusions of SAASW would be observed per year judging from their association with ring shedding. Meeuwis and van Rensburg (1995) have estimated that these intrusions are present at the Agulhas Retroflection approximately 17 % of the time.

iii. Establish the persistence of these SAASW intrusions at the Agulhas Retroflection. This is difficult to do with only infrared satellite imagery. Persistent cloudiness at the STC, makes serial tracking of SAASW intrusion events difficult. The surface heating of these cold features makes their detection by thermal infrared difficult as well. Satellite altimeter data from TOPEX-POSEIDON and ERS were, therefore, used instead. Altimetric (microwave) measurements effectively makes cloud cover seem transparent to the satellite giving "cloud free" sea surface height anomalies.

iv. Determine the hydrographic structure of these SAASW intrusion events. This include their vertical extent in the water column and a water mass analysis confirming whether these intrusions are indeed SAASW in nature.

Chapter 5

Data and Methodology

This chapter outlines the data used in answering the research questions formulated in the previous chapter and the methodology employed to arrive at the answers. It also presents some sources of error within the data and the corrections made to minimise this error.

5.1. Mean sea surface thermal and salinity expression.

Figure 5.1 shows the geographic area used to study SAASW intrusions. Sea surface temperature (SST) and salinity data were obtained form the Southern African Data Centre for Oceanography (SADCO). They were collected mainly by merchant ships and ships of opportunity over a period spanning the years 1910 to 1990.

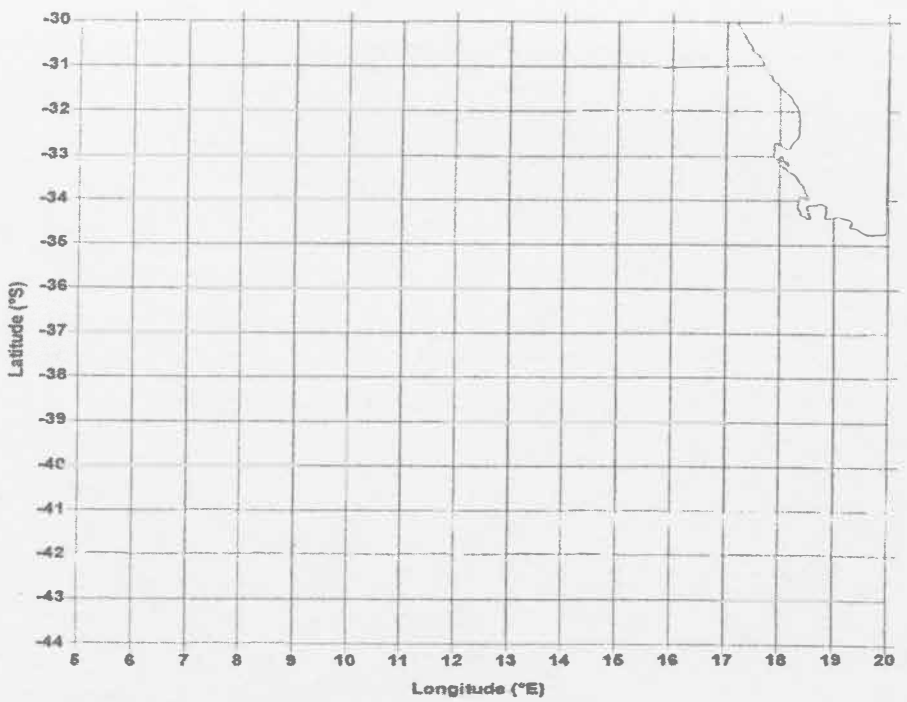

Figure 5.1. The study area used to analyse SAASW intrusions from surface hydrographic data and satellite images. The region was subdivided into 1°x1° latitude/longitude grid cells for the analysis of SST and sea surface salinity using the available historic data.

The study area 5 °E to 21 °E and 30 °S to 45 °S was subdivided into 1^{o} x 1^{o} longitude/latitude squares and the mean temperature and salinity were calculated along with their respective standard deviations for each square. Data corrections performed were as follows:

1. The temperature records between 1910 and 1940 were increased by 0,49 °C [Villacastin-Herrero *et al.*, 1990 in accordance with the analysis by Jones *et al.*, 1986]. This correction was made to account for the systematic error in temperature measurements due to the conversion from canvas buckets, which is subject to evaporative cooling.

2. During 1940 the temperature records were increased by 0,19 °C, while the records between 1941 and 1945 were reduced by 0,1 °C. This correction takes into account heating of water from engine intake (the conversion from sail to steam ship as well as the ship size) [Villacastin-Herrero *et al.*, 1990 in accordance with factors employed by Folland *et al.*, 1984].

No corrections were made to salinity measurements. The accuracy of salinity data from research cruises was considered reasonable for the analysis done here [*e.g.* Villacastin-Herrero *et al.*, 1990].

The number of temperature observations per grid cell (Figure 5.2) increases considerably towards to coast. Further away from the coast the number of observations is almost entirely based on research cruises and the data gathered is very scant. The main reason for this is the fact that the oceanic region west of Africa was/is very infrequently traversed. The number of research data (both temperature and salinity) given in Figure 5.3 is even less and suggests that inferences made, based on these salinity measurements farther away from the coast, may be questionable since they are based on very few observations.

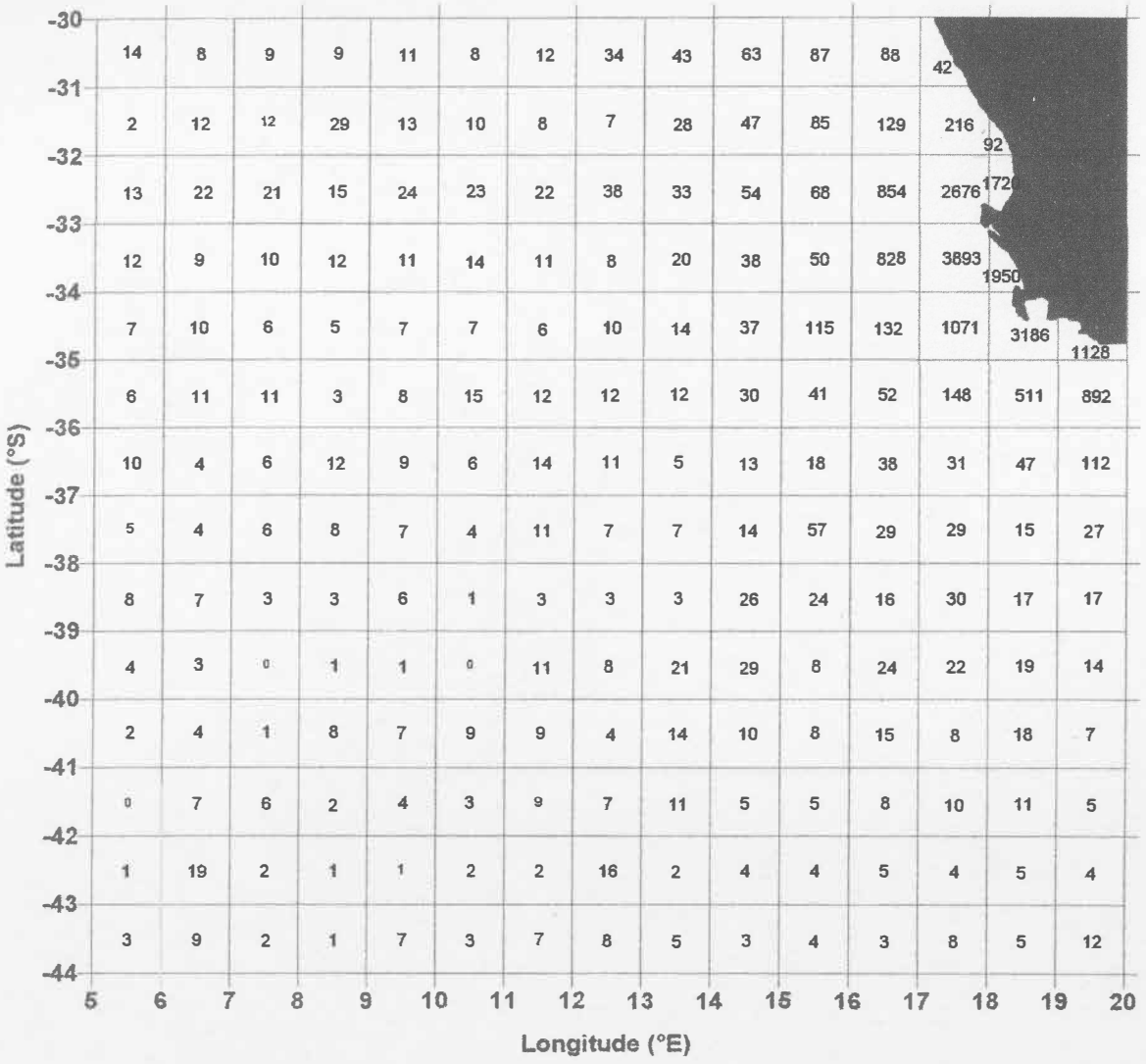

Figure 5.2 The number of available sea surface temperature observations in 1° latitude x 1° longitude cells for the study area southwest of the African continent.

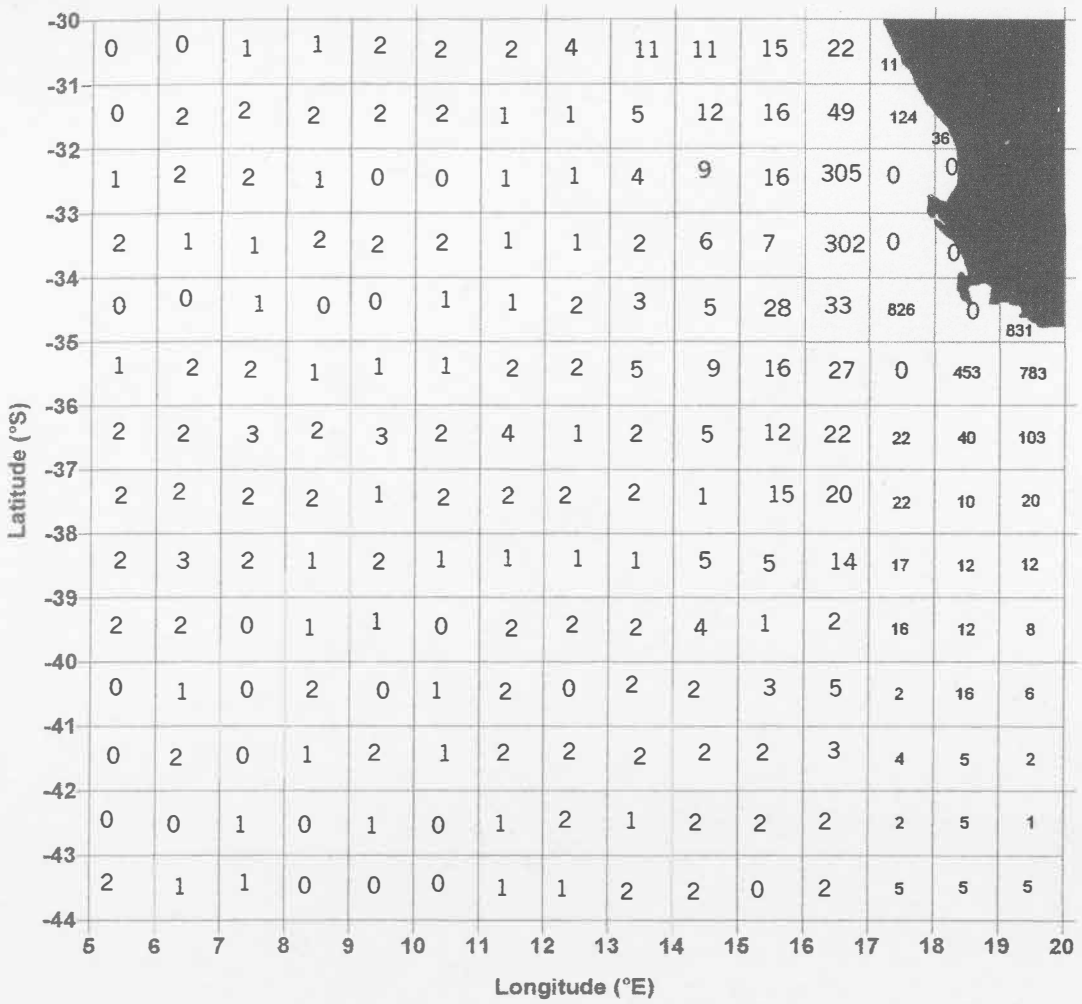

Figure 5.3 The number of available sea surface salinity observations per grid of 1° latitude x 1° longitude cells in the study region southwest of the African continent.

5.2. Thermal infrared analysis

Thermal infrared images from the geostationary satellites METEOSAT I and METEOSAT II as well as from the near-polar orbiting satellites NOAA 4, 5, and 9 were used to study the thermal nature of the surface waters of the Agulhas Retorflection.

The geostationary satellites measured in the range between 10.5 μm and 12.5 μm over the ocean and have a *nadir* resolution of 5x5 km over the equator. The geographic resolution becomes considerably poorer with increased distance form the equator, reaching about 8x8 km around the region of interest.

The near-polar orbiting Very High Resolution Radiometer (VHRR) satellites NOAA 4 and 5 and the Advanced Very High Resolution Radiometer (AVHRR) NOAA 9 measured in the range 10.5 μm and 11.5 μm and have a *nadir* resolution of between 800 m and 1.5 km along the subsatellite track. These images facilitate the identification of much smaller oceanographic phenomena than those observed through the METEOSAT images.

Generally, the data from both satellite series (METEOSAT and NOAA) were not atmospherically corrected or calibrated and therefore the images could not be used to determine absolute sea surface temperature. However, for the purposes of this investigation, finer resolution or calibration was found to be unnecessary in the region [*e.g.* Lutjeharms and van Ballegooyen, 1988; Lutjeharms and Cooper, 1996]. This notwithstanding, a number of images of illustrative SAASW intrusion episodes were geometrically corrected and calibrated for SST and are shown in chapter 6.

5.2.1. Analysis of satellite thermal infrared images

The study region is geographically located within an area of persistent cloudiness [Lutjeharms and Valentine, 1988], which makes continuous serial oceanic feature tracking over lengthy periods rarely possible.

NOAA satellite images were used mainly to examine the fine scale features of these intrusions. Their usefulness in contouring surface hydrographic data is apparent. However, useful images from these near-polar orbiting satellites are rare. The satellite tracks cross the southern reaches of Africa approximately two or three times a day, however, the coverage of relatively cloud-free satellite images, housed at the Oceanography Department at the University of Cape Town, is of the order if two or three times a week over different areas. This makes long-term serial tracking of SAASW intrusion events south of Africa very difficult. Persistent cloud cover, therefore, hinders the temporal analysis over the study region.

METEOSAT images were available for this investigation for nearly every day of the year from 1981 onward. These geostationary satellites stay at a fixed distance from the earth's surface at a fixed location above the equator. Their infrared images proved particularly useful in creating temporal composite diagrams used in this thesis. Unfortunately persistent cloud cover over the study region also mars the usefulness of these METEOSAT images to the present study.

5.2.2. Determination of SAASW intrusion frequency

To determine the occurrence frequency of the intrusions the satellite images were analysed in the manner shown of Figure 5.4.

Useless images are those images that were extensively covered with cloud or the image was of the wrong area (for NOAA images). Useful images are those images that had little cloud cover within the study area.

Total number of Satellite images

Number of useful images

Number of useless images

Images with intrusions

Images without intrusions

Figure 5.4. Sorting of METEOSAT and NOAA thermal infrared images.

The following statistical analysis were performed on the data to obtain the occurrence frequencies, yearly and seasonally of these cold water intrusions:

$$\text{The occurrence frequency} = \frac{\text{The number of images that have cold water filaments}}{\text{Total number of useful images}}$$

$$\text{The seasonal frequency} = \frac{\text{The number of images with intrusions in the season}}{\text{The total number of useful images for the season.}}$$

The occurrence frequency (OF) was calculated as the proportion of SAASW intrusions in useful images to the total number of useful images. This proportion was then assumed to

be distributed normally about the true proportion OF and errors to the approximation of frequency could therefore be calculated for the 9-year period for which METEOSAT images were available. The assumption of normality was not tested due to the large number (more than 10 % of total number of days in study period) of clear images in the 9-year study period in accordance with the statistical law of large numbers [Rice, 1988, Underhill, 1984].

5.3. Altimetric observations

Owing to persistent cloud cover over the study period, thermal infrared images are not entirely reliable in determining how long these SAASW intrusions are present at the Agulhas retroflection. Moreover the surface temperature of cold-water intrusions as they move northward may be warmed by the air temperature and the temperature of ambient waters making them indistinguishable from the surrounding surface water features using infrared remote sensing. To overcome this problem, altimetric measurements of the sea surface height variability from the ERS and TOPEX-Poseidon satellites were used since cloud cover does not effect these measurements.

The general procedure was to use thermal infrared images of the NOAA series to identify very distinct and well developed SAASW intrusion events and then to follow these in their sea surface height expression both backward and forward, temporally to obtain a reasonable estimate of the residence time of SAASW intrusions.

Since November 1995 NOAA has been generating "Real-time Geophysical Data Records" (RGDRs) for ERS-1 (launched in August 1991) and has continued this since May 1996 with ERS-2. Fast delivery altimeter data containing only crude satellite vector information comprises a range measurement between the satellite and the sea surface. These data arrive at NOAA within 6 hours of acquisition. In order to compute changes in the sea surface topography, it is also necessary to have accurate satellite orbit information. These orbits are calculated by the Delft Institute for Earth-Oriented Space Research (in

the Netherlands) and are called JGM-3 orbits. JGM-3 orbits consist of a computed orbit segment (7 days) plus a predicted extension of that orbit of 6.5 days. The predicted orbit phase is necessary because of delays in tracking data between consecutive satellite passes. "Interim Geophysical Data Records" IGDRs, used with the TOPEX/Poseidon satellite may be obtained by simply replacing the predicted segment of the JGM-3 orbits with the best part of the computed orbit. The Laboratory for Satellite Altimetry (LSA, Silver Spring, USA) combines the altimeter range data with these JGM-3 orbits, adds corrections for travel time delays of the radar pulse through the troposphere and ionosphere and removes the tidal components of sea level since these are not related to large scale ocean circulation. IGDRs can be computed within 3 days. These data have orbit errors of ~ 10 cm, and are suitable for large scale interannual ocean monitoring. The IGDR data is assimilated into a coupled ocean/atmosphere model running at NOAA, as is being done with TOPEX/Poseidon altimetry.

Near real-time, final RGDRs and IGDRs are distributed *via* the Internet at http://www-ccar.colorado.edu/~realtime/global-historical_vel/ for the period 1 May 1994 to 20 October 1997. Sea surface anomaly maps of the area spanning the geographical area of 0 °E to 21 °E and 30 °S to 45 °S were used in conjunction with concurrent thermal infrared images of the NOAA series to study the residence time of SAASW intrusions at the Agulhas retroflection region.

5.4. Hydrographic Data

Hydrographic sections from two previous studies have been redrawn in this thesis with fresh interpretation on some of the features present *e.g* :

i. Data gathered on the ARC (Agulhas Retroflection Cruise) on board the *R.V. Knorr* and *R.V. Meiring Naude* was analysed by Gordon *et al.* (1987). Some CTD (conductivity-temperature-depth meter) sections from this cruise are redrawn in this investigation.

ii. Data gathered during the SCARC (Subtropical Convergence and Agulhas Retroflection Cruise) on board the *S. A. Agulhas* have been analysed by Rigg (1995). These sections are redrawn in this investigation.

Individual Potential temperature-Salinity (Θ-S) diagrams and temperature profiles of stations of particular interest were also drawn for finer analysis of specific features using CTD measurements. The CTD data from both these cruises are archived at the Ocean Climatology Group, in the Department of Oceanography, at the University of Cape Town, in the form of data reports [Camp *et al.*, 1986; Valentine *et al.*, 1988].

The CTD used in the ARC cruise was a modified Neil Brown Instrument Systems, Inc. CTD-02 combined with a 24 position 10 litre rosette sampler. The Physical and Chemical Data Facility (PACDF) of Scripps Institute of Oceanography provided the instruments and data acquisition system. Various sensor corrections, decimations and calibrations were performed by Lamont-Doherty Geological Observatory of Columbia University and are described in by Camp *et al.* (1986)

During processing of the ARC CTD data it was discovered that a salinity-temperature mismatch occurred at the sea surface. The pressure at which the first good match was found was therefore extrapolated to the surface. All the stations used in this thesis were carried out to a depth of 1 500 m.

The CTD used in the SCARC cruise was a standard Neil Brown Instrument System Mark III CTD. A smoothing and reduction procedure was followed to obtain one-decibar levels between the stations of interest to this thesis. A running mean was then calculated on this subset by way of interpolation, resulting in a maximum uncertainty in represented levels of 0,5 db. Typically, the selected values are between 0,2 db of the desired levels.

Various sensor calibrations were performed (Valentine *et al.*, 1988). However, no corrections were made for sensor response times. Also, no attempt was made to calibrate the Beckham oxygen sensor.

Samples of near surface water were collected from the scientific sea water supply; the inlet of which was situated at approximately 3 m depth. Seawater samples through the water column were collected by means of eight Niskin bottles in line of a cable, triggered by a messenger.

It is clear that the available resources (both traditional and non-traditional) to study SAASW intrusions encompass a wide spectrum and they were all employed here to gain as much information as possible. The results of these analyses are given and discussed in the next chapter.

Chapter 6

Mean oceanic environment and satellite infrared analysis.

This chapter presents the results of the historic sea surface temperature and salinity mean used to determine the geographical location of SAASW intrusions at the surface. Thermal infrared satellite images show various types of cold water intrusions present at the Agulhas retroflection. Five colder water intrusions are observed per year which are present at the Agulhas Retroflection approximate 38 percent of the satellite infrared coverage in the study period. A tentative seasonal analysis of SAASW occurrence is also discussed.

6.1. Mean flow field southwest of Africa.

The mean sea surface temperature for the region of interest, based on hydrographic data, is given on Figure 6.1. This figure shows a clear southeasterly-northwesterly alignment of warm surface water (~ 18 °C) seemingly emanating from the Agulhas Retroflection, the position of which is suggested in the warm patch of water > 20 °C directly south of the African continent. This distribution of warm water corresponds to the trajectories of warm Agulhas rings into the southeastern Atlantic Ocean [Lutjeharms and van Ballegooyen, 1988; Duncombe-Rae, 1991 (*cf.* Figure 2.11)] as well as the movement of Agulhas filaments [Lutjeharms and Stockton, 1987 (*cf.* Figure 2.10 A); Lutjeharms and Cooper, 1996]. Lower SSTs along the southwestern Cape coast (< 16 °C) reflect the cooling effect of coastal upwelling [Shannon, 1985].

The STC at the 14 °C isotherm [*e.g.* Lutjeharms, 1985; Matthysen, 1997] seems to be consistently situated at approximately 42 °S east of 12 °E. Matthysen (1997) has found that this front generally lies at approximately 41 °S, however variation in the latitudinal location of the STC is typical of the behaviour of this front south of Africa [Harris and Stavropoulos, 1978; Lutjeharms, 1985; Matthysen, 1997]. The number of SST observations west of 12 °E is very small (*cf.* Figure 5.2) and as a result the location of the STC may not be as reliably defined here than for the eastern areas.

A warm feature situated in the mean temperature field at approximately 8 °E, 42 °S seems to be the consequence of too few data in that area (Figure 5.2). The standard

deviations for the sea surface temperature data are given on Figure 6.2. This suggests that this warm feature should be viewed with suspicion in light of the extremely high standard deviations (14 °C) found in that area. The overall SST standard deviation of 2 °C may be a result of seasonal variation within the SST around Southern Africa [Villacastin-Herrero *et al.*, 1990].

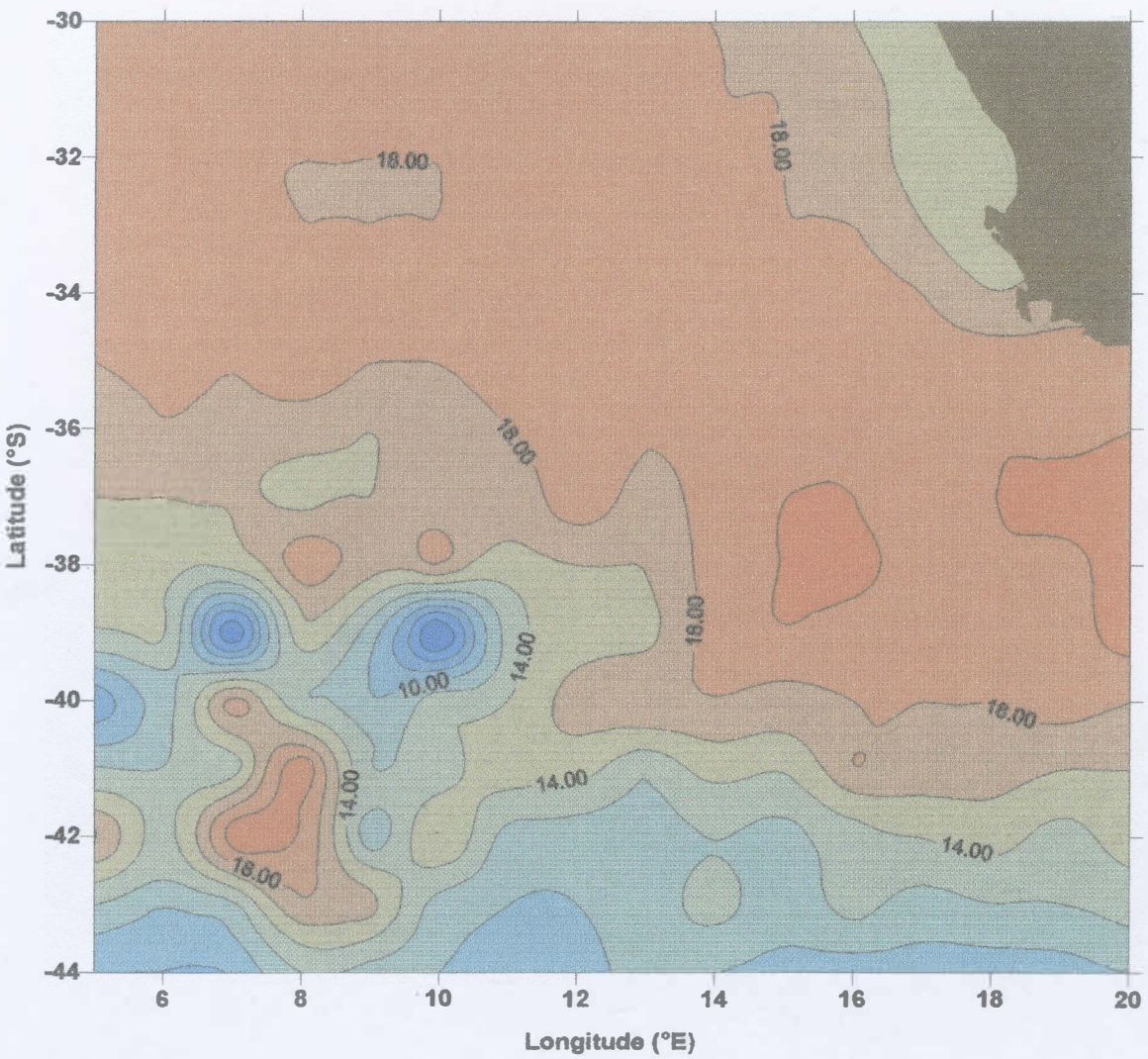

Figure 6.1. A map of the mean sea surface temperature using ship's data contoured in 2 °C intervals.

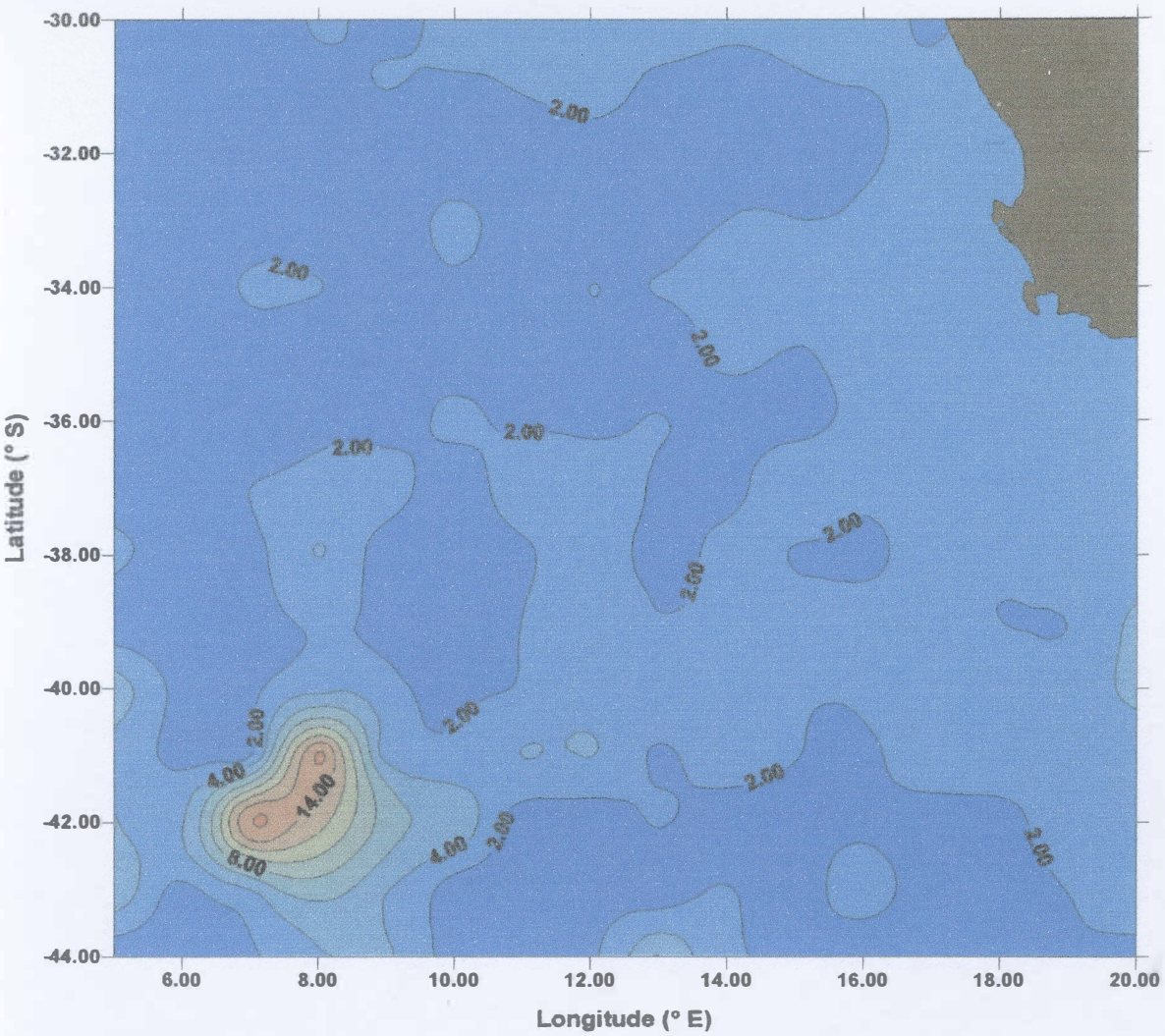

Figure 6.2. A map for the standard deviations for Figure 6.1 contoured in 2 °C intervals.

Two pools of cold water < 14 °C (Figure 6.1) are evident at approximately 10 °E, 39 °S and 7 °E, 39 °S. The easterly cold anomaly seems to originate at 6 °E, 44 °S. Taking into consideration the locations of known intrusions of SAASW in this general area [Shannon *et al.*, 1989], these bodies of colder water might be of Subantarctic origin.

The mean sea surface salinity for all available data is given in Figure 6.3. The southeasterly-northwesterly alignment of high salinity water is similar to the alignment of high surface temperature on Figure 6.1. This water extends from the relatively high surface salinity water of the Agulhas Retroflection and may therefore, to some degree, reflect the course of Agulhas rings and filaments into the southeastern Atlantic Ocean as suggested earlier for SSTs depicted in Figure 6.1.

The effect of upwelling on the west coast of South Africa is even more clearly seen on the sea surface salinity diagram than on the sea surface temperature diagram, while the warm feature centred near 8 °E, 42 °S in Figure 6.1 is not in evidence. This is possibly due to the fact that SST changes with the atmospheric conditions more rapidly than salinity *i.e.* salinity is conserved better at the sea surface than temperature and is therefore probably more reliable in investigating the lateral extent of SAASW intrusions.

Apparent intrusions of low salinity water (< 35) across the STC (which seems to be situated at approximately 42 °S on the salinity analysis as well) are observed at 19 °E and 11 °E. The easternmost intrusion is only visible as a slight deflection in the 14 °C isotherm on Figure 6.1.

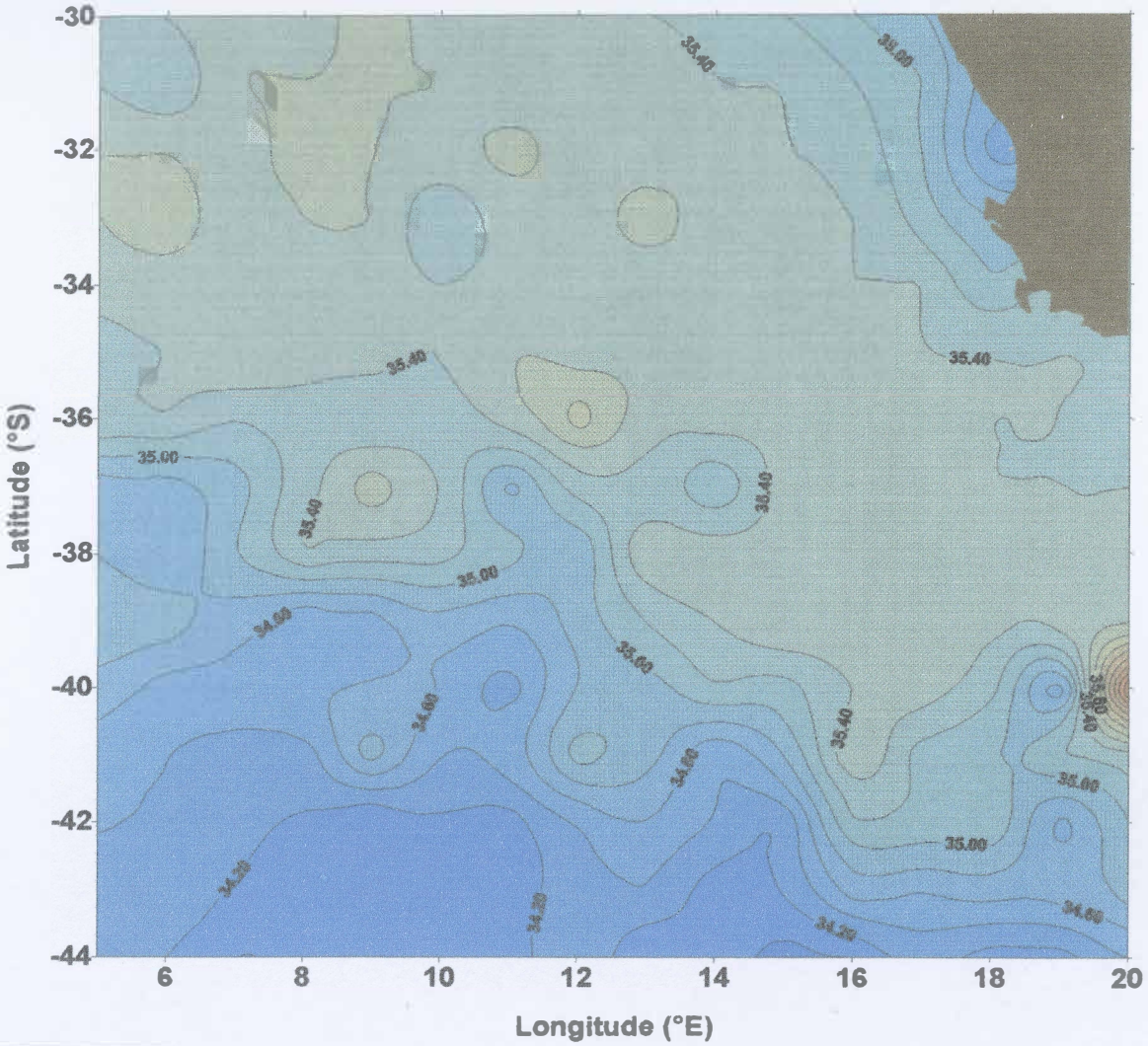

Figure 6.3. A map of the mean sea surface salinity using ship's data contoured in 0.2 intervals.

The approximate location of the STC seems to be 42 °S for data points east of 12 °E in both the temperature and the salinity mean fields. West of 12 °E the position of the STC cannot be unambiguously estimated owing to little data in the area. The SST as well as the sea surface salinity diagrams suggest intrusions of cold (< 14 °C) and low salinity (< 35) water at approximate locations 6 °E, 10 °E and 19 °E; the suggested easterly intrusion showing slightly higher geographic permanence in the salinity diagram than in the temperature diagram. This suggests that cold water intrusions are frequent features of the Agulhas Retroflection region and may have a definite role to play in the Agulhas retroflection dynamics. It should however be borne in mind that these are means spanning approximately 70 years and individual filament characteristics will not show in this analysis.

On average, the westerly intrusions penetrate north to approximately 36 °S, suggesting that the intrusion of SAASW reported by Shannon *et al.* (1989) was indeed an unusual occurrence. That extreme intrusion penetrated as far north as 33 °S and could have interrupted and even impeded Agulhas Current leakage *via* filaments into the Atlantic Ocean; at least at the sea surface.

The frequency of SAASW intrusion events could therefore suggest a measure of how often Agulhas filaments are impeded or interrupted. However it would be instructive to consider what these intrusions look like in the satellite infrared altimetry *i.e.* the types of SAASW intrusions.

6.2. Types of intrusions

Various types of intrusions have been observed through the use of both NOAA and METEOSAT images of which three representative examples are presented in Figures 6.4 to 6.6. It is worthwhile to note that while the absolute temperatures of cold features in these images have quite a wide range they were not considered in these analyses. It is assumed that the SST of cold water upon moving northward gets altered quickly by ambient warmer waters from the Agulhas retroflection and "pinched off" Agulhas rings as well as the overlying warmer atmosphere. Warm *versus* cold in this analysis only reflect the high contrast in heat as depicted in the infrared images.

Most intrusions are broad and solitary, spanning a surface area of approximately 20 000 km^2 on average (*e.g.* Figure 6.4). This illustrative intrusion of cold (< 14 °C) water was ~100 km wide and 200 km long located at approximately 17 °E, 39 °S. In Figure 6.4 an Agulhas Current filament (~20 °C surface water) directly south of the continent may be observed to the northeast on this cold-water intrusion. Clouds cover most of the satellite image from 5 ° to 12 °E. Very cold water along the South African west coast (< 14 °C) reflects the effects of coastal upwelling the area is known for.

Figure 6.5 shows an illustrative example of intrusions occupying a fairly larger surface area, ~50 000 km^2, than that in Figure 6.4. This type of intrusion consisted of two or more solitary intrusions and are not as frequent as the solitary ones (Figure 6.4). They are observable through infrared remote sensing for a much longer time, as will be seen in the next chapter. It will be shown later in this chapter that this particular intrusion is actually quite exceptional consisting of two intrusions at longitudinal positions 15 °E and (possibly) 11 °E of waters < 17 °C and have been discussed at length by Shannon *et al.*, (1989). The slightly higher overall ocean temperature (compared to Figure 6.4) surrounding the cold water intrusions could be due to the fact that this infrared satellite image was taken during the austral summer of 1986 while that of Figure 6.4 was taken during the Autumn of 1985. A warm core Agulhas Current ring [Shannon *et al.*, 1989] is observed at 14 °E, 38 °S. A false warm core feature, marked by a dashed line is possibly

due to sensor interference from sun glare [Shannon *et al.*, 1989]. Cloud covers most of the area between 5 °E and 10 °E.

Figure 6.6 shows a clear double cold water intrusion at longitudinal positions 19 °E and 12 °E. The two intrusions seem to be of the same temperature (~16 to 17 °C) range. The easterly intrusion was ~ 50 km wide, 300 km long and covered an area of ~15 000 km^2. The westerly intrusion, however was about 100 km wide and 400 km long covering a surface area of ~ 40 000 km^2. The higher sea surface temperature found between the cold water filaments suggests an Agulhas ring embedded between the two intrusions. In this figure the surrounding ocean waters was almost a degree higher that that of Figure 6.5, creating a strong temperature contrast between SAASW intrusions and the surrounding oceans.

These three examples of cold intrusion images were reasonably cloud free and have been colour coded, calibrated and geometrically corrected for illustrative purposes. Most images used were, however, not calibrated and geographically corrected and were usually not as cloud free. Composite sketches of these images were drawn and are given in Addendum A.1 and will be discussed next.

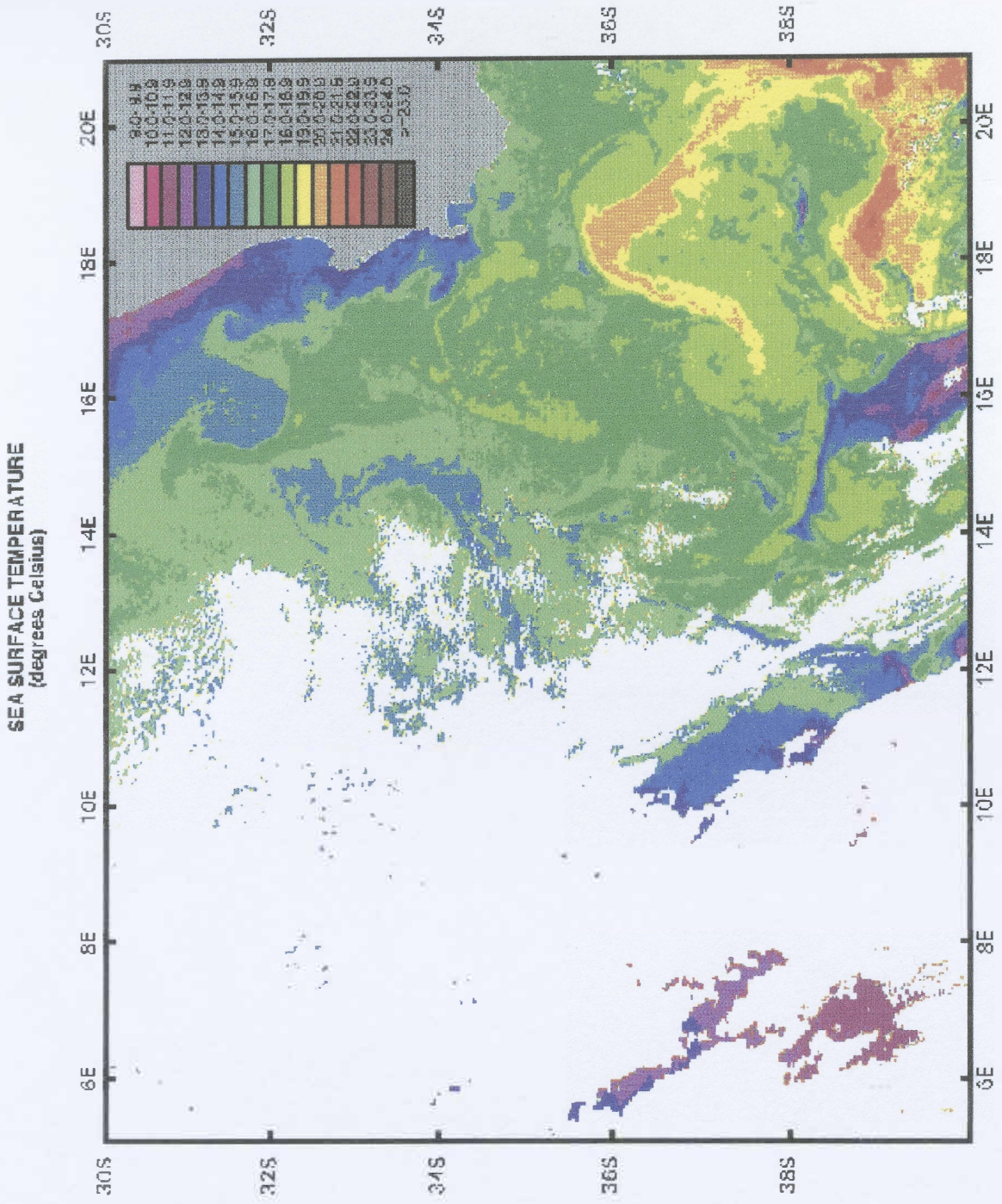

Figure 6.4 Calibrated and geographically corrected image of the sea surface temperature southwest of Africa on May 1985 (NOAA 4). This figure shows a clear, broad, solitary cold (<14 °C) water intrusion at ~ 17 °E. Warm water to the east is associated with the Agulhas Current. An Agulhas Current filament at ~ 19 °E, 37 °S is shown to emanate from the Agulhas Current. Very cold water to the west of the continent reflects coastal upwelling. White represents clouds.

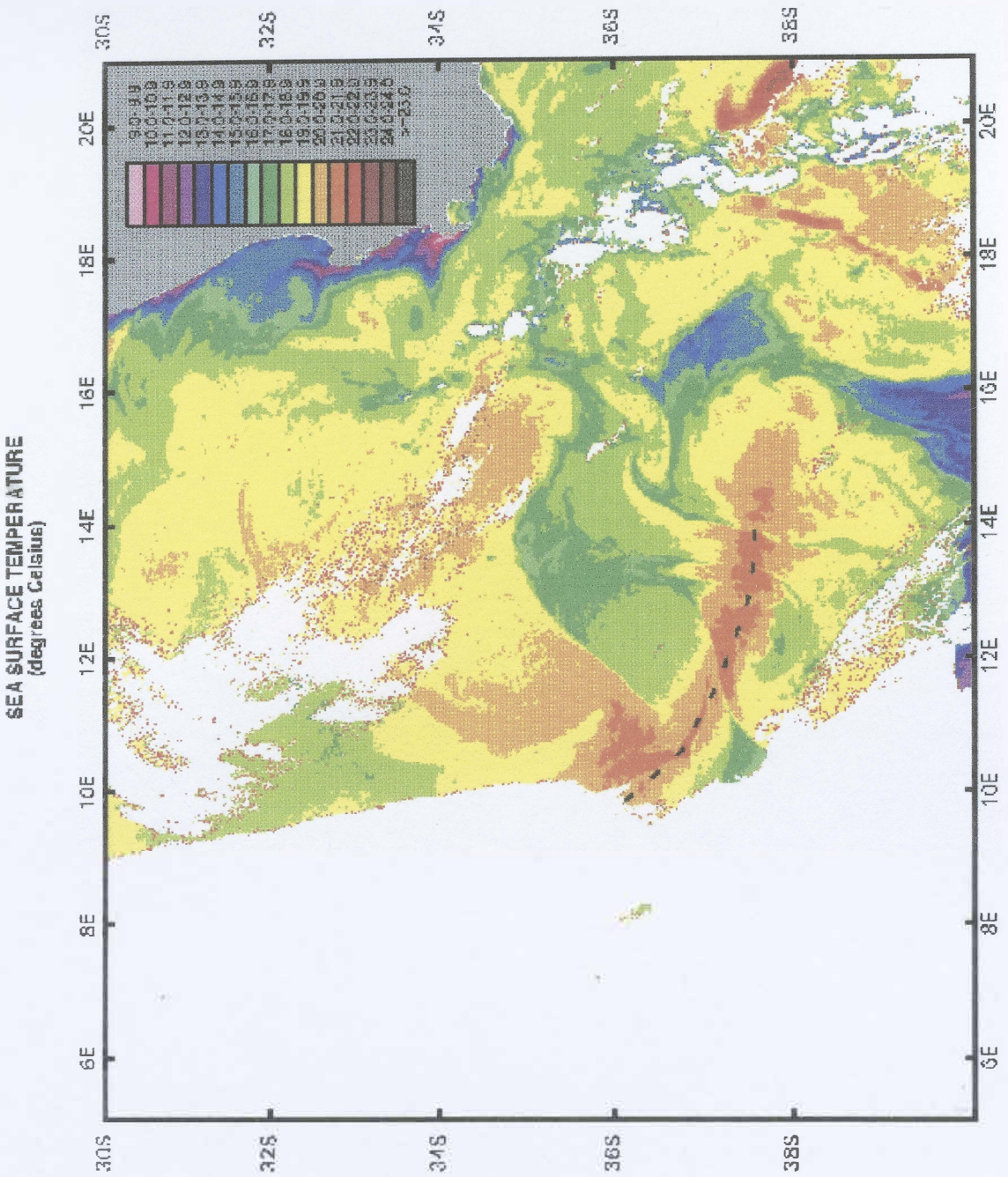

Figure 6.5 Calibrated and geographically corrected image of the sea surface temperature southwest of Africa on 10 December 1986 (NOAA 9). A dashed line indicates interference from sun glare. (*cf.* Figure 3.3). Two intrusions of cold water are observed at longitudes 15 °E and 11 °E. The coastal upwelling, with temperatures in places below 10 °C, is clearly circumscribed off the South African west coast. White regions represent clouds.

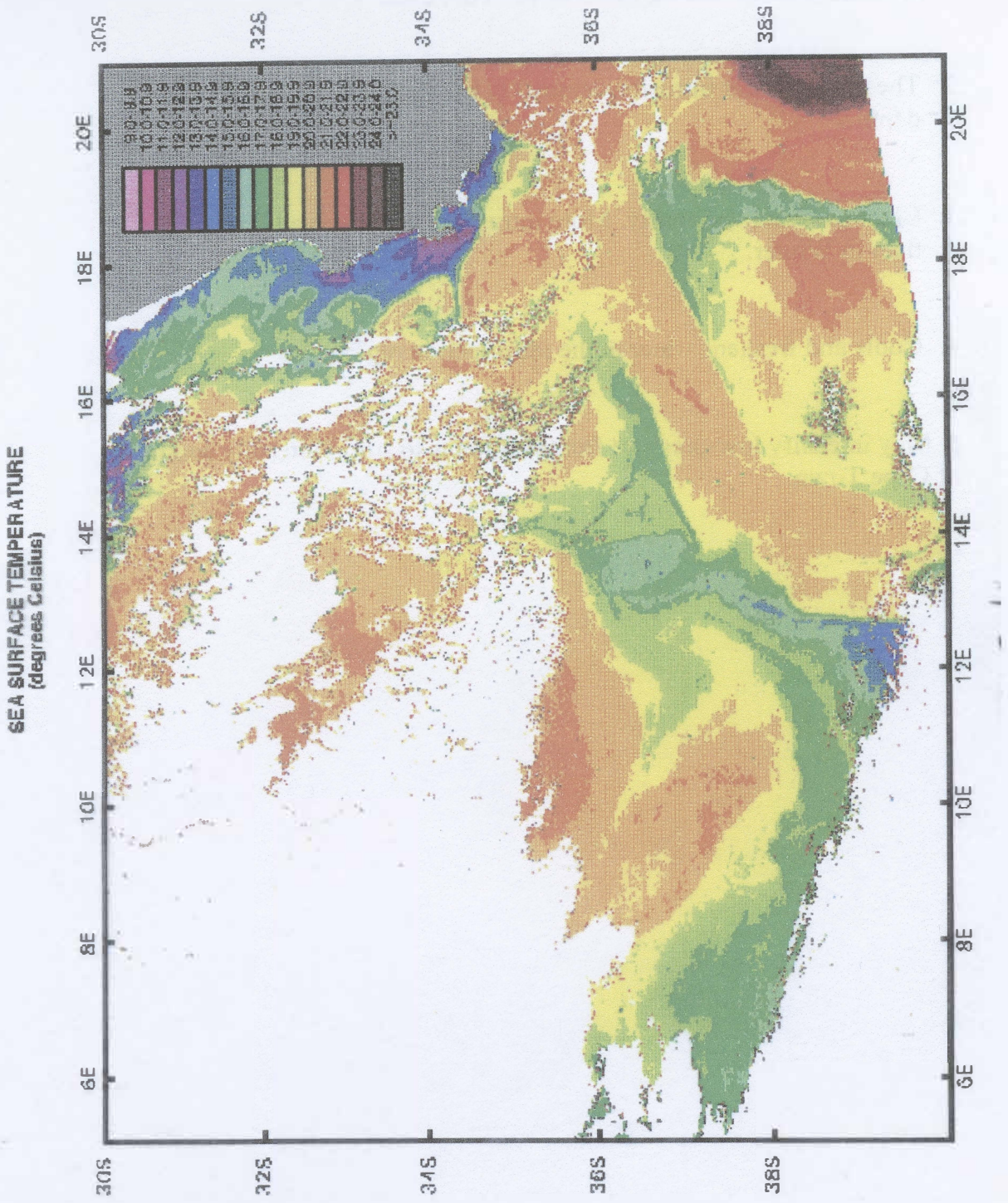

Figure 6.6 Calibrated and geographically corrected image of the sea surface temperature southwest of Africa on 28 February 1988 (NOAA 9). Two very pronounced intrusions of cold water (~ 16 to 17 °C) are observed at longitudinal positions 19 °E and 12 °E with an Agulhas ring probably embedded between these intrusions. The Agulhas retroflection is presented by the patch of warm water (~23 to 24 °C. The white regions represent clouds.

6.3. Satellite Composite Analysis

Thermal infrared images from the METEOSAT series were used to draw serial composite diagrams of individual cold water intrusion events. These composite diagrams are given in Addendum A.1. Yearly composite diagrams of all the SAASW intrusions are also given in Addendum A.2. From these figures it is evident that dual intrusions of cold water are not as unusual as originally thought and seem to be present during most of these intrusion events. In fact, during some events three cold-water filaments were observed.

Therefore, "extreme" cases of SAASW intrusions are classified as those intrusions that approximate (in lateral dimensions) the cold-water intrusion described by Shannon *et al.*, (1989) and are visible in satellite imagery for more than 1 month. The intrusions described by Shannon *et al.* (1989) consisted of a double intrusion with a collective aerial coverage of approximately 200 000 km^2.

The longitudinal orientation of cold water intrusions was found to be predominantly northeasterly for the intrusions observed through the satellite remote sensing during 1981 to 1990 (Figure 6.7). This orientation is in direct interception of the paths of Agulhas filaments from the Agulhas Current (*cf.* Figure 2.10) and may, therefore, interrupt the Agulhas Current filaments moving into the southeastern Atlantic Ocean. Hydrographic data at depth through these intrusions will be used later in this thesis to investigate the effectiveness of SAASW intrusions in "cutting off" Agulhas filaments.

From Figure 6.7 it seems that cold water intrusions are distributed from near 20 °E and into the southeastern Atlantic Ocean in a north-westerly curve. The association of SAASW intrusions with Agulhas rings, likewise distributed, has been discussed in chapter 3. East of ~20 °E the meridional instabilities in the STC could be attributed to the Agulhas Plateau situated at approximately 23 °E.

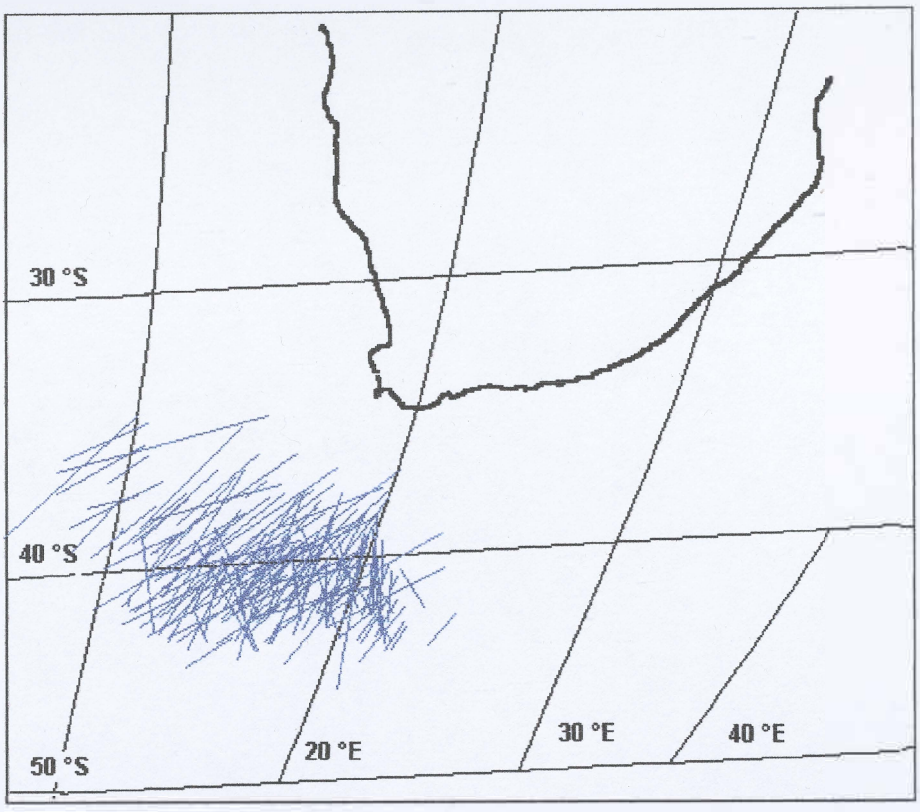

Figure 6.7. The lengthwise orientation of Sub-antarctic surface water intrusions during 1981 to 1990 as observed through satellite remote sensing of the METEOSAT satellite series.

The locations of these cold water intrusions on the STC (Figure 6.8) seem to show a slightly curve-like tendency starting from approximately 20 °E along 40 °S and then northwesterly into the southeastern Atlantic also indicating the association of these SAASW intrusions with the paths of Agulhas rings. As these rings move further north west they rapidly lose their surface thermal expression, therefore, the temperature contrast between these rings and the surrounding ocean waters, including SAASW become less distinguishable in thermal infrared sensing instruments of satellites.

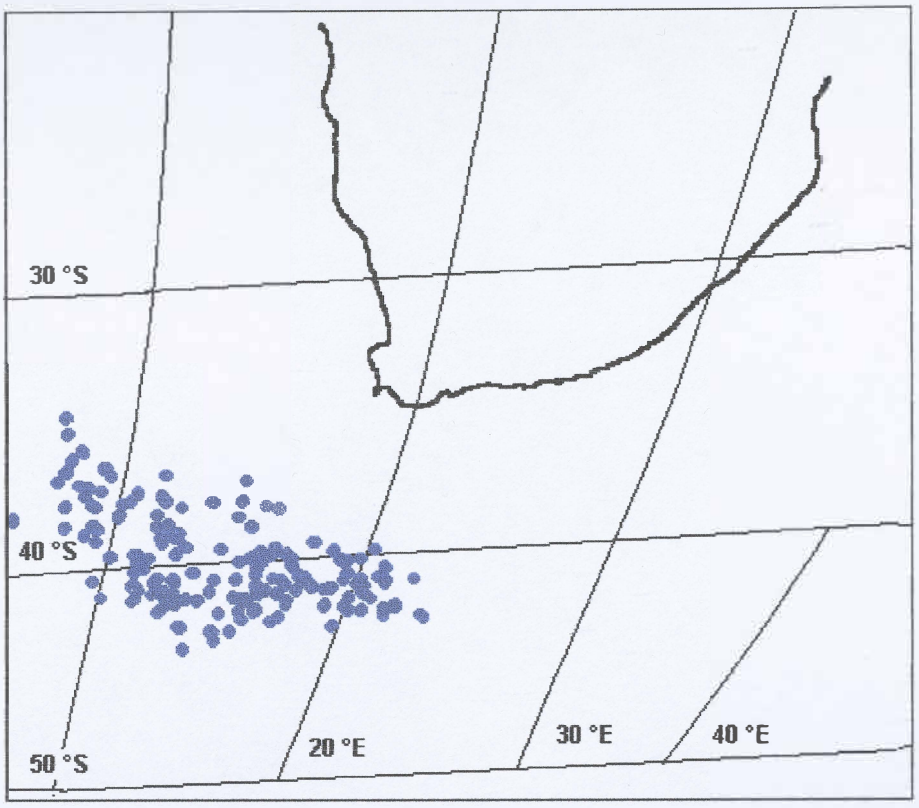

Figure 6.8. The location of sub-antarctic surface water intrusions on the subtropical convergence for the period 1981 to 1990 as observed *via* satellite remote sensing using the METEOSAT series.

It is clear from the above analysis that large meridional variation occurs within the STC southwest of Africa in which voluminous amounts of cold water are introduced into the Agulhas retroflection system. It is also suggested that these cold water intrusions could be quite effective in impeding the movement of Agulhas Current filaments into the southeastern Atlantic Ocean at the surface. Their association with Agulhas current rings were alluded to due to their associated movement into the southeastern Atlantic Ocean. In order, therefore, to calculate the frequency of the cold-water intrusions we have to consider individual events.

6.4. Composite diagrams of individual SAASW intrusion events

Drawing individual SAASW intrusion composite diagrams proved to be particularly difficult. In certain cases the surface nature of these intrusions as depicted by infrared satellite remote sensing makes distinguishing between two or more consecutive events very unclear.

A Table summarizing the satellite composite analyses performed is given in Addendum A.3. These results were calculated from the composite individual sketches given in Addendum A.1.

Most often, two intrusions are observed at a time, each with a width of 175 ± 99 km and a length of 413 ± 215 km (Addendum A.3). These intrusions cover an average 158 520 ± 118 256 km^2 of the retroflection region with colder water from south of the STC. The Table also shows that these intrusions are normally found at approximately 15 °E, 40 °S. It should be stressed that these summarising quantities are based on satellite infrared images that were NOT geometrically corrected and serve only as a rough approximation of the magnitude of cold water intrusions south of the African continent.

Immediately obvious is the immensity of the intrusion described by Shannon *et al.*, 1989 (January and February 1987 – Addendum A.3.). This intrusion covered an area of 733 784 km^2, which is almost 5 standard deviations higher than the calculated mean area cover for cold water intrusions at the retroflection, making this a truly exceptional event. The closest event to it, in terms of area covered by cold water was that of Summer 1984/ 1985. However, that event covered a mere (comparatively) 369 630 km^2 of the retroflection region.

"Extreme" cold water intrusion events could now be defined as events in which the total aerial coverage of cold water exceeds the average of 158 520 km^2. These events are as follows:

The Summer of 1983/ 1984 covered a total surface area of 246 420 km^2.

The Summer of 1984/ 1985 covered an area of 369 630 km^2. This intrusion seem to continue to Winter 1985 covering an area of approximately 328 560 km^2 in that season. September 1985 saw an area of 219 040 km^2 covered with colder water. The Winter of 1986 (284 752 km^2) lead to the massive 1986/ 1987 Summer intrusion already mentioned. The effects of this intrusion were still observable through April and September 1986. The summer of 1990 saw an area of 164 280 km^2 of the sea surface at the retroflection covered with cold water.

From this analysis a Table describing the yearly distribution of cold water intrusions are given in Table 6.1.

Year	**Number of Intrusions**	**Number of extreme Intrusions**
1983	6	1
1984	4	2
1985	6	2
1986	3	1
1987	6	1
1988	3	1
1989	4	0
1990	6	1
Mean per year	5	1

Table 6.1. The number of normal and extreme intrusions of SAASW for the years 1983 to 1990.

On average there seem to be 5 intrusions of cold SAASW per year for the period 1983 to 1990 with one extreme intrusion per year although some yearly variation may occur. This estimate of the number of SAASW intrusions agree with the annual estimate of the number of rings found by Gordon and Haxby (1990) using altimetric observations.

It therefore appears that cold water intrusions may reside at the Agulhas retroflection for a substantial amount of the time. The very extreme intrusion of Summer 1986/ 1986 was observable through satellite remote sensing for more than four months. It will therefore be instructive to consider the frequency of these cold water intrusions. This will be done in the next section.

6.5. Frequency of SAASW intrusions

The estimation of the frequency of these intrusions from the available satellite images from the NOAA series is given on Table 6.2 (a). A total of 1 459 images were available for the entire 11-year study period. The number of days within the study period totals 4 018. Thus the number of NOAA images represents only about 36 % of the days within the study period. Approximately 316 of these images were useful. This number of useful images (316), therefore, represents a mere 8 % of the total number of days in the study period, and it is therefore difficult to establish how representative they are of the study period of 11 years.

	T	NU	WI	N	E	OF (%)	OFN (%)	OFE (%)
1980	146	18	3	1	2	17	6	11
1981	167	4	0	0	0	0	0	0
1982	183	5	2	2	0	40	40	0
1983	209	17	5	1	4	29	6	24
1984	217	27	8	5	3	30	19	11
1985	187	103	39	31	8	38	30	8
1986	79	25	13	9	4	52	3	16
1987	68	37	14	8	6	38	22	16
1988	72	30	11	9	2	37	30	7
1989	87	30	11	11	0	37	37	0
1990	44	20	3	3	0	15	15	0
Total	1459	316	109	80	29	34	25	9

Table 6.2. (a) Estimation of the number of SAASW intrusions using the NOAA satellite series. T: Total number of available images; NU: Total number of useful images; WI: Total number of useful images with SAASW intrusions; N: Normal intrusions; E: Double intrusions; OF: Occurrence frequency of all the intrusions; OFN: Occurrence frequency of the normal intrusions; OFE: Occurrence frequency of double intrusions.

From Table 6.2 (a) it appears as if SAASW is present at the Agulhas Retroflection region approximately 34 % of the time during the 11-year study period. Approximately 25 % of the time these intrusions are of the normal kind while 9 % of the time multiple intrusions were observed covering a substantially larger area of the retroflection.

The occurrence frequency of SAASW intrusions varied considerably from year to year. While there were no SAASW intrusions observed during 1981, these intrusions were observed to be present 40 % of the time (based on only 5 useful images, however) in 1982 and 52 % of the time during 1986 (25 useful images).

The estimation of the frequency of the intrusions using METEOSAT images offers more encouraging prospects for statistical analysis (Table 6.2 (b)). A total of 3 054 images were available for the 10 year period (1981 to 1990) of which 1 145 images were deemed useful. This represents approximately 76% of the total number of days in the study period for which images were available - of which 28% were useful. Therefore statistical analysis was performed to give an approximation of the frequency of these intrusions in the satellite images.

	T	NU	WI	N	E	OF (%)	OFN (%)	OFE (%)
1981	15	3	1	1	0	33	33	0
1982	295	134	37	31	6	28	23	4
1983	270	111	56	49	7	50	44	6
1984	356	132	48	43	5	36	33	4
1985	365	223	94	71	23	42	32	10
1986	359	130	50	37	13	38	28	10
1987	361	138	51	33	18	37	24	13
1988	343	85	33	20	13	39	24	15
1989	345	69	34	20	14	49	29	20
1990	345	120	34	16	18	28	13	15
Total	3054	1145	438	321	117	38	28	10

Table 6.2(b) Estimation of SAASW intrusions using the METEOSAT satellite series. T: Total number of available images; NU: Total number of useful images; WI: Total number of useful images with SAASW intrusions; N: Normal intrusions; E: Double intrusions; OF: Occurrence frequency of all the intrusions; OFN: Occurrence frequency of the normal intrusions; OFE: Occurrence frequency of multiple intrusions.

Although some intrusions and even extreme intrusion events were observed in 1982, they were from photographic images and of varying scale. They were, therefore, unsuitable for serial composite drawing.

The proportion of useful images with SAASW intrusions was found to be 38 % (Table 6.2 (b)). To calculate the reliability of this estimate, the statistical method described by Underhill (1985) was used.

P, the estimate of the true 10 year proportion Π, were assumed to be approximately Normally distributed about Π, with a variance of $P(1-P)(N-n)/n(N-1)$ where N is the total number of days in the study period and n is the total number of useful images. From this the reliability of P as an estimate of Π can be calculated as:

$$\text{Reliability} = 1{,}96\sqrt{\frac{P(1-P)(N-n)}{n(N-1)}}$$

Substituting into the above equation it was found that P, which is 38 %, falls within 2,3 % of Π approximately 95 % of the time for the 10 year period for which satellite images were available. Therefore, it can be safely assumed that cold water intrusions south of Africa are present at the retroflection region approximately 38 % of the time.

It should be noted that n, the number of useful images, depends largely on the extent of cloud cover over the retroflection region and would, therefore be biased towards summer months. Analysis of the seasonal variability of this OF is, therefore, invaluable to support our estimate P. This will be done later in this section.

From Table 6.2 (b) 28 % of the intrusions were found to be of the kind judged to be normal while 10 % of the intrusions were believed to be of the extreme kind; judging from their lateral extent in the infrared images and categorized in the previous section. Thus extreme intrusions of SAASW are not as infrequent as originally thought. This

could be due to the fact that although one composite intrusion was observed during one particular year, it may show its effects on a number of infrared images.

The average yearly occurrence frequencies (OF) of the intrusions, as calculated from Equation 1 (Chapter 5) using METEOSAT images, are given in Figure 6.9. This figure shows two years of higher occurrence frequency (1983 and 1989) of approximately 50% and two years of lower frequency (1982 and 1990) of approximately 27%. A slight increase of approximately 42% within the occurrence frequency is evident in 1985 while the occurrence frequency for 1984, 1986, 1987, and 1988 seem to approximate the mean yearly frequency of 38% (dashed line).

Figure 6.9 also shows that the largest yearly increase in the frequency of SAASW intrusions occurred between 1982 and 1983 while the largest yearly decrease in the occurrence frequencies are found to have occurred between 1989 and 1990. The increase in the occurrence frequency between 1982 and 1983 seems to coincide with the 1982/1983 Pacific El Niño [Preston-Whyte and Tyson, 1988; Jury, 1992] while the peak at 1989 seems to coincide with the end of the 1988/1989 Pacific La Niña occurrence. This analysis of SAASW intrusion occurrence frequency therefore does not reflect the findings in the composite analysis; in particular the extreme Summers of 1983/ 1984 and 1986/ 1987 does not show any significant effect in Figure 6.9.

Since El Niño and La Niña occurrences are largely summer phenomena, it is instructive to consider the seasonal variation of these SAASW intrusions. The analysis of the seasonal frequency of these intrusions using the METEOSAT series is given in Table 6.3. January and February of a particular year is grouped with the December of the previous year and is analysed as Summer of the previous year. Thus DJF for 1981, for example, includes December 1981, January 1982 and February 1982.

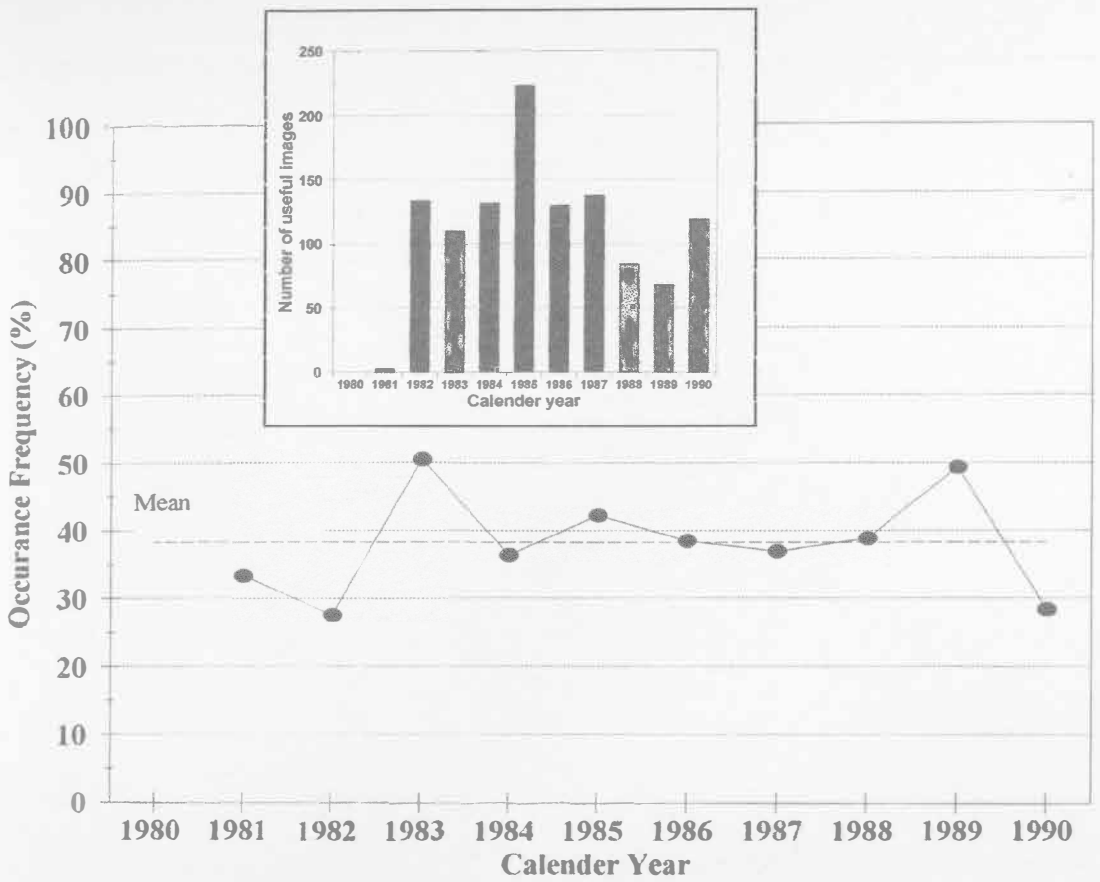

Figure 6.9. Yearly occurrence frequency of SAASW intrusion for all the years of the study period. The inset shows the yearly variation in the number of useful images per year for the 11 year study period. Dashed line denotes the 10 year mean OF.

	NU		WI		OF	
	JJA	DJF	JJA	DJF	JJA	DJF
1980						
1981		26		1		3.8
1982	33	6	9	1	9	16.6
1983	32	51	5	42	15.6	82.4
1984	25	60	12	21	48	35
1985	49	46	17	12	34.7	26
1986	29	50	10	15	34.5	30
1987	32	24	5	8	15.6	33.3
1988	21	29	7	11	33.3	37.9
1989	15	26	6	16	40	61.5
1990	29	51	12	33	41	64.7
Total	265	369	83	160	31.3	43.4

Table 6.3. Analysis of the seasonal frequency of SAASW intrusions. NU: Number of useful images, WI: Number of useful images with SAASW intrusions. JJA: June, July and August; DJF: December of that year, January and February of the next year. OF is given as a percentage.

On average, the total number of useful images is less in Winter (265) than in Summer (369) and the occurrence frequency of Winter (31 %) is less than that of Summer (43 %). The percentage of clear images is lower in winter than in summer due to the northward displacement of the STC (associated with persistent cloudiness) during Winter [Preston-White and Tyson, 1988]. Cloud cover should not, however, introduce bias in the estimate of occurrence frequency since division by the total number of cloud free images should normalize for this.

The yearly variation of the seasonal percentage occurrence of cold SAASW intrusions as calculated from Equation 2 (Chapter 5) is given on Figure 6.10. An increase in the occurrence frequency during 1982/1983 is evident in the peak for the 1983 summer. Following a sharp decrease in the winter percentage occurrence of SAASW in 1987 there has been a steady increase in the SAASW occurrence frequency during the remaining years of the study period in summer. This increase is only interrupted by a slight increase in frequency during the summer of 1988/1989.

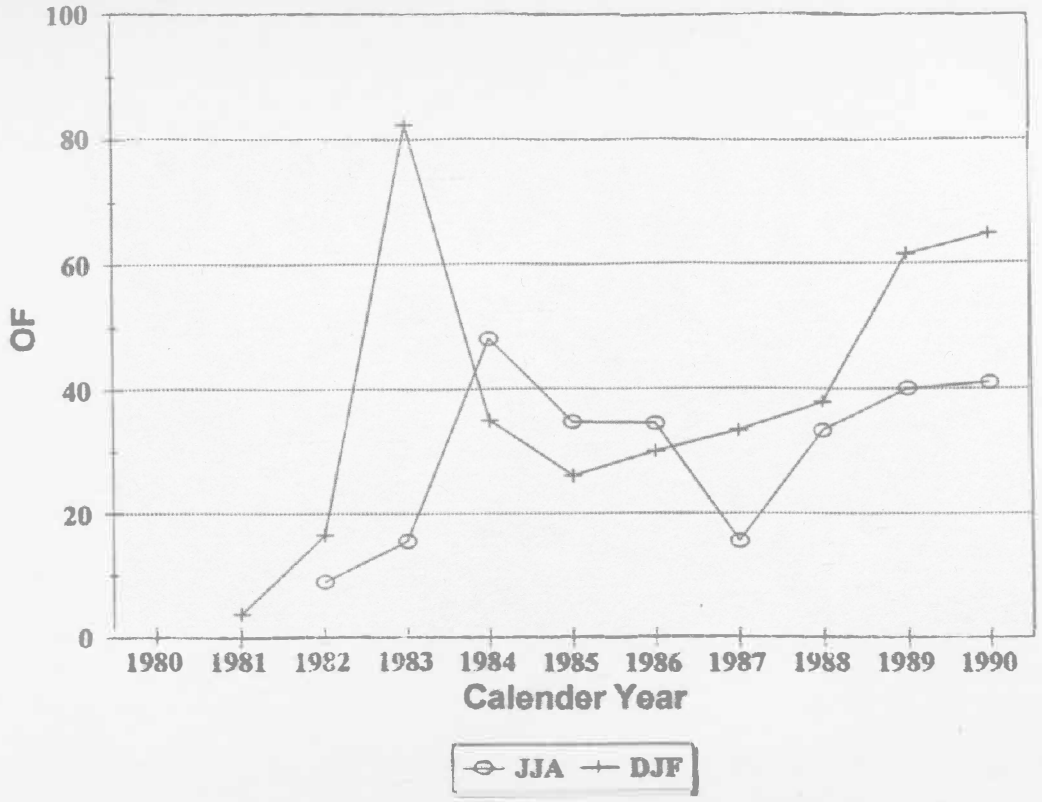

Figure 6.10. Seasonal distribution of SAASW occurrence frequency during the study period from 1981 to 1990. JJA: June July and August, DJF: December of the previous year and January and February of that year.

In general, the frequency of SAASW is higher in summer than in winter except during the period 1984 to 1986. The winter yearly frequency variation seems to mirror that of summer with a lag of one year from 1981 to 1985, judging from the similar shapes of the graphs during those years. A sharp increase was observed in 1984 and a distinct drop in the occurrence frequency is observed during the winter of 1987. After this sharp decrease in occurrence frequency, the Winter SAASW intrusion frequency seems to increase for the remaining years of the study period.

To investigate the lag relationship between Winter and Summer occurrence frequency a linear regression was performed. The correlations coefficients are plotted on Figure 6.11. Lag 0 means that the Winter OF was directly correlated to that of summer. A negative correlation means that the Winter OF was shifted 6 months back and correlated to that of

summer. A positive correlation means that the winter OF was shifted 6 months ahead and correlated to that of Summer.

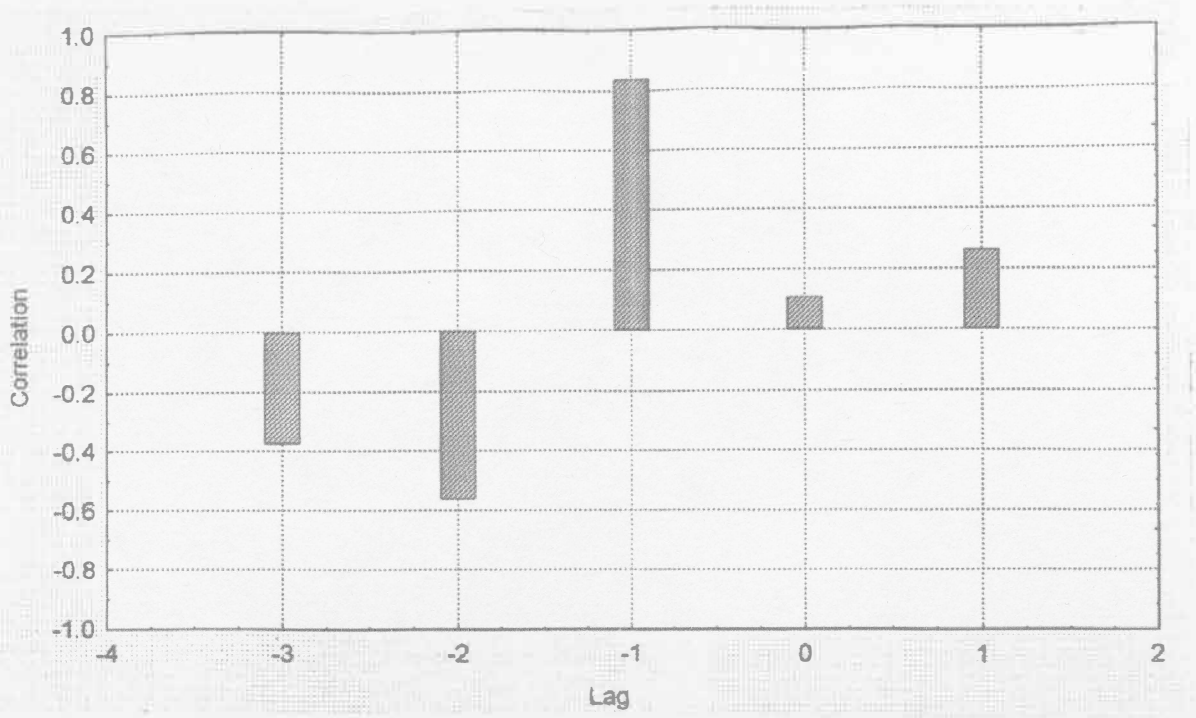

Figure 6.11 Plot of correlation coefficients against lag (in 6 month intervals) for the regression of summer OF against winter OF.

Figure 6.11 shows, judging from the correlation coefficients alone, that there is a near linear relationship between the occurrence frequency of cold water intrusion in summer and that of cold water intrusion frequency of the subsequent winter (Lag –1 has a significance of <0,025 for correlation coefficient of 0,84). This relationship is even more dramatically shown in Figure 6.12, plotting the correlation scatter plots for winter/summer and for lags –2 to 0. At lag –2 and 0 a very wide 95% confidence interval was observed and the correlation coefficient r seems to show little relationship between the winter and summer OF. However, the scatter plot for lag –1, shows a very high correlation, a very narrow confidence interval and a near linear scatter plot of points.

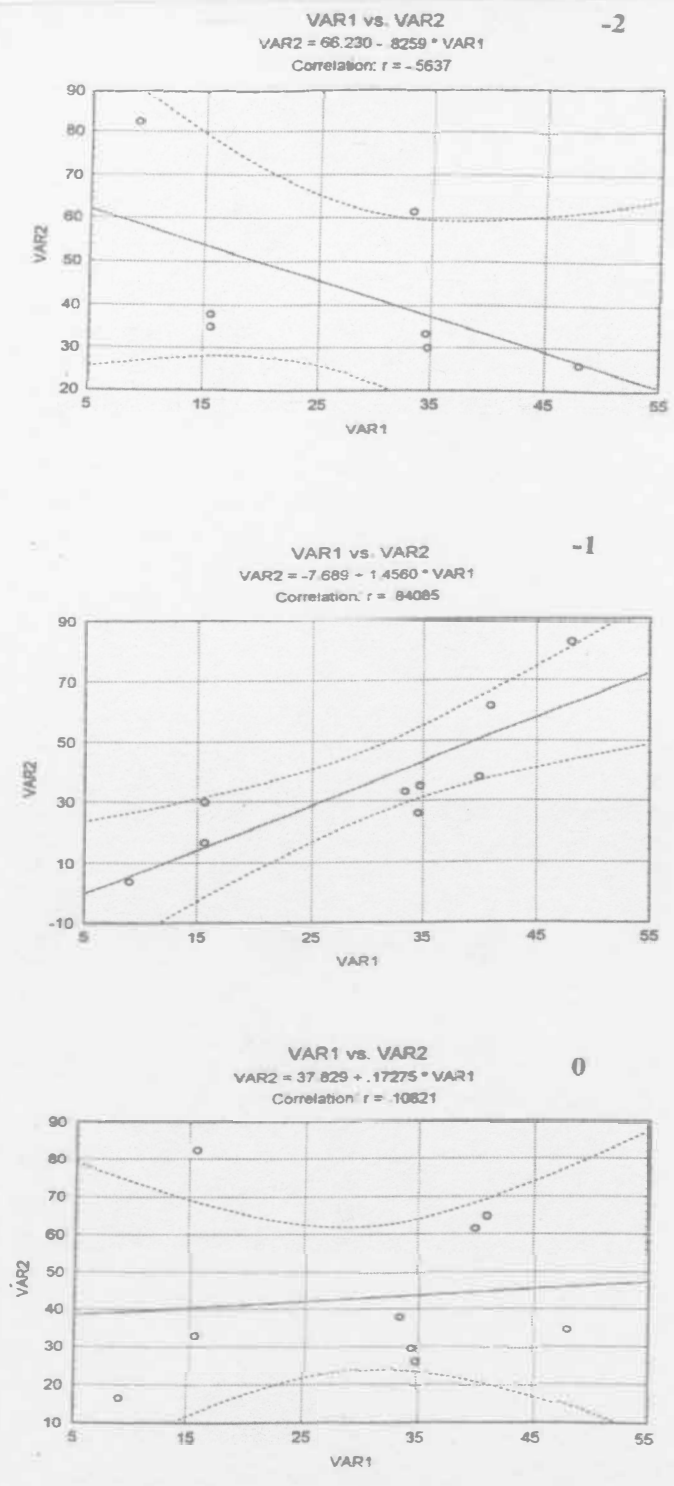

Figure 6.12 Scatter plots for the regression analysis of OF in Summer against the OF in winter of cold water intrusions observed *via* satellite remote sensing for lags –2, -1 and 0 respectively. The dashed lines indicate the 95% confidence interval. VAR1= OF in winter. VAR2= OF in summer.

This means that it is possible to predict the OF in winter (OFW) based on the occurrence frequency of the previous summer (OFS) from:

$$OFW=12,6+0,5(OFS)$$

A possible link between the advent of a Pacific El Niño and an increase in the frequency of SAASW intrusions was suggested earlier. It would therefore be instructive to consider environmental and oceanic changes around Southern Africa during El Niño and La Niña events.

El Niño can be described as a perturbation within a linked series of zonal circulation cells known collectively as the Walker circulation [Preston-Whyte and Tyson, 1988]. This cell is directly responsive to sea surface temperatures over the eastern and western Pacific Ocean. As these SSTs change a major pressure oscillation (the Southern Oscillation) is set up between the Indian and Pacific oceans. This oscillation is measured by observing the air pressure difference between Tahiti and Darwin at the western and eastern Pacific Ocean respectively.

During the Southern Oscillation high phase (positive temperature difference) the SST at Indonesia is high and the upper level pressure falls. The opposite occurs at Darwin (the eastern Pacific). The Walker circulation then has the characteristics indicated in Figure 6.13(a). During the low phase of the Oscillation the SST in the eastern Pacific undergoes an increase to the extent that the pressure gradient between that region and Indonesia reverses and the Walker circulation cell weakens or reverses as shown on Figure 6.13(b).

The implications of the Southern Oscillation low phase (El Niño) for South Africa is that the zone of convergence and ascent (cloud formation and rain) over eastern Africa moves eastward out to sea over the Indian ocean and descending, divergent air (associated with drought) sets in over South Africa. The most extreme El Niño experienced in this

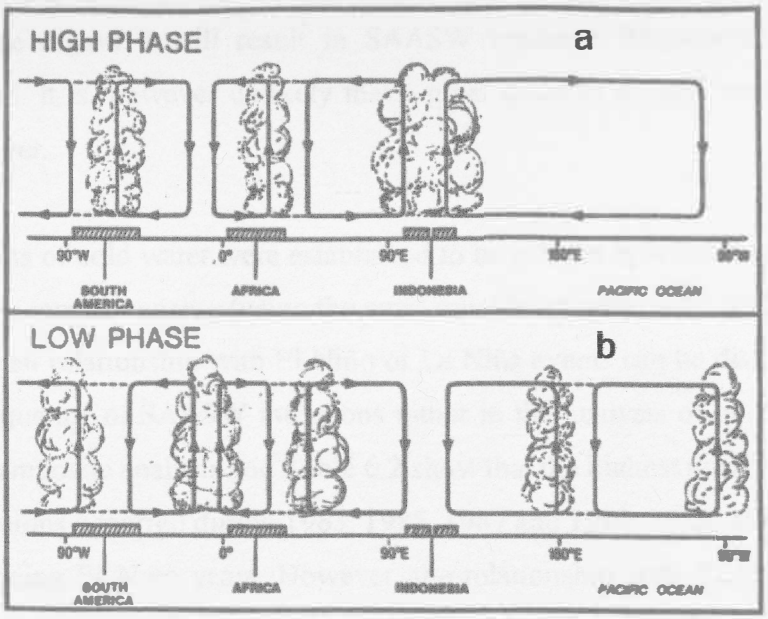

Figure 6.13 The Walker circulation during the Southern Oscillation high and low phase [Preston-Whyte and Tyson, 1988 after Lindesay, 1987].

century was the 1982/1983 event and was associated with catastrophic droughts in South Africa [Preston-Whyte and Tyson, 1988].

During the Southern Oscillation high phase, however, cloud bands are located preferentially over southern Africa and rainfall is higher. An intensified high phase El Niño (La Niña) [e.g. Jury, 1990] is not as common as a low phase El Niño and usually follows some El Niños.

Therefore El Niño may affect cloud cover over the study period; the high phase causing more cloud cover while the low phase may cause less cloud cover. Again, the effect of cloud cover in the calculation of SAASW occurrence frequency has been dealt with by division by the number of cloud free images. Moreover, it is unlikely that El Niño or La Niña events will directly influence SAASW intrusions at the oceanic level in the region southwest of Africa.

Another possibility for possible bias in the estimate of SAASW intrusion occurrence may be within the assumption of the independence of SAASW intrusions to the total number

of cloud free images. If it can be shown that SAASW intrusion may in fact cause cloud cover over the region it will result in SAASW intrusion frequencies being highly underestimated. It is, however unlikely that a great expanse of cold water could cause such cloud cover.

Thus, intrusions of cold water were established to be present approximately 38 % of the time in satellite remote sensing (using the more reliable estimate from METEOSAT). No evidence of their relationship with El Niño or La Niña events can be discerned from the individual frequency of SAASW intrusions either in the analysis of normal or extreme events. The composite analysis and Table 6.2 show that the highest number of individual SAASW intrusions occurred during 1983, 1985, 1987 and 1990; 1983, 1987 and to some extent 1990 being El Niño years. However, the relationship with El Niño or La Niña seems rather tentative. A longer study period could perhaps shed more light on this connection between SAASW intrusions and advents of El Niño and La Niña.

The duration of SAASW intrusions can not be satisfactorily established through infrared remote sensing where persistent cloud cover in the study area makes serial tracking of these intrusions nearly impossible. The use of altimetry in ocean science has been proven very useful on various occasions [*e.g.* Gordon and Haxby, 1990]. This oceanographic tool was used to determine the persistence of the cold SAASW intrusions at the retroflection region and will be discussed in the next chapter.

Chapter 7

Altimetry

In establishing the lateral dimensions and especially the occurrence frequency of these cold water intrusions, the problem of cloud cover in the region was a considerable hindrance for concrete findings. The advent of satellite altimetry as well as its easy availability makes serial tracking of cold water intrusions possible. The altimeter on board the TOPEX- POSEIDON does not suffer from the disadvantages of infrared remote sensing in light of the fact that cloud cover does not affect it. This chapter attempts to determine the residence time of SAASW intrusions at the Agulhas Retroflection.

Sea surface height anomalies are readily available *via* the Internet and at reasonable time intervals as explained in Chapter 5. However, the altimeter data falls outside the study period used thus far of 1980 to 1990. Sea surface height anomaly diagrams are available from May 1994 to October 1997. Therefore, SAASW intrusion events during the period May 1994 to October 1997 were selected through their thermal expression in satellite infrared sensing and were used to determine the persistence of these intrusion events at the Agulhas Retroflection region through the use of their sea surface height anomaly expression.

Figure 7.1 shows the thermal expression of two broad intrusions of SAASW intrusions southwest of Africa on 3 May 1994. These intrusions were followed using altimetric information from TOPEX-Poseidon/ ERS and the serial diagram is given in Figure 7.2.

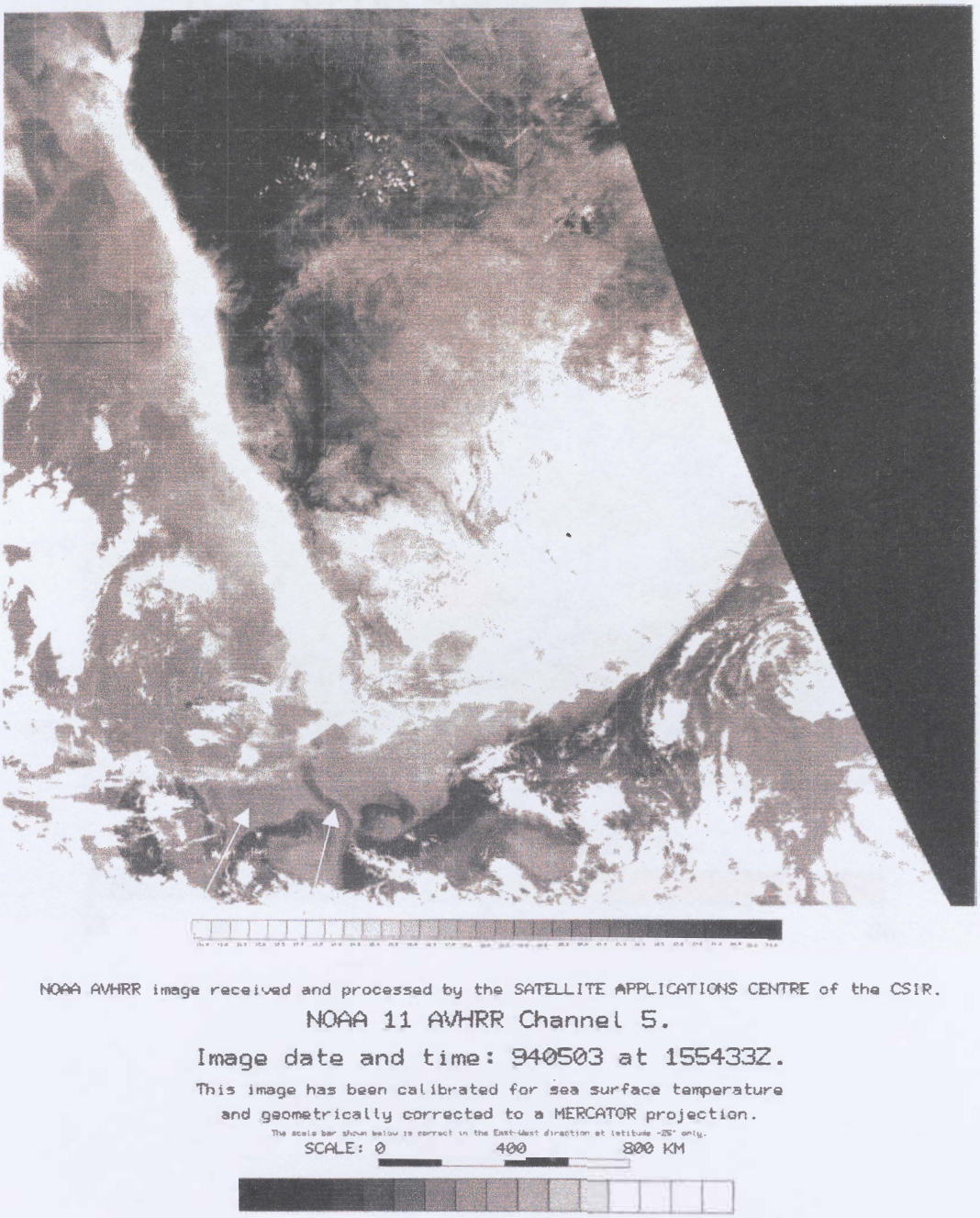

Figure 7.1 Thermal infrared NOAA AVHRR image of the sea surface around Southern Africa on 3 May 1994. This image was calibrated for absolute temperatures and geometrically corrected to a Marcator projection. The white arrows indicate the paths of the SAASW intrusions. [Received and processed by the Satellite Applications Centre at the CSIR].

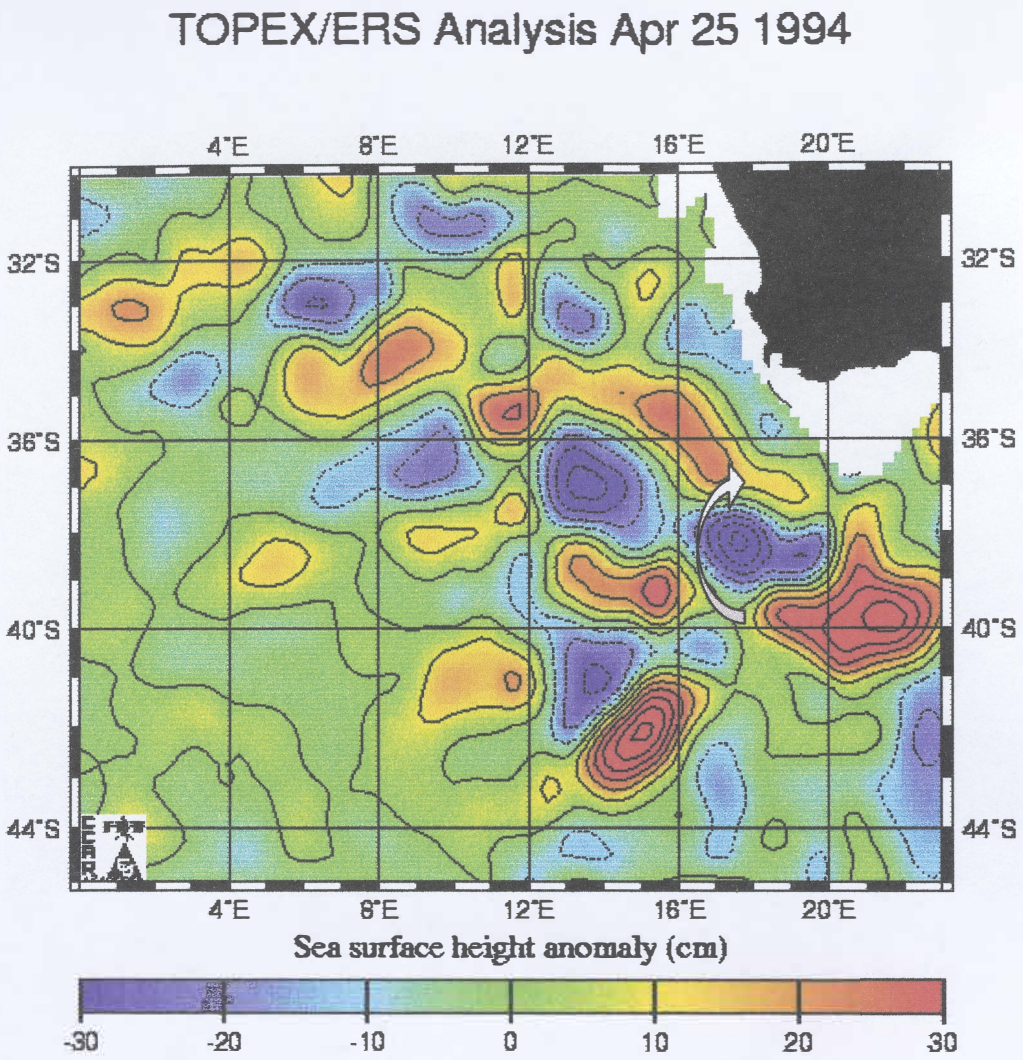

Figure 7.2. Sea surface height anomalies for the oceanic environment southwest of Africa for the region 0 °E to 21 °E and 30 °S to 45 °S. Areas shallower than 200m are coloured white around the coastline. The series spans the period 25 April 1994 to 15 May 1994. The cold water intrusion is indicated by a broad, white arrow.

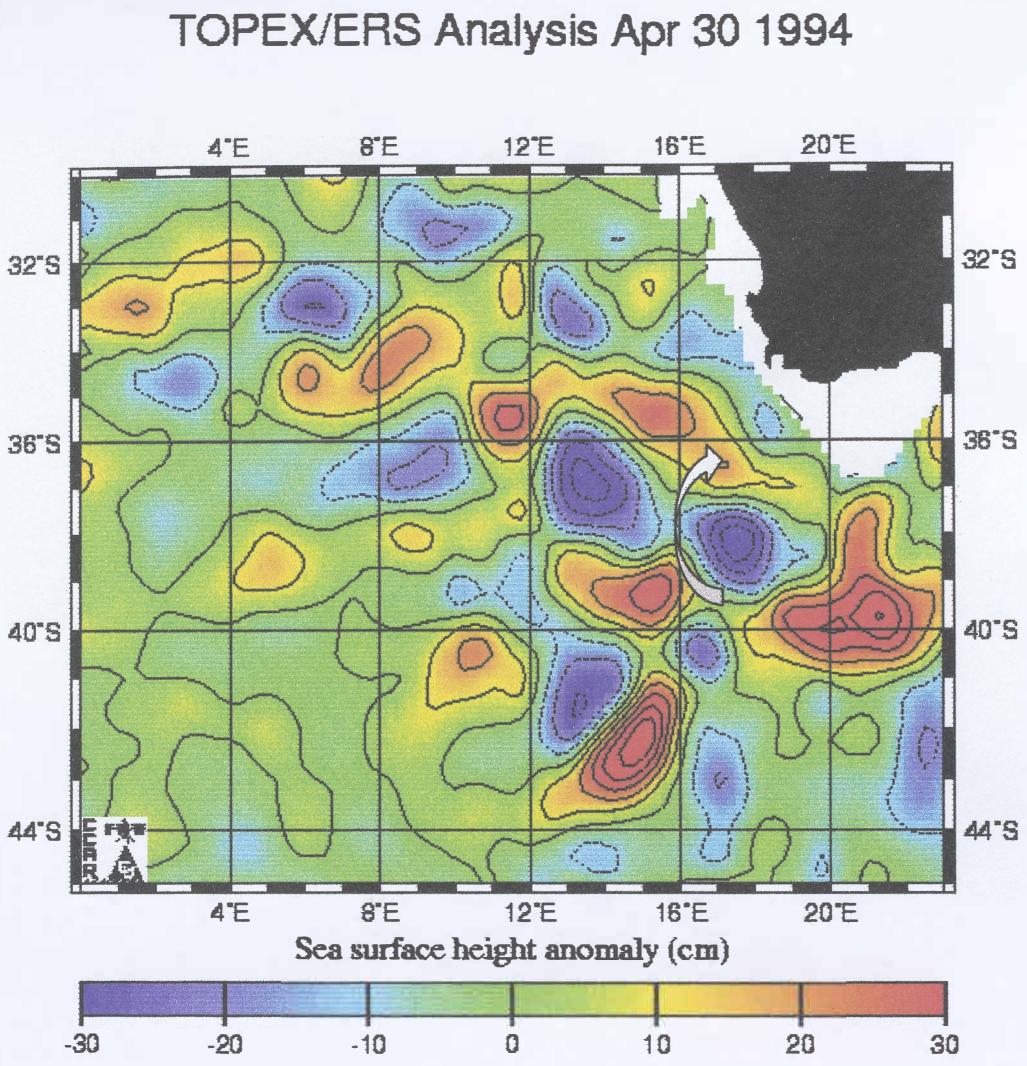

Figure 7.2. Sea surface height anomalies for the oceanic environment southwest of Africa for the region 0 °E to 21 °E and 30 °S to 45 °S. Areas shallower than 200m are coloured white around the coastline. The series spans the period 25 April 1994 to 15 May 1994 *Continued...*

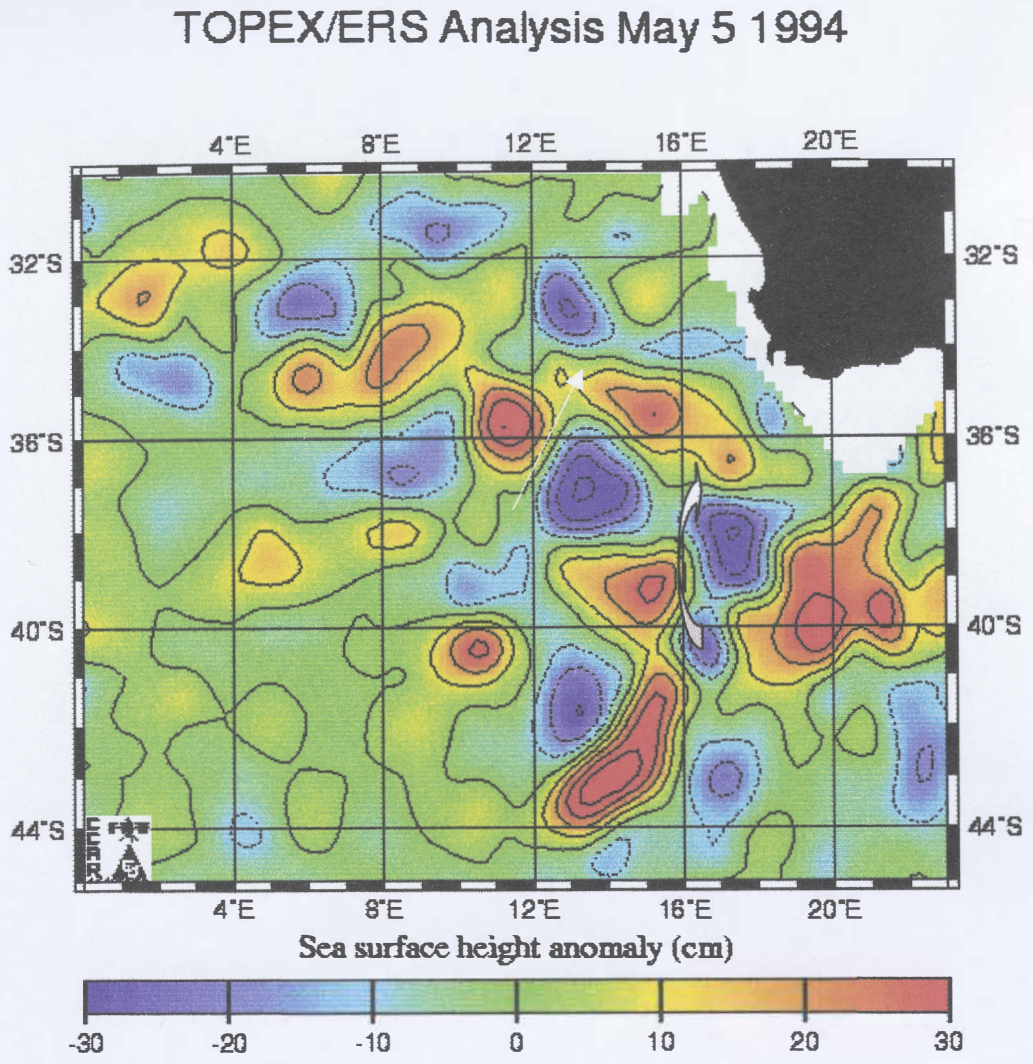

Figure 7.2. Sea surface height anomalies for the oceanic environment southwest of Africa for the region 0 °E to 21 °E and 30 °S to 45 °S. Areas shallower than 200m are coloured white around the coastline. The series spans the period 25 April 1994 to 15 May 1994 *Continued...*

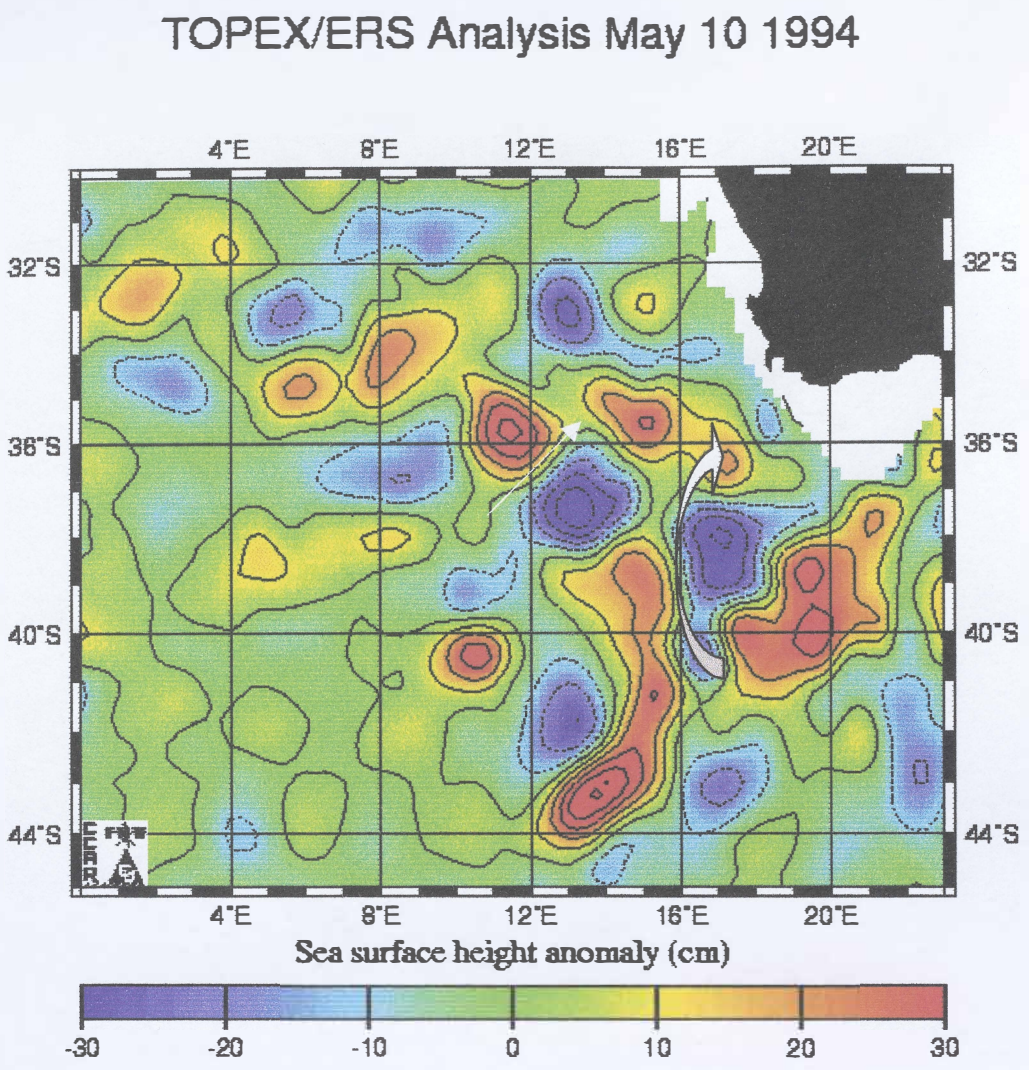

Figure 7.2. Sea surface height anomalies for the oceanic environment southwest of Africa for the region 0 °E to 21 °E and 30 °S to 45 °S. Areas shallower than 200m are coloured white around the coastline. The series spans the period 25 April 1994 to 15 May 1994 *Continued...*

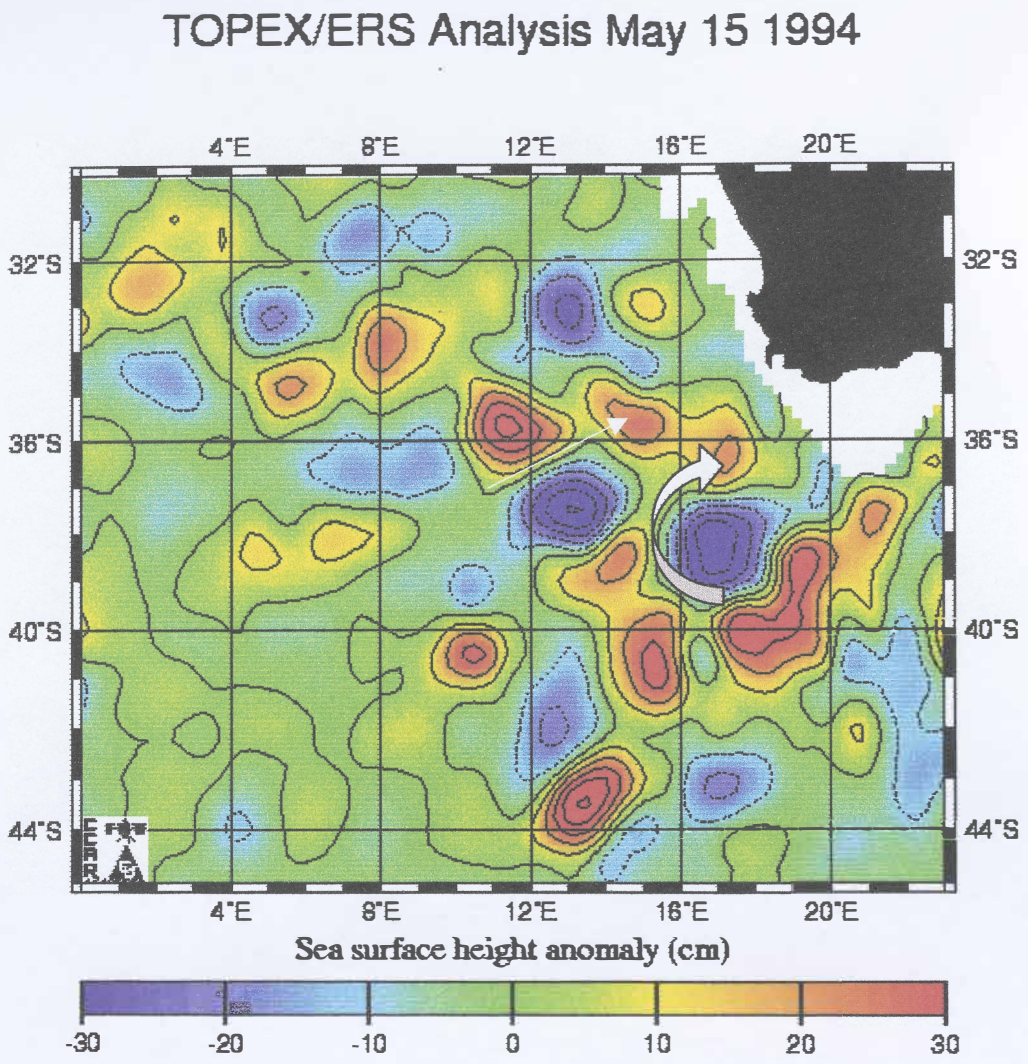

Figure 7.2. Sea surface height anomalies for the oceanic environment southwest of Africa for the region 0 °E to 21 °E and 30 °S to 45 °S. Areas shallower than 200m are coloured white around the coastline. The series spans the period 25 April 1994 to 15 May 1994 *Continued...*

In Figure 7.2 the cold water intrusion appears as an elongated very low sea surface height anomaly at ~ 18 °E, 30 °S on 5 May , 1994. This elongated anomaly is also present on 10 May 1994. It appears from these anomaly charts that the intrusion probably started at around 25 April 1994 and lasted about 20 days to 15 May 1994. On 25 April 1994, a negative or cyclonic perturbation in the oceanic flow field was observed at about 19 °E, 39 °S just west of the anticyclonic movement of water associated with the Agulhas Retroflection, directly south of the continent at about 40 °S. This cyclonic surface anomaly persisted right through to the satellite image date of 3 May 1994 (Figure 7.1), approximated by the anomaly map of 5 May 1994. No pronounced cyclonic/ anticyclonic circulation conducive to northward movement of water was observed beyond 15 May 1994.

The second example of a SAASW intrusion at the Agulhas retroflection is presented in the thermal infrared satellite image of 27 December 1994 in Figure 7.3. This image shows a narrow intrusion of cold water southwest of the continent and its altimetric expression is given in the serial sea surface anomaly map of Figure 7.4.

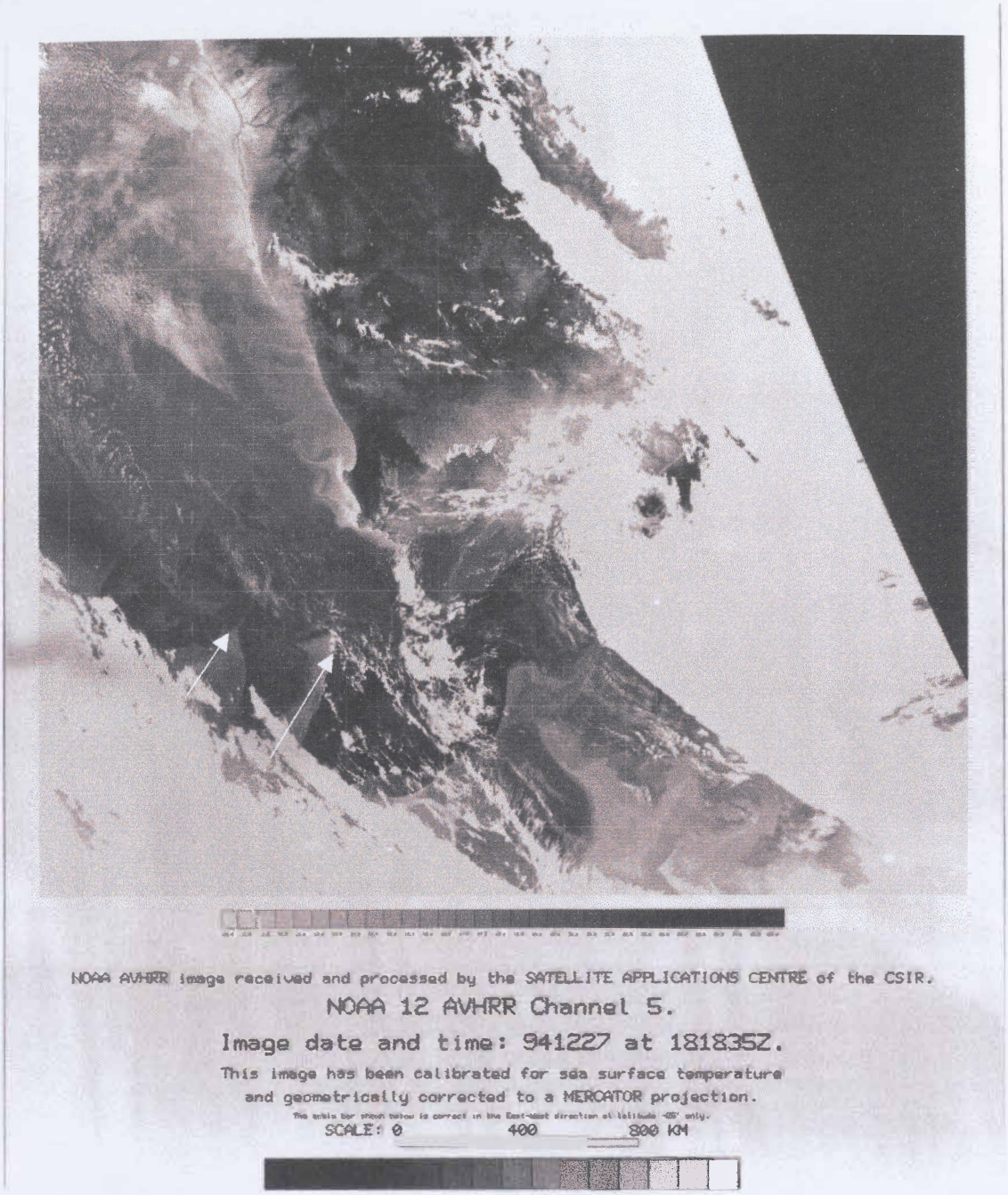

Figure 7.3 Thermal infrared NOAA AVHRR image of the sea surface around Southern Africa on 27 December 1994. This image was calibrated for absolute temperatures and geometrically corrected to a Marcator projection. The white arrow indicates the paths of the SAASW intrusions. [Received and processed by the Satellite Applications Centre at the CSIR].

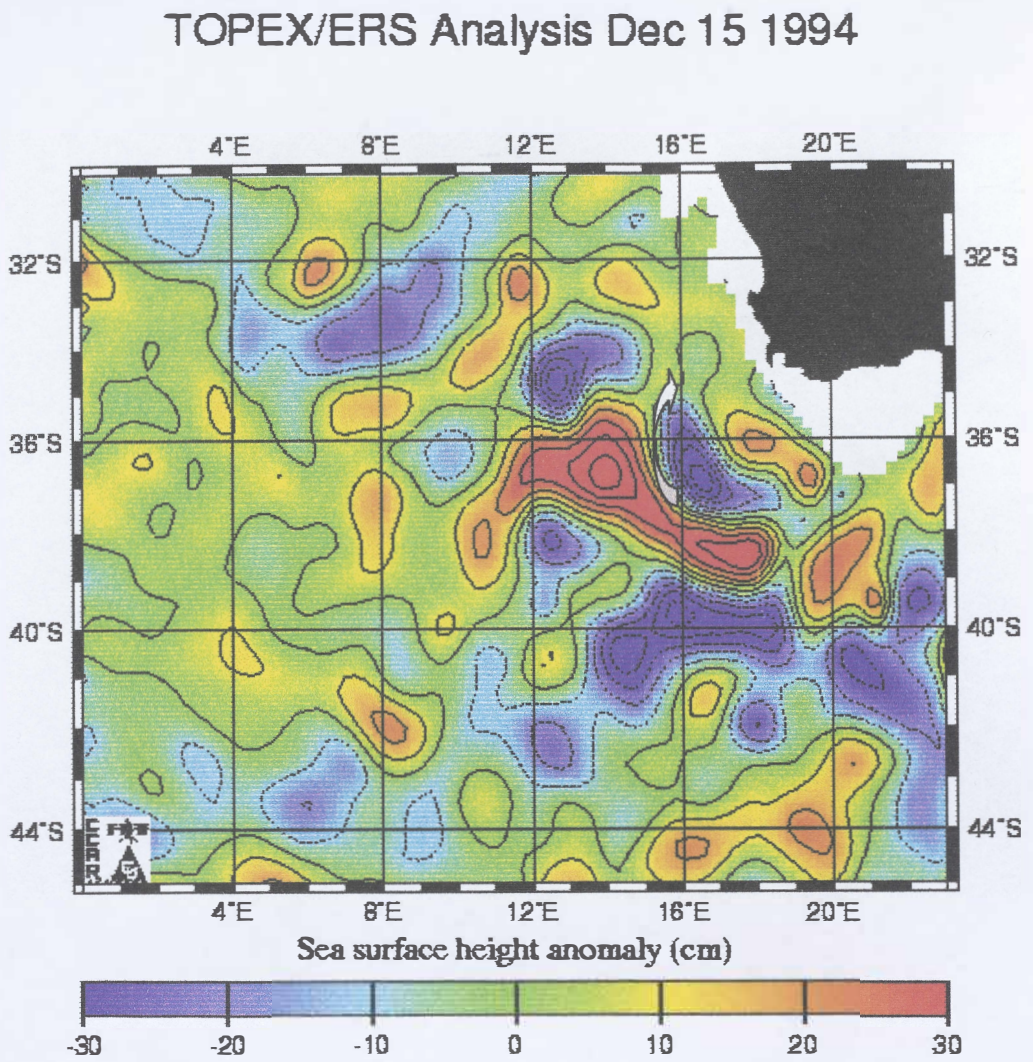

Figure 7.4. Sea surface height anomalies for the oceanic environment southwest of Africa for the region 0 °E to 21 °E and 30 °S to 45 °S. Areas shallower than 200m are coloured white around the coastline. The series spans the period 15 December 1994 to 10 January 1995. The white arrows indicate the path of cold intrusions.

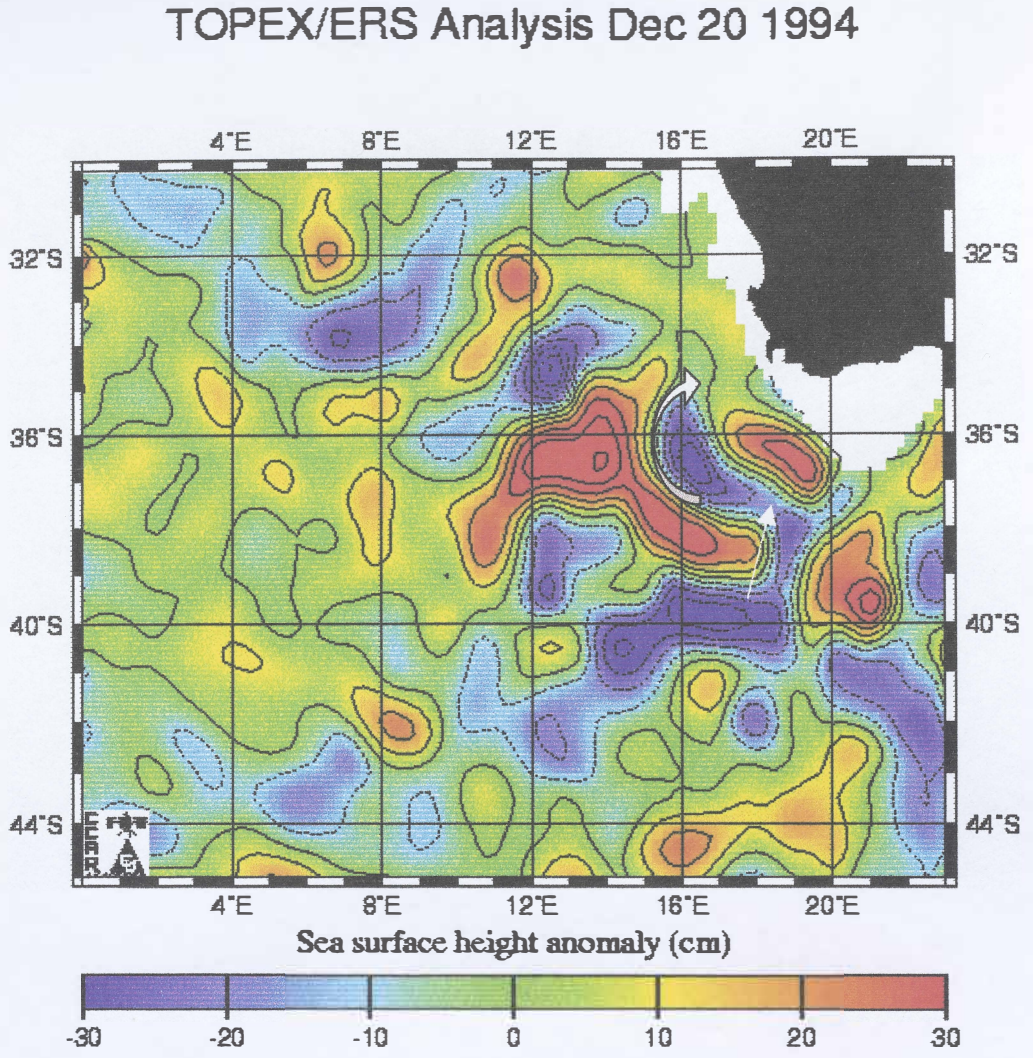

Figure 7.4. Sea surface height anomalies for the oceanic environment southwest of Africa for the region 0 °E to 21 °E and 30 °S to 45 °S. Areas shallower than 200m are coloured white around the coastline. The series spans the period 15 December 1994 to 10 January 1995. *Continued...*

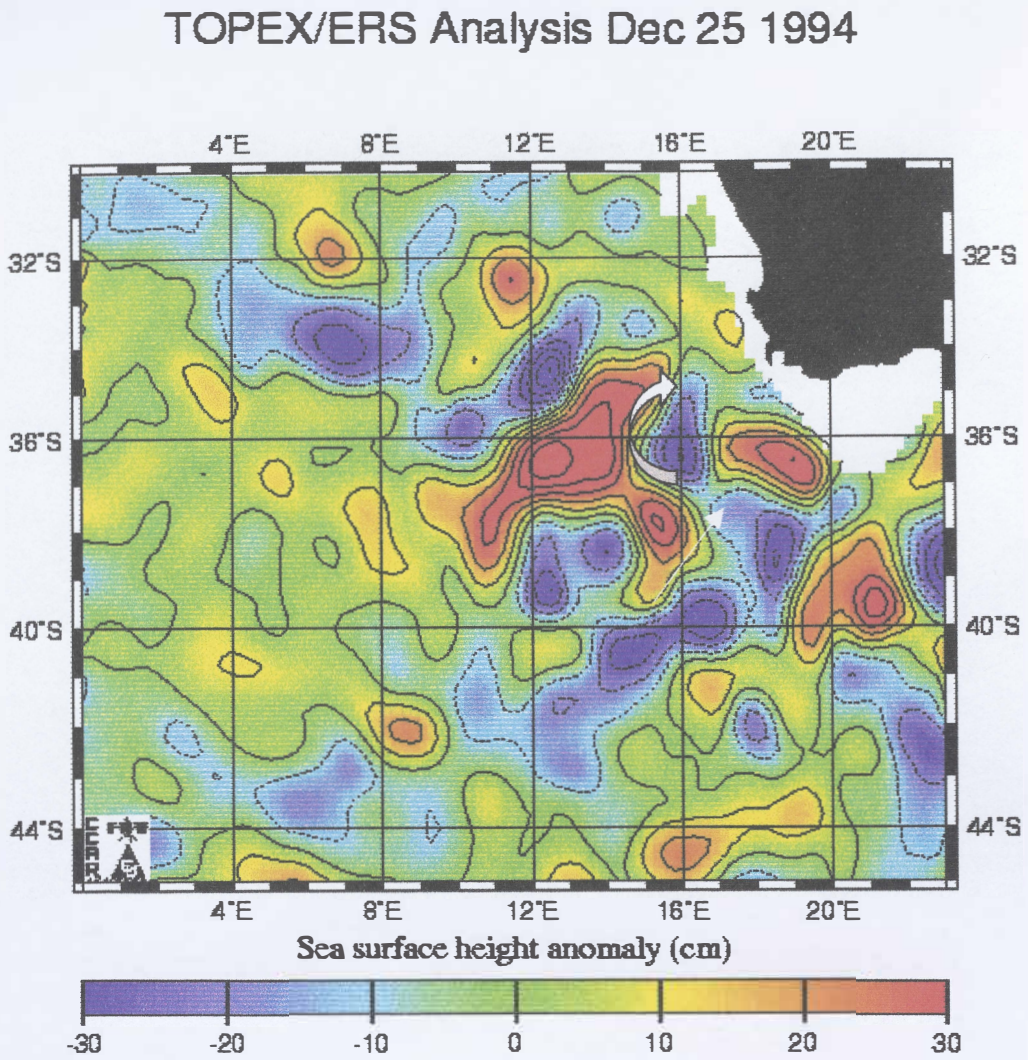

Figure 7.4. Sea surface height anomalies for the oceanic environment southwest of Africa for the region 0 °E to 21 °E and 30 °S to 45 °S. Areas shallower than 200m are coloured white around the coastline. The series spans the period 15 December 1994 to 10 January 1995. *Continued...*

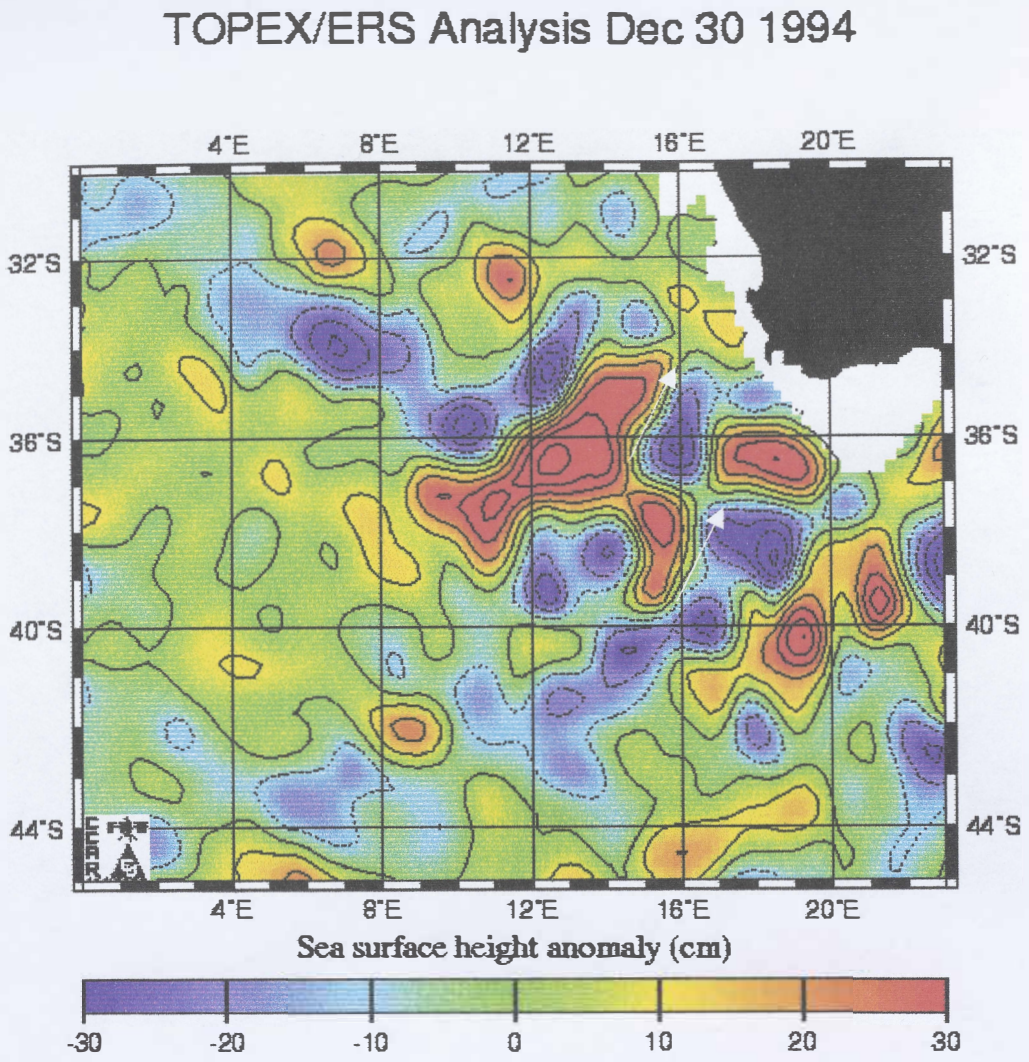

Figure 7.4. Sea surface height anomalies for the oceanic environment southwest of Africa for the region 0 °E to 21 °E and 30 °S to 45 °S. Areas shallower than 200m are coloured white around the coastline. The series spans the period 15 December 1994 to 10 January 1995. *Continued...*

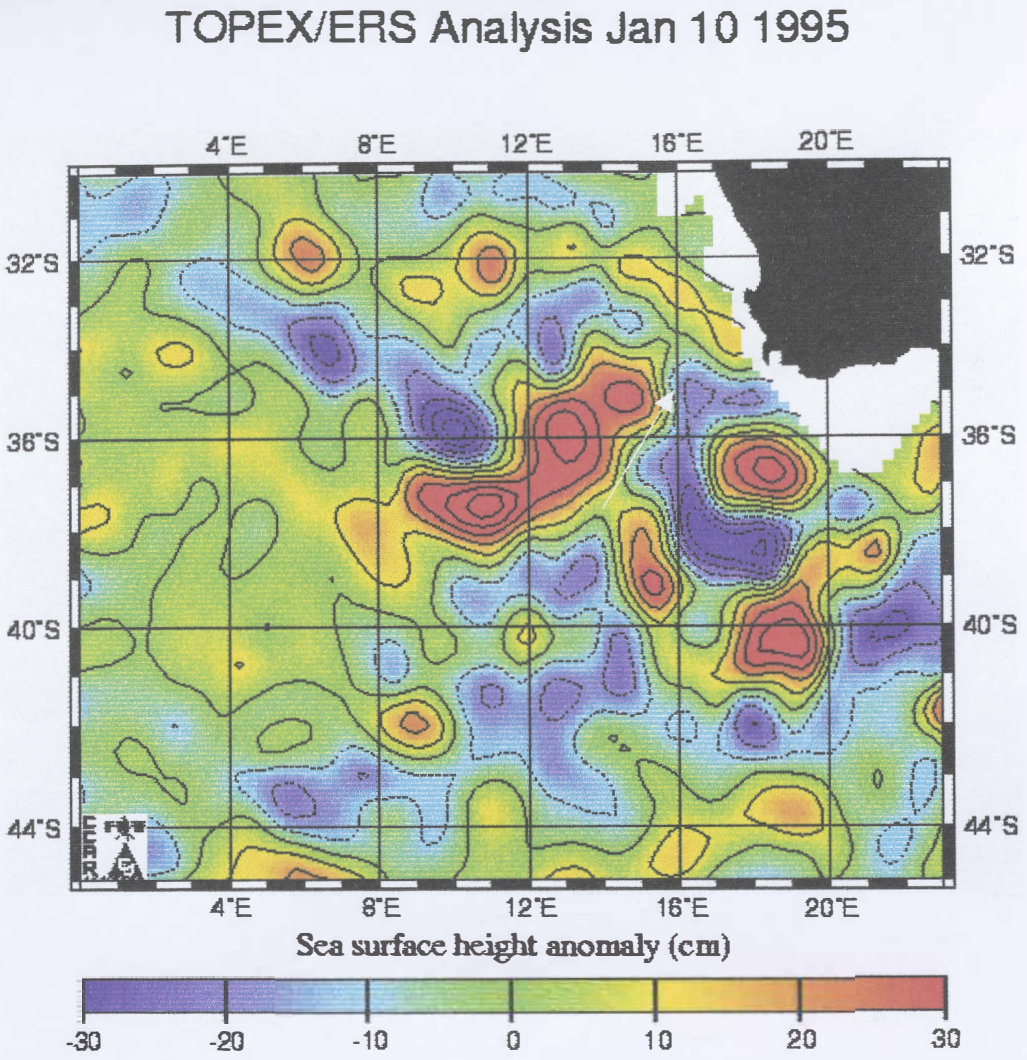

Figure 7.4. Sea surface height anomalies for the oceanic environment southwest of Africa for the region 0 °E to 21 °E and 30 °S to 45 °S. Areas shallower than 200m are coloured white around the coastline. The series spans the period 15 December 1994 to 10 January 1995. *Continued...*

The image of the sea surface anomalies (Figure 7.4) shows the same elongated negative sea surface height anomaly at ~ 19 °E, 40 °S as observed in Figure 7.2. From the series it appears as if the cyclonic anomaly probably formed at around 15 December 1994, started growing on 20 December 1994 and took on its elongated form on about 20 December 1994. No cyclonic-anticyclonic anomalous circulation is seen after 10 January 1995. The estimate of the persistence of this intrusion of SAASW is therefore 25 days.

The third example of SAASW intrusion is presented in Figure 7.5. This figure shows a broad intrusion of cold water in the thermal infrared on 11 December 1995 and its altimetric expression series is presented on Figure 7.6.

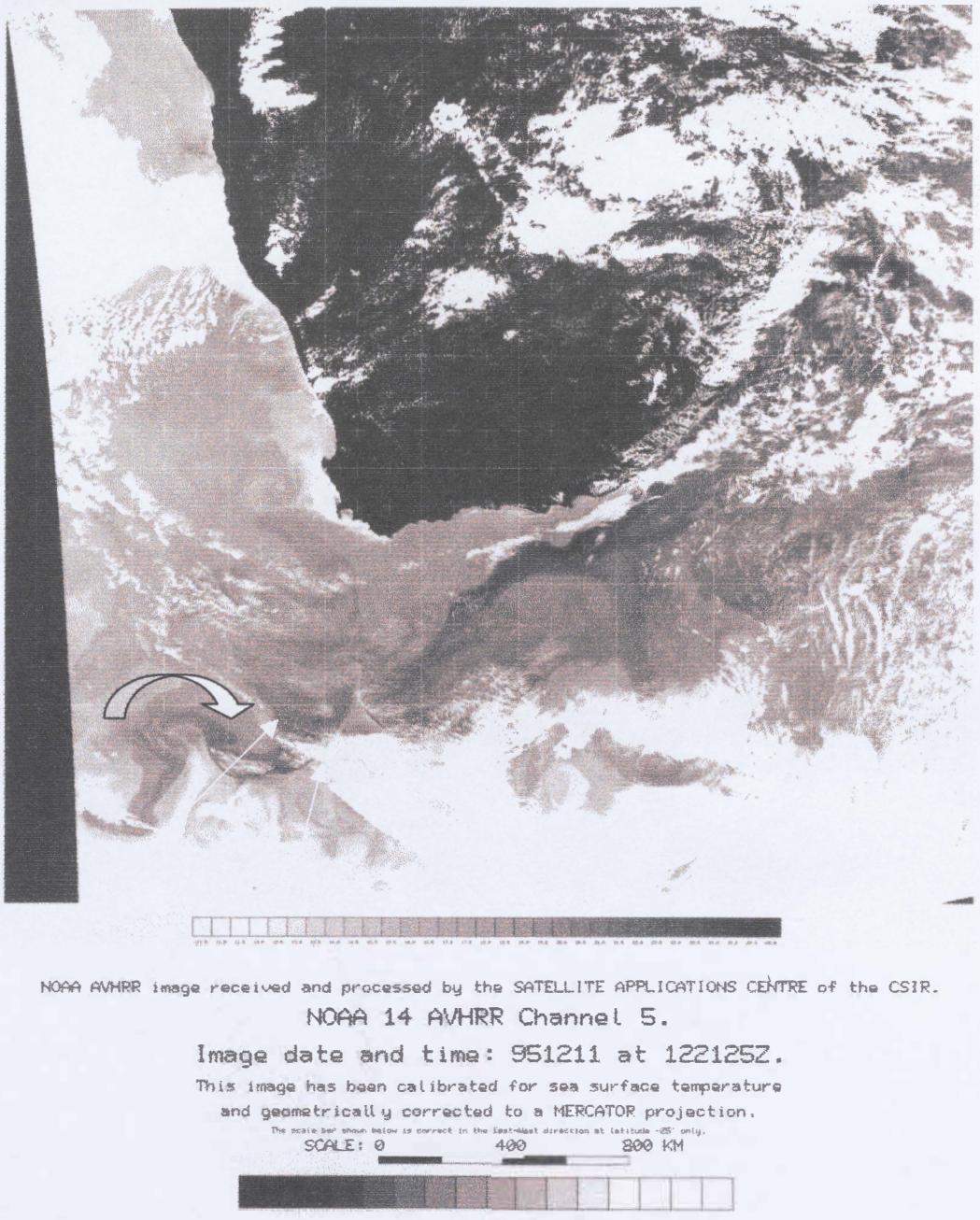

Figure 7.5 Thermal infrared NOAA AVHRR image of the sea surface around Southern Africa on 11 December 1995. This image was calibrated for absolute temperatures and geometrically corrected to a Marcator projection. The white arrow indicates the paths of the SAASW intrusions. [Received and processed by the Satellite Applications Centre at the CSIR].

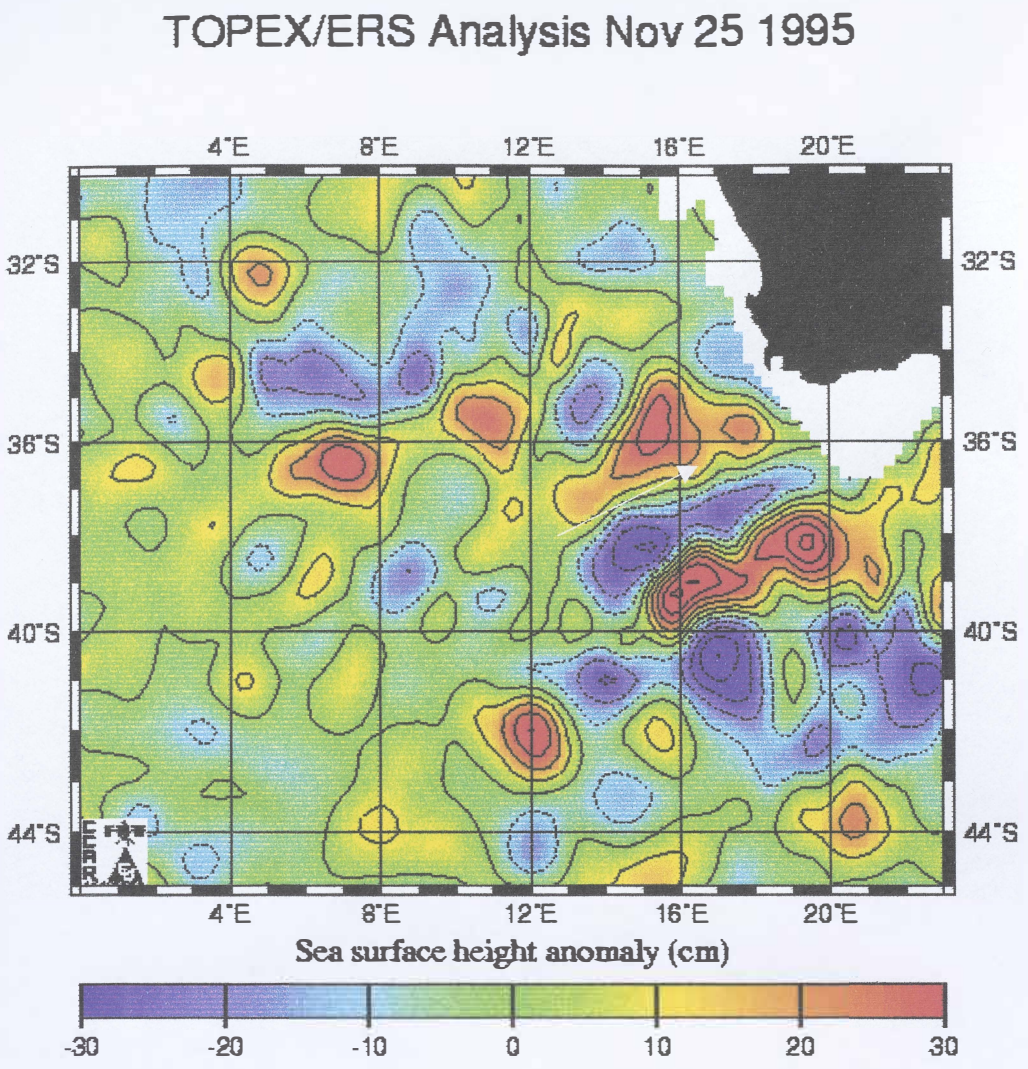

Figure 7.6 Sea surface height anomalies for the oceanic environment southwest of Africa for the region 0 °E to 21 °E and 30 °S to 45 °S. Areas shallower than 200m are coloured white around the coastline. The series spans the period 25 November 1995 to 10 January 1996. The arrows indicate the paths of cold water intrusions.

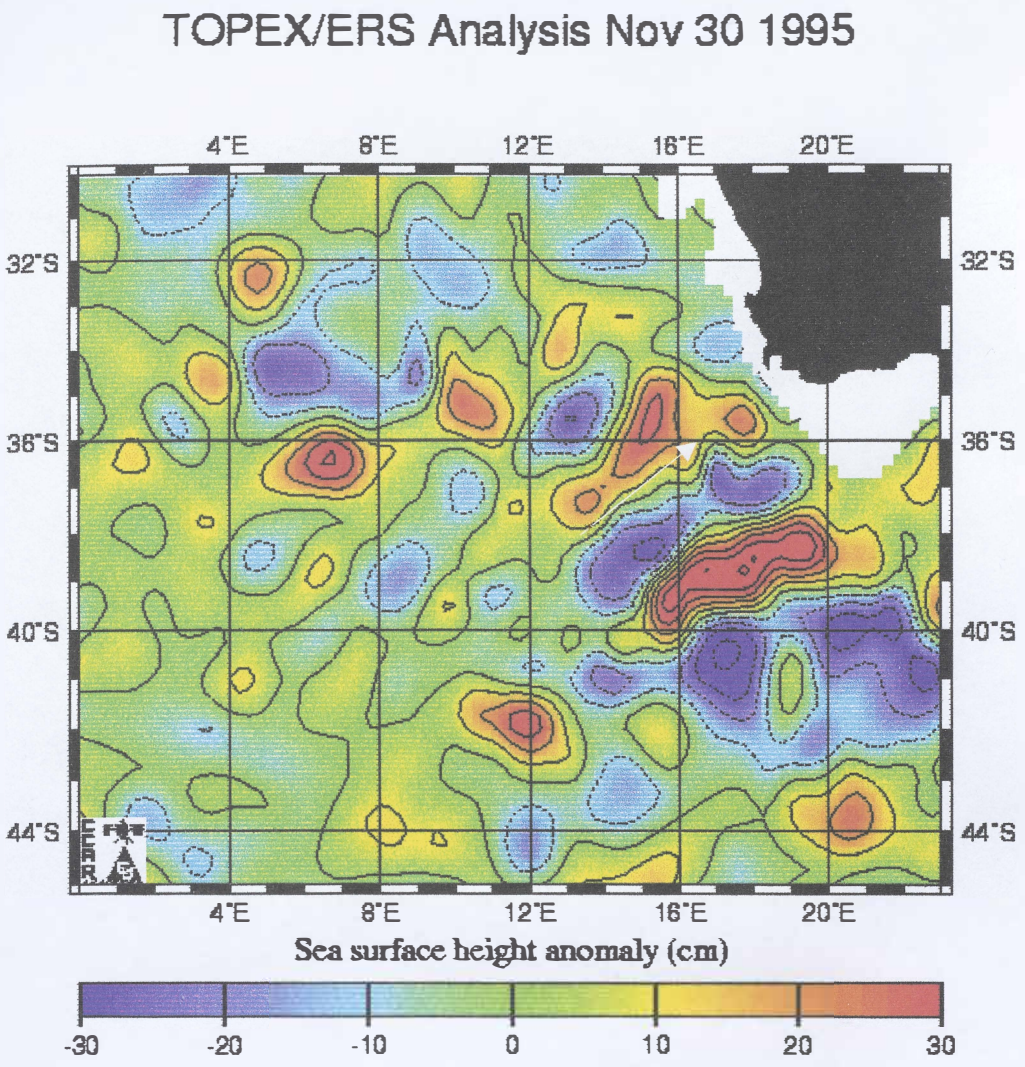

Figure 7.6 Sea surface height anomalies for the oceanic environment southwest of Africa for the region 0 °E to 21 °E and 30 °S to 45 °S. Areas shallower than 200m are coloured white around the coastline. The series spans the period 25 November 1995 to 10 January 1996. *Continued...*

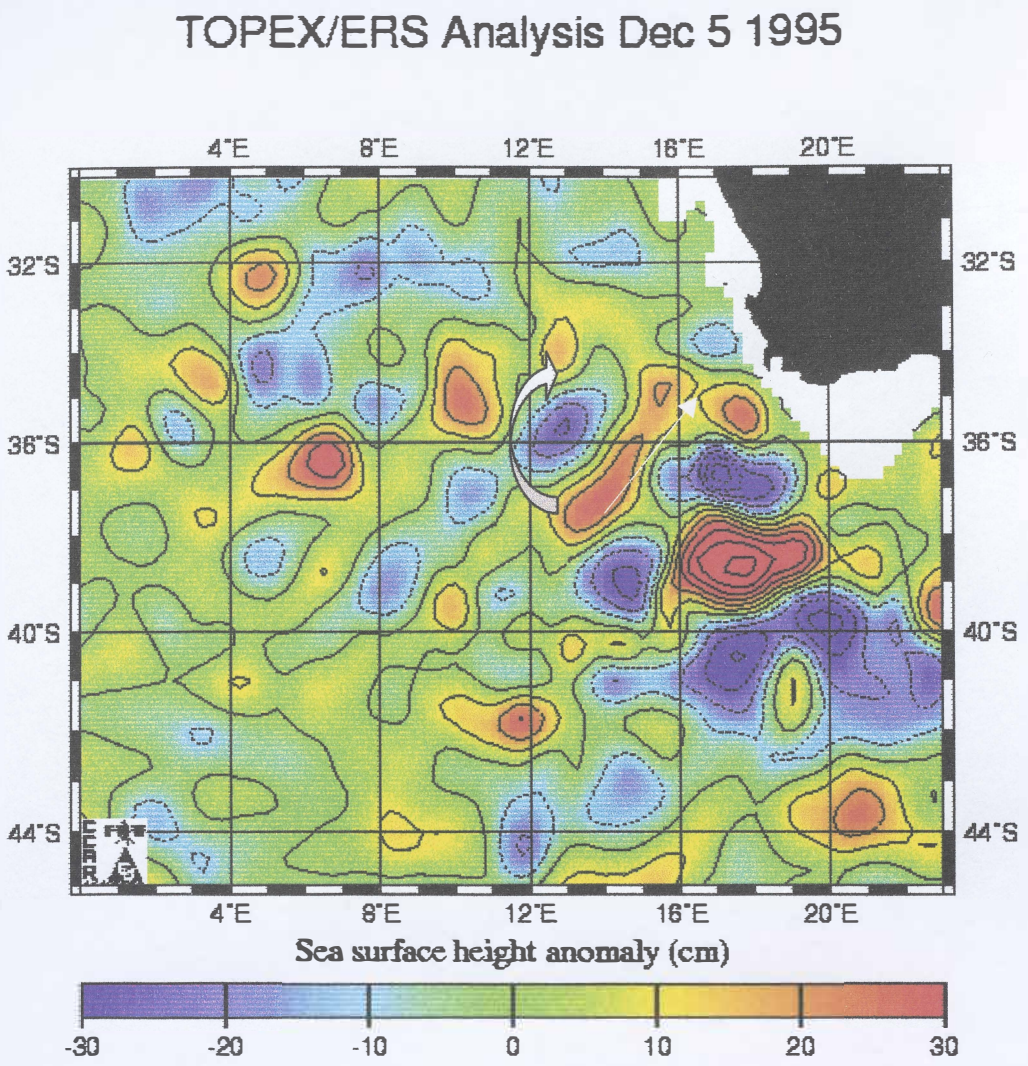

Figure 7.6 Sea surface height anomalies for the oceanic environment southwest of Africa for the region 0 °E to 21 °E and 30 °S to 45 °S. Areas shallower than 200m are coloured white around the coastline. The series spans the period 25 November 1995 to 10 January 1996. *Continued...*

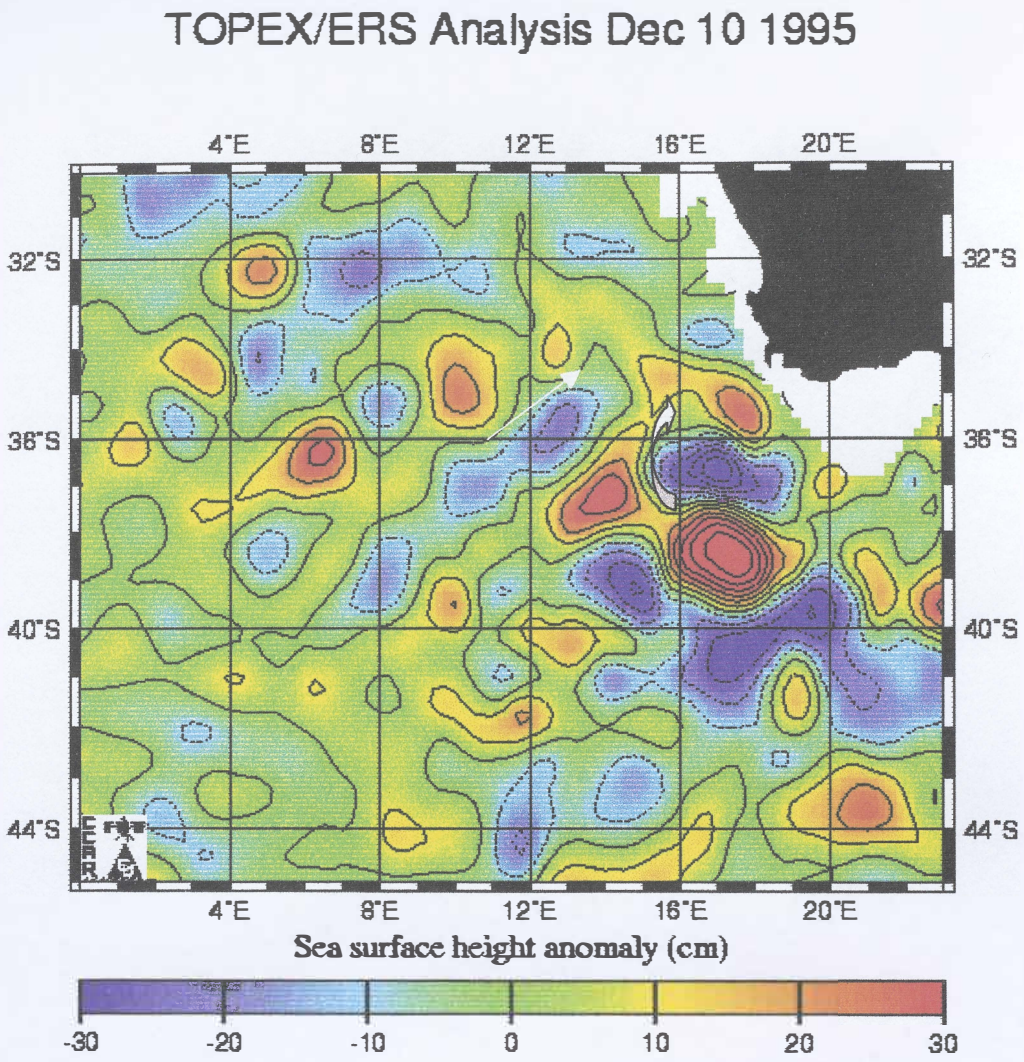

Figure 7.6 Sea surface height anomalies for the oceanic environment southwest of Africa for the region 0 °E to 21 °E and 30 °S to 45 °S. Areas shallower than 200m are coloured white around the coastline. The series spans the period 25 November 1995 to 10 January 1996. *Continued...*

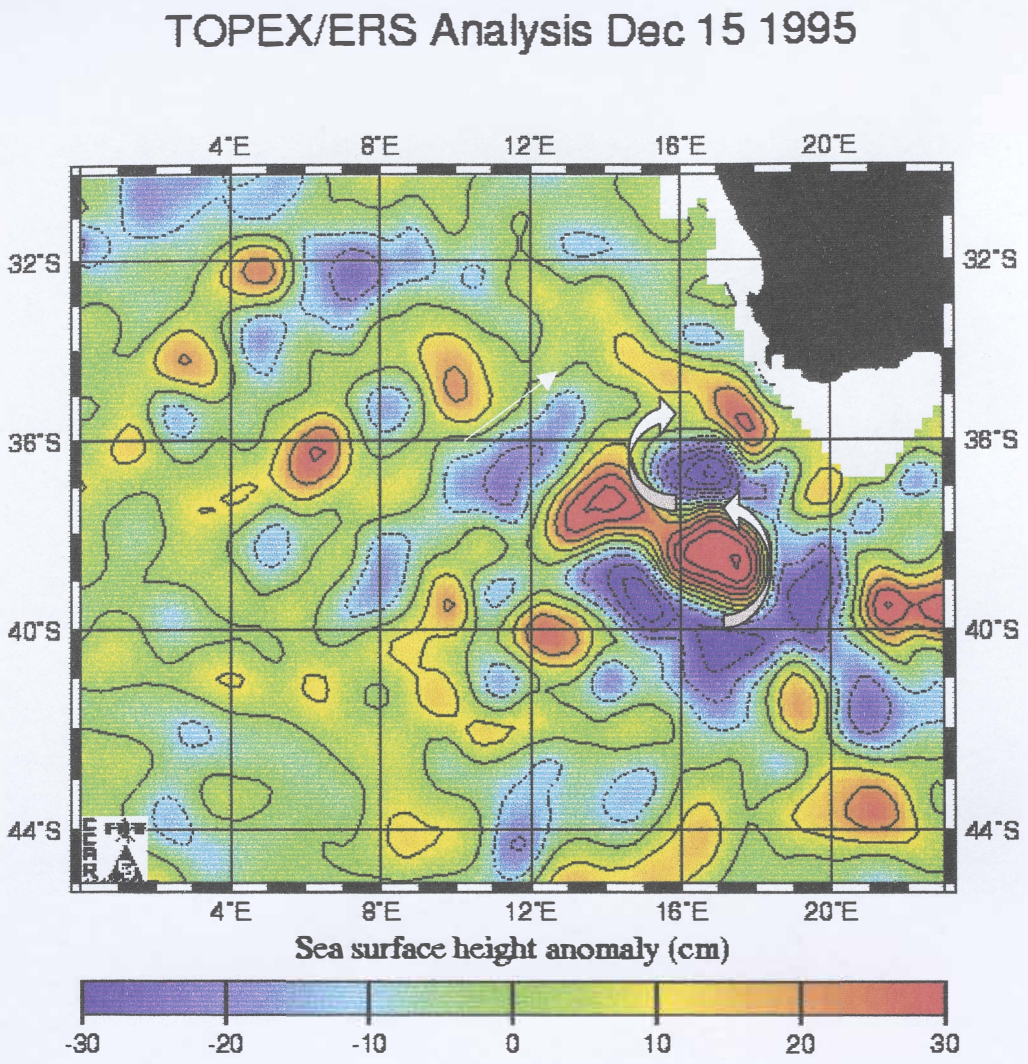

Figure 7.6 Sea surface height anomalies for the oceanic environment southwest of Africa for the region 0 °E to 21 °E and 30 °S to 45 °S. Areas shallower than 200m are coloured white around the coastline. The series spans the period 25 November 1995 to 10 January 1996. *Continued...*

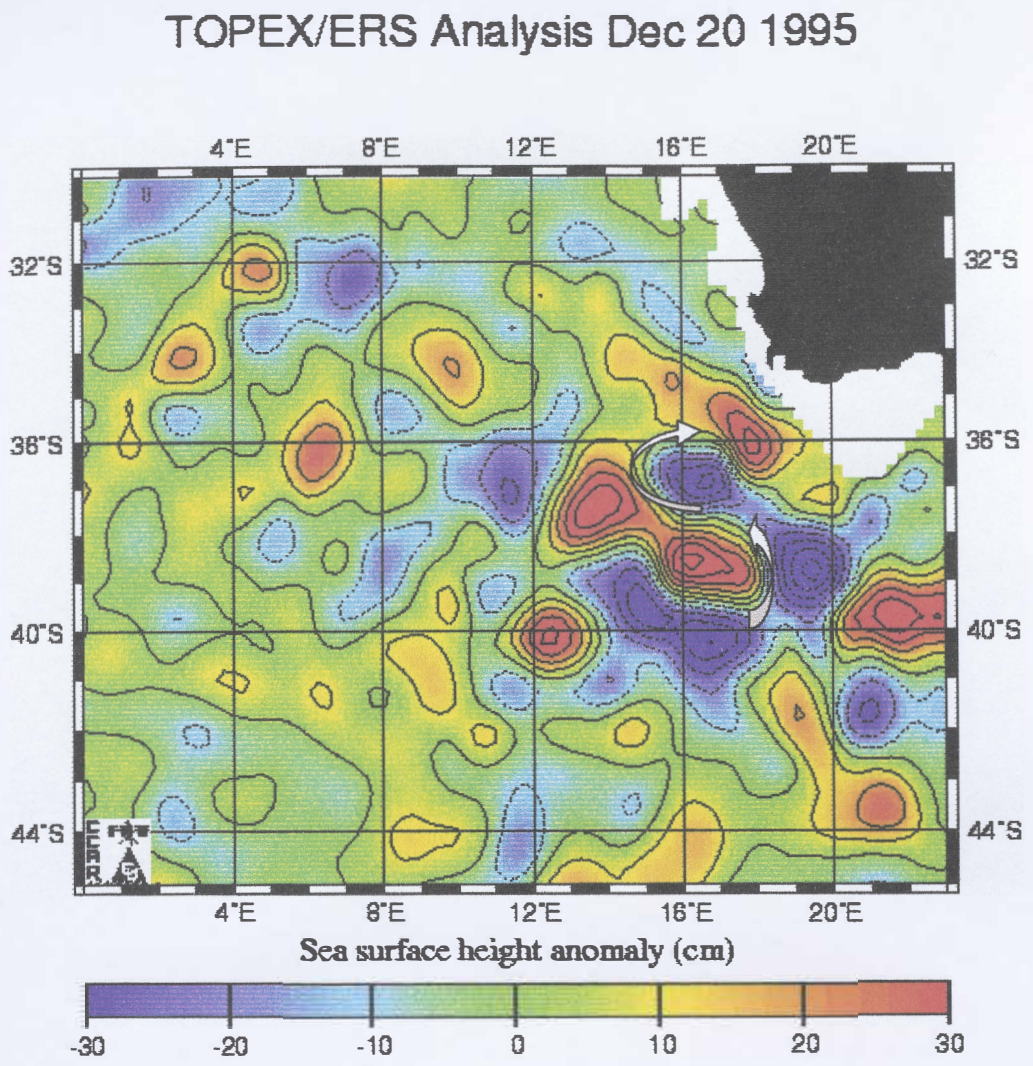

Figure 7.6 Sea surface height anomalies for the oceanic environment southwest of Africa for the region 0 °E to 21 °E and 30 °S to 45 °S. Areas shallower than 200m are coloured white around the coastline. The series spans the period 25 November 1995 to 10 January 1996. *Continued...*

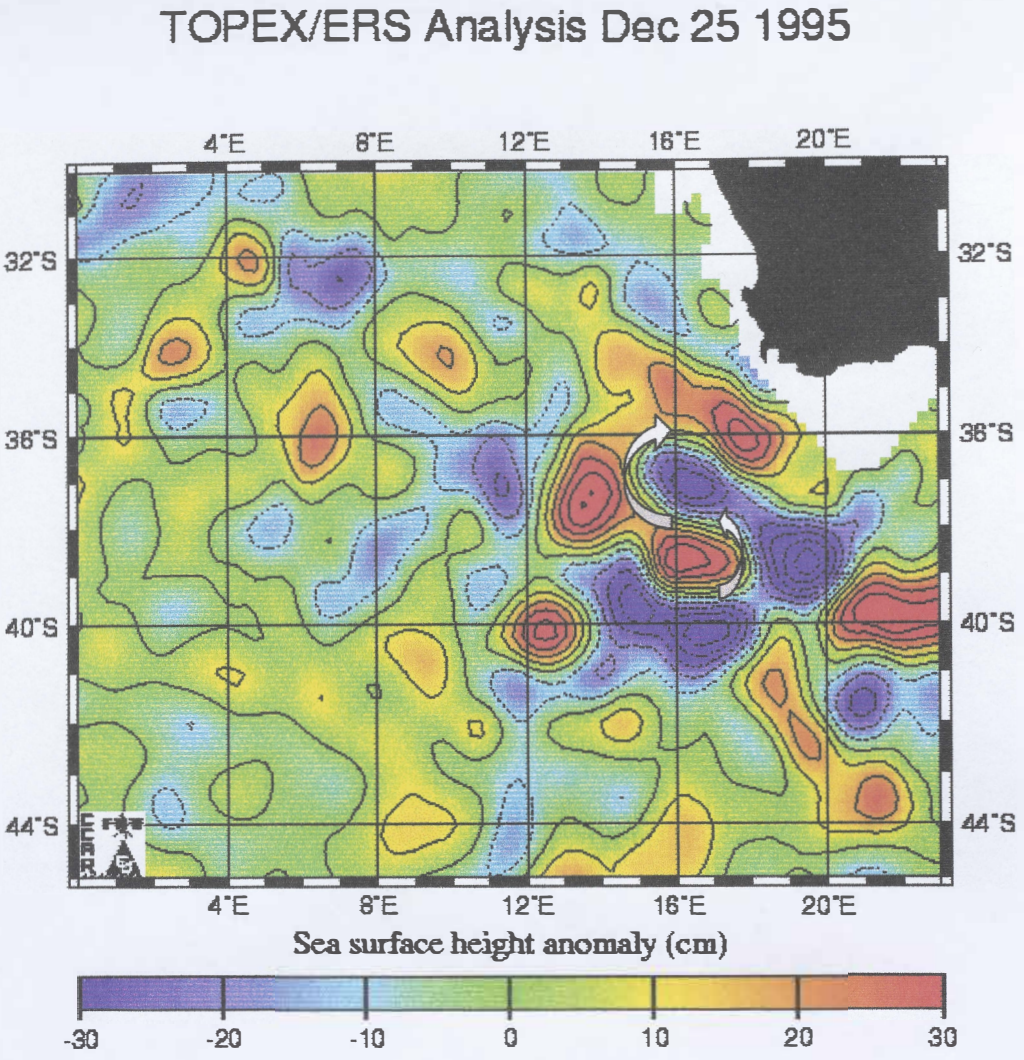

Figure 7.6 Sea surface height anomalies for the oceanic environment southwest of Africa for the region 0 °E to 21 °E and 30 °S to 45 °S. Areas shallower than 200m are coloured white around the coastline. The series spans the period 25 November 1995 to 10 January 1996. *Continued...*

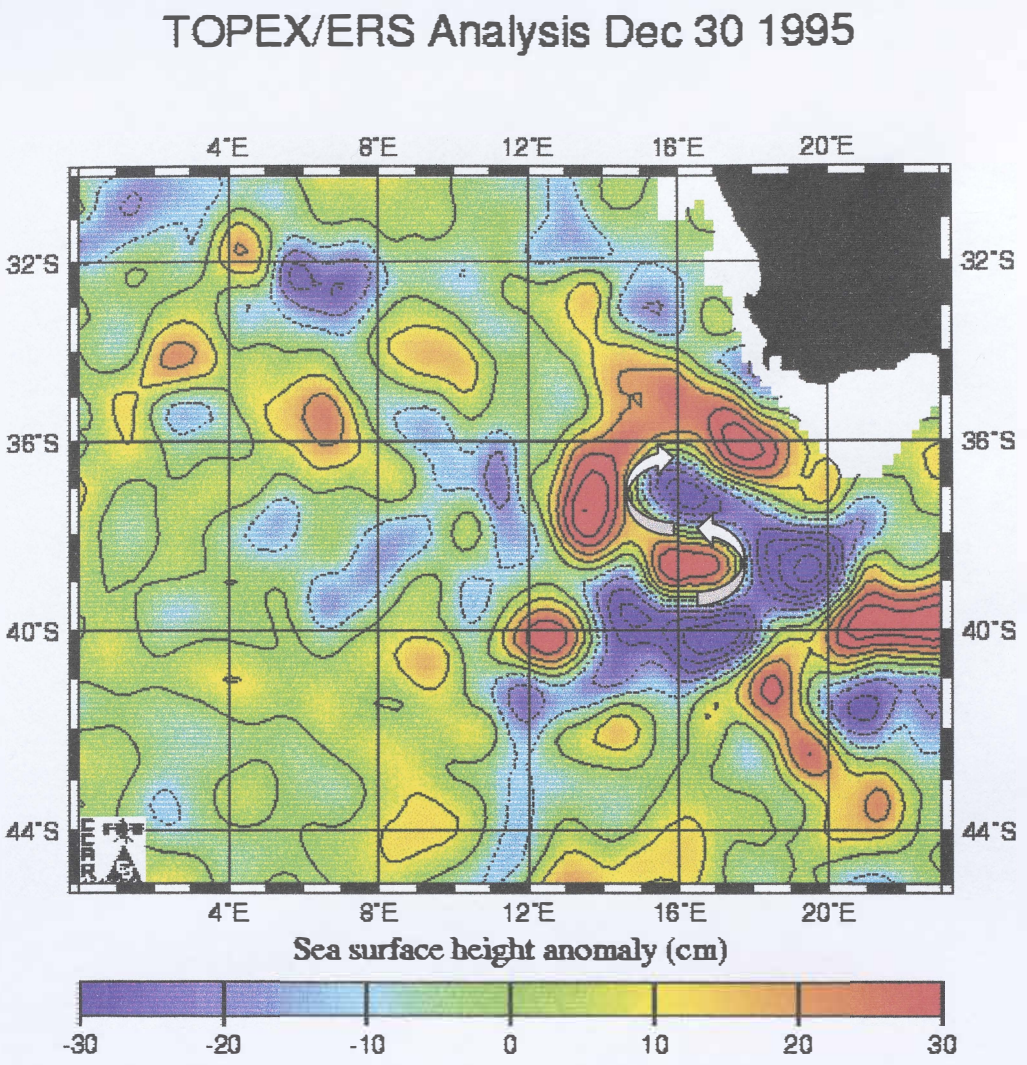

Figure 7.6 Sea surface height anomalies for the oceanic environment southwest of Africa for the region 0 °E to 21 °E and 30 °S to 45 °S. Areas shallower than 200m are coloured white around the coastline. The series spans the period 25 November 1995 to 10 January 1996. *Continued...*

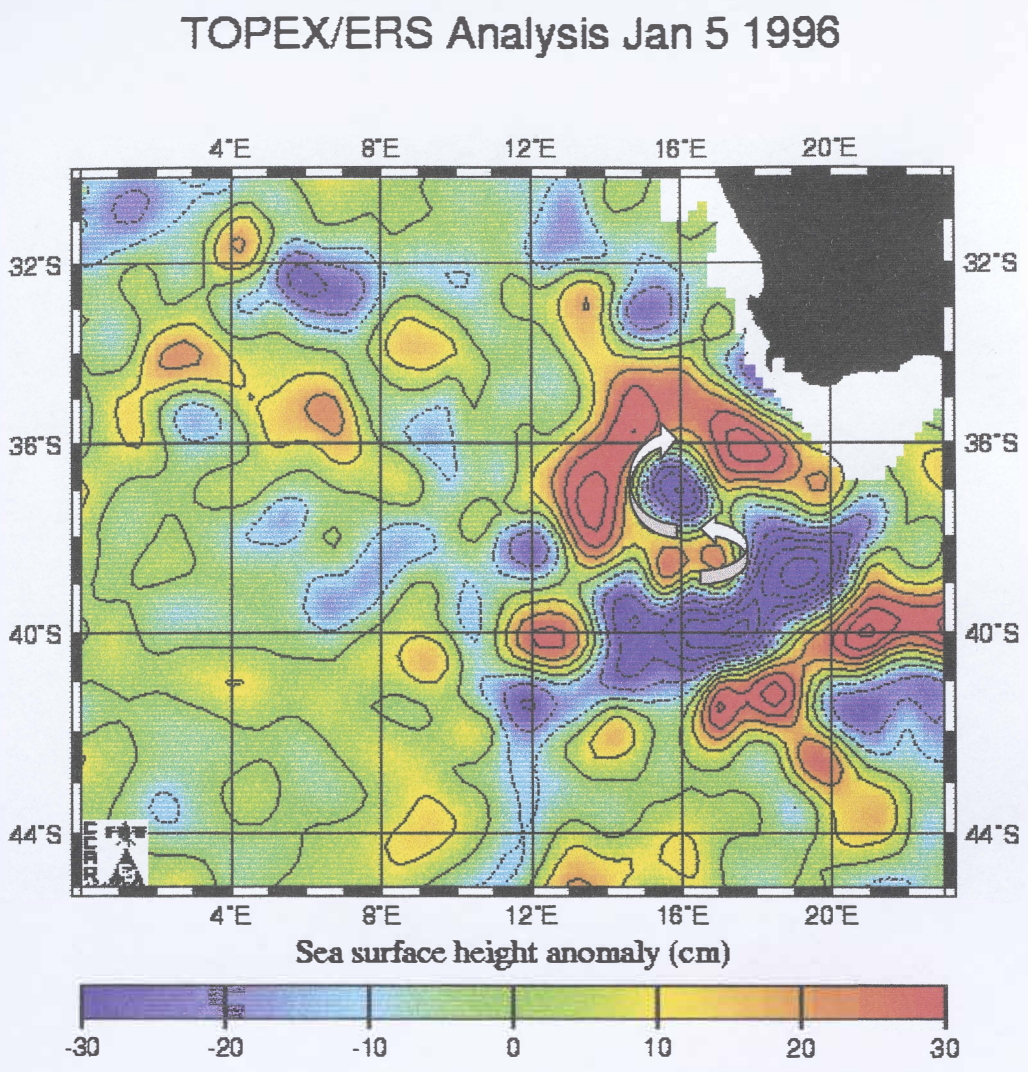

Figure 7.6 Sea surface height anomalies for the oceanic environment southwest of Africa for the region 0 °E to 21 °E and 30 °S to 45 °S. Areas shallower than 200m are coloured white around the coastline. The series spans the period 25 November 1995 to 10 January 1996. *Continued...*

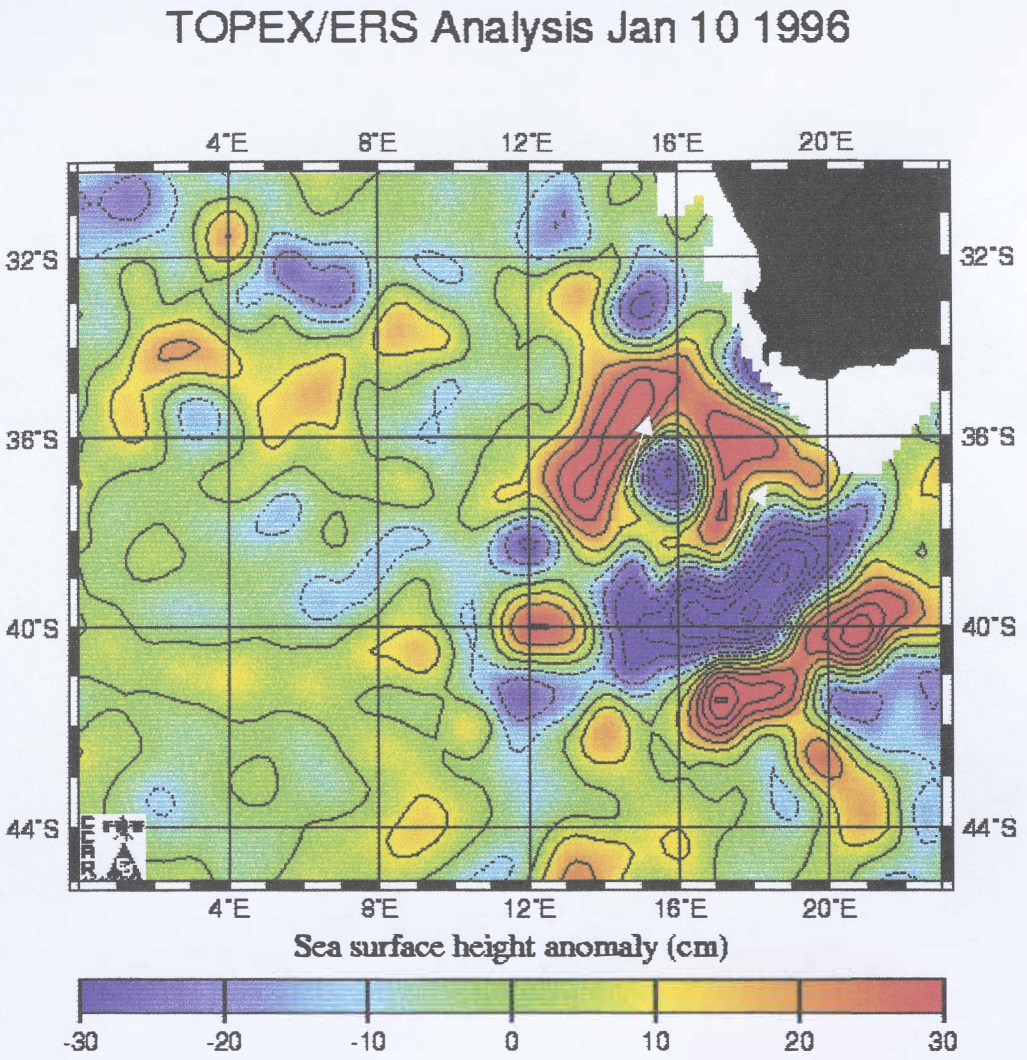

Figure 7.6 Sea surface height anomalies for the oceanic environment southwest of Africa for the region 0 °E to 21 °E and 30 °S to 45 °S. Areas shallower than 200m are coloured white around the coastline. The series spans the period 25 November 1995 to 10 January 1996. *Continued...*

The altimeter record shows that the intrusion of cold water on 10 December 1995 had a sea surface height anomaly expression very much conducive to northward movement of water at between 18 °E and 20 °E at 40 °S. This expression is characterized by an alongside anticyclonic / cyclonic anomaly and can be traced back in the altimetry to about 5 December 1995; the anomalies of 25 November and 30 November 1995 are added for comparison. The sea surface anomaly expression of this event seem to grow progressively more pronounced through December becoming a broad band of anomalous flow at around 5 January 1996, approximately 30 days after its presumed initial conception. This broad anomaly event continued to dominate the flow field southwest of Africa (at least in the anomaly pattern) until around 25 January 1996, a further 20 days after initial conception, when the western part of the anomaly at around 15 °S seemed to migrate northward. An infrared satellite image of the intrusion on 4 February 1996 is given on Figure 7.7 showing the presence of a broad intrusion of cold water still present southwest of the continent.

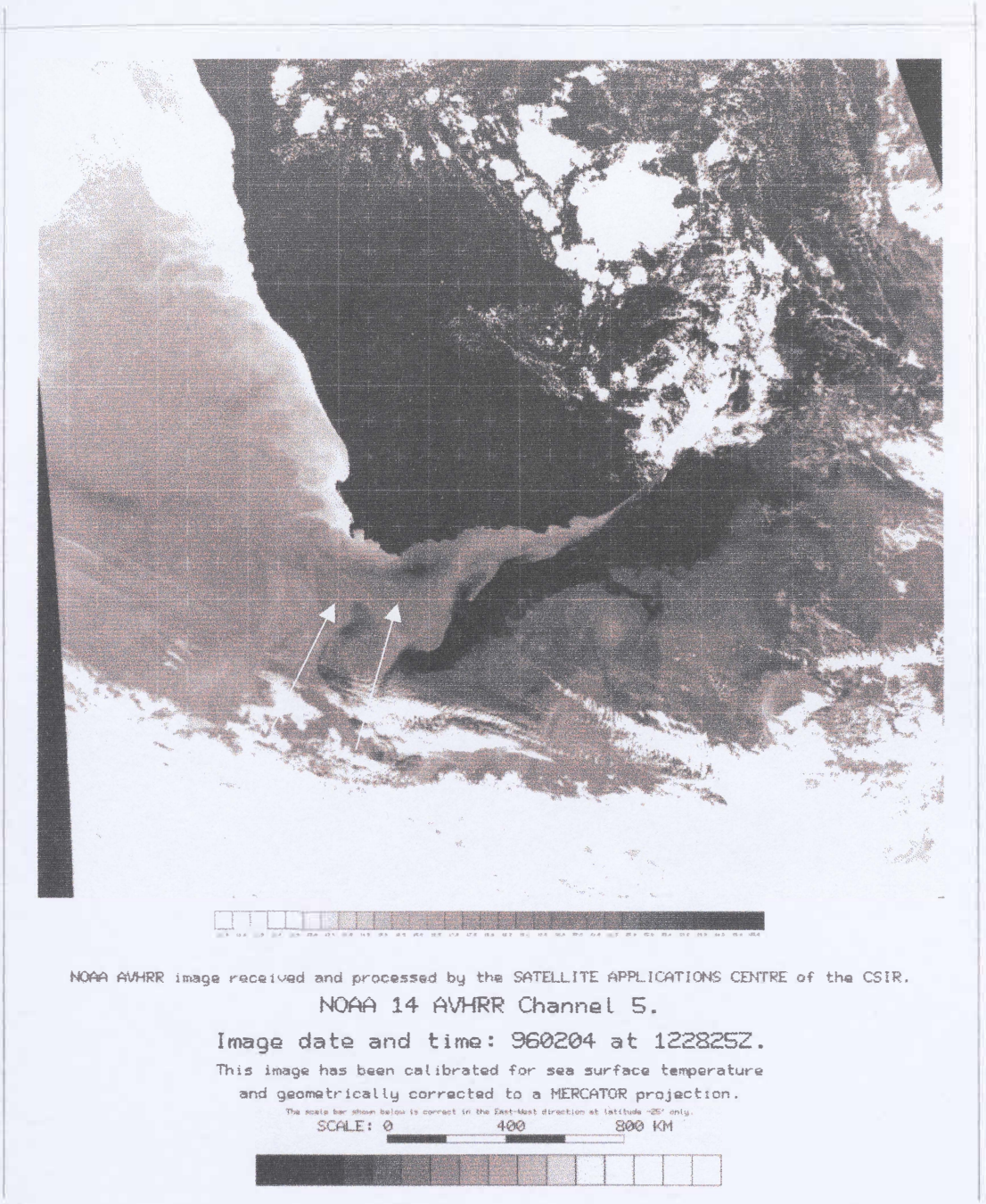

Figure 7.7 Thermal infrared NOAA AVHRR image of the sea surface around Southern Africa on 4 Febraury 1996. This image was calibrated for absolute temperatures and geometrically corrected to a Marcator projection. The arrows indicate the paths of the SAASW intrusions. [Received and processed by the Satellite Applications Centre at the CSIR].

The altimetric record (Figure 7.6) shows this northward displacement of the westerly part of the sea surface anomaly pattern southwest of Africa to be present at the retroflection region through February 1996 to about 5 March, 1996; a further 35 days after initial conception; when a broad easterly anomaly again seemed to develop through March to about 30 March 1996; a further 25 days after initial conception. The sea surface anomaly expression of this intrusion was lost on 10 April 1996. This intrusion is therefore observed to have been present at the retroflection region for 110 days. The durability of this intrusion suggests that some intrusions may be a collection of smaller intrusions succeeding one another. The lack of concurrent satellite infrared images that are sufficiently cloud free in order to construct serial composite diagrams of these intrusions based on their thermal expressions are therefore felt.

Figure 7.8 shows the last example of cold water intrusion in the study region southwest of the African continent. The sea surface height anomaly (Figure 7.9) shows a broad band of anomalous flow between 16 and 20 °E, 40 °S. This broad sea surface anomaly may be traced back to approximately 15 May 1997 from which date it grew and developed through the latter half of May and June losing its anomaly expression at approximately 25 June 1997. This event seem to last for approximately 40 days.

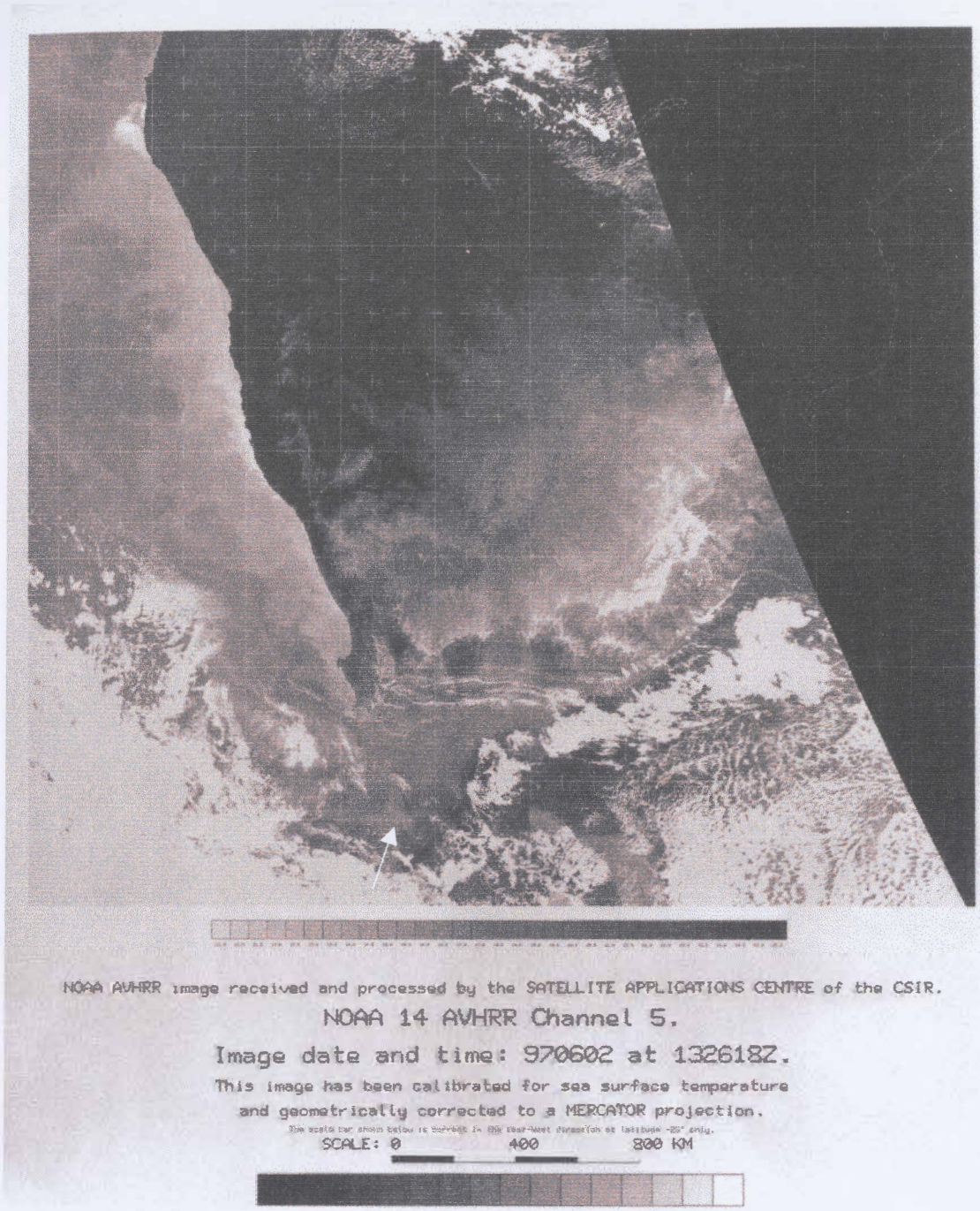

Figure 7.8 Thermal infrared NOAA AVHRR image of the sea surface around Southern Africa on 2 June 1997. This image was calibrated for absolute temperatures and geometrically corrected to a Marcator projection. The white arrow indicates the paths of the SAASW intrusions. [Received and processed by the Satellite Applications Centre at the CSIR].

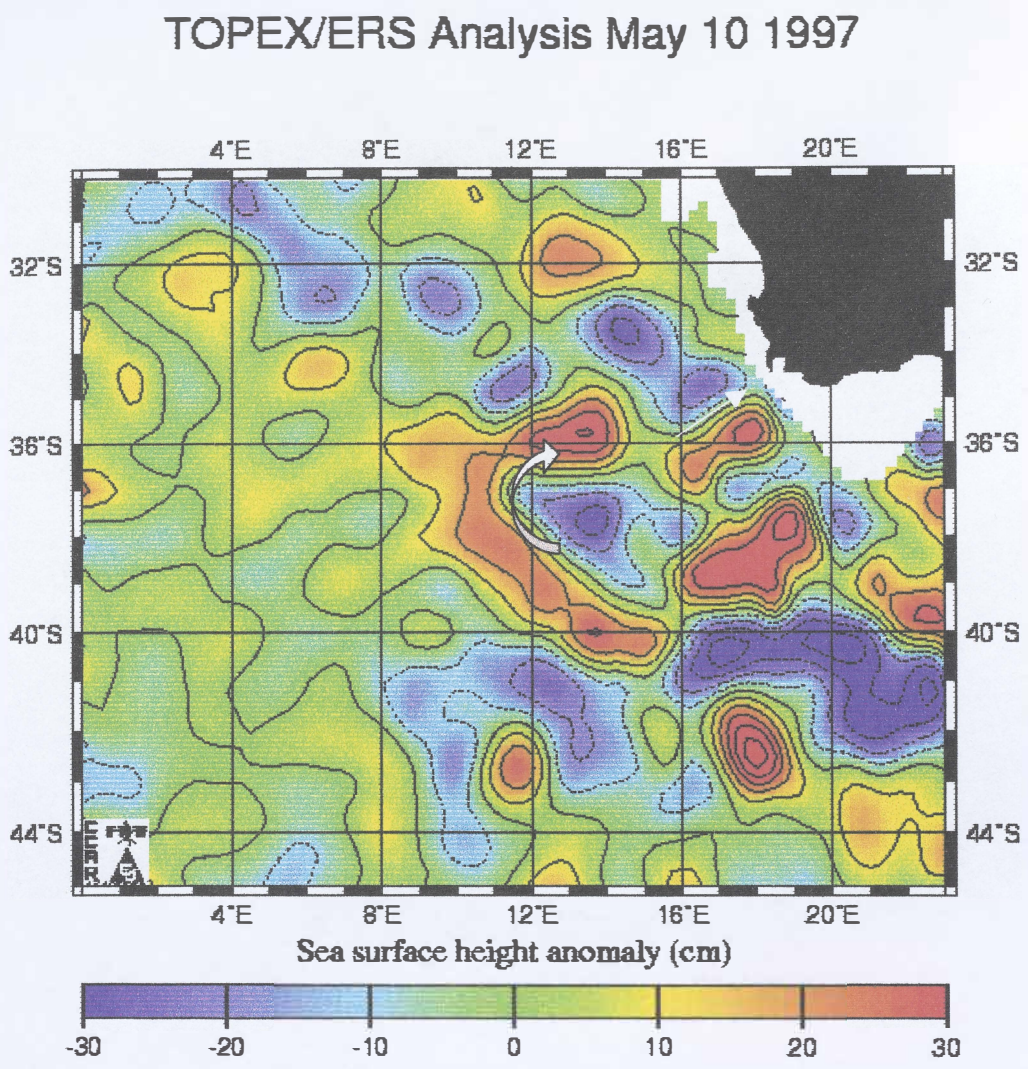

Figure 7.9 Sea surface height anomalies for the oceanic environment southwest of Africa for the region 0 °E to 21 °E and 30 °S to 45 °S. Areas shallower than 200m are coloured white around the coastline. The series spans the period 10 May 1997 to 25 June 1997. The white arrows indicate the path of the cold intrusions.

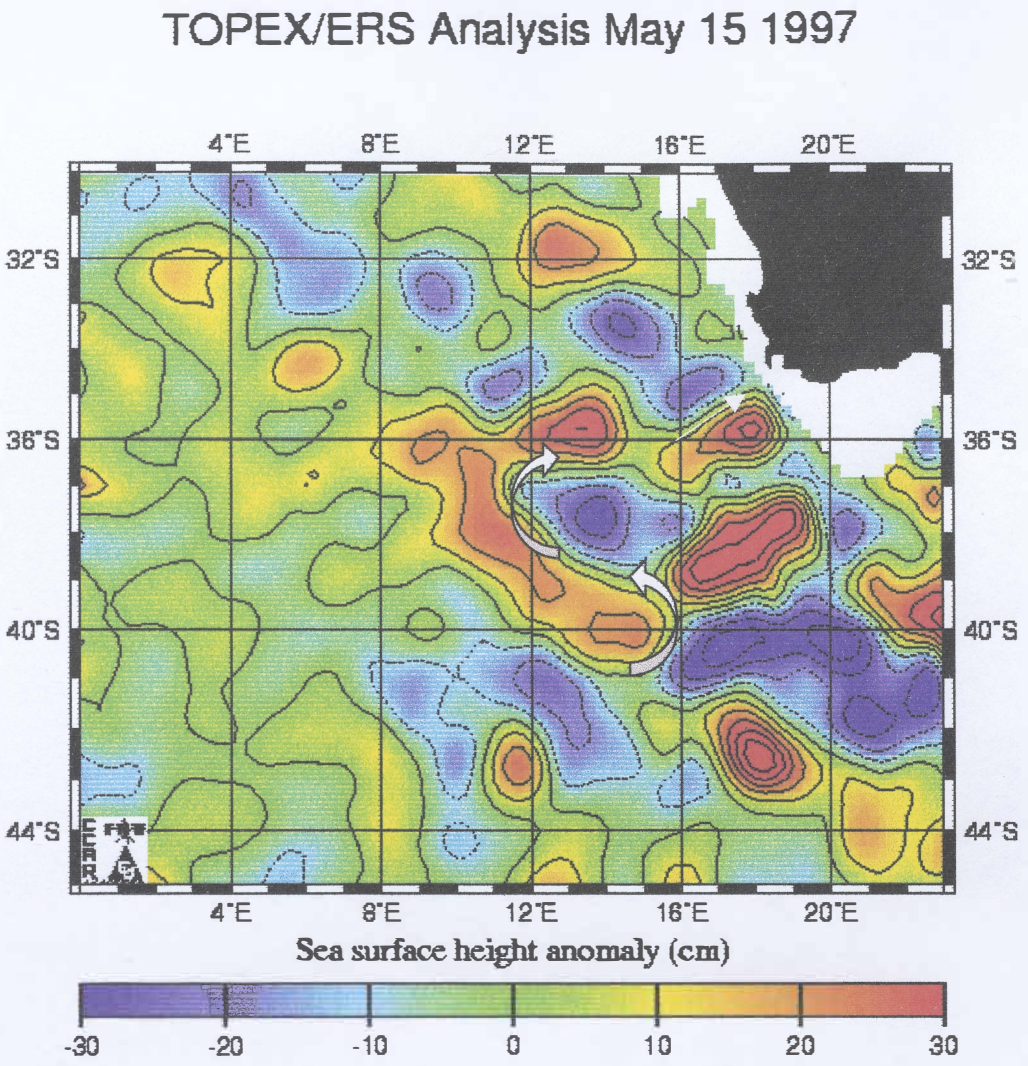

Figure 7.9 Sea surface height anomalies for the oceanic environment southwest of Africa for the region 0 °E to 21 °E and 30 °S to 45 °S. Areas shallower than 200m are coloured white around the coastline. The series spans the period 10 May 1997 to 25 June 1997. *Continued*

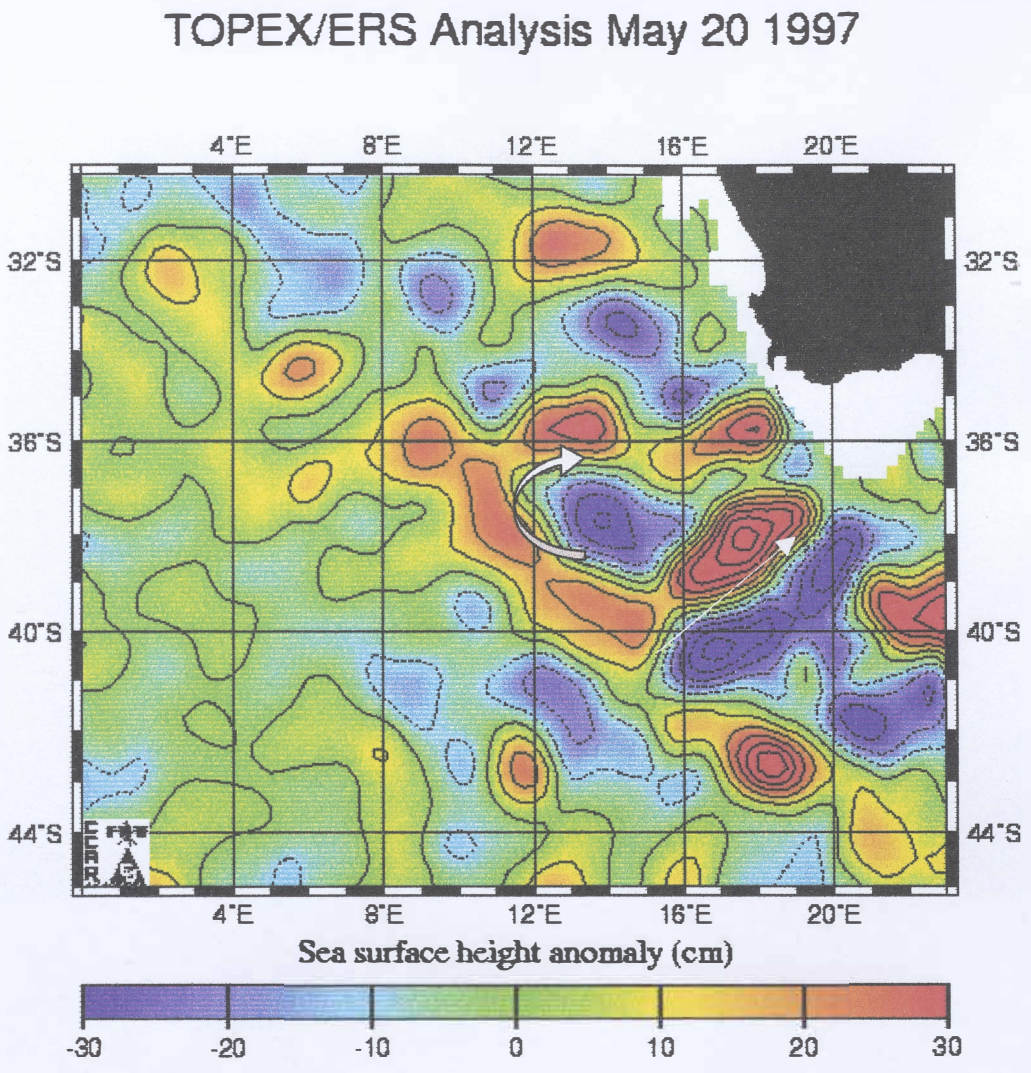

Figure 7.9 Sea surface height anomalies for the oceanic environment southwest of Africa for the region 0 °E to 21 °E and 30 °S to 45 °S. Areas shallower than 200m are coloured white around the coastline. The series spans the period 10 May 1997 to 25 June 1997. *Continued*

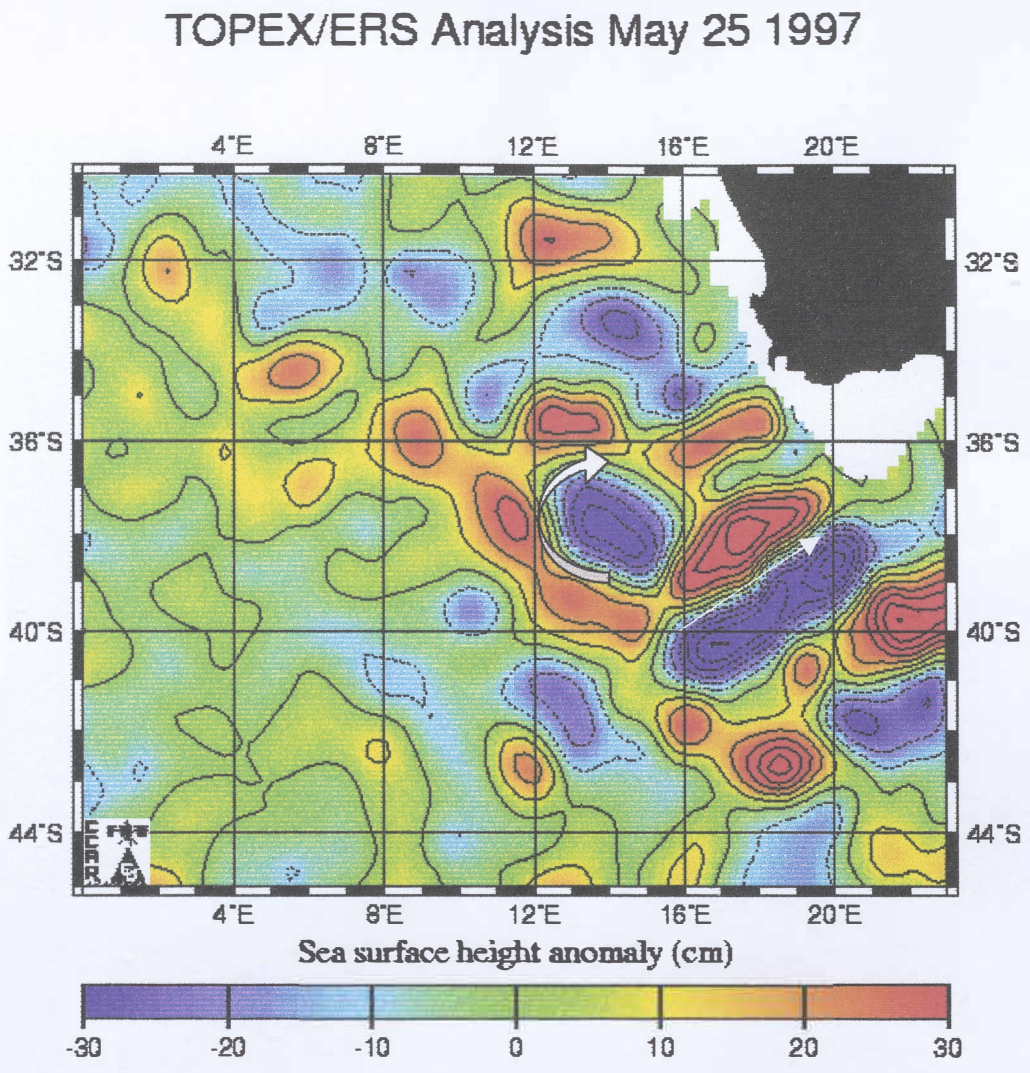

Figure 7.9 Sea surface height anomalies for the oceanic environment southwest of Africa for the region 0 °E to 21 °E and 30 °S to 45 °S. Areas shallower than 200m are coloured white around the coastline. The series spans the period 10 May 1997 to 25 June 1997. *Continued*

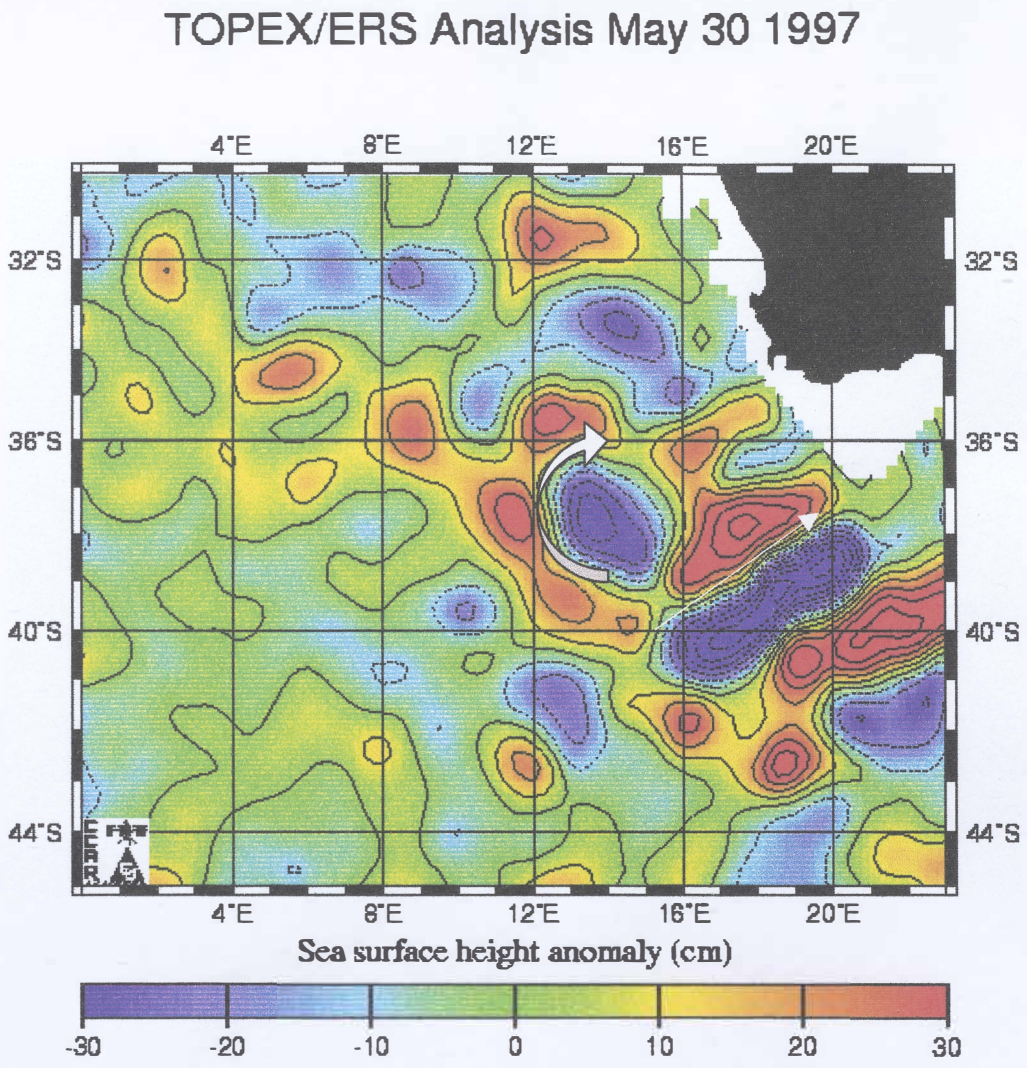

Figure 7.9 Sea surface height anomalies for the oceanic environment southwest of Africa for the region 0 °E to 21 °E and 30 °S to 45 °S. Areas shallower than 200m are coloured white around the coastline. The series spans the period 10 May 1997 to 25 June 1997. *Continued*

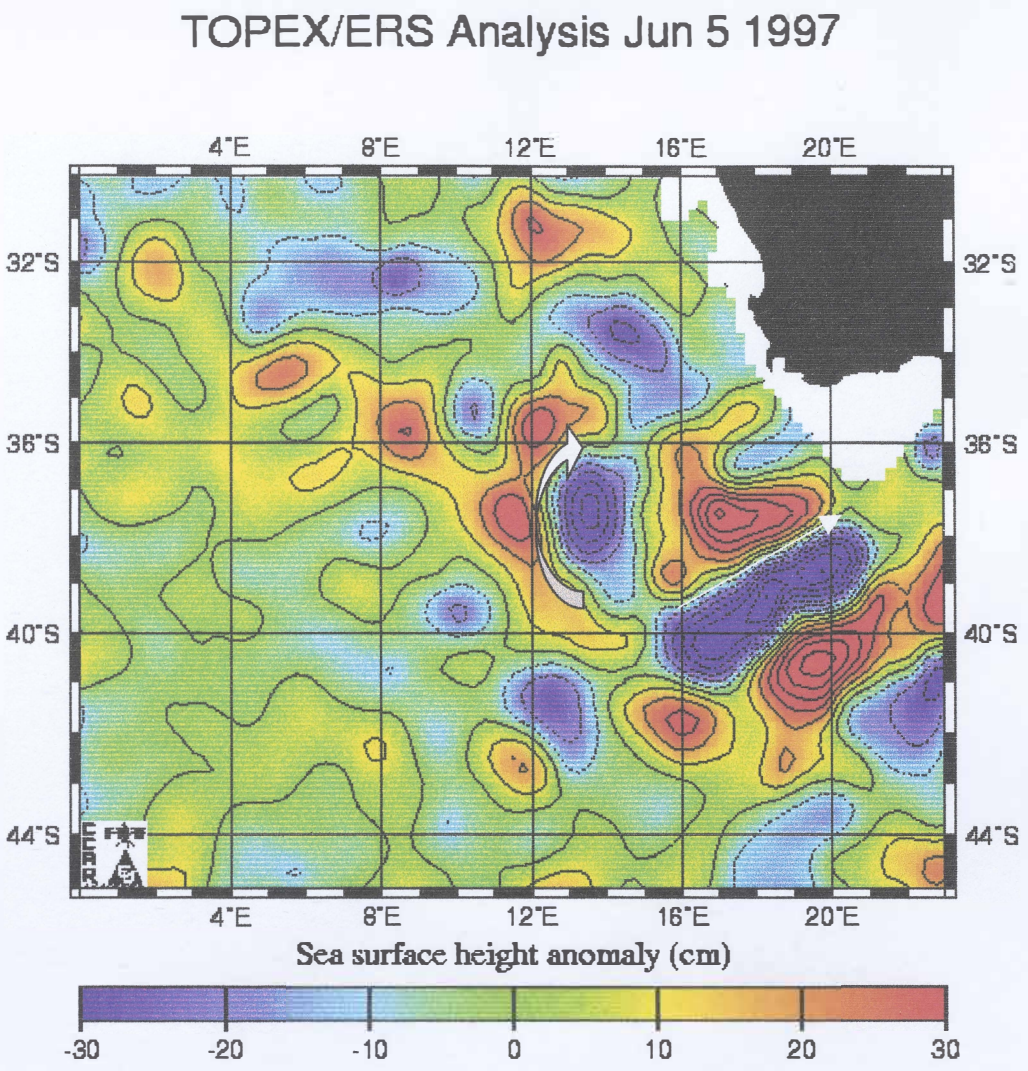

Figure 7.9 Sea surface height anomalies for the oceanic environment southwest of Africa for the region 0 °E to 21 °E and 30 °S to 45 °S. Areas shallower than 200m are coloured white around the coastline. The series spans the period 10 May 1997 to 25 June 1997. *Continued*

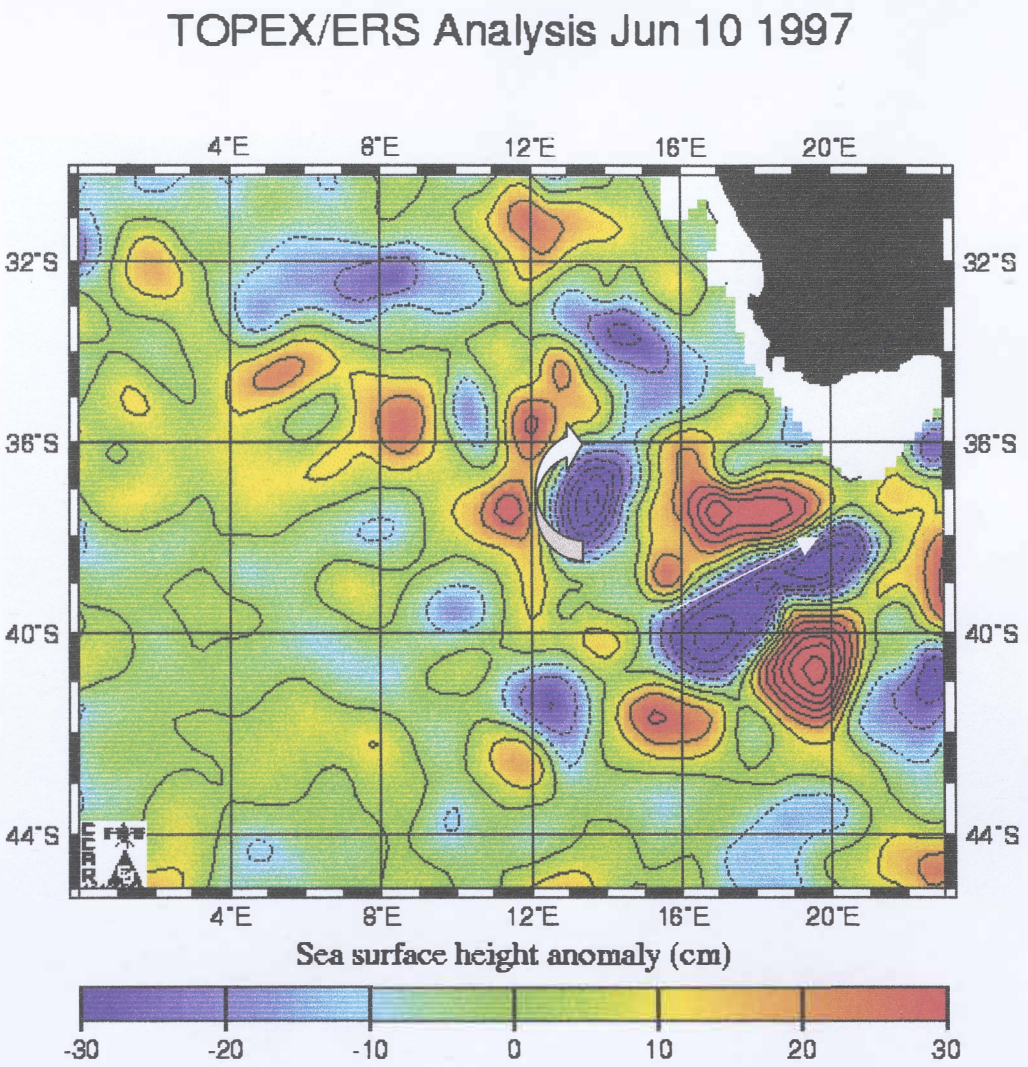

Figure 7.9 Sea surface height anomalies for the oceanic environment southwest of Africa for the region 0 °E to 21 °E and 30 °S to 45 °S. Areas shallower than 200m are coloured white around the coastline. The series spans the period 10 May 1997 to 25 June 1997. *Continued*

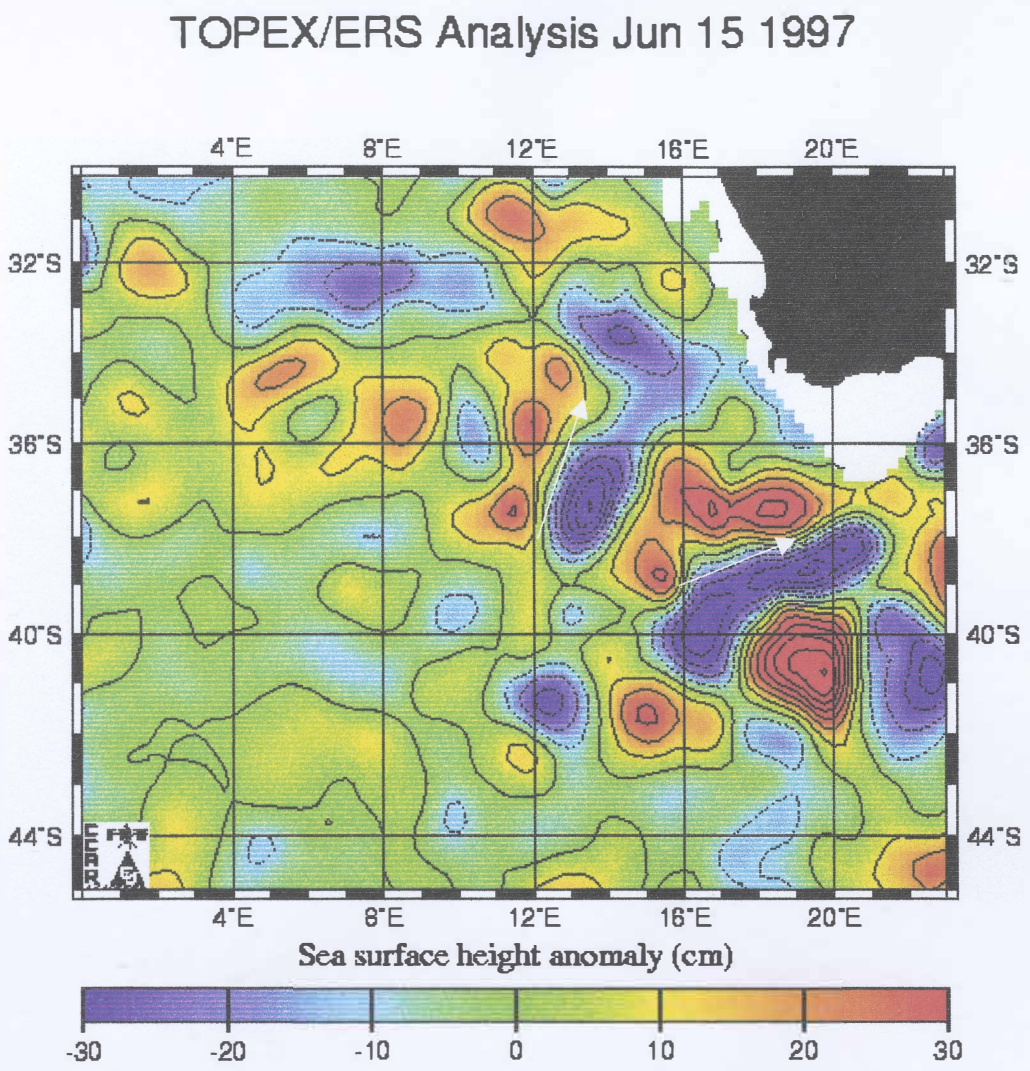

Figure 7.9 Sea surface height anomalies for the oceanic environment southwest of Africa for the region 0 °E to 21 °E and 30 °S to 45 °S. Areas shallower than 200m are coloured white around the coastline. The series spans the period 10 May 1997 to 25 June 1997. *Continued*

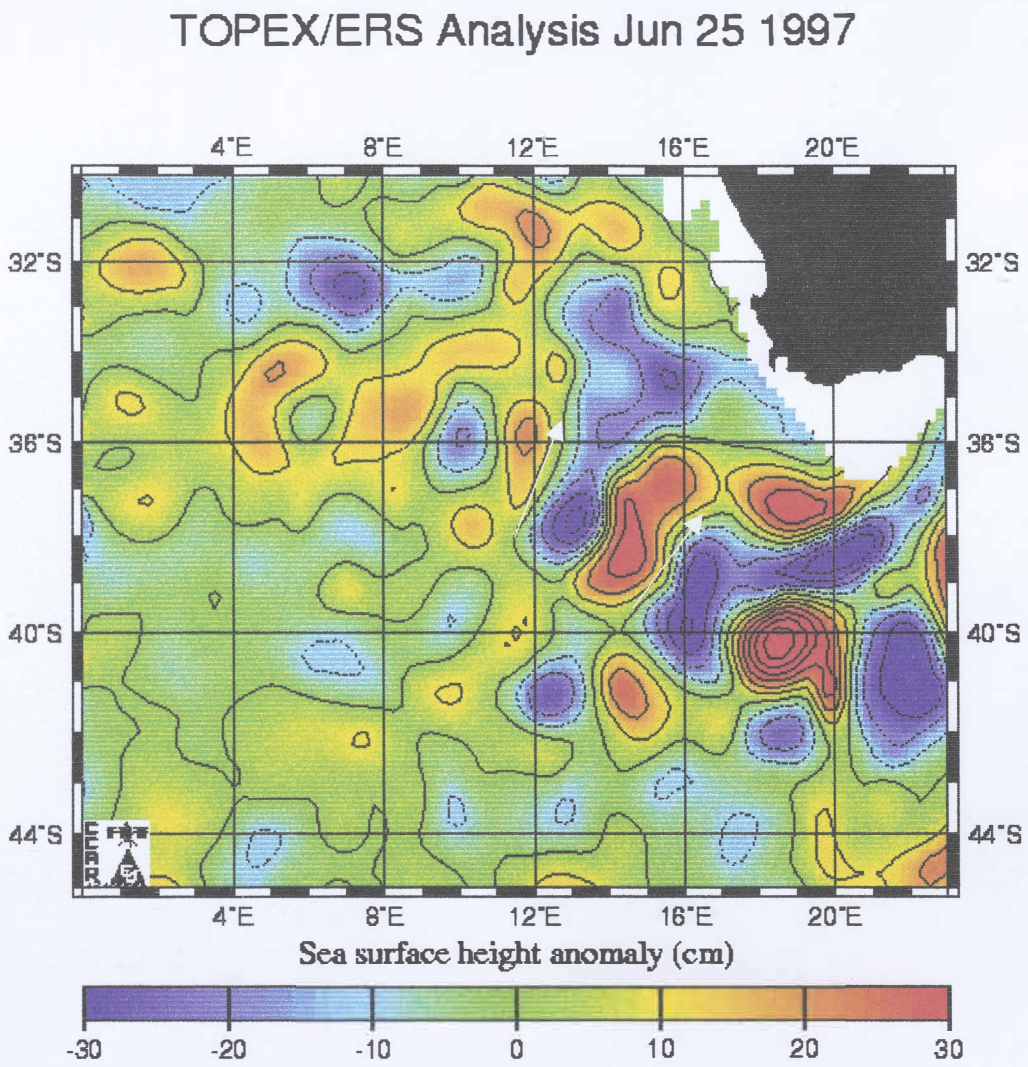

Figure 7.9 Sea surface height anomalies for the oceanic environment southwest of Africa for the region 0 °E to 21 °E and 30 °S to 45 °S. Areas shallower than 200m are coloured white around the coastline. The series spans the period 10 May 1997 to 25 June 1997. *Continued*

From the above four examples of SAASW intrusion and tracing their sea surface anomaly expression through satellite altimeter data a table of approximate residence times of SAASW intrusions may be constructed.

Intrusion	**Approximate residence time (days)**
25 April 1994 to 15 May 1994.	20
15 December 1994 to 10 January 1994.	25
25 November 1995 to 10 April 1996.	30, 20, 35, 25
10 May 1997 to 25 June 1997.	40
Average	**28 (n=7)**

Table 7.1. Estimated residence time of SAASW intrusions at the Agulhas Retroflection based on their thermal expressions through satellite infrared images and their sea surface anomaly height measurements determined by satellite altimetric records.

Table 7.1 shows the estimated residence times of SAASW intrusions based on the 4 examples studied. The intrusion of 25 November 1995 to 10 April 1996 is assumed to consist of four individual intrusions successively following one another to form one intrusion. In order to calculate the residence time, this big intrusion was analysed as four separate intrusions as discussed in the text.

The average residence time of SAASW intrusions were calculated to be 28 days varying between 20 days to 40 days for the seven examples used. Intrusion may also be succeeding one another very closely to form massive intrusion events. Between 25 November 1995 and 10 April 1996 one such intrusion occurred consisting of 4 individual intrusions forming a 110 day intrusion event.

Having established the frequency of individual intrusions of SAASW as well as the duration of these events at the Agulhas Retroflection at the surface, their hydrographic structure would give a good indication of the vertical nature of these events through the water column.

Chapter 8

Hydrographic Structure of SAASW intrusions

Data from research vessels in the study area are scant but, nevertheless, a few cruises afforded a reasonable indication of the hydrographic structure of SAASW intrusions. Results from analyzed cruise tracks are given here. They are believed to be sufficient to determine the representative hydrographic structure of SAASW intrusion events.

8.1. The Agulhas Retroflection Cruise (ARC)

Gordon *et al.* (1987) have analyzed the data from the R.V. *Meiring Naudè* (October 1983) and the R.V. *Knorr* (November to December 1983) mentioned in Chapter 2. The R.V. *Knorr* data set covers the entire retroflection (Figure 8.1).

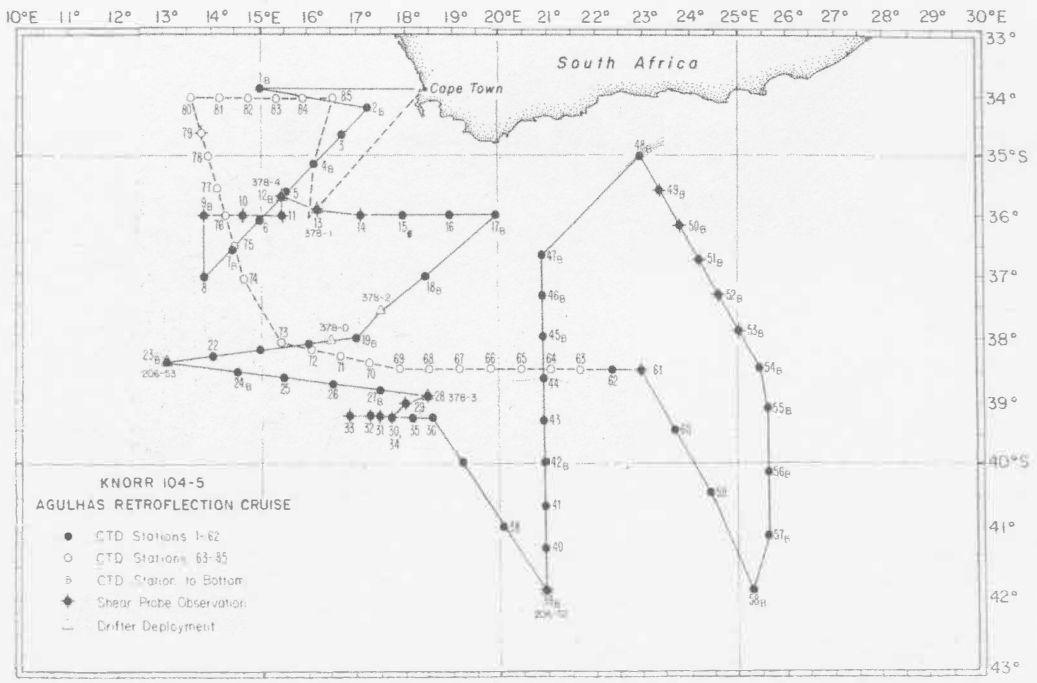

Figure 8.1. The cruise tracks of the R. V. *Knorr* in November/ December 1983. The cruise essentially covers the entire retroflection region. [Camp *et al.*, 1986].

A sketch of part of the cruise track and the sea surface temperature distribution is given in Figure 8.2. The intrusions of cold water are seen on the latter figure to be situated at approximately 17 °E, 39 °S and 13 °E, 38 °S.

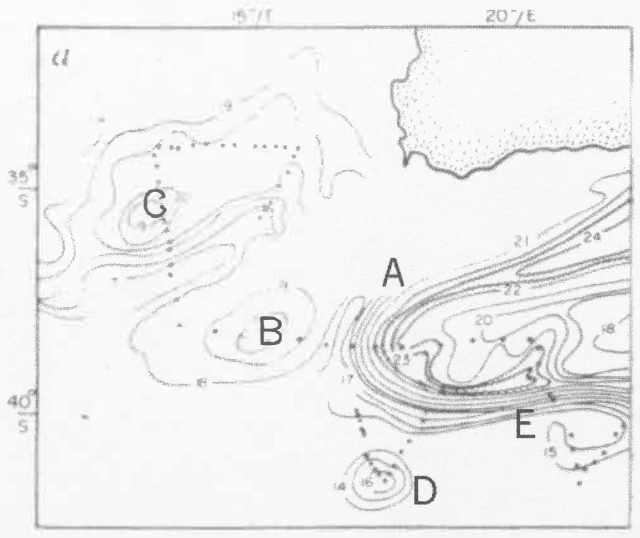

Figure 8.2. Surface isotherms of the Agulhas retroflection during the Agulhas Retroflection Cruise (ARC). Measurements were made by the R. V. *Knorr* after the shedding of an Agulhas ring. A= Agulhas retroflection, B= newly spawned Agulhas Current ring, C= an older Agulhas Current ring, D= eddy south of the Subtropical Convergence, E= Agulhas Return Current, [Lutjeharms and Gordon, 1987].

Figure 8.2 shows a clear, strong front between the warm tropical and subtropical surface water within the Agulhas retroflection and the cold water believed to be SAASW. Directly west of the Retroflection a tongue of cold water is evident. Immediately to the west of this tongue of cold water a newly spawned Agulhas ring is observed (marked B on the diagram). Between this ring and an "older" ring (marked C on Figure 8.2) the presence of cold water was also observed during a northward leg of the cruise (CTD stations 73 to 80 in Figure 8.1). Two sections were analyzed in order to verify whether these cold water intrusions were indeed SAASW and to determine to what depth they extended.

The potential temperature section between CTD stations 61 and 73 (*viz.* Figure 8.1) is given in Figure 8.3. A clear wedge-like intrusion of cold water (between CTD stations 65 and 69) is seen to penetrate between the Agulhas Retroflection to the right of the wedge and a newly spawned Agulhas ring (indicated as a warm, trough-like pool of water) to the west of the cold water intrusion. The two cores of warm water within the ring between CTD 69-70 and 71-72 in the upper 100 m form part of the annulus shape of the warmest surface water of this Agulhas ring.

An interesting feature about this particular cold intrusion is that it seemed to display a double wedge structure, shallowest at CTD stations 66 and 68. The western wedge is expressed at the surface at CTD station 68 while the eastern wedge seems to be impeded from reaching the surface by the warm water of the Agulhas Retroflection. The double wedge structure seems to continue right through the water column to ~900 m where the eastern intrusion starts to dominate the vertical structure of the wedge. From this temperature structure it is observed that this cold water wedge seems to have reached vertically downward to below 1500m at CTD 66. This indicates that at least the whole upper 1500 m of the water column was involved in cold water penetration episodes and not just the upper 200 to 300 m [Shannon *et al.*, 1989] associated with SAASW.

The salinity for this section between CTD stations 61 and 73 (Figure 8.1) is given as Figure 8.4. High salinity water dominated the surface of the retroflection region at this section. This high salinity water indicated the positions of the Agulhas retroflection to the east and the Agulhas current ring to the west of a wedge of lower salinity water between CTD stations 65 and 68 creating a salinity front at approximately 200 m depth. The salinity section seems to show the same double wedge structure as seen in the temperature (Figure 8.3). An intrusion of low salinity water to ~600 m with a mild single surface expression between CTD 68 and 64 is evident. A salinity minimum at 800 m at CTD 68 is clearly seen and appears to reach levels ~1000 m deep suggesting that these intrusions may reach as deep as the AAIW. The deep local salinity maximum at CTD station 66 below ~1000 m suggests the involvement of NADW in the northward intrusion as well.

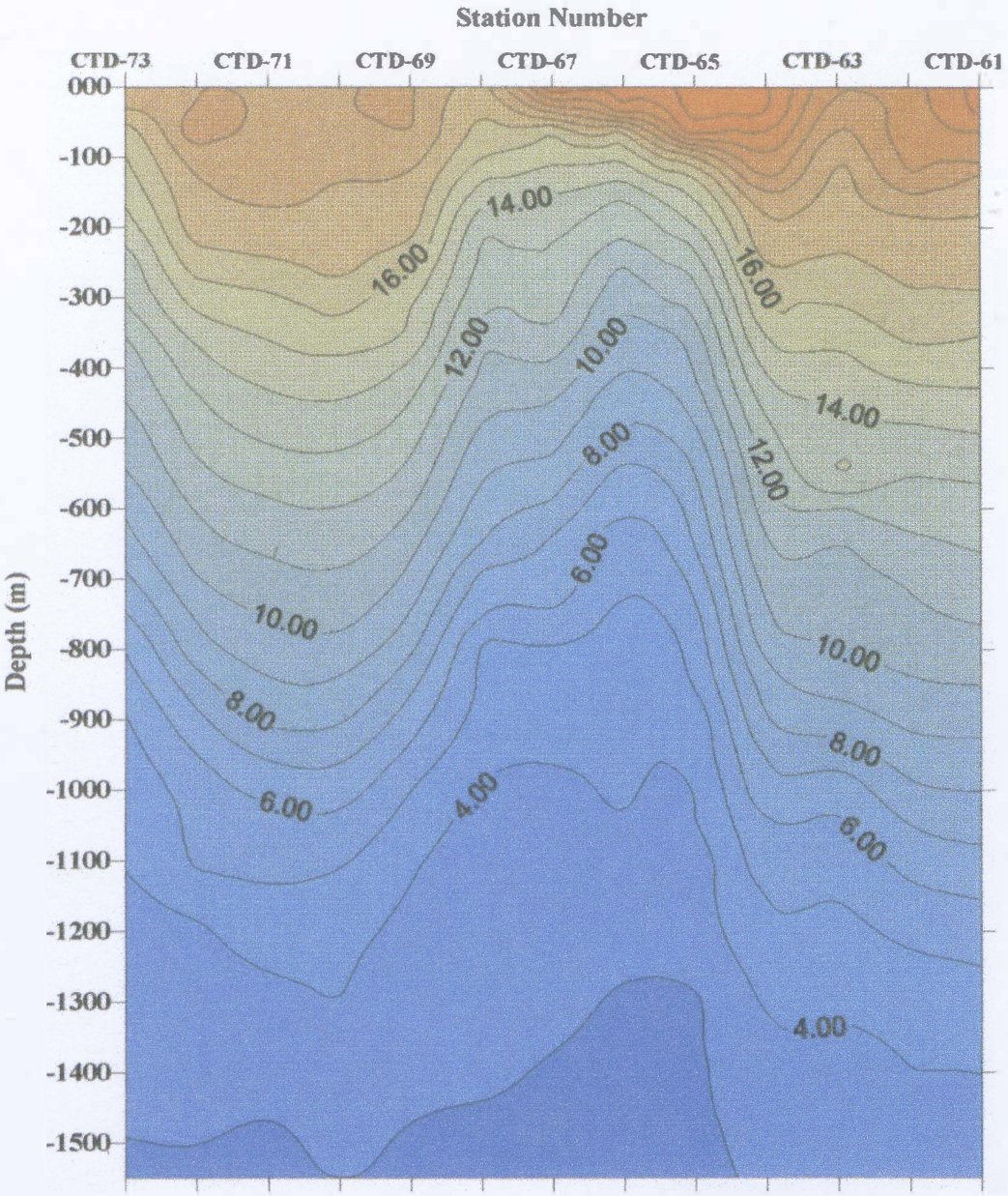

Figure 8.3. Potential temperature section between CTD stations 61 and 73 of the Agulhas Retroflection Cruise (ARC). This section intersects a wedge-like cold water intrusion.

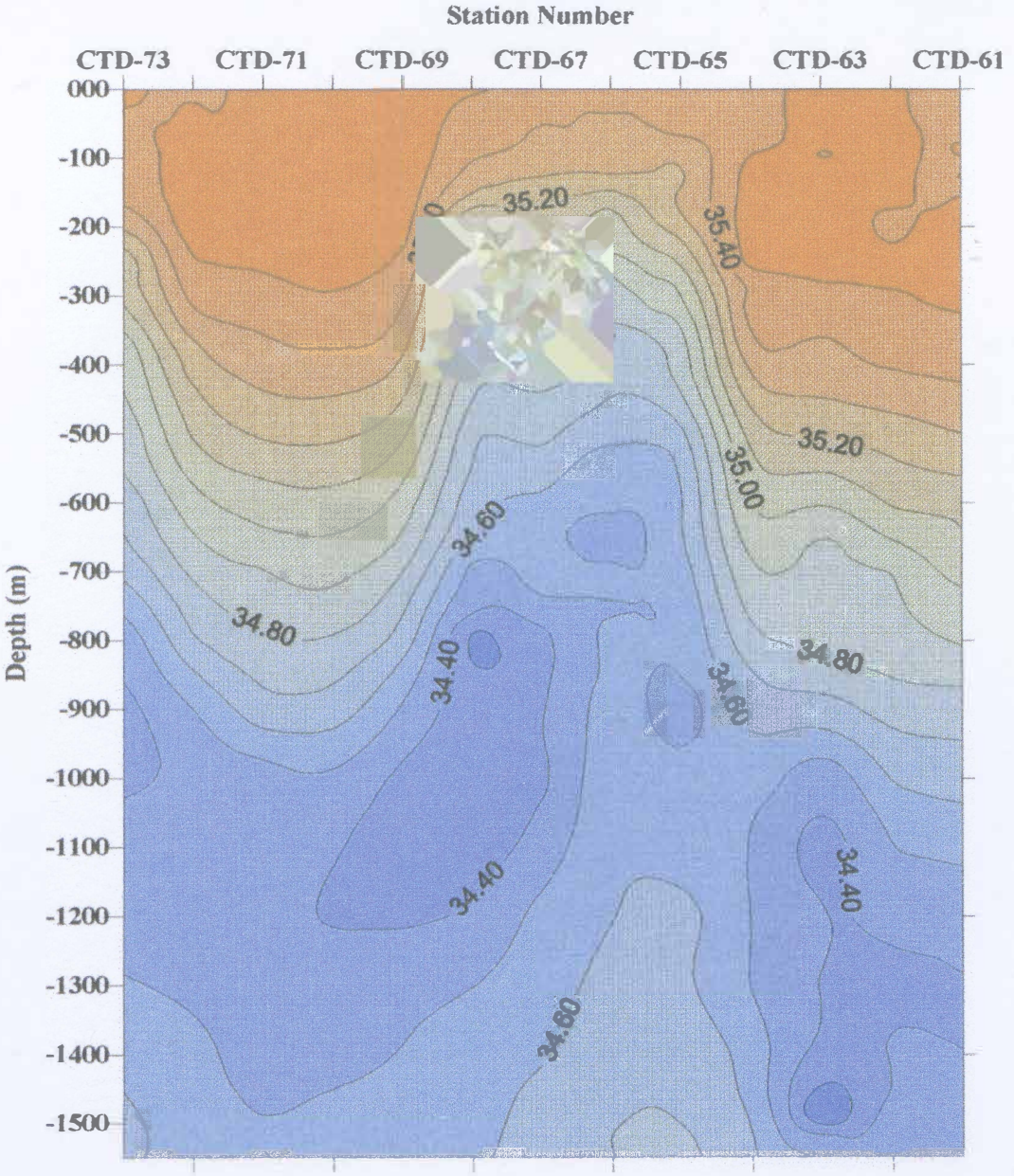

Figure 8.4. Salinity section between CTD stations 61 and 73 of the Agulhas Retroflection Cruise (ARC). This section intersects a wedge-like cold water intrusion.

Thus, a clear low temperature, low salinity water intrusion is seen between the Agulhas retroflection and a newly spawned Agulhas ring throughout the water column to the AAIW level of ~1000 m in both temperature and salinity. The wedging of this cold water may even be linked to the low temperature, high salinity water of NADW (below 1000 m) as seen at station 66 in Figure 8.3 and 8.4.

A Θ-S plot for the above hydrographic section is given in Figure 8.5 in order to study the water masses entering the retroflection region from the south. At the surface the usual Tropical and Subtropical Surface Water were observed as well as Tropical thermocline water as described in Chapter 2. Beneath that layer the SICW spans the linear part of the diagram from salinity ~ 35.5 to 34.8 and temperature 8 to 15 °C. An AAIW stratum present above the local deep salinity maximum created by NADW [Gordon *et al.*, 1987]. The high salinity Red Sea Water at the same depth as AAIW is also observed. Chapter 2 provides a more comprehensive discussion of these water masses at the retroflection [see also Gordon *et al.*, 1987].

From analyses of Figures 8.3 and 8.4 SAASW seem to be situated above the AAIW stratum. The near surface intrusion of cold water above the AAIW stratum was classified as Sub-antarctic in nature. The high oxygen content of the SAASW (Gordon *et al.*, 1987) indicates recent contact with the atmosphere.

For comparison, the Θ-S plots of CTD stations 66 and 68 in the direct paths of the double-wedged intrusion are given in Figures 8.6 and 8.7 respectively. CTD 66 shows clear Tropical Thermocline Water at the surface and the deeper SICW mass. At the AAIW stratum some SAASW is indicated to be present and even some low oxygen Red Sea Water. However, CTD station 68 (Figure 8.7) clearly shows a SAASW presence above the AAIW stratum as well as the presence of Subtropical surface water and the absence of Red Sea water.

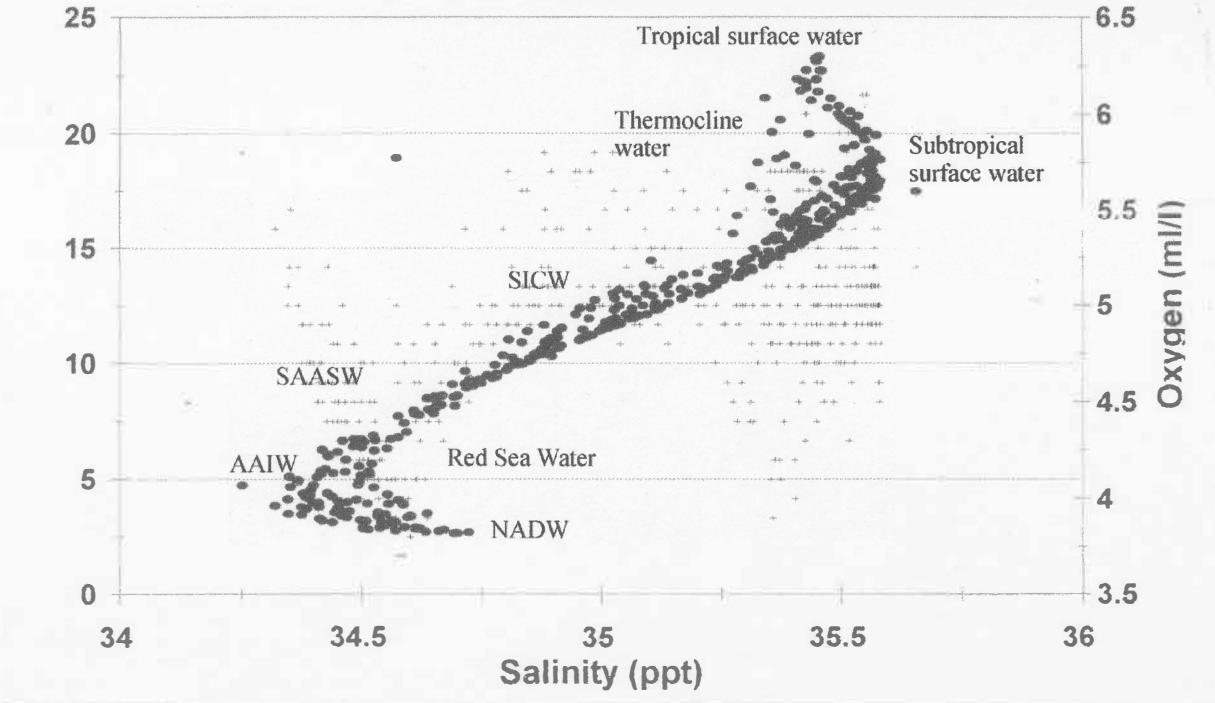

Figure 8.5 Potential temperature-salinity diagram of the ARC section shown in Figures 7.4 and 7.5. Oxygen is also marked as a function of salinity. The different water masses are named. SICW= South Indian Central Water, AAIW= Antarctic Intermediate Water, NADW= North Atlantic Deep Water. SAASW marks the proposed location of Sub Antarctic Surface Water.

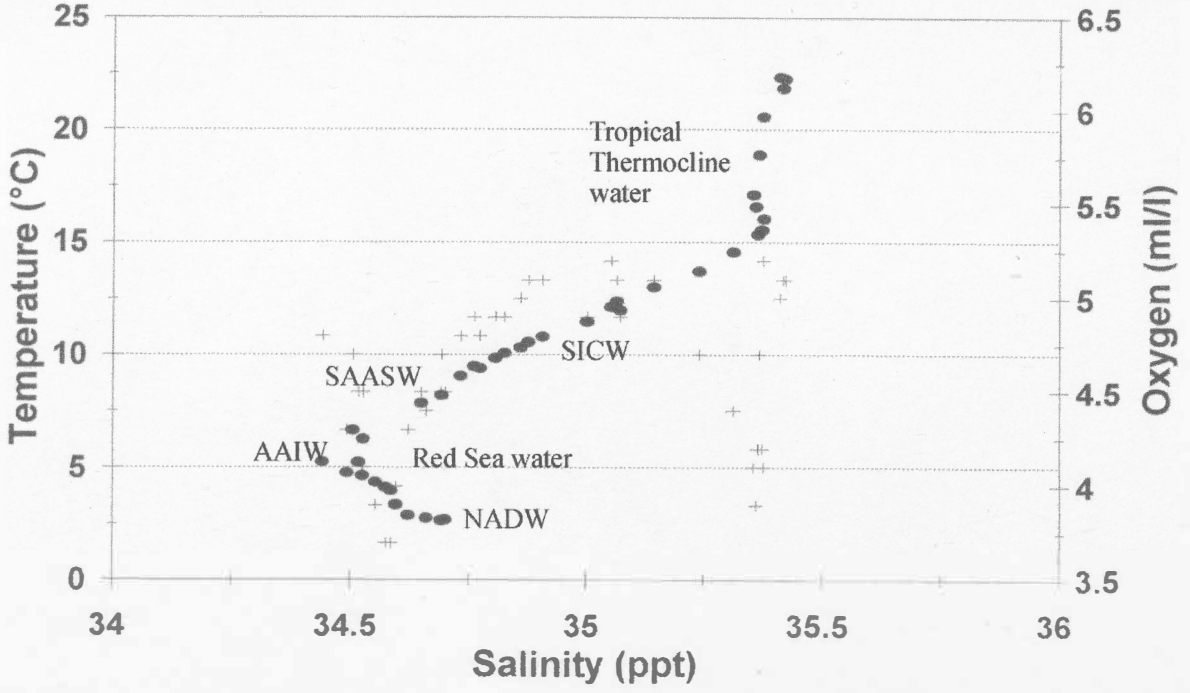

Figure 8.6. Potential temperature- salinity diagram for CTD station 66 of the Agulhas Retroflection Cruise (ARC), showing the different water masses present at one wedge path of the SAASW surface water intrusion.

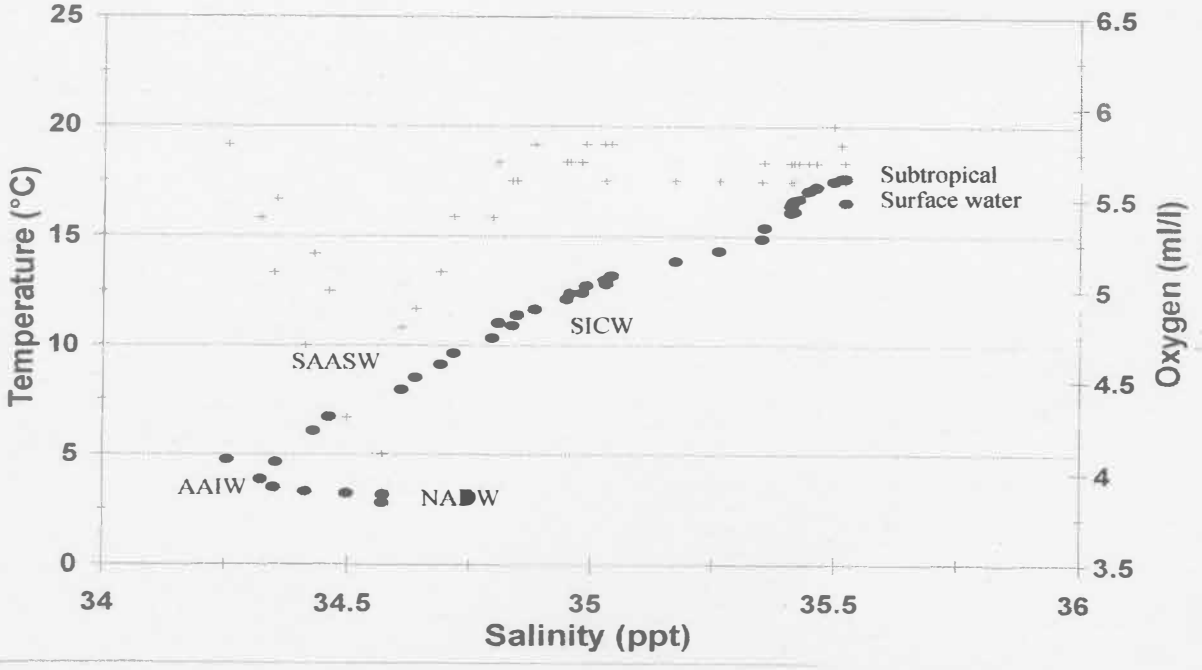

Figure 8.7. Potential temperature- salinity diagram for CTD station 68 of the Agulhas Retroflection Cruise (ARC), showing the different water masses present at one wedge path of the SAASW surface water intrusion.

Station 68 (visible at the surface through its temperature expression (Figure 8.2)) may therefore be assessed to have been the main intrusion path of SAASW between the Agulhas Retroflection and the newly spawned Agulhas ring, based on Figures 8.3 and 8.4 as well as Figures 8.5 and 8.6 and this penetrated the water column to ~800 to 900 m. This wedge of cold SAASW seems to have involved deeper water masses like AAIW (~1000 m) and even NADW.

Therefore a massive amount of water was advected northward during this cold water intrusion spanning a width of over 400 km and reaching a depth of over 1500 m.

Figures 8.8 and 8.9 show the individual temperature and salinity profiles respectively of CTD stations 66 to 69. The temperature profiles (Figure 8.8) show that between 100 and 900m, CTD station 66 seems to be coldest (except near the sea surface) while the profiles of CTD stations 67 and 68 approximate one another throughout the water column; CTD station 68 becoming colder between ~400 and 700 m. CTD station 69 shows values that are clearly higher as expected since it falls outside the path of the SAASW wedge. The salinity profiles (Figure 8.9) show very much the same situation; CTD 66 having lower salinity values between 250 m and 700 m (*viz.* Figure 8.4). The AAIW salinity minimum at ~900 m is clearly seen and below that the deep salinity maximum of NADW is also clearly observed.

Although no explanation can be offered for this massive wedging of water it is interesting to note that these intrusions occur in the vicinity of prominent topographic features; in this case the Agulhas Rise situated at ~18 ° 32, 68' E, 38 ° 29, 28' S. Shannon *et al.*, (1989) have speculated on topographic control in their analysis of the 1987 SAASW extreme intrusion event (this will be discussed later).

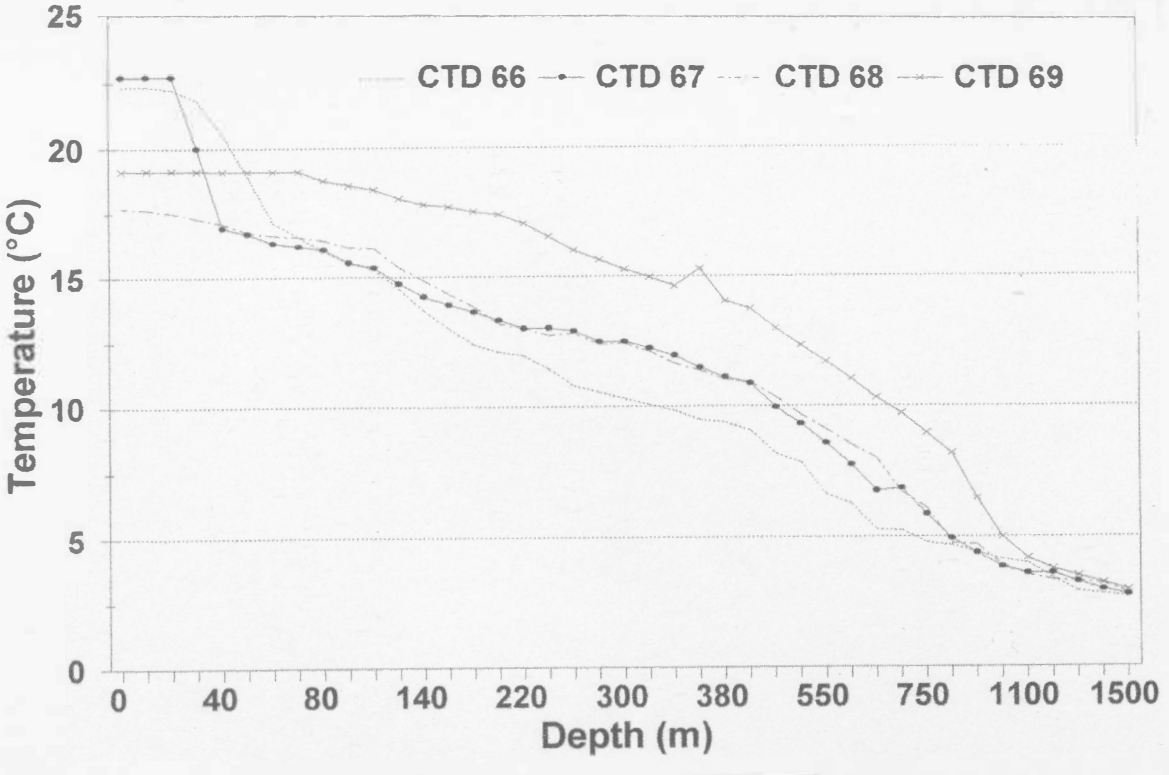

Figure 8.8. Temperature profiles of CTD stations 66 to 69 of one transect of the Agulhas Retroflection Cruise (ARC) undertaken during November/ December 1983.

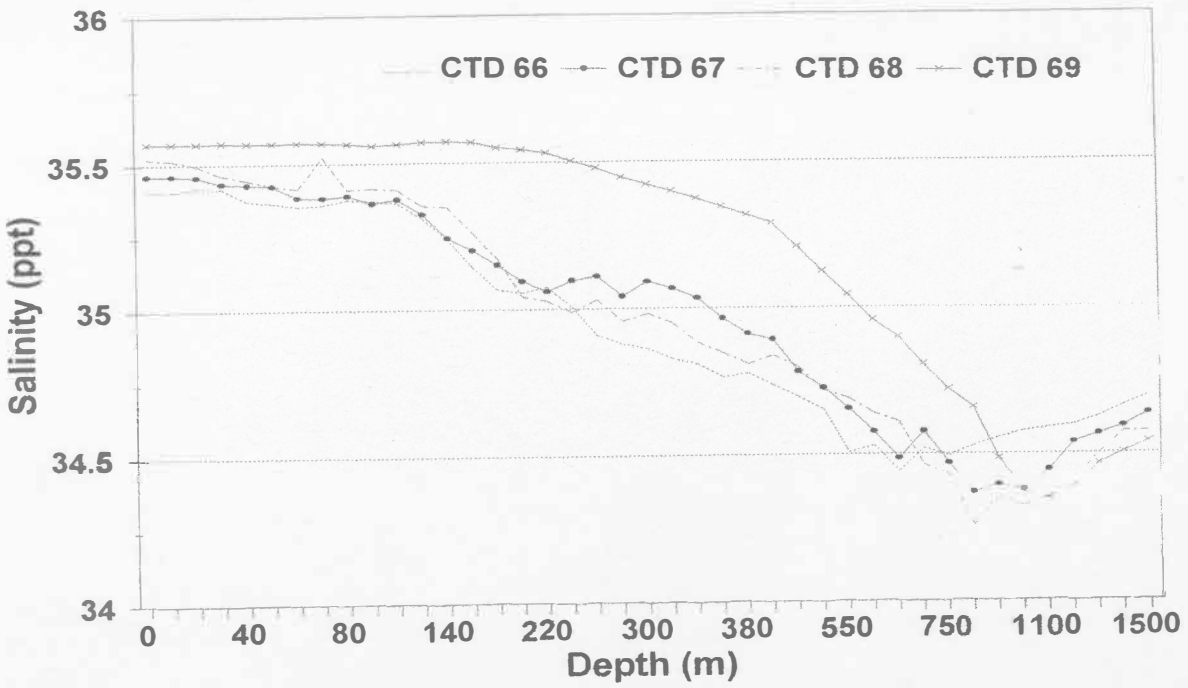

Figure 8.9. Salinity profiles of CTD stations 66 to 69 of one transect of the Agulhas Retroflection Cruise (ARC) undertaken during November/ December 1983.

The temperature and salinity transects of the more northerly ARC section consisting of CTD stations 73 to 80 (see Figure 8.1) are given in Figures 8.10 and 8.11 respectively. This is the northward continuation of the ARC section discussed above. From the temperature and salinity diagrams a single clear intrusion of cold, low salinity water seems to wedge from approximately 1100 m depth. The cold water wedge is lodged between two rings delineated by high temperature, high salinity troughs. Both penetrated to a depth of at least 1000 m. The main path of the intrusion seems to have been between CTD stations 74 and 75 in both the temperature and salinity sections. The temperature and salinity expressions of this cold water intrusion compared well with that of the southerly section. A huge amount of water ~300 km wide and over 1500 m deep is involved in this cold water intrusion. The intrusion occurred in the vicinity of the Erica Seamount situated at ~37 °S, 14 °E.

In summarizing the analysis of the ARC data set it is concluded that the water penetrating between the Agulhas Retroflection and newly spawned rings and between two rings themselves is indeed SAASW in the upper layers. However these intrusions seem to penetrate to much greater depth than was originally thought [Meeuwis and van Rensburg, 1995; Shannon *et al.*, 1989; Gordon et al., 1987] reaching the AAIW (at ~1000 m) and even the NADW below. Analysis of two sections through the direct paths of cold water intrusions show that these intrusions have massive dimensions, ~400 km wide reaching a depth of more than 1500 m.

Figure 8.12 shows the volume and accumulated volume transports of the above ARC transects. This figure shows two prominent peaks in the volume transport of 60 Sv at CTD station 66 and ~50 Sv at CTD station 74 (relative to 1500 db) and accumulated transports of 15 and 5,5 Sv to the north respectively. It has been established that these intrusions are visible at the sea surface at least 5 times per year indicating that a massive amount of water is advected northward into the Southeastern Atlantic Ocean per year.

However, we have only looked at sections from one cruise at one particular time. Would the same conclusions hold for other cruises in the area? Oceanographic cruises in the study area are very scarce. The only other cruise data with the same synoptic coverage as the ARC cruise was that of Subtropical Convergence and Agulhas Retroflection Cruise (SCARC) [Valentine *et al.*, 1988] and will be discussed next.

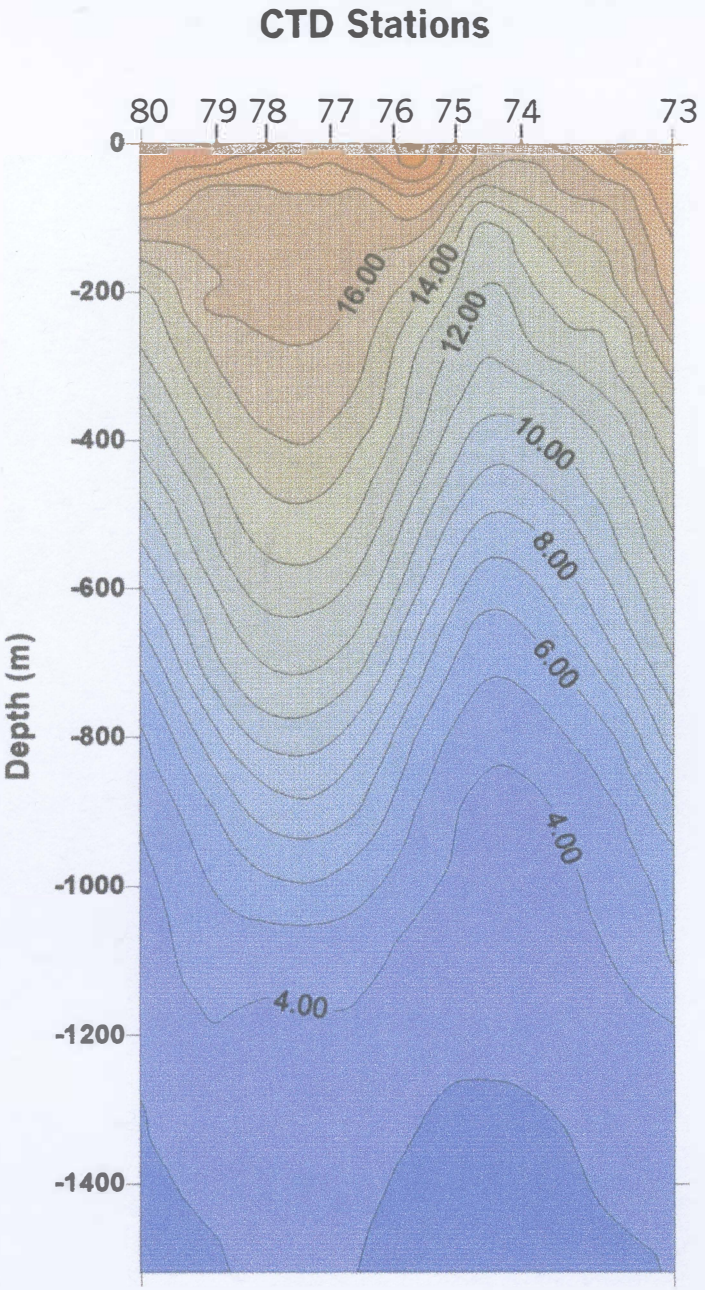

Figure 8.10. Potential temperature section between CTD stations 73 and 80 of the Agulhas Retroflection Cruise (ARC). This section intersects a wedge-like cold water intrusion at CTD station 74

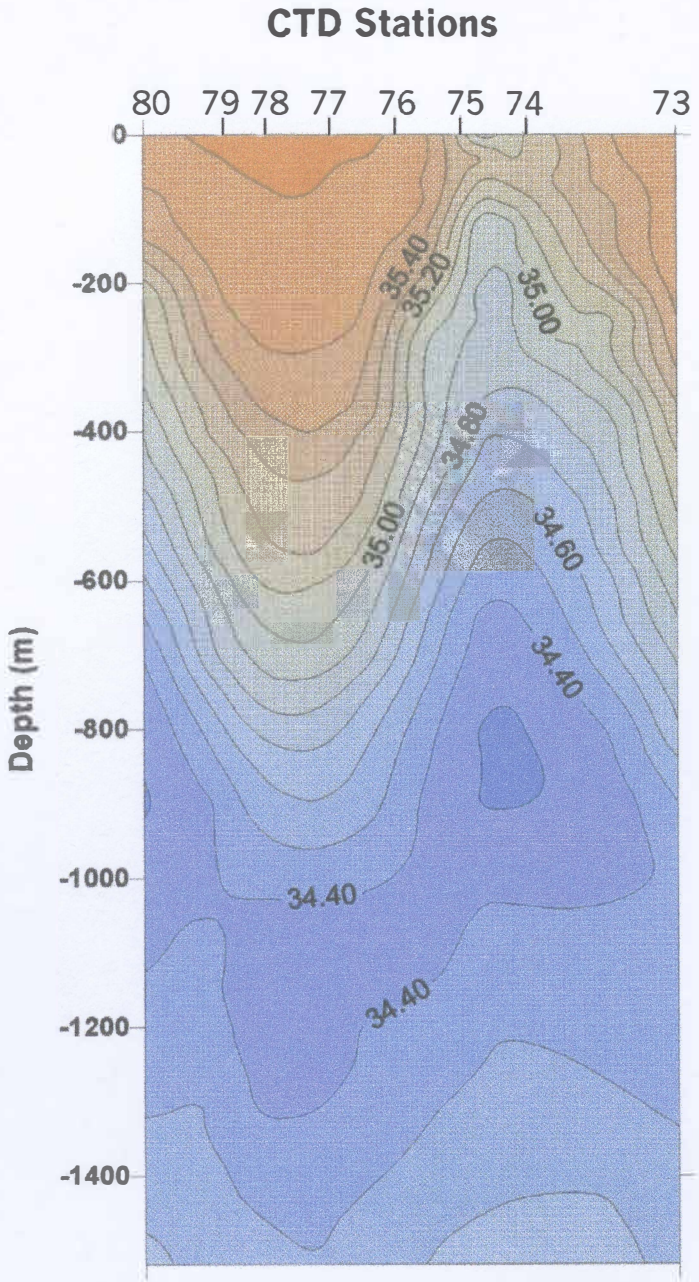

Figure 8.11 Salinity section between CTD stations 73 and 80 of the Agulhas Retroflection Cruise (ARC). This section intersects a wedge-like cold water intrusion at CTD station 74.

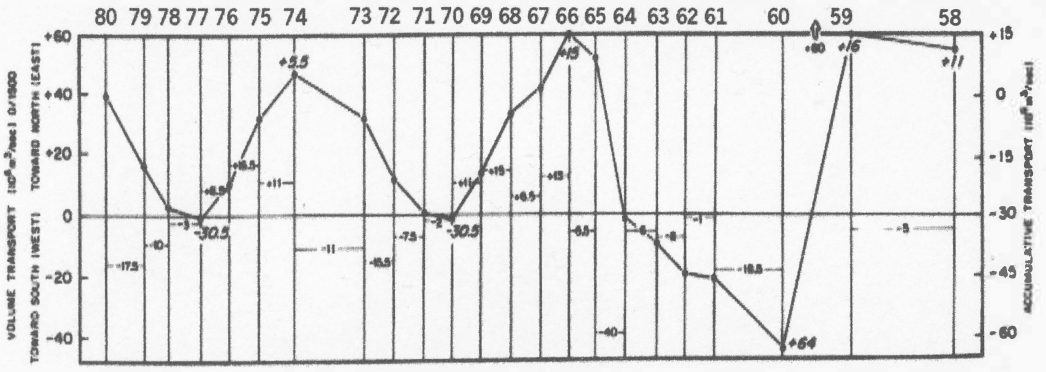

Figure 8.12. Volume transport and accumulated volume transport between CTD stations 58 and 80 of the Agulhas Retroflection Cruise (ARC) in Sverdrups including sections CTD 61 to 73 and 73-80 discussed earlier [Gordon *et al.*, 1987].

8.2. The Subtropical Convergence and Agulhas Retroflection Cruise (SCARC).

The surface thermal expression of the Agulhas Retroflection region from satellite remote sensing during the Subtropical Convergence and Agulhas Retroflection Cruise (SCARC)- from 12 February to 4 March 1987- cruise is given in Figure 3.3 and Figure 6.5. The cruise track for the SCARC is given on Figure 8.13 and covers a large part of the retroflection region with the same synoptic coverage as that of the ARC cruise in 1983. Figure 8.14 gives a contour plot of the depth of the 10 °C isotherm with an overlay of this SCARC cruise track. This Figure shows a clear intrusion of cold water penetrating northward into the Agulhas Retroflection region at CTD station 38. This cold water feature is lodged between the Agulhas retroflection to the east and a warm Agulhas ring centered at CTD 37 to the west of the intrusion. The CTD section from CTD stations 36 to 41 therefore shows similar oceanic features as that observed in the ARC section CTD 73 to CTD 80 approximately four years earlier. Other features at the retroflection are secondary rings with their cores at CTD stations 16, between CTD stations 5 and 6 as well as at CTD station 30. The temperature and salinity of the section between CTD stations 36 and 41 is given in Figures 8.15 and 8.16 respectively.

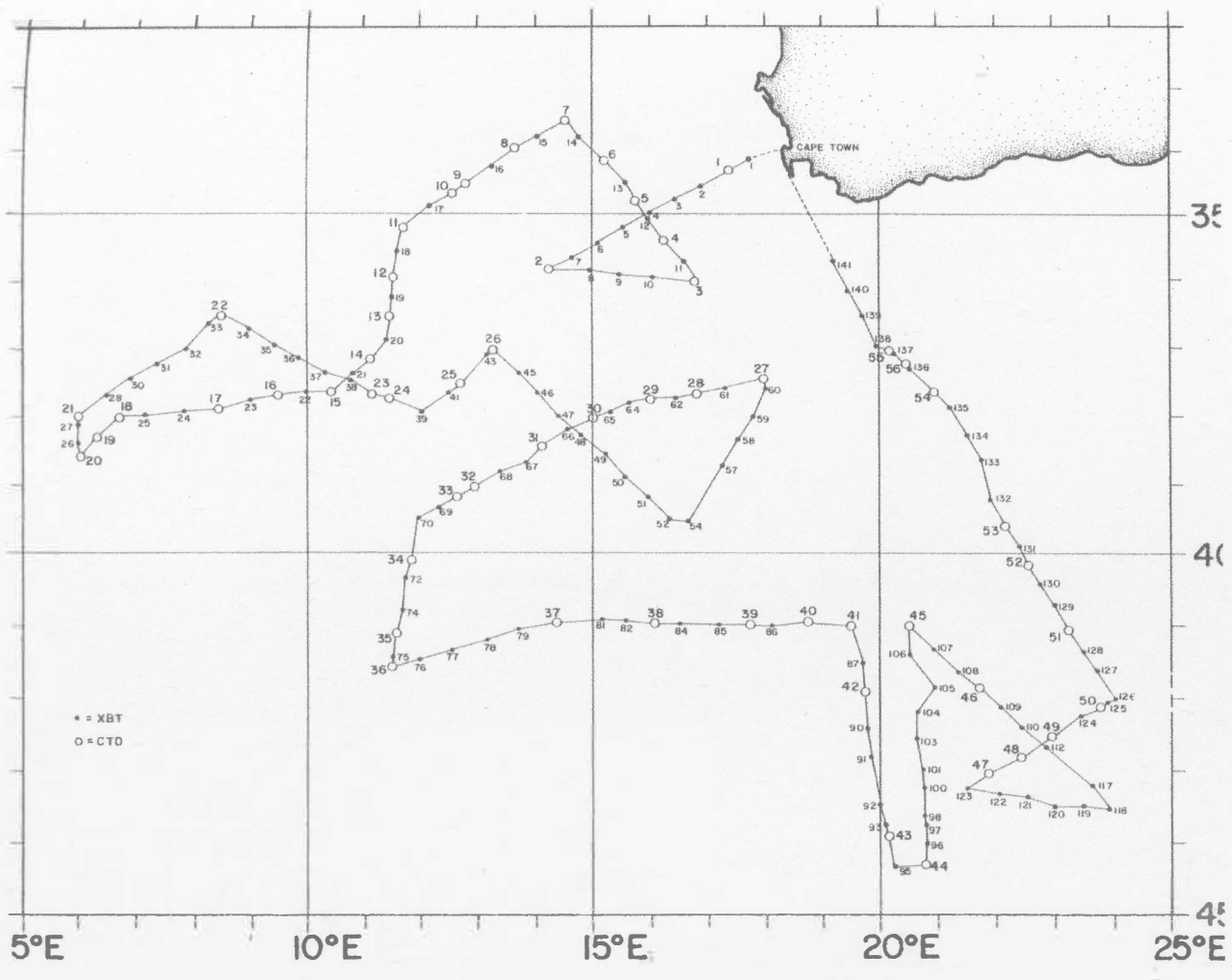

Figure 8.13. The cruise track for the Subtropical Convergence and Agulhas Retroflection Cruise (SCARC) undertaken in February and March 1987. The cruise covered a large part of the Agulhas retroflection region.

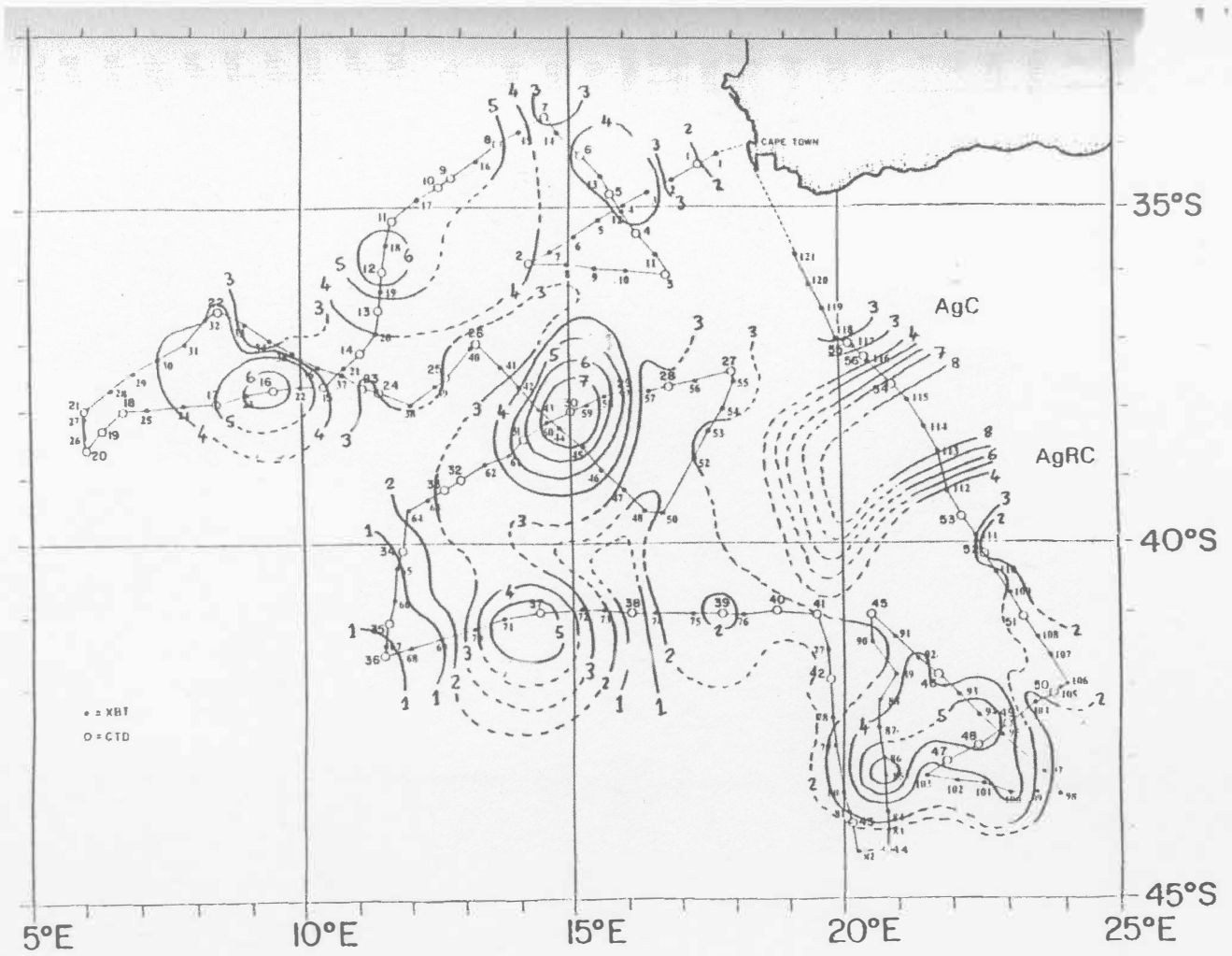

Figure 8.14. Depth contours of the 10 °C isotherm with an overlay of this SCARC cruise track. The Agulhas Current is marked AgC and the Agulhas Return Current is marked AgRC on the diagram. [Rigg, 1995]

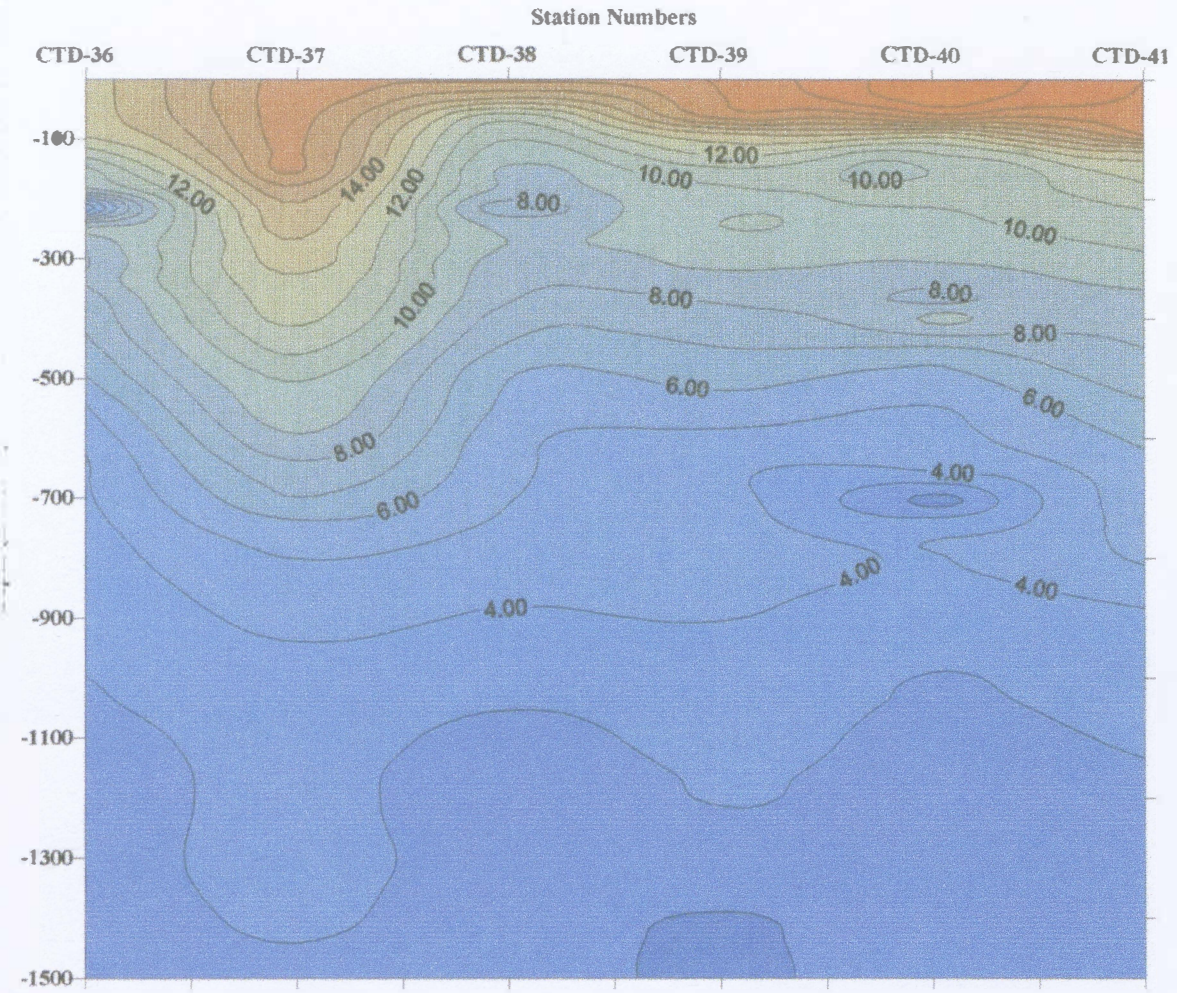

Figure 8.15 Potential temperature section between CTD stations 36 and 41 of the Subtropical Convergence and Agulhas Retroflection Cruise (SCARC). This section intersects a wedge-like cold water intrusion at CTD station 38.

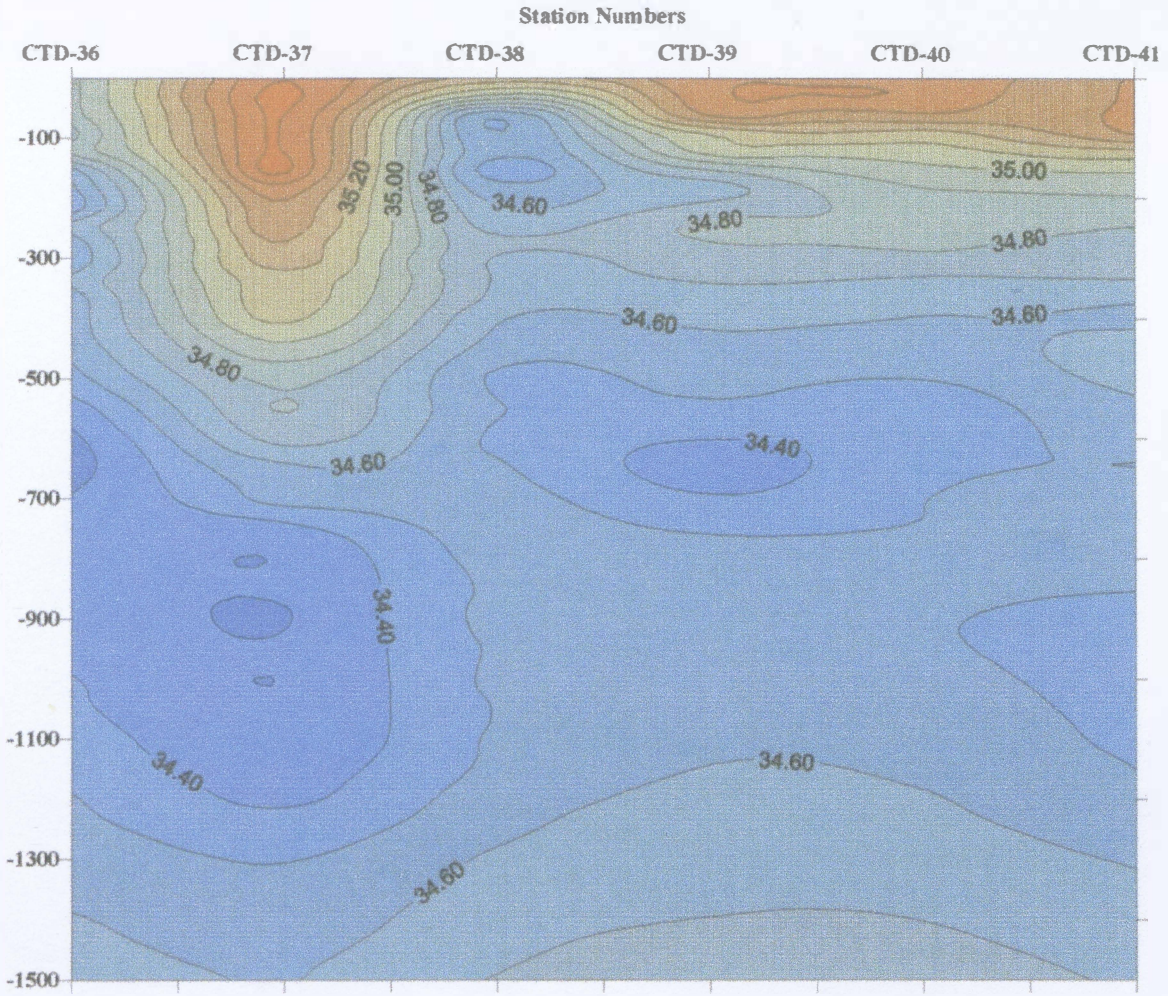

Figure 8.16. Salinity section between CTD stations 36 and 41 of the Subtropical Convergence and Agulhas Retroflection Cruise (SCARC). This section intersects a wedge-like cold water intrusion at CTD station 38.

An intrusion of cold water can be seen at CTD station 38 and a possible intrusion is situated at CTD station 36. The core of the Agulhas Retroflection is seen between CTD stations 39 and 40. This Retroflection is shallower than the retroflection observed for the ARC (~ 1000 m) reaching a depth of approximately 200 m where a strong thermal and salinity front may be observed. To the west of the cold water intrusion a shallower Agulhas current ring than the one observed to the west of the ARC CTD station 66 intrusion is observed. This ring seems to reach a depth of approximately 700 to 800 m.

SAASW seem to wedge upward through the water column to a depth of approximately 300 m in both the temperature and salinity sections (Figures 8.15 and 8.16). During the ARC cruise it was seen that the entire water column wedged upward. However, in the SCARC cruise this wedging of water below 700 m at station 38 is unclear. AAIW is found at a shallower depth of ~700 m and shows no wedge characteristics like its ARC counterpart. Below ~1000 m, however, the NADW mass seem to show some wedging.

A possible explanation for the shallower nature of this SCARC section could lie in the timing of the cruise. The ARC cruise was undertaken in December during the onset of a ring spawning and SAASW intrusion event (from satellite analyses in Chapter 6) while the SCARC cruise was undertaken almost 2 months after the onset of the SAASW intrusion. Therefore this intrusion might have lost some of its onset characteristics.

Figure 8.17 shows the Θ-S diagram for the SCARC section under discussion. AASW and SAASW seem to be present at the AAIW stratum above the NADW. The SAASW is however much more clearly defined here than in the ARC Θ-S section diagrams (Figures 8.3 and 8.4). Other water masses show the distribution normally found for the water of the Agulhas Retroflection *i.e.* Tropical Thermocline Water, Subtropical Surface Water and SICW (Gordon *et al.*, 1987).

The individual Θ-S diagram for CTD station 38 is given in Figures 8.18. The dominant water mass for this station seems to be SAASW above the NADW and AAIW/ Red Sea Water stratum. The surface layer comprises Tropical Thermocline Water and no SICW is present at depth. Thus, the water mass between the Agulhas Retroflection and the newly spawned Agulhas Current ring is indeed SAASW in the upper layers.

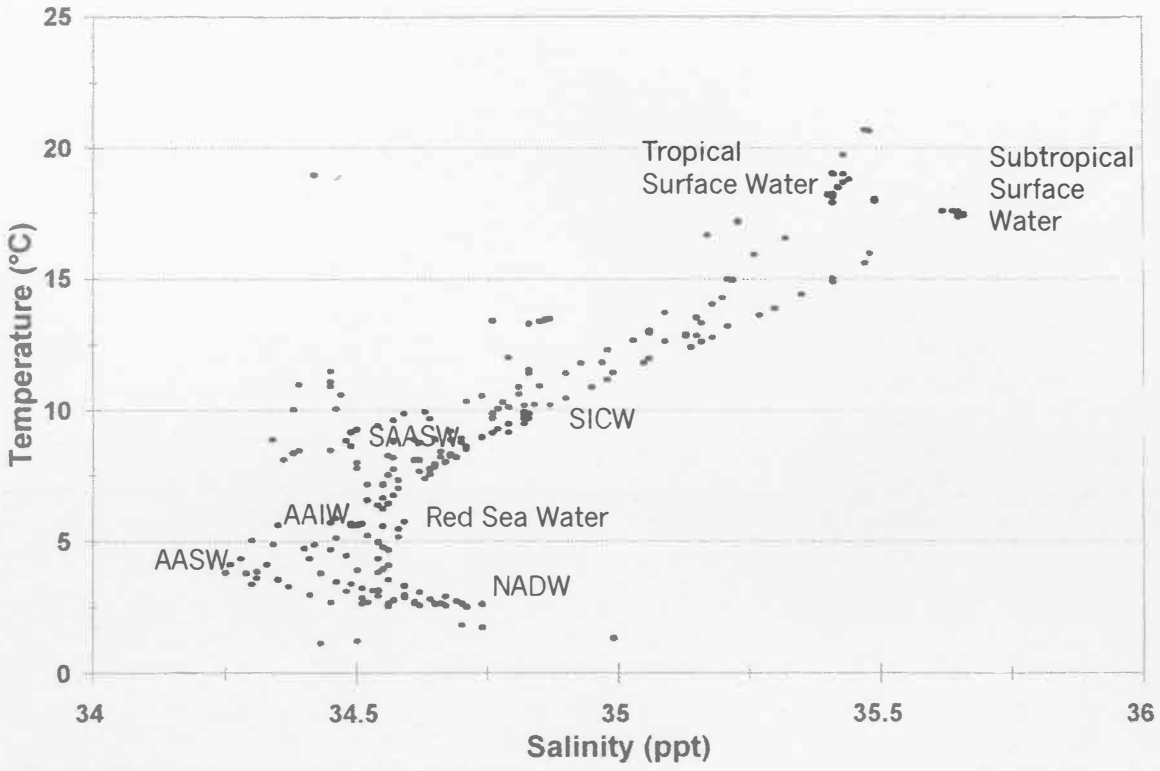

Figure 8.17 Potential temperature-salinity diagram of the SCARC section shown in Figure 8.15 and 8.16 The different water masses are named. SICW= South Indian Central Water, AASW= Antarctic Surface Water, AAIW= Antarctic Intermediate Water, NADW= North Atlantic Deep Water. SAASW marks the proposed location of Sub Antarctic Surface water.

Figure 8.19 shows the vertical temperature profiles for all stations comprising the section of CTD stations 36 to 41. The surface water of CTD station 38 is clearly cooler than that of the surrounding water. A strong thermocline at ~40 m deep is observed; the water above the thermocline being Tropical and Subtropical water associated with the Agulhas Current as observed in the temperature section in Figure 7. 16. Judging from the traces in

Figure 8.19 SAASW seems to be present between the depths 40 m and 200 m at CTD station 38. Below 240 m there does not seem to be any marked differences between the temperature profiles between CTD station 38 and the profiles for the rest of the CTD stations on that section. A distinct spike at 220 m at CTD stations 38 and 36 in Figure 8.19 may be the result of instrumental error.

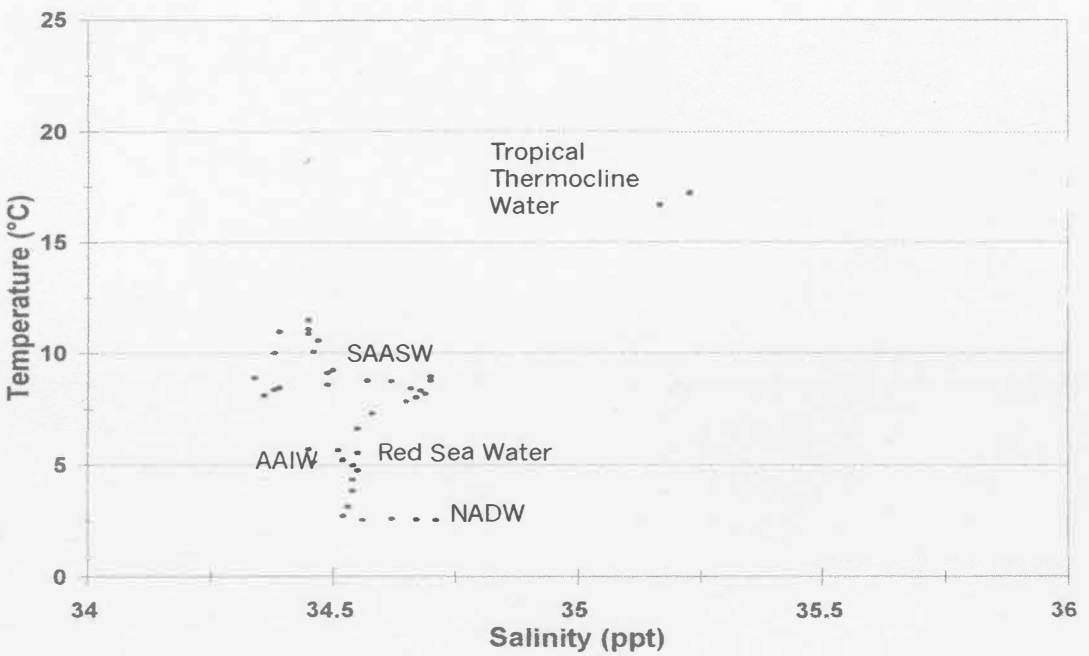

Figure 8.18. Potential Temperature-Salinity plot of Station 38 of the Subtropical Convergence and Agulhas Retroflection Cruise (SCARC) showing a clear presence of SAASW.

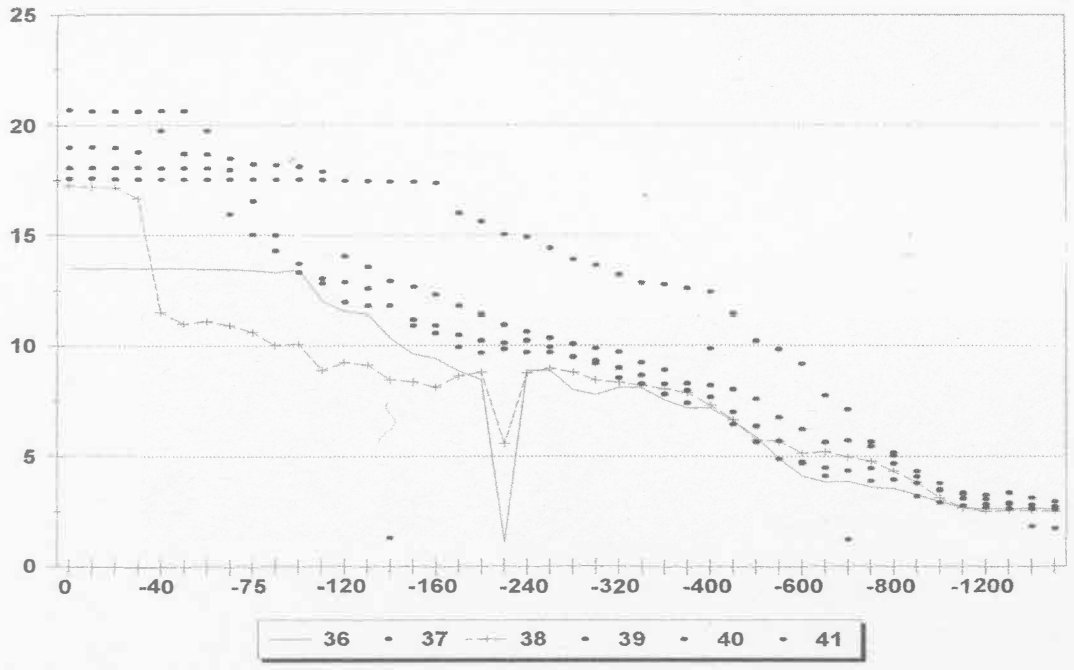

Figure 8.19. Vertical temperature profiles for the Subtropical Convergence and Agulhas Retroflection Cruise (SCARC). The distinct peak of very low temperatures observed at 220 m depth at CTD stations 36 and 38 is most probably the result of instrumental error.

The wedging of the NADW stratum seem to occur at CTD station 39 situated at 40° 56,7' S and 17° 56,446' E which is at the western side of the Agulhas Ridge. The intrusion at CTD station 36 is situated at 41° 31,8' S and 11° 31.2' E. The position seems to fall on the Erica, Schmitt-Ott and Panzarini Seamount chain. Thus topographic control of these intrusions is a possibility.

Thus, the surface lateral dimensions of SAASW intrusions are now known, the duration at which it occurs at the Agulhas Retroflection and the frequency at which they may be observed through satellite infrared remote sensing. Altimetry afforded an indication of the persistence of these SAASW intrusions and the hydrographic analysis gave an indication of the vertical structures of SAASW intrusions. Therefore, a summary of the findings are reported in the next section as well as a exegesis of the implications these findings may have both oceanographically and meteorological.

Chapter 9

Summary and Conclusions

This chapter summarises the results presented in the previous three chapters and presents subjective implications of these results within the restraints of the data and study period used. Extra analyses and data summaries are presented in the Addendum at the end of the thesis.

This thesis does not claim to answer all the possible questions on SAASW intrusions but the data used were sufficient in establishing a basis from which further research could continue. It would therefore be instructive to revisit the original research objectives of the thesis and consider to what extent these research questions were answered:

9.1. The lateral dimensions of SAASW intrusions.

Composite images from the METEOSAT range were used to establish the lateral dimensions of cold water intrusions observed between 1983 and 1990. These intrusions were found to have a width of 174 ± 99 km and a length of 413 ± 215 km, covering an area of 158 520 ± 118 256 km^2. It should, however, be noted that these results are estimates from geographically uncorrected METEOSAT images. These estimates do, however, agree fairly well with those calculated for three illustrative examples of SAASW intrusions from geometrically corrected images.

9.2. Location of SAASW intrusions

The geostationary satellite was again utilized to establish the position of these SAASW intrusions. This is found to be 15 ± 4° E and 40 ± 2° S. The latitudinal estimate is obvious since the STC was considered to be the base from which these SAASW intrusions extend. This agrees well with Meeuwis and van Rensburg (1995) who estimated the longitudinal position of SAASW at 12 ± 2 °E and 15 ± 2 °E, using 3 years of METEOSAT images.

Maps of the mean sea surface temperature and salinity using ship's data clearly shows that the average penetration of cold water generally occurs at approximately 11° E and 19 °E which is at the extremes of the current estimate of SAASW intrusion events.

9.3 Frequency and persistence

About 5 intrusions per year are observed. This agrees very well with the frequency of ring shedding at the retroflection and they are observable through satellite remote sensing about 38% of the time. Meeuwis and van Rensburg (1995) estimated that SAASW might be observable by infrared remote sensing only 17 % of the time.

The estimate of observability depends on the classification of a "bad" or "useless" image. This estimate, therefore, depends on the amount of cloud cover over the region of interest which may account for the mismatch in occurrence frequency of SAASW intrusions.

To eliminate the effect of cloud cover in the estimate of the persistence of SAASW intrusions altimetry was used instead. It was found that SAASW intrusions are present at the Agulhas Retroflection for an average of 28 days before their surface expression is assimilated in the dynamic heights anomalies at the retroflection. This suggests that the penetration of Agulhas filaments into the South Atlantic Ocean, at least at the surface, is halted for this period, cutting off a valuable source of heat and salt to the Atlantic ocean needed to drive the thermohaline circulation cell associated with NADW.

9.4. Hydrographic structure

Two fortuitous cruises afforded the structural investigation of SAASW through the water column. Θ-S diagrams revealed that it is indeed modified SAASW wedging northward over the STC. Potential temperature and salinity sections also suggests that this northward wedging may even involve deeper water such as SAAIW and NADW alluding to possible topographic influence by prominent bathymetric structures; the most obvious being the Agulhas Ridge at ~18° E and the Panzarini seamount at ~11° E.

Shannon *et al.* (1989) have shown that this SAASW shoals northward to approximately 200 m. Their example of a SAASW intrusion was indeed an extreme event lasting for more that 3 months and covering an area of approximately 733 784 km^2.

All available data, both traditional and untraditional were used to study SAASW intrusions southwest of Africa and the findings are reported in the previous three chapters. Although Shannon *et al.* (1989) have commented on the 1986/ 1987 extreme SAASW intrusion event, no focussed research on SAASW intrusions has been carried out to date. This thesis has shown that cold water intrusions involve the northward movement of a massive amount of low temperature, low salinity water to a depth of between 800 m and 1000 m. The biological, oceanographical and meteorological implications of this with regard to the transfer of heat, water and biomass between the Southern, Atlantic and Indian Ocean cannot be ignored in light of the sheer dimensions of these features.

References

Bang N.D., 1970: Dynamic interpretations of a detailed surface temperature chart of the Agulhas Current retroflexion and fragmentation area. *South African Geographical Journal*. **52**: 67 - 76.

Belkin I.M., 1989: Thermohaline structure, hydrological fronts and flux of the Antarctic Circumpolar Current in the central part of the Indian sector of the Southern Ocean. In : *The Antarctic. The Committee Reports*. Nauka, Moskow. **28**: 97 - 112.

Belkin I.M., 1993: Frontal structure of the South Atlantic. In : *Pelagic Ecosystems of the Southern Ocean*. N.M. Voronica (ed.). Nauka, Moskow: 40 - 53.

Brundrit G.B. and L.V. Shannon, 1989: Cape storms and the Agulhas Current : a glimpse of the future ? *South African Journal of Science*. **85 (10)**: 619 - 620.

Camp D. B., E. H. Haines, B. A. Huber, S. E. Rennie and A. L. Gordon, 1986: Agulhas Retroflection Cruise. November-December 1983. Hydrographic Data. *Office of Naval Research, 800 N. Quincy Street, Arlington, VA 22216.* **LDGO-86-1**: 390pp.

Chapman P. and L.V. Shannon, 1985: The Benguela ecosystem 2. Chemistry and related processes. In : *Oceanography and Marine Biology. An Annual Review.* Barnes M. (ed.) Aberdeen, University Press. **23**: 183 - 251.

Duncombe Rae C.M., 1991: Agulhas retroflection rings in the South Atlantic Ocean; an overview. *South African Journal of Marine Science*. **11**: 327 - 344.

Duncombe Rae, C. M., F. A. Shillington, J. J. Agenbach, J. Taunton-Clark and M. L. Gründlingh, 1992: An Agulhas ring in the South Atlantic Ocean and its interaction with the Benguela upwelling frontal system. *Deep-Sea Research.* **39(11/12)**: 2009 - 2027.

Feron R. C. V., W.P.M. de Ruijter and D. Oskam, 1992: Ring-shedding process in the Agulhas Current system. *Journal of Geophysical Research.* **97 (C6)**: 9467 - 9477.

Folland C.K., D.E. Parker and F.E. Kates, 1984: Worldwide marine temperature fluctuations 1856-1981. *Nature.* **310**: 670-673.

Gillooly J.F. and N.D. Walker, 1984: Spatial and temporal behaviour of sea-surface temperatures in the South Atlantic. *South African Journal of Science.* **80 (2)**: 97 - 100.

Gordon A. L., 1986: Interocean exchange of thermocline water. *Journal of Geophysical Research.* **91(C4)**: 5037 - 5046.

Gordon A.L., 1996: Comment on the South Atlantic's role in global circulation. *The South Atlantic: Present and Past Circulation*. Wefer G, Berger W.H., Sieder G and Webb D.J. (eds). Springer-Verslag, Berlin Heidelberg. **1996**: 121 - 124.

Gordon A.L. and W.F. Haxby, 1990: Agulhas Eddies invade the South Atlantic - evidence from GEOSAT altimeter and shipboard conductivity-temperature-depth survey. *Journal of Geophysical Research.* **95 (C3)**: 3117 - 3125.

Gordon A.L., J.R.E. Lutjeharms and M.L. Gründlingh, 1987: Stratification and circulation of the Agulhas Retroflection. *Deep-Sea Research.* **34 (4)**: 565 - 599.

Gründlingh M.L., 1985: Occurrence of Red Sea Water in the south-western Indian Ocean, 1981. *Journal of Physical Oceanography*. **15**: 207-212.

Gründlingh M.L. and J.R.E. Lutjeharms, 1990: Deep-sea circulation patterns off Southern Africa. In: *Marine Science and Technology in South Africa*. J.F. Herbst (ed). Foundation for Research Development (**pub**.): 13 – 16.

Harris T. F. W. and C.C. Stavropoulos, 1978: Satellite-Tracked Drifters between Africa and Antarctica. *Bulletin of the American Meteorological Society*. **59 (1)**: 51 - 59.

Harris T. F. W. and D. van Foreest, 1978: The Agulhas Current in March 1969. *Deep-Sea Research*. **25**: 549 – 561.

Jones P.D., T.M.L. Wigley and P.B. Wright, 1986: Global temperature variations between 1861 and 1984. *Nature*. **322**: 430 – 434.

Jury M.R., 1992: A climatic dipole governing the interannual variability of convection over the S.W. Indian Ocean and S.E. Africa region. *Trends in Geophysical Research*. **1**: 165-172.

Lutjeharms J.R.E., 1981: Features on the Southern Agulhas circulation from satellite remote sensing. *South African Journal of Science*. **77(5)**: 231 - 236.

Lutjeharms J.R.E., 1985: Location of frontal systems between Africa and Antarctica: some preliminary results. *Deep-Sea Research*. **32 (12)**: 1499 - 1509.

Lutjeharms J.R.E., 1991: Twintig jaar van fisiese oseanologie in Suid-Afrika: 'n persoonlike beskouing. *South African Journal of Marine Science*. **10**: 305 - 320.

Lutjeharms, J.R.E., 1996: The Exchange of Water Between the South Indian and the South Atlantic Oceans. *The South Atlantic: Present and Past Circulation*. Wefer G, Berger W.H., Sieder G and Webb D.J. (eds). Springer-Verslag, Berlin Heidelberg. **1996**: 125 - 162.

Lutjeharms J.R.E. and J. Cooper, 1996: Interbasin leakage through Agulhas Current filaments. *Deep-Sea Research*. **43 (2)**: 213 - 238.

Lutjeharms J.R.E. and A.L. Gordon, 1987: Shedding of an Agulhas ring observed at sea. *Nature*. **325 (7000)**: 138 - 140.

Lutjeharms J. R. E. and H. R. Roberts, 1988: The Natal Pulse: An extreme transient on the Agulhas Current. *Journal of Geophysical Research*. **93 (C1)**: 631 – 645.

Lutjeharms J.R.E. and P.L. Stockton, 1987: Kinematics of the upwelling front off Southern Africa.. In : *The Benguela and comparable ecosystems*. A.I.L. Payne, J.A. Gulland and K.H. Brink (eds). *South African Journal of Marine Science*. **5**: 35 - 49.

Lutjeharms J.R.E. and H.R. Valentine, 1987: Water Types in the S. E. Atlantic Upwelling Regime. In: The Benguela and Comparable Ecosystems. *South African Journal of Marine Science*. **5**: 63 - 71

Lutjeharms J.R.E. and H.R. Valentine, 1988: Eddies at the Subtropical Convergence South of Africa. *Journal of Physical Oceanography*. **18**: 761 - 774.

Lutjeharms J.R.E. and R.C. van Ballegooyen, 1988: The retroflection of the Agulhas Current. *Journal of Physical Oceanography*. **18**: 1570 - 1583.

Lutjeharms J.R.E., N.D. Bang and C.P. Duncan, 1981: Characteristics of the currents east and south of Madagascar. *Deep-Sea Research*. **28 (9)**: 879 - 899.

Lutjeharms J.R.E., R. Catzel and H.R. Valentine, 1989: Eddies and other border phenomena of the Agulhas Current. *Continental Shelf Research*. **9 (7)**: 597 - 616.

Lutjeharms J.R.E., W.P.M. de Ruijter and R.G. Peterson, 1992: Interbasin exchange and the Agulhas retroflection; the development of some oceanographic concepts. *Deep-Sea Research*. **39 (10)**: 1791-1807.

Majodina M., 1995: Composite analysis of Winter Storms South of Africa. *Honours Thesis, 1995*. University of Cape Town, South Africa: 30pp + 15pp diagrams.

Matthysen C. P., 1997: Detail of the Thermal Structure of the oceanic fronts in the Southern Ocean south of Africa. *Master of Science Thesis, 1997*. University of Cape Town, South Africa: 74 pp.

Meeuwis J.M. and P.A.J. van Rensburg, 1995: The changing patterns of cold Sub-antarctic Surface Water into the Agulhas System. *International Geosphere-Biosphere Programme. Global Environmental Change : Implications for Southern Africa. Regional Conference*, 24 to 26 April 1995: 158 - 159.

Nelson G., D.W. Japp and R.J.Q. Tarr, 1992: The 1980s - a decade of change in the Benguela ecosystem. *South African Journal of Marine Science*. **12**: 271 - 296.

Pickard G.L., 1963: Descriptive Physical Oceanography. *Pergamon Press Ltd. Headington Hill Hall, Oxford*. 200pp.

Preston-White R.A. and P.D. Tyson, 1988: The Atmosphere and Weather of Southern Africa. *Oxford University Press, Harrington House, Barrack Street, Cape Town 8001, South Africa*: 374pp.

Rice J. A., 1988: Mathematical Statistics and Data Analysis. *Wadsworth & Brooks/ Cole, Belmont*: 595pp.

Rigg G. M., 1995: The hydrography and dynamics of rings and eddies of the Agulhas Retroflection February-March 1987. *Master of Science Thesis, graduate 1995*. University of Cape Town, South Africa: 270pp.

Schmitz W. J., 1996: On the World Ocean circulation: Volume 1: Some global features/ Norht Atlantic circulation. *Technical Report WHOI-96-03*. Woods Hole Oceanographic Institute, Woods Hole, Massachusetts: 141pp.

Schumann E. H., 1990: Physical oceanography. In: *Marine Science and Technology in South Africa*. J.F. Herbst (Ed.). Foundation for Research Development (**pub**.): 2 -3.

Schumann E.H. and L.J. Beekman, 1984: Ocean Temperature structures on the Agulhas Bank. *Transactions of the Royal Society of South Africa*. **45 (2)**: 191 – 203.

Shannon L.V., 1985: The Benguela Ecosystem Part I. Evolution of the Benguela, physical features and processes. *Oceanography and Marine Biology. Annual Review*. **23**: 105 - 182.

Shannon L.V., 1990: The Benguela Current System. In: *Marine Science and Technology in South Africa*. J.F. Herbst (Ed.). Foundation for Research Development (**pub**.): 17 - 19.

Shannon L.V. and J.J. Agenbag, 1990: A large scale perspective on the interannual variability in the environment in the south-east Atlantic. *South African Journal of Marine Science*. **9**: 161 - 168.

Shannon L.V., J.J. Agenbag, N.D. Walker, J.R.E. Lutjeharms, 1990: *A major perturbation in the Agulhas Retroflection area in 1986*. Deep-Sea Research. **37 (3)**: 493 to 512.

Shannon L.V., A.J. Boyd, G.B. Brundrit and J. Taunton-Clark, 1986: On the existence of an El Niño-type phenomenon in the Benguela system. *Journal of Marine Science*. **44 (3)**: 495 - 520.

Shannon L.V. and Chapman P., 1991: Evidence of Antarctic Bottom Water in the Angola Basin at 32 °S. *Deep-Sea Research*. **38 (10)**: 1299 - 1304.

Shannon L.V. and D Hunter, 1988: Notes on Antarctic Intermediate Water around Southern Africa. *South African Journal of Marine Science*. **6**: 107 – 117.

Shannon L.V., J.R.E Lutjeharms and J.J. Agenbag, 1989: Episodic input of Sub-antarctic Water into the Benguela region. *South African Journal of Science*. **85(5)**: 317 - 322.

Shannon L.V. and G. Nelson, 1996: The Benguela: Large Scale Features and Processes and System Variability. *The South Atlantic: Present and Past Circulation*. Wefer G, Berger W.H., Sieder G and Webb D.J. (eds). Springer-Verslag, Berlin Heidelberg. **1996**: 163 - 210.

Siegfried W.R. and J.R.E. Lutjeharms, 1990: Introduction. In: *Marine Science and Technology in South Africa*. J.F. Herbst (ed). Foundation for Reseach Development Publ.: 70 pp.

Stramma L. and J.R.E. Lutjeharms, 1997: The flow field of the subtropical gyre of the South Indian Ocean. *Journal of Geophysical Research*. **C 102 (3)**: 5513 - 5530.

Stramma L and R.G. Peterson, 1989: Geostrophic transport in the Benguela Current region. *Journal of Physical Oceanography* **19**: 1440 - 1448.

Tomczak M and J. S. Godfrey, 1994: Regional oceanography: An Introduction. *Oxford: Pergamon Press*. 422pp.

Toole J. M. and B. A. Warren, 1993: A hydrographic section across the subtropical South Indian Ocean. *Deep-sea Research*. **40 (10)**: 1973 – 2019.

Tyson P.D., 1986: Climate Change and Variability in Southern Africa. Oxford University Press, Cape Town: 220pp.

Underhill L. G., 1984: Introstat (3rd Ed). *Juta and Company, Kenwyn*: 383 pp.

Valentine H. R., C. M. Duncombe Rae, R. C. van Ballegooyen and J. R. E. Lutjeharms, 1988: The Subtropical Convergence and Agulhas Retroflection Cruise (SCARC) Data Report. *National Research Institute for Oceanology, CSIR, P. O. Box 320, Stellenbosch, 7600, South Africa.*

van Ballegooyen R.C., M.L. Gründlingh and J.R.E. Lutjeharms, 1994: Eddy fluxes of heat and salt from the south-west Indian Ocean into the South-east Atlantic Ocean: a case study. *Journal of Geophysical Research*. **99 (C7)**: 14053 - 14070.

van Ballegooyen R.C., H.R. Valentine and J.R.E. Lutjeharms, 1991: Modelling of the Agulhas Current System. *South African Journal of Science*. **87 (11/12)**: 569 - 571.

van Leeuwen P. J., W. P. M. de Ruijter and J. R. E. Lutjeharms, 2000: Natal pulses and the formation of Agulhas rings. *Journal of Geophysical Research*. **105 (C3)**: 6425 – 6436.

Villacastin-Herrero C.A., L.G. Underhill, R.J.M. Crawford and L.V. Shannon, 1990: Sea surface temperature of the oceans surrounding subequatorial Africa: seasonal patterns, spatial coherence and long-term trends. *South African Journal of Science*. **92 (4)**: 189 - 197.

Webb D.J., 1996: The Southern Boundary of the South Atlantic. *The South Atlantic: Present and Past Circulation*. Wefer G, Berger W.H., Sieder G and Webb D.J. (eds), 1996. Springer-Verslag, Berlin Heidelberg: 211 - 217.

Weeks S.J. and F.A. Shillington, 1996: Phytoplancton pigment distribution and the frontal structure if the South Indian Ocean. *Journal of Geophysical Research*. **101 (C3)**: 6377 - 6391.

Whitworth T. and W. D. Nowlin, 1987: Water Masses and Currents of the Southern Ocean at the Greenwich Meridian. *Journal of Geophysical Research.* **92 (C6)**: 6462 – 6476.

Wyrtki K., 1971: Oceanic Atlas of the International Indian Ocean Expedition. *National Science Foundation*, Washington DC: 531 pp.

Addenda

A.1. Composite METEOSAT images (1983 to 1990)

These are composite sketches of infrared images from the METEOSAT series of individual SAASW intrusions at the STC and were used to determine the geographic location of SAASW intrusions as well as their lateral dimensions. It also gives an indication of the various types and shapes of the intrusions at the Agulhas Retroflection.

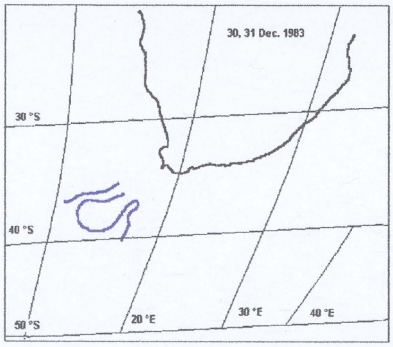
30, 31 Dec. 1983
30 °S
40 °S
50 °S
20 °E
30 °E
40 °E

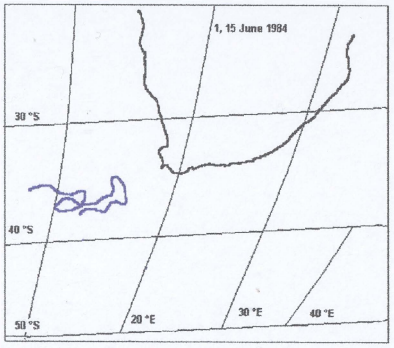
1, 15 June 1984
30 °S
40 °S
50 °S
20 °E
30 °E
40 °E

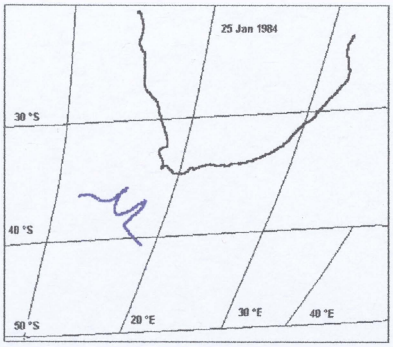
25 Jan 1984
30 °S
40 °S
50 °S
20 °E
30 °E
40 °E

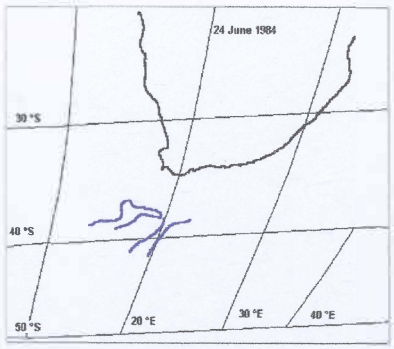
24 June 1984
30 °S
40 °S
50 °S
20 °E
30 °E
40 °E

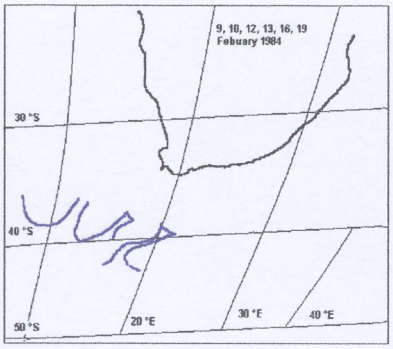
9, 10, 12, 13, 16, 19
Febuary 1984
30 °S
40 °S
50 °S
20 °E
30 °E
40 °E

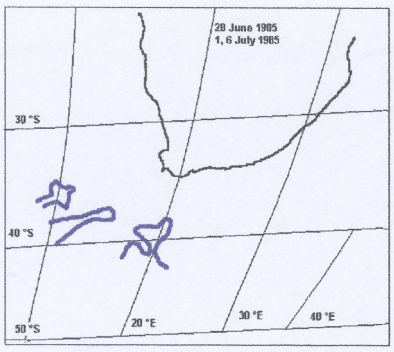
28 June 1985
1, 6 July 1985
30 °S
40 °S
50 °S
20 °E
30 °E
40 °E

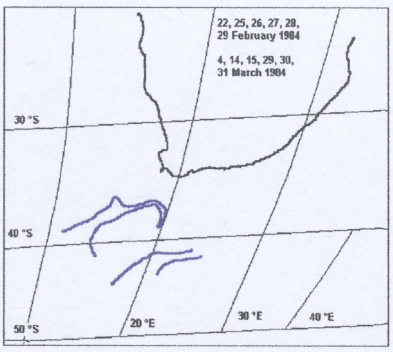
22, 25, 26, 27, 28,
29 February 1984
4, 14, 15, 29, 30,
31 March 1984
30 °S
40 °S
50 °S
20 °E
30 °E
40 °E

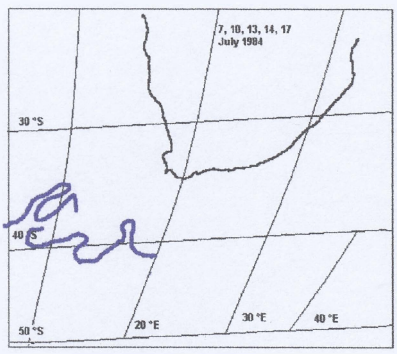
7, 10, 13, 14, 17
July 1984
30 °S
40 °S
50 °S
20 °E
30 °E
40 °E

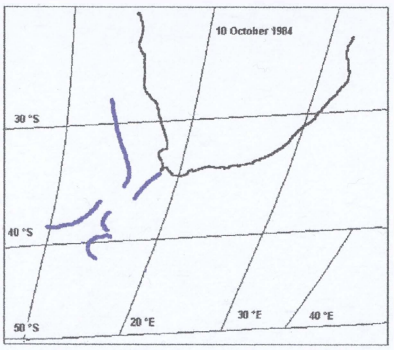
10 October 1984
30 °S
40 °S
50 °S
20 °E
30 °E
40 °E

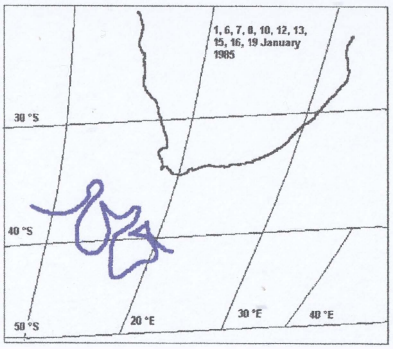
1, 6, 7, 8, 10, 12, 13, 15, 16, 19 January 1985
30 °S
40 °S
50 °S
20 °E
30 °E
40 °E

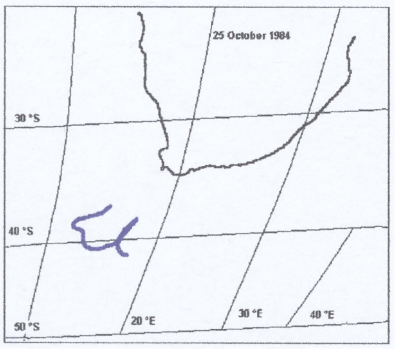
25 October 1984
30 °S
40 °S
50 °S
20 °E
30 °E
40 °E

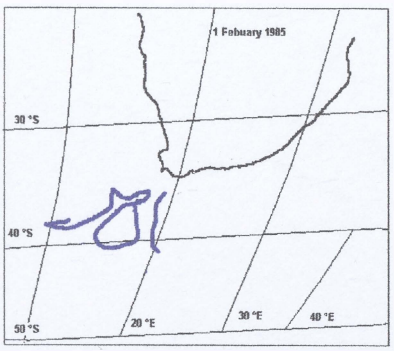
1 Febuary 1985
30 °S
40 °S
50 °S
20 °E
30 °E
40 °E

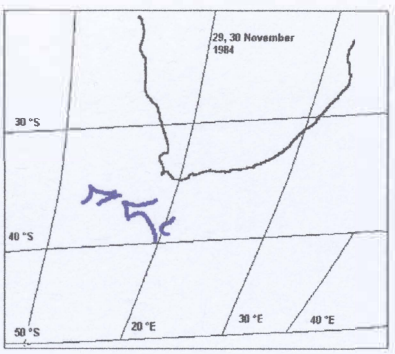
29, 30 November 1984
30 °S
40 °S
50 °S
20 °E
30 °E
40 °E

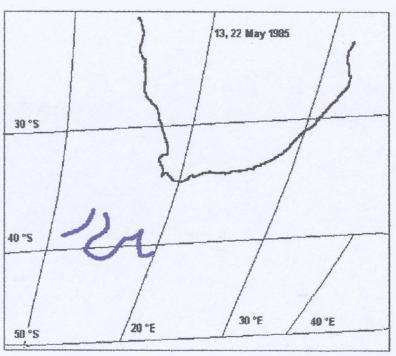
13, 22 May 1985
30 °S
40 °S
50 °S
20 °E
30 °E
40 °E

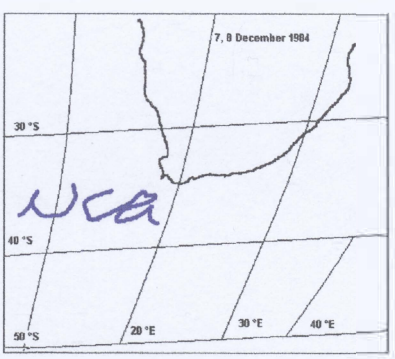
7, 8 December 1984
30 °S
40 °S
50 °S
20 °E
30 °E
40 °E

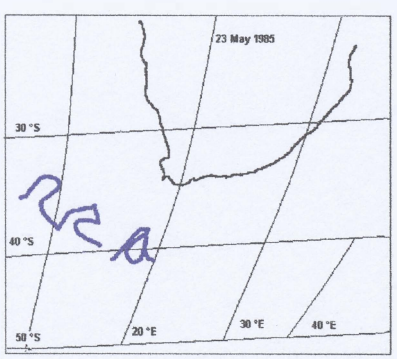
23 May 1985
30 °S
40 °S
50 °S
20 °E
30 °E
40 °E

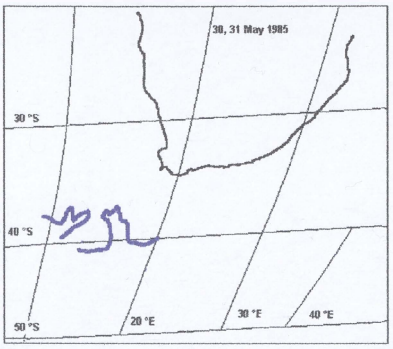
30, 31 May 1985
30 °S
40 °S
50 °S
20 °E
30 °E
40 °E

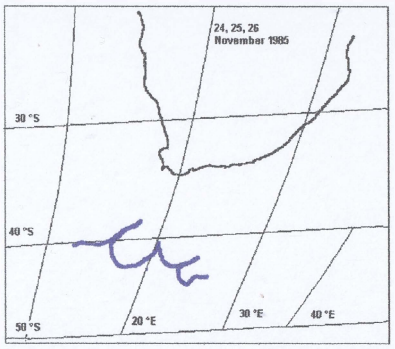
24, 25, 26
November 1985
30 °S
40 °S
50 °S
20 °E
30 °E
40 °E

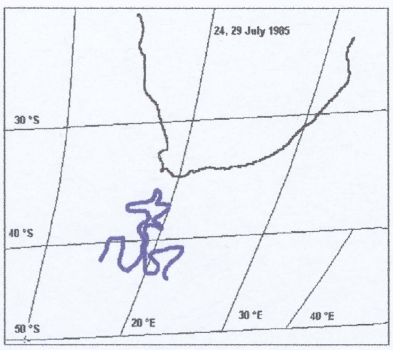
24, 29 July 1985
30 °S
40 °S
50 °S
20 °E
30 °E
40 °E

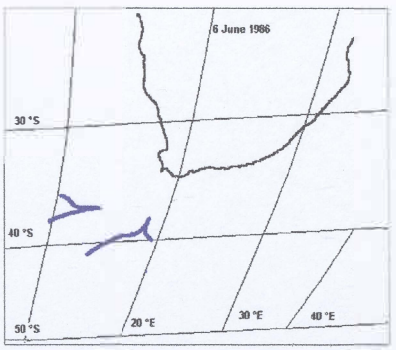
6 June 1986
30 °S
40 °S
50 °S
20 °E
30 °E
40 °E

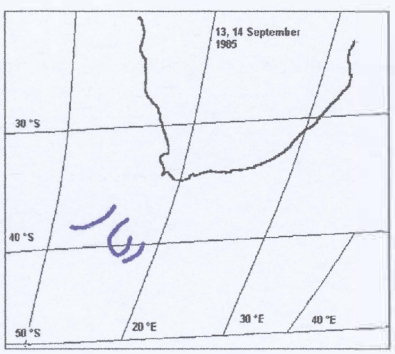
13, 14 September
1985
30 °S
40 °S
50 °S
20 °E
30 °E
40 °E

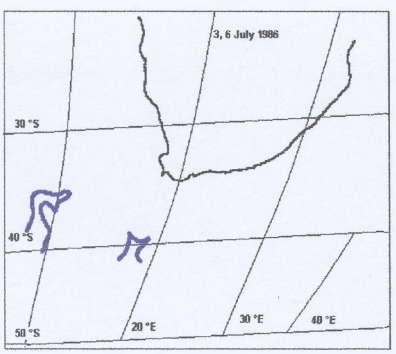
3, 6 July 1986
30 °S
40 °S
50 °S
20 °E
30 °E
40 °E

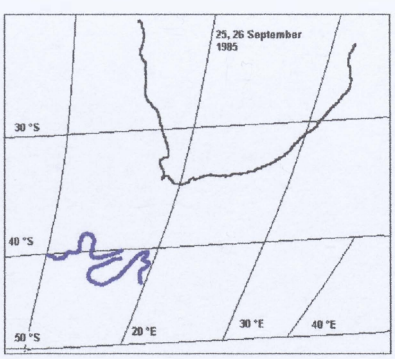
25, 26 September
1985
30 °S
40 °S
50 °S
20 °E
30 °E
40 °E

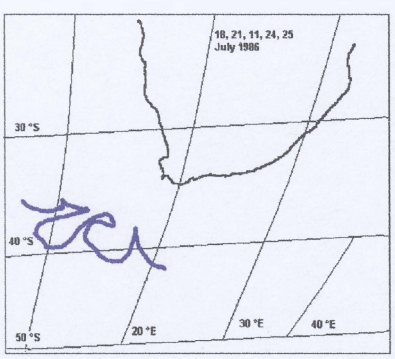
18, 21, 11, 24, 25
July 1986
30 °S
40 °S
50 °S
20 °E
30 °E
40 °E

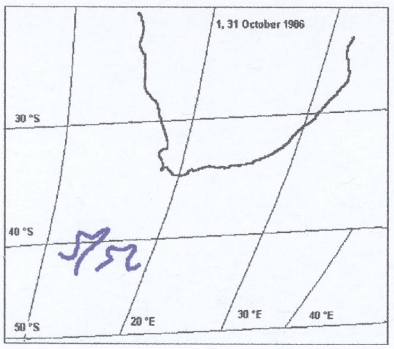
1, 31 October 1986
30 °S
40 °S
50 °S
20 °E
30 °E
40 °E

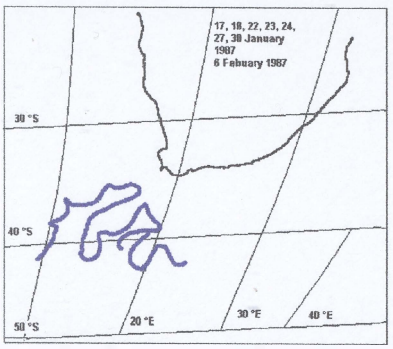
17, 18, 22, 23, 24, 27, 30 January 1987
6 February 1987
30 °S
40 °S
50 °S
20 °E
30 °E
40 °E

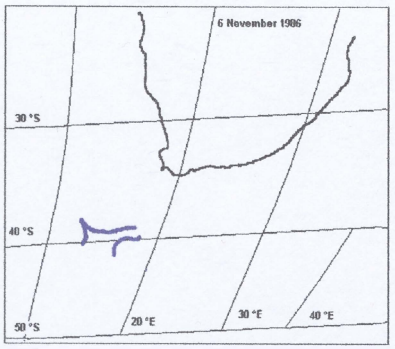
6 November 1986
30 °S
40 °S
50 °S
20 °E
30 °E
40 °E

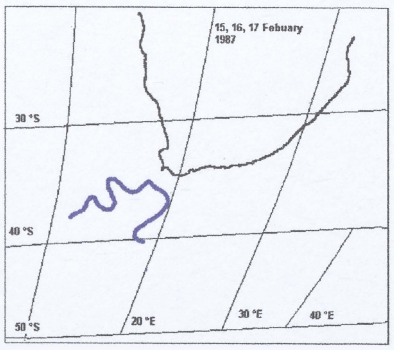
15, 16, 17 Febuary 1987
30 °S
40 °S
50 °S
20 °E
30 °E
40 °E

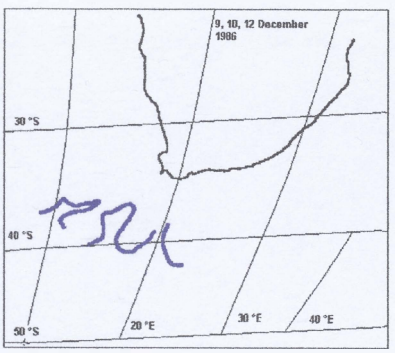
9, 10, 12 December 1986
30 °S
40 °S
50 °S
20 °E
30 °E
40 °E

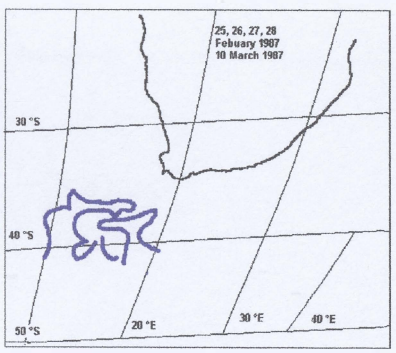
25, 26, 27, 28 Febuary 1987
10 March 1987
30 °S
40 °S
50 °S
20 °E
30 °E
40 °E

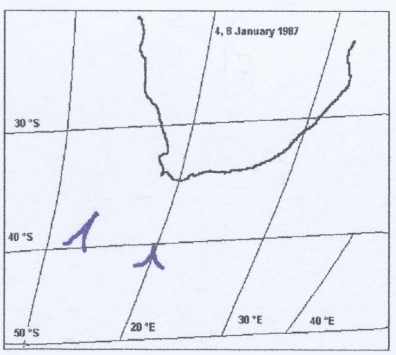
4, 8 January 1987
30 °S
40 °S
50 °S
20 °E
30 °E
40 °E

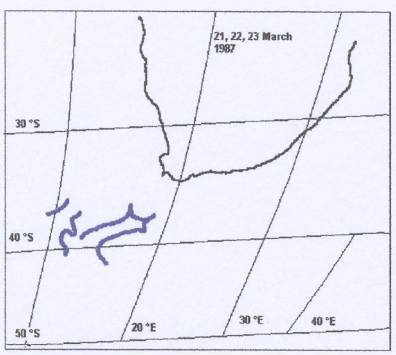
21, 22, 23 March 1987
30 °S
40 °S
50 °S
20 °E
30 °E
40 °E

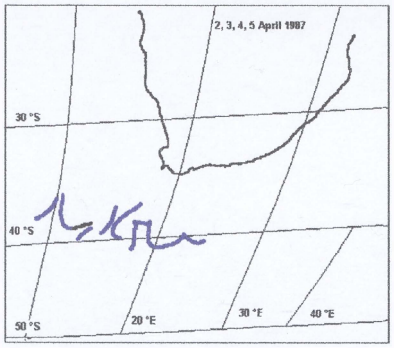
2, 3, 4, 5 April 1987
30 °S
40 °S
50 °S
20 °E
30 °E
40 °E

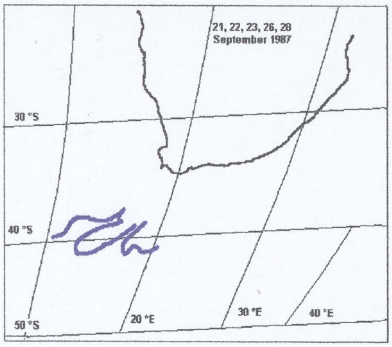
21, 22, 23, 26, 28
September 1987
30 °S
40 °S
50 °S
20 °E
30 °E
40 °E

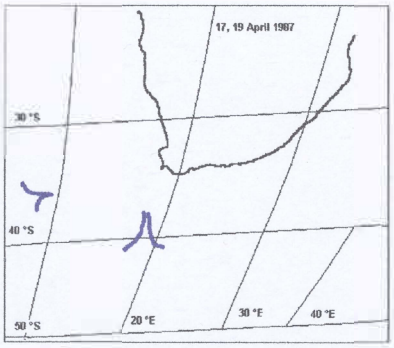
17, 19 April 1987
30 °S
40 °S
50 °S
20 °E
30 °E
40 °E

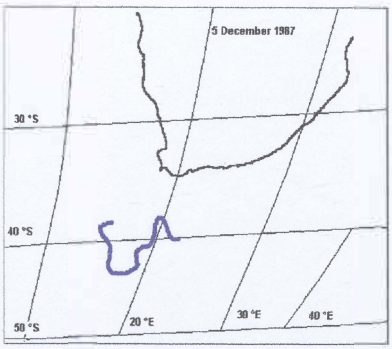
5 December 1987
30 °S
40 °S
50 °S
20 °E
30 °E
40 °E

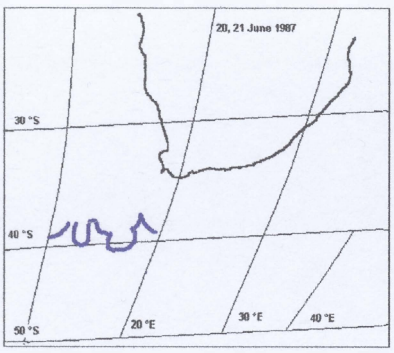
20, 21 June 1987
30 °S
40 °S
50 °S
20 °E
30 °E
40 °E

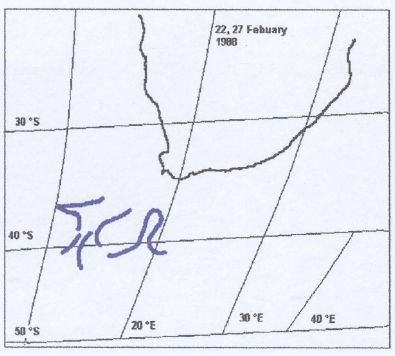
22, 27 Febuary
1988
30 °S
40 °S
50 °S
20 °E
30 °E
40 °E

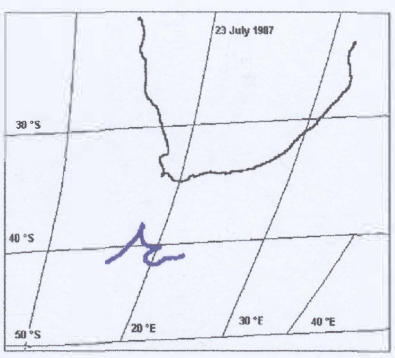
23 July 1987
30 °S
40 °S
50 °S
20 °E
30 °E
40 °E

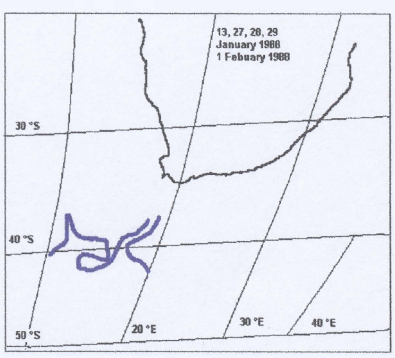
13, 27, 28, 29
January 1988
1 Febuary 1988
30 °S
40 °S
50 °S
20 °E
30 °E
40 °E

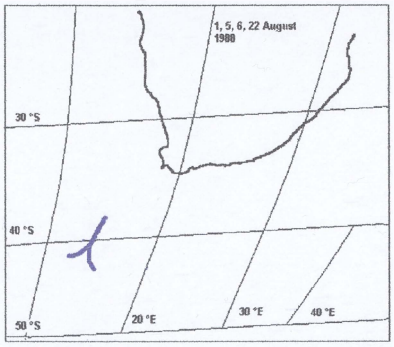
1, 5, 6, 22 August
1988
30 °S
40 °S
50 °S
20 °E
30 °E
40 °E

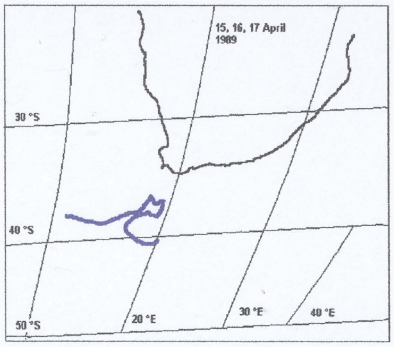
15, 16, 17 April
1989
30 °S
40 °S
50 °S
20 °E
30 °E
40 °E

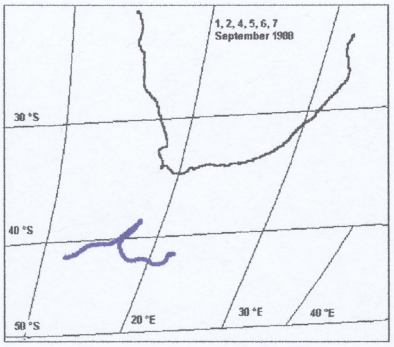
1, 2, 4, 5, 6, 7
September 1988
30 °S
40 °S
50 °S
20 °E
30 °E
40 °E

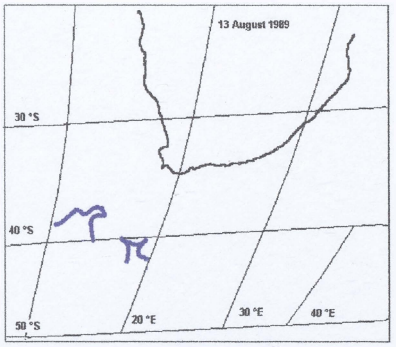
13 August 1989
30 °S
40 °S
50 °S
20 °E
30 °E
40 °E

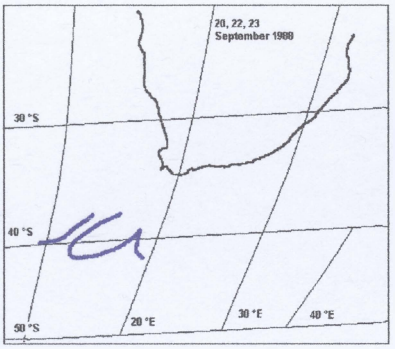
20, 22, 23
September 1988
30 °S
40 °S
50 °S
20 °E
30 °E
40 °E

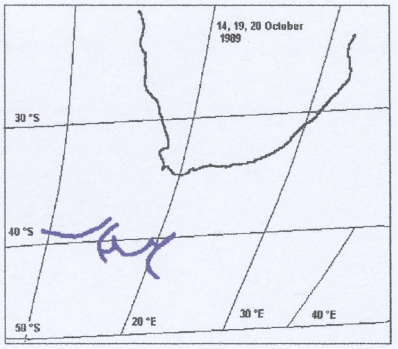
14, 19, 20 October
1989
30 °S
40 °S
50 °S
20 °E
30 °E
40 °E

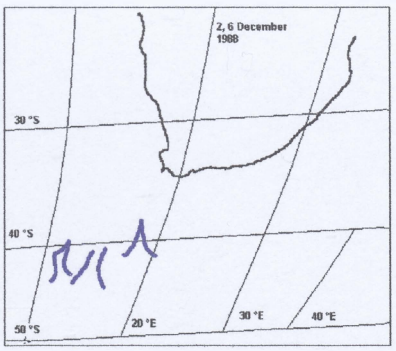
2, 6 December
1988
30 °S
40 °S
50 °S
20 °E
30 °E
40 °E

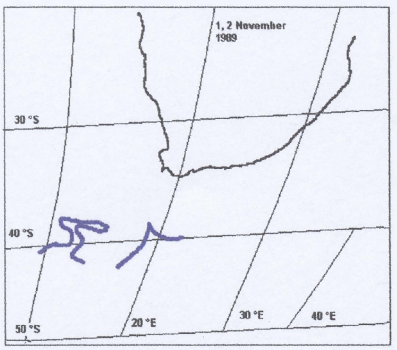
1, 2 November
1989
30 °S
40 °S
50 °S
20 °E
30 °E
40 °E

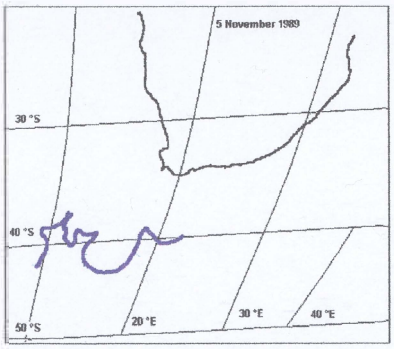
5 November 1989
30 °S
40 °S
50 °S
20 °E
30 °E
40 °E

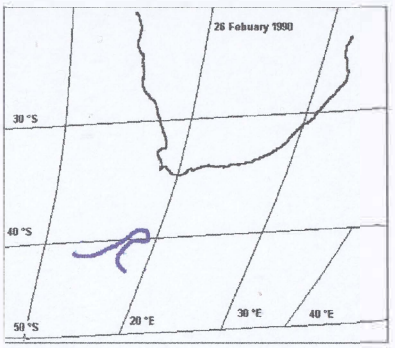
26 Febuary 1990
30 °S
40 °S
50 °S
20 °E
30 °E
40 °E

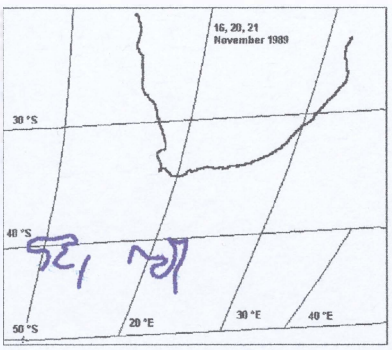
16, 20, 21
November 1989
30 °S
40 °S
50 °S
20 °E
30 °E
40 °E

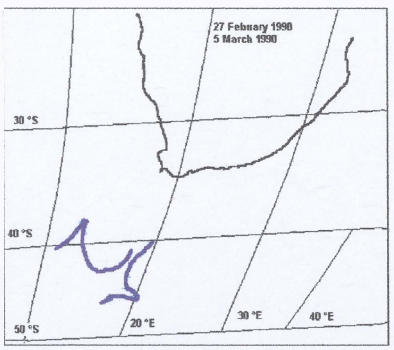
27 Febuary 1990
5 March 1990
30 °S
40 °S
50 °S
20 °E
30 °E
40 °E

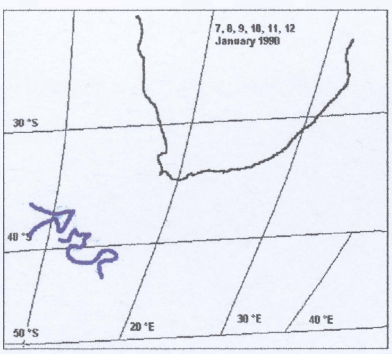
7, 8, 9, 10, 11, 12
January 1990
30 °S
40 °S
50 °S
20 °E
30 °E
40 °E

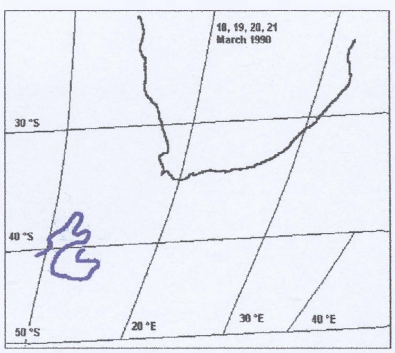
18, 19, 20, 21
March 1990
30 °S
40 °S
50 °S
20 °E
30 °E
40 °E

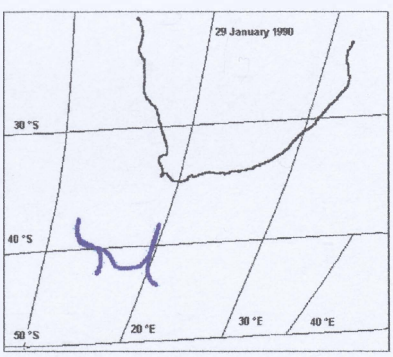
29 January 1990
30 °S
40 °S
50 °S
20 °E
30 °E
40 °E

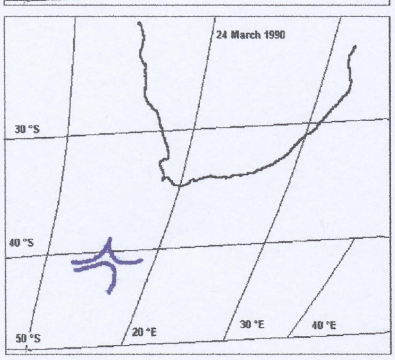
24 March 1990
30 °S
40 °S
50 °S
20 °E
30 °E
40 °E

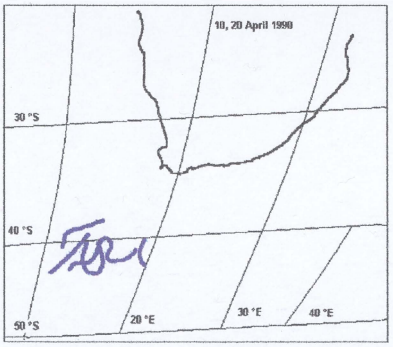
10, 20 April 1990
30 °S
40 °S
50 °S
20 °E
30 °E
40 °E

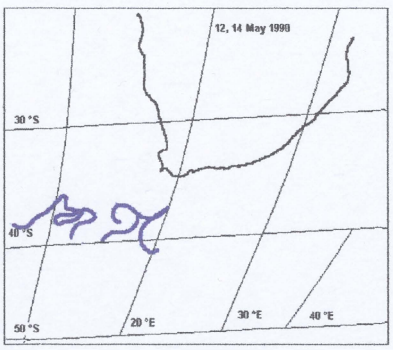
12, 14 May 1990
30 °S
40 °S
50 °S
20 °E
30 °E
40 °E

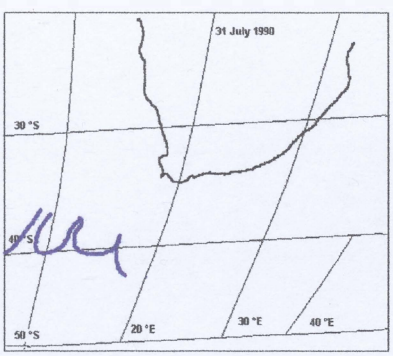
31 July 1990
30 °S
40 °S
50 °S
20 °E
30 °E
40 °E

A.2. Yearly composite diagrams

Yearly composite sketches of METEOSAT images showing (a) the position and (b) the orientation of SAASW intrusions.

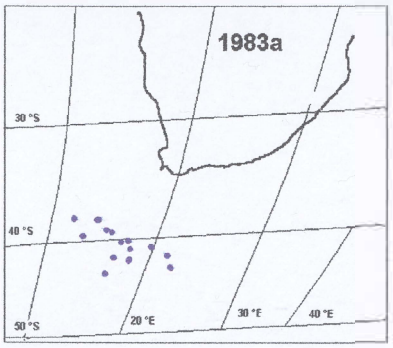
1983a
30 °S
40 °S
50 °S
20 °E
30 °E
40 °E

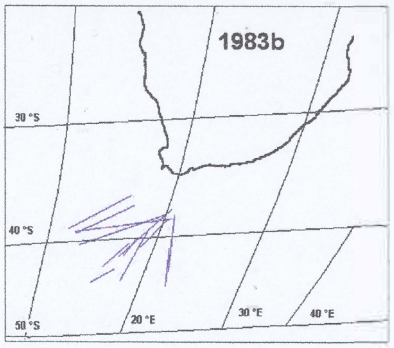
1983b
30 °S
40 °S
50 °S
20 °E
30 °E
40 °E

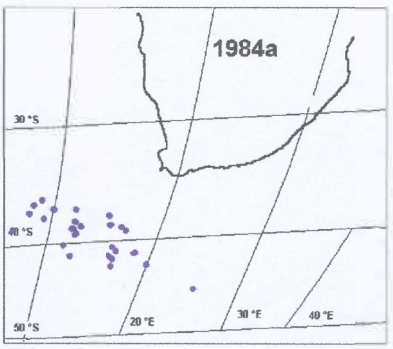
1984a
30 °S
40 °S
50 °S
20 °E
30 °E
40 °E

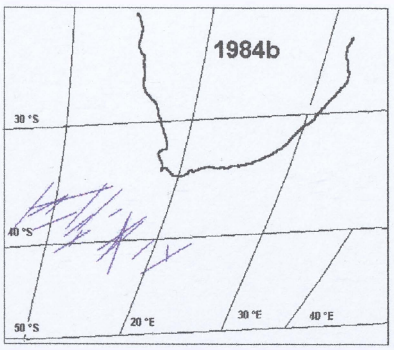
1984b
30 °S
40 °S
50 °S
20 °E
30 °E
40 °E

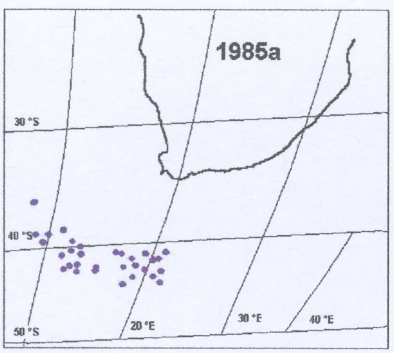
1985a
30 °S
40 °S
50 °S
20 °E
30 °E
40 °E

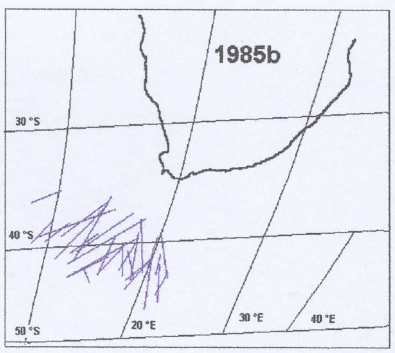
1985b
30 °S
40 °S
50 °S
20 °E
30 °E
40 °E

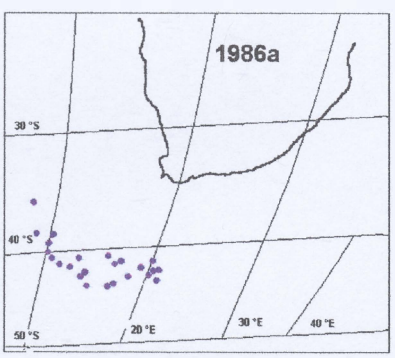
1986a
30 °S
40 °S
50 °S
20 °E
30 °E
40 °E

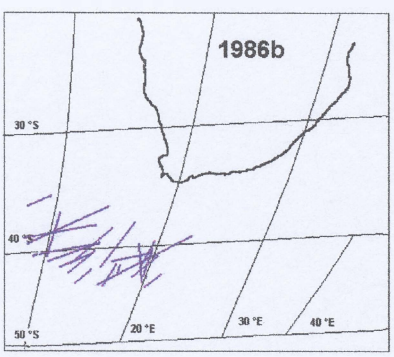
1986b
30 °S
40 °S
50 °S
20 °E
30 °E
40 °E

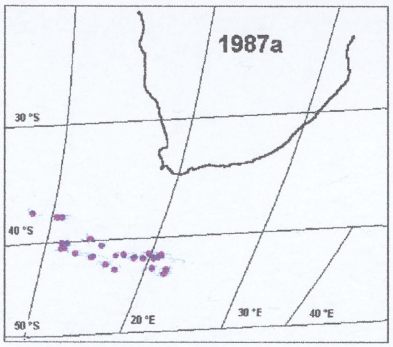
1987a
30 °S
40 °S
50 °S
20 °E
30 °E
40 °E

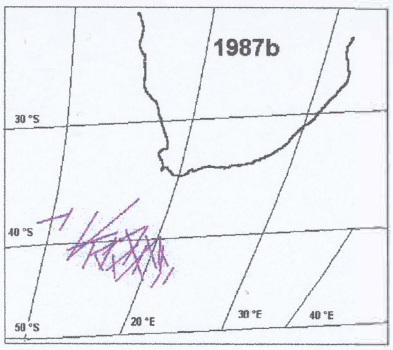
1987b
30 °S
40 °S
50 °S
20 °E
30 °E
40 °E

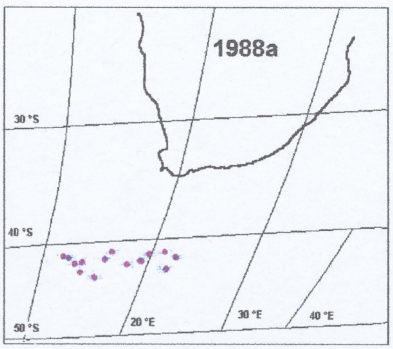
1988a
30 °S
40 °S
50 °S
20 °E
30 °E
40 °E

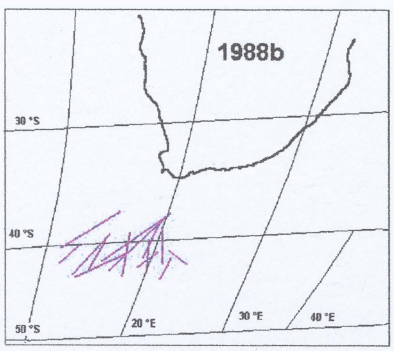
1988b
30 °S
40 °S
50 °S
20 °E
30 °E
40 °E

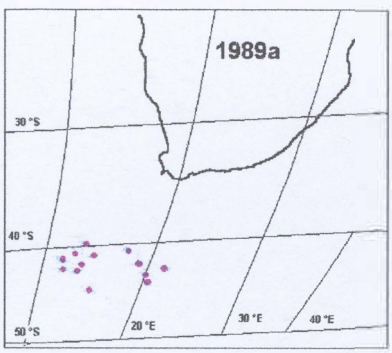
1989a
30 °S
40 °S
50 °S
20 °E
30 °E
40 °E

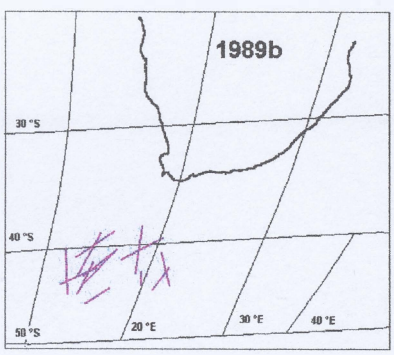
1989b
30 °S
40 °S
50 °S
20 °E
30 °E
40 °E

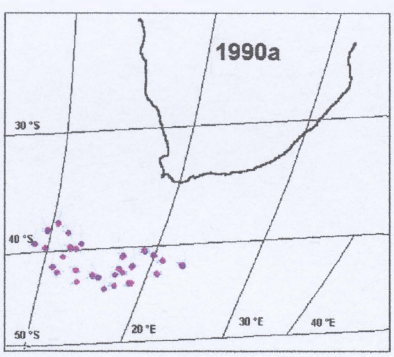
1990a
30 °S
40 °S
50 °S
20 °E
30 °E
40 °E

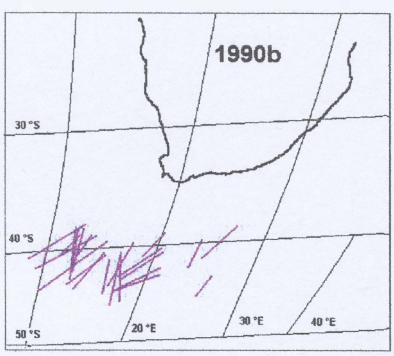
1990b
30 °S
40 °S
50 °S
20 °E
30 °E
40 °E

A.3. Summary of statistical analyses

These are statistical analyses done on satellite composite sketches given in Addendum A1.

Date	No of intrusions	Breadth (km)	Width (km)	Area Covered (km^2)	Total Area Covered (km^2)	Longitude (° E)	Latitude (° S)
30, 31 December 1983	2	111	592	65 712	120 472	11	37
		148	370	54 760		15	40
25 January 1984	2	74	296	21 904	43 808	15	37
		74	296	21 904		16	38
9,10, 12, 13, 16, 19 February 1984	3	222	370	82 140	175 232	11	38
		111	444	49 284		15	40
		74	592	43 808		17	42
22, 25, 26, 27, 28, 29 February1984	2	148	740	109 520	246 420	12	40
		185	740	136 900			
4, 14, 15, 29, 30, 31 March 1984						20	42
1, 15 June 1984	2	222	370	82 140	139 638	10	36
		111	518	57 498		12	37
24 June 1984	2	148	444	65 712	131 424	15	39
		148	444	65 712		19	41
7, 10, 13, 14, 17 July 1984	3	74	592	43 808	114 996	9	38
		222	222	49 284		11	40
		74	296	21 904		18	41
10 October 1984	1	222	1110	246 420	246 420	12	40
25 October 1984	2	74	444	32 856	65 712	12	39
		74	444	32 856		17	41
29, 30 November 1984	2	111	222	24 642	106 782	12	36
		222	370	82 140		20	40
7, 8 December 1984	4	111	222	24 642	139 638	8	38
		222	444	98 568		12	38
		111	518	16 428		15	38
		111	148			18	38
1, 6, 7, 8, 10, 12, 13, 15, 16, 19 January 1985	3	222	740	164 280	369 630	12	38
		222	740	164 280		15	42
		111	370	41 070		20	42

		185	370	68 450		20	40
4, 8 January 1987	2	111	444	49 284	76 664	16	40
		148	185	27 380		20	42
17, 18, 22, 23, 24, 27,		370	1110	410 700		12	41
30 January 1987	3	370	740	273 800	733 784	15	42
6 February 1987		222	222	49 284		20	42
15, 16, 17 February 1987	1	740	740	547 600	547 600	15	39
25, 26, 27, 28 February 1987		185	740	136 900		11	41
10 March 1987	2	185	444	82140	219 040	17	42
21, 22, 23 March 1987	2	370	296	109 520	246 420	10	38
		185	740	136 900		14	39
		518	296	153 328		10	39
2, 3, 4, 5 April 1987	3	111	370	41 070	221 778	15	40
		148	185	27 380		17	42
17, 19 April 1987	2	148	185	27 380	82 140	7	36
		185	296	54 760		18	42
		185	148	27 380		11	40
20, 21 June 1987	3	185	148	27 380	76 664	15	40
		148	148	21 904		18	40
23 July 1987	1	222	296	65 712	65 712	17	42
21, 22, 23, 26, 28 September 1987	2	185	814	150 590	216 302	11	40
		111	592	65 712		16	42
5 December 1987	1	444	111	49 284	49 284	20	42
13, 27, 28, 29 January 1987	2	222	370	82 140	156 066	12	41
1 February 1988		111	666	73 926		17	42
22, 27 February 1987	2	185	592	109 520	158 804	14	40
		111	444	49 284		18	42
1, 5, 6, 22 August 1988	1	74	592	43 808	43 808	13	42
1, 2, 4, 5, 6, 7 September 1988	1	74	370	27 380	27 380	16	42

20, 22, 23 September 1988	2	111 111	592 370	65 712 41 070	106 782	12 18	40 42
2, 6 December 1988	3	111 111 111	296 444 370	32 856 49 284 41 070	123 210	12 15 18	43 44 42
15, 16, 17 April 1989	1	111	518	57 498	57 498	16	39
13 August 1989	2	296 148	296 148	87 616 21 904	109 520	13 18	38 42
14, 19, 20 October 1989	2	185 148	444 444	82 140 65 712	147 852	14 19	40 42
1, 2 November 1989	2	111 74	1184 74	131 424 5 476	136 900	13 19	41 41
5 November 1989	3	222 74 148	185 148 111	41 070 10 952 16 428	68 450	11 13 18	40 41 41
16, 20, 21 November 1989	3	148 296 74	296 111 444	43 808 32 856 32 856	109 520	12 20 23	42 43 43
7, 8, 9, 10, 11, 12 January 1990	3	222 111 111	370 222 222	82 140 24 642 24 642	131 424	7 12 15	37 40 42
29 January 1990	2	74 37	740 518	54 760 19 166	73 926	16 20	43 43
26 February 1990	1	148	518	76 664	76 664	17	43
27 February 1990 5 March 1990	2	222 111	370 740	82 140 82 140	164 280	13 18	41 44
18, 19, 20, 21 March 1990	1	222	592	131 424	131 424	11	42
24 March 1990	1	111	222	24 642	24 642	15	42
10, 20 April 1990	3	148 111 74	296 222 148	43 808 24 642 10 952	79 402	13 15 18	42 42 42

		148	222	32 856		10	38
12, 14 May 1990	3	111	296	32 856	120 472	12	38
		148	370	54 760		17	40
		185	444	82 140		7	40
31 July 1990	3	111	370	41 070	139 638	12	40
		74	222	16 428		16	41
Average		**175**	**413**		**158 520**	**15**	**40**
Standard deviation		**99**	**215**		**118 256**	**4**	**2**

A.4. Weather ship data

This insert presents thermograph data collected by the vessel *F. H. Hughes* on fortnightly sea crossings from Cape Town to a point 10° E and 40° S between 1969 and 1974. An illustrative cruise track is given as well as a brief analysis of the thermograph data. The results of this analysis are discussed at the end of the section.

A.4. Weather ship data

This insert presents thermograph data collected by the vessel *F. H. Hughes* on fortnightly sea crossings from Cape Town to a point 10° E and 40° S between 1969 and 1974. An illustrative cruise track is given as well as a brief analysis of the thermograph data. The results of this analysis are discussed at the end of the section.

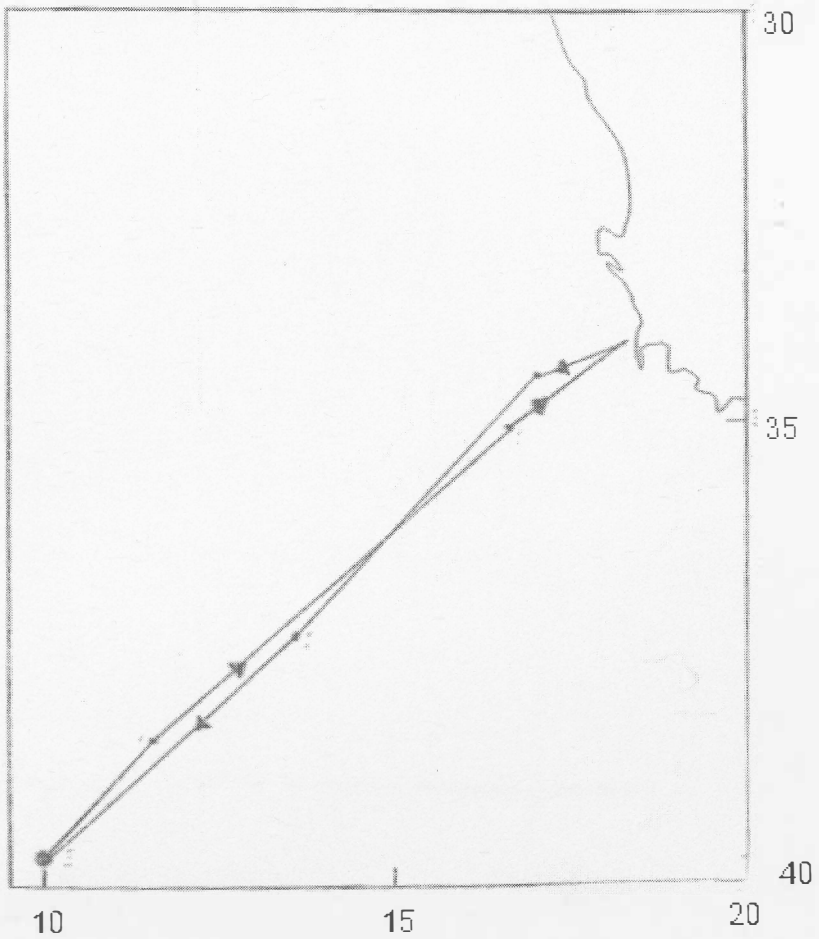

Figure A1. An illustrative cruise track of the weather ship F. H. Hughes on fortnightly sea crossings from Cape Town to a point 10° E, 40° S.

The data available were hand-drawn temperature versus longitude plots and are given overleaf.

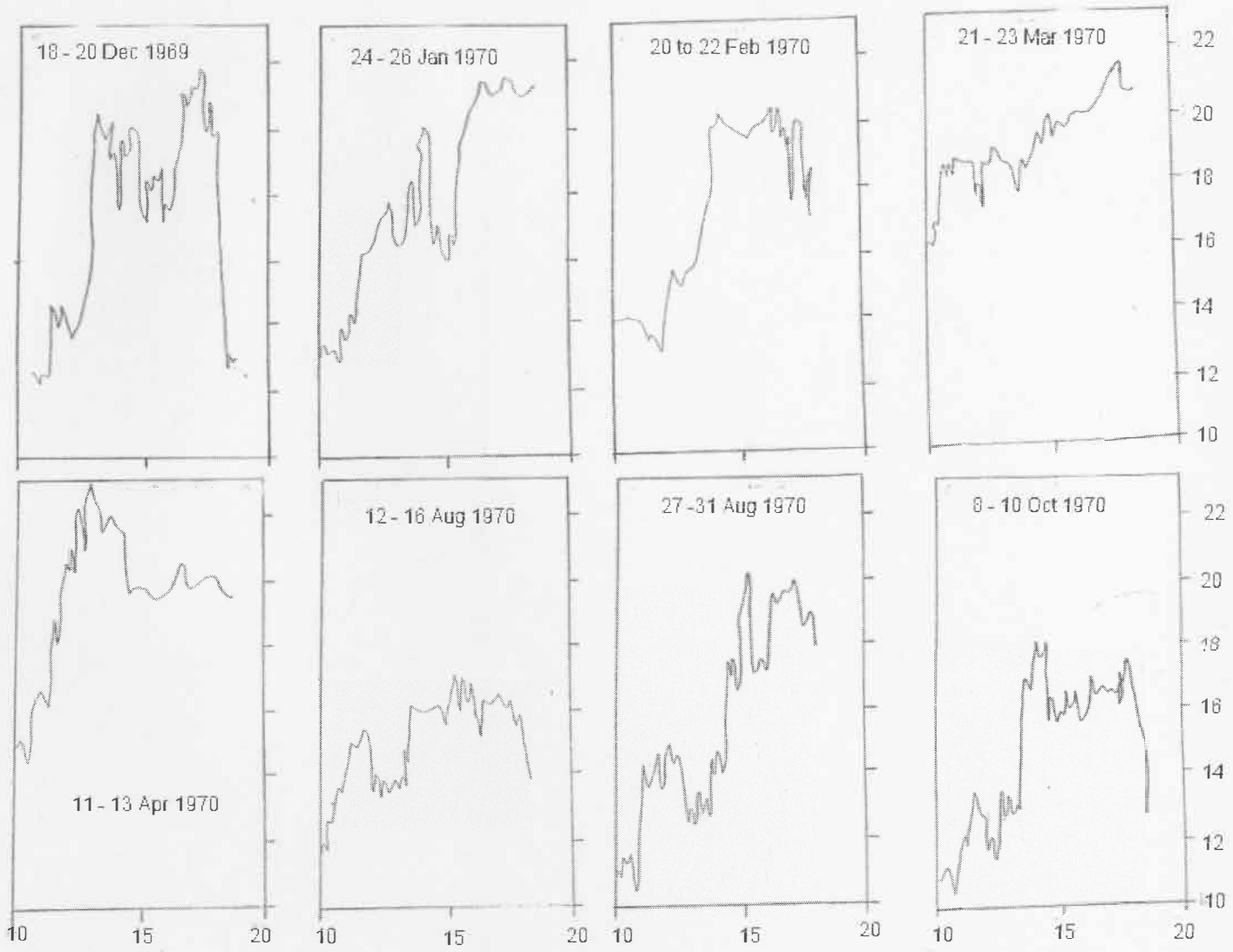
18 - 20 Dec 1969
24 - 26 Jan 1970
20 to 22 Feb 1970
21 - 23 Mar 1970
11 - 13 Apr 1970
12 - 16 Aug 1970
27 - 31 Aug 1970
8 - 10 Oct 1970
10
12
14
16
18
20
22
10
15
20

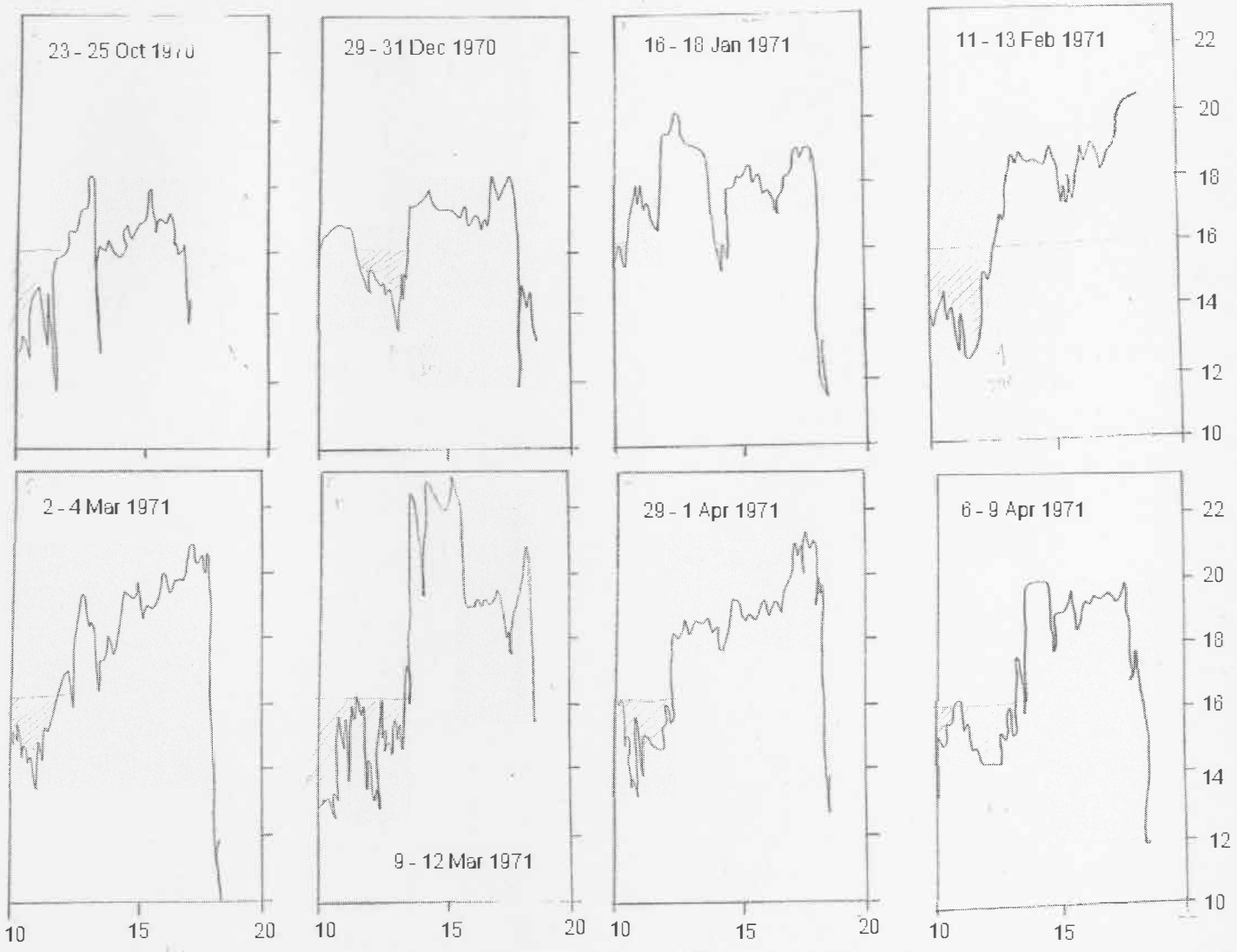
23 - 25 Oct 1970
29 - 31 Dec 1970
16 - 18 Jan 1971
11 - 13 Feb 1971
2 - 4 Mar 1971
9 - 12 Mar 1971
29 - 1 Apr 1971
6 - 9 Apr 1971
10
12
14
16
18
20
22
10
15
20

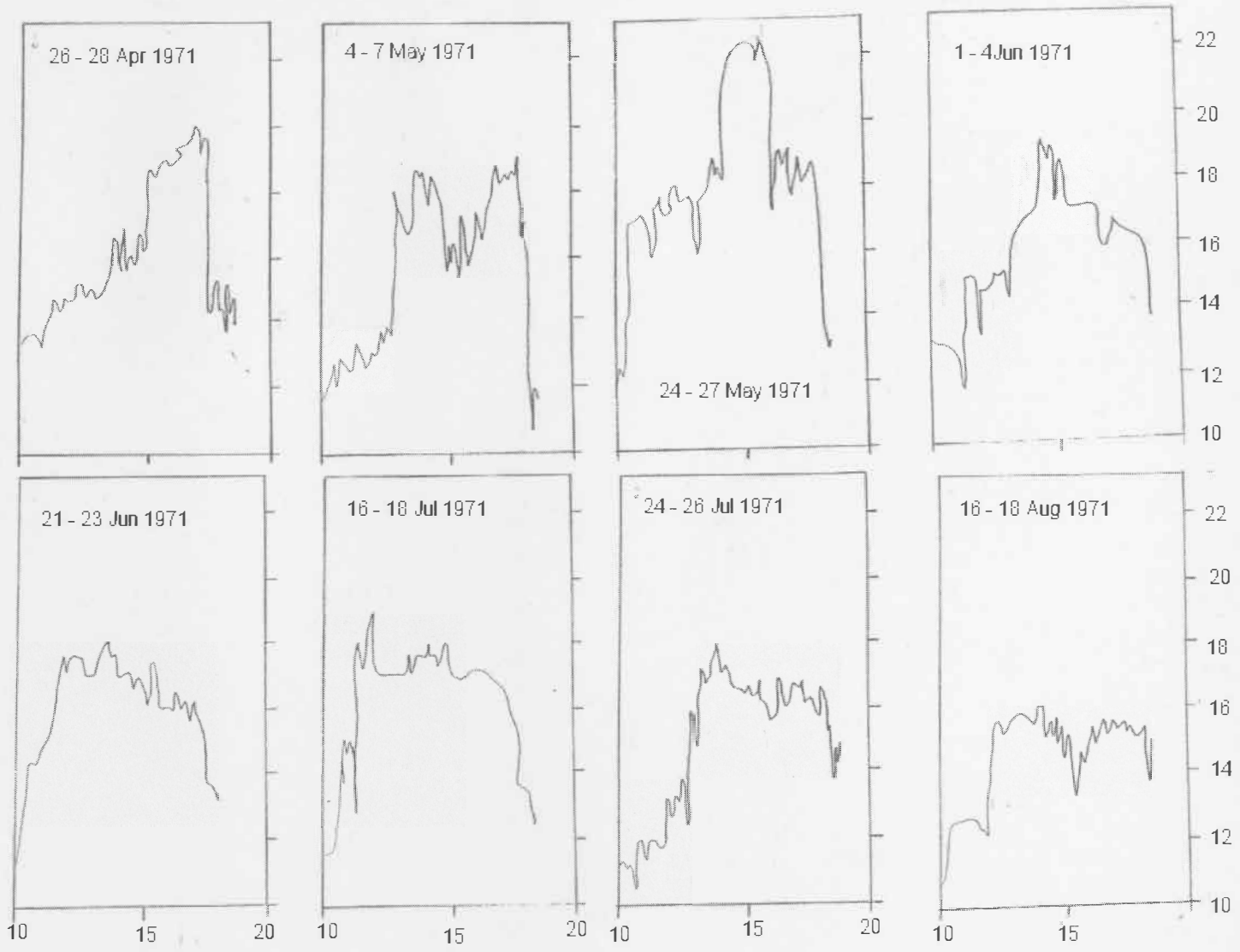
26 - 28 Apr 1971
4 - 7 May 1971
24 - 27 May 1971
1 - 4Jun 1971
21 - 23 Jun 1971
16 - 18 Jul 1971
24 - 26 Jul 1971
16 - 18 Aug 1971
10
12
14
16
18
20
22
10
15
20

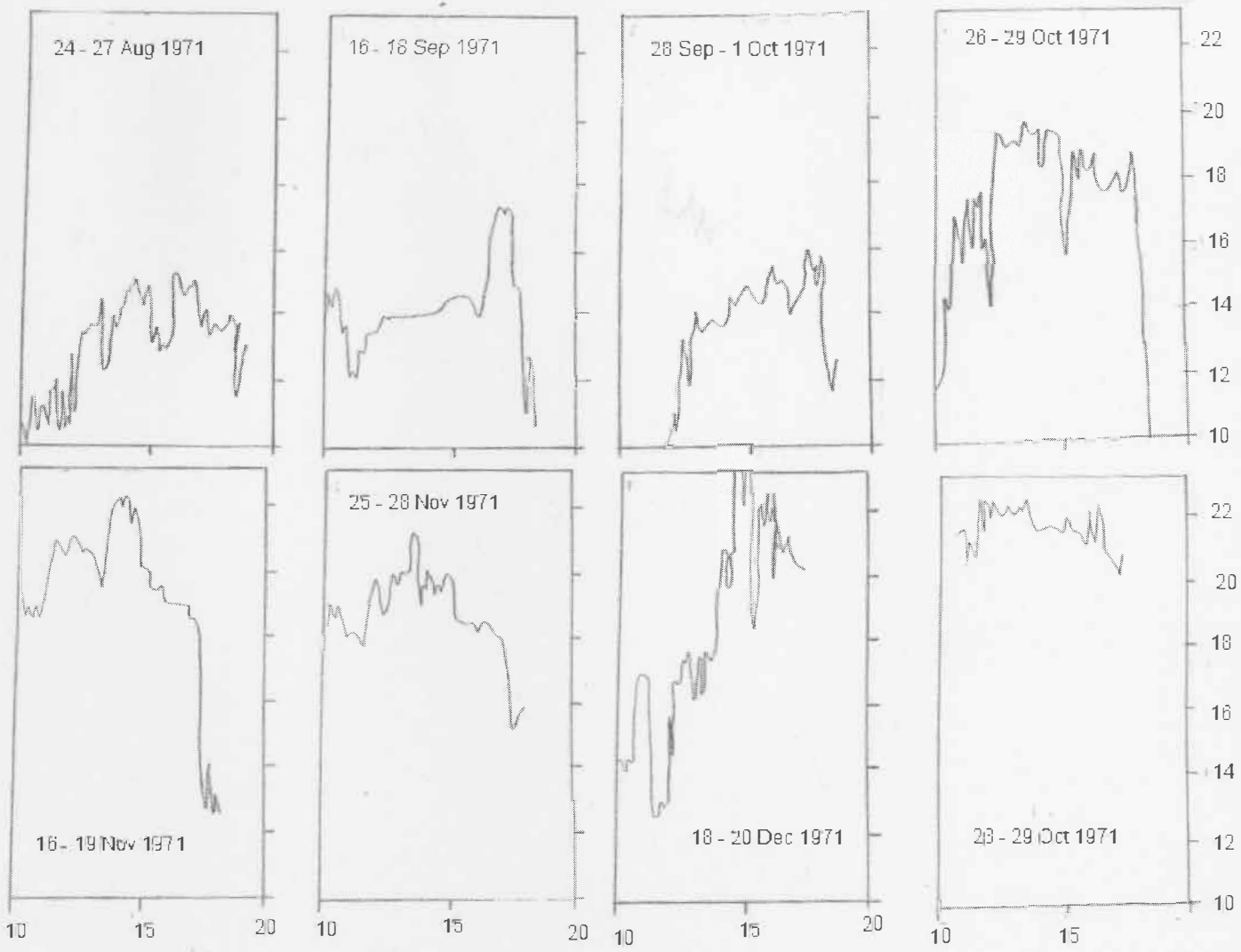
24 - 27 Aug 1971
16 - 18 Sep 1971
28 Sep - 1 Oct 1971
26 - 29 Oct 1971
16 - 19 Nov 1971
25 - 28 Nov 1971
18 - 20 Dec 1971
28 - 29 Oct 1971
10
12
14
16
18
20
22
10
15
20

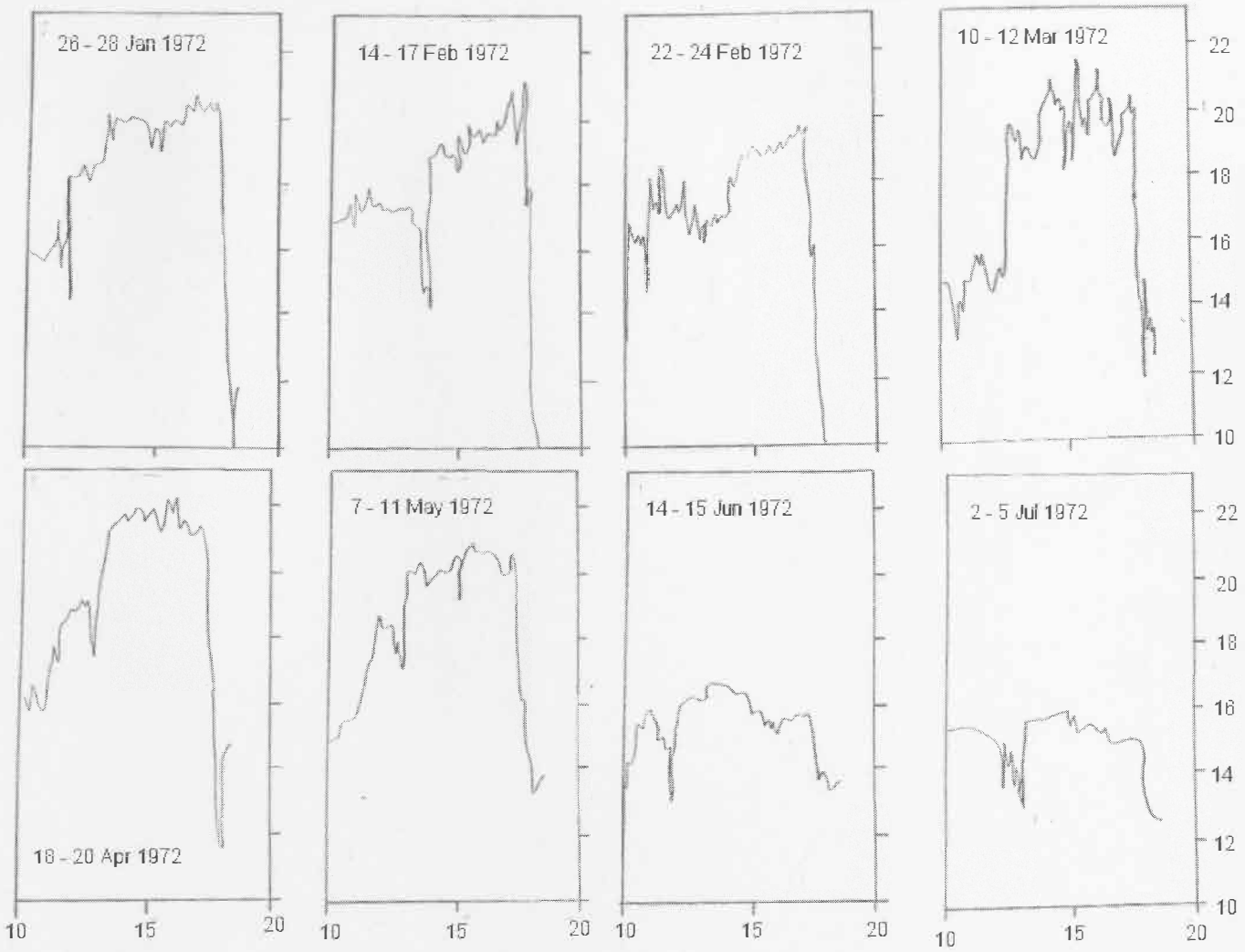
26 - 28 Jan 1972
14 - 17 Feb 1972
22 - 24 Feb 1972
10 - 12 Mar 1972
18 - 20 Apr 1972
7 - 11 May 1972
14 - 15 Jun 1972
2 - 5 Jul 1972
10
12
14
16
18
20
22
10
15
20

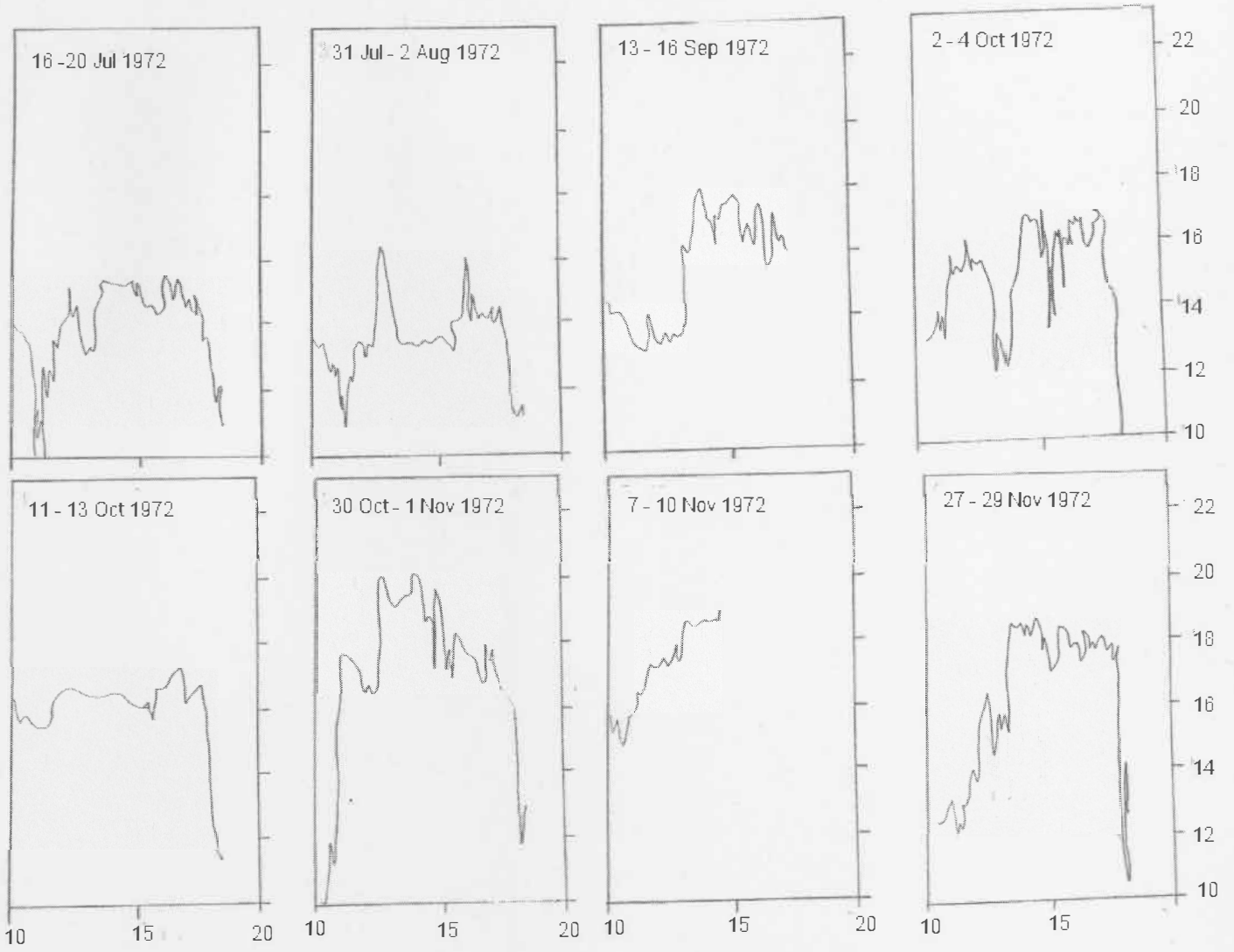
16 -20 Jul 1972
31 Jul - 2 Aug 1972
13 - 16 Sep 1972
2 - 4 Oct 1972
11 - 13 Oct 1972
30 Oct - 1 Nov 1972
7 - 10 Nov 1972
27 - 29 Nov 1972
10
12
14
16
18
20
22
10
15
20

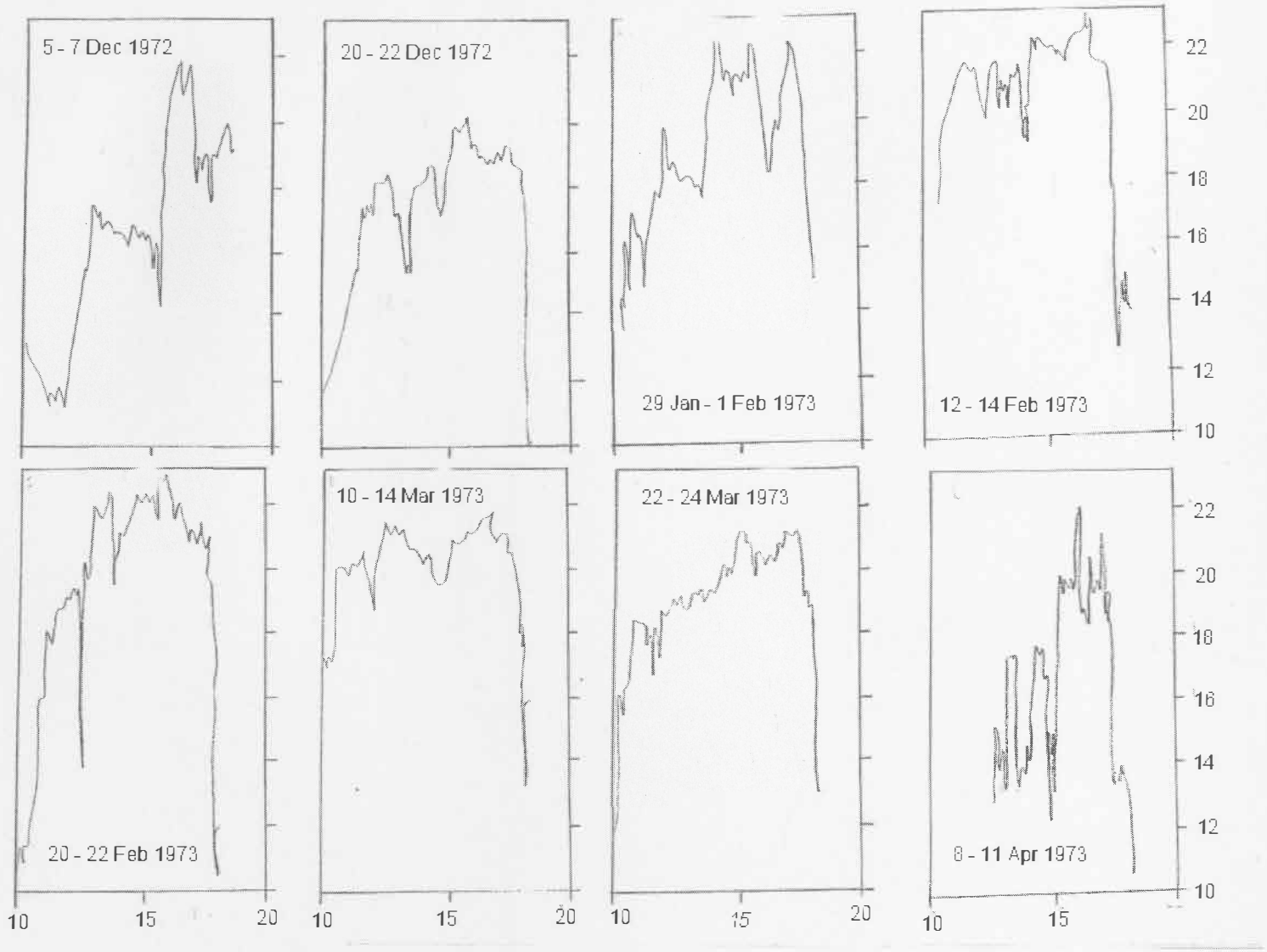
5 - 7 Dec 1972
20 - 22 Dec 1972
29 Jan - 1 Feb 1973
12 - 14 Feb 1973
20 - 22 Feb 1973
10 - 14 Mar 1973
22 - 24 Mar 1973
8 - 11 Apr 1973
10
12
14
16
18
20
22
10
15
20

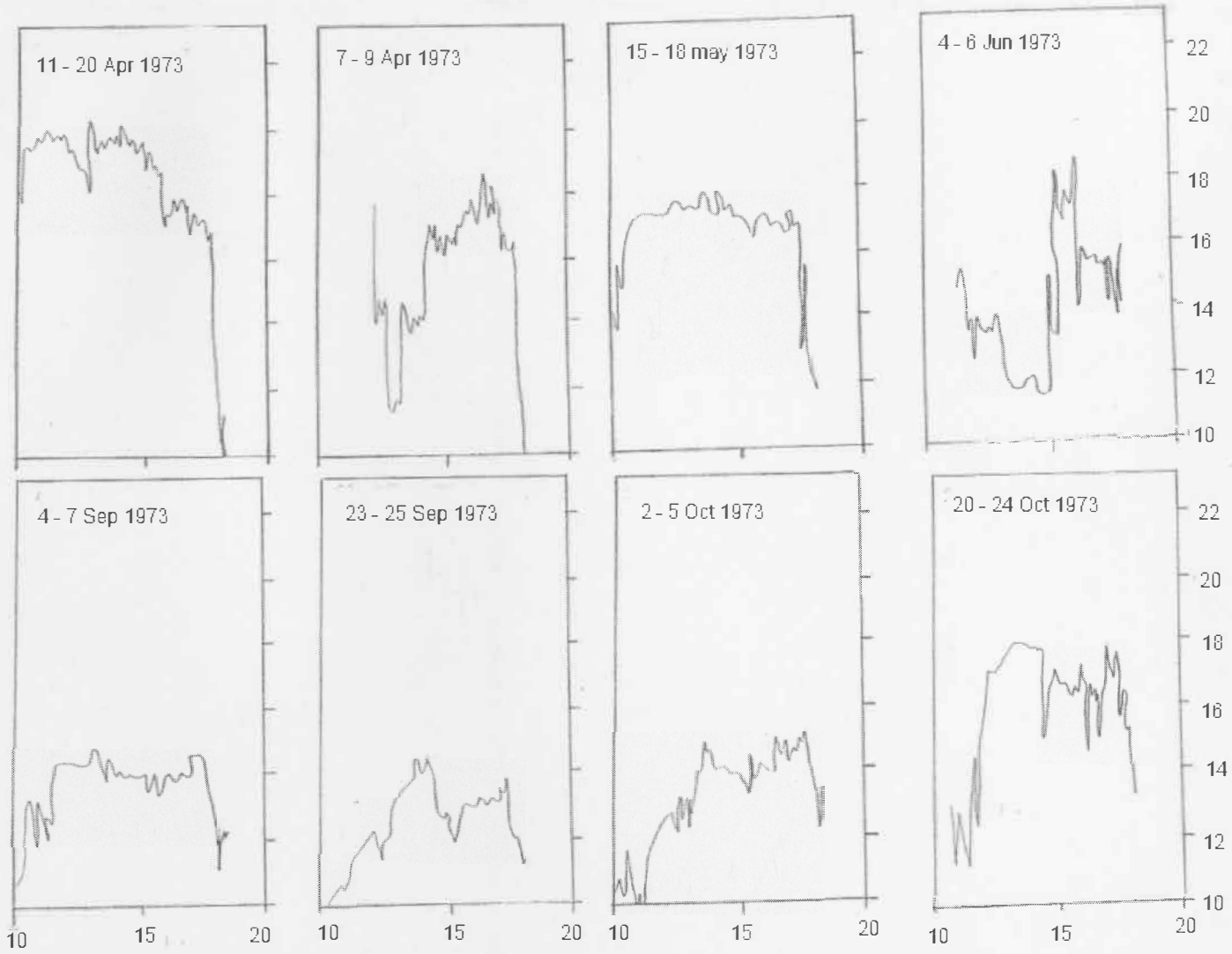
11 - 20 Apr 1973
7 - 9 Apr 1973
15 - 18 may 1973
4 - 6 Jun 1973
4 - 7 Sep 1973
23 - 25 Sep 1973
2 - 5 Oct 1973
20 - 24 Oct 1973
10
12
14
16
18
20
22
10
15
20

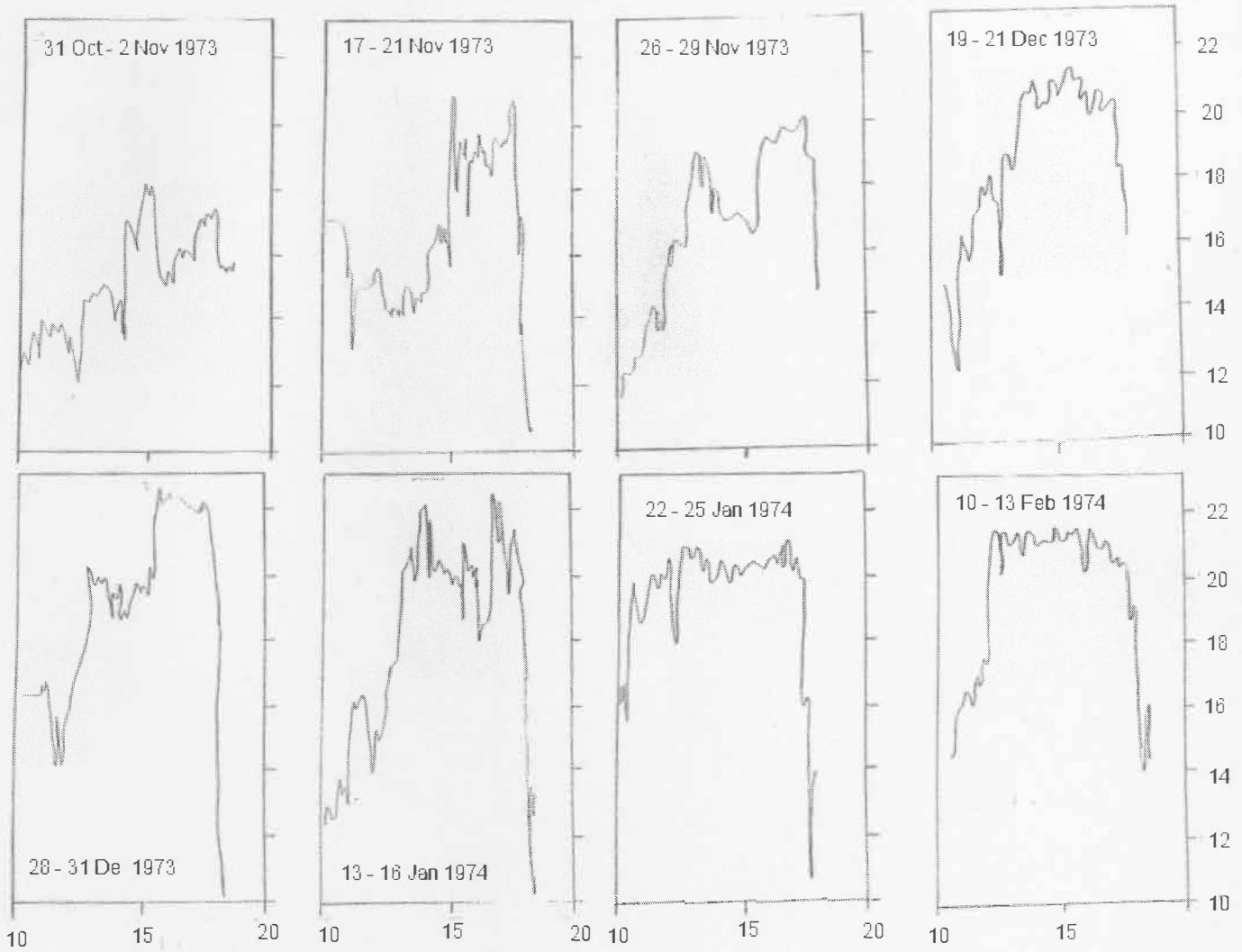
31 Oct - 2 Nov 1973
17 - 21 Nov 1973
26 - 29 Nov 1973
19 - 21 Dec 1973
28 - 31 De 1973
13 - 16 Jan 1974
22 - 25 Jan 1974
10 - 13 Feb 1974
10
15
20
22
18
16
14
12

The data is not included in the body of the thesis because of the uncertainly with regards to the hand drawn diagrams as well as the uncalibrated nature of the ship's thermograph on which these measurements depended. Moreover, although Figure A1 illustrates an example of a cruise track, the assumption can not be verified that all crossings followed this same cruise track. Nevertheless, these data were used to give a rough estimate of the longitudinal position of SAASW intrusion. This was done by determining the longitudinal frequency of water that is < 16° C, assumed to be modified SAASW. This is illustrated in Figure A2.

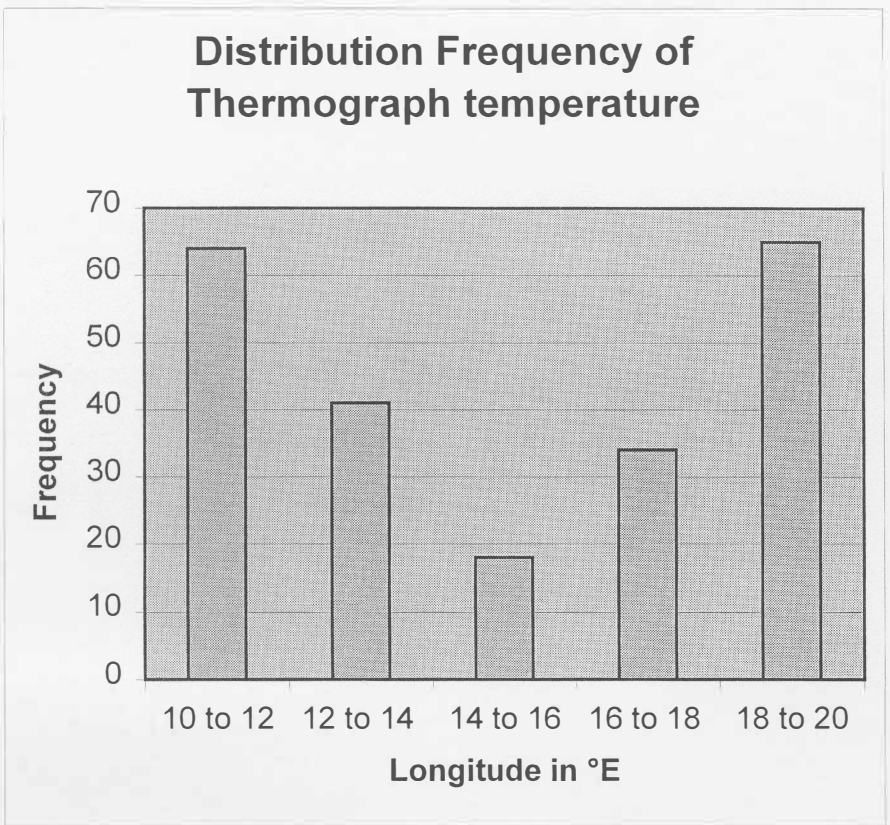

Figure A2. Histogram showing the distribution frequencies of water colder than 16° C on the cruise track similar to that illustrated in Figure A1.

It is interesting to note that this Figure shows a tendency for colder surface water to occur at approximately 11° E and 19° E which is in exact agreement with the historical mean estimate of cold water intrusion at the STC.